Studies of Experimental Cerebral Ischaemia using Magnetic Resonance Imaging and Autoradiography

Mark F. Lythgoe

Submitted for the Degree of
Doctor of Philosophy

1999

Royal College of Surgeons Unit of Biophysics
Institute of Child Health and
Great Ormond Street Hospital
University of London

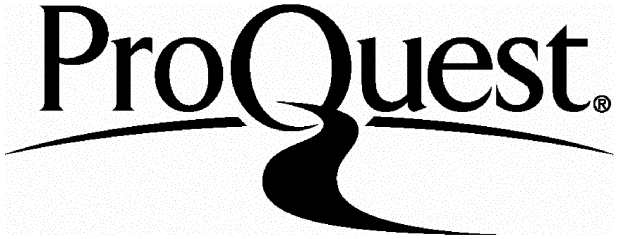

Studies of experimental cerebral ischaemia using magnetic resonance imaging and autoradiography

Following a stroke, the ability to discriminate between areas of non-recoverable tissue and potentially salvageable tissue remains a goal of diagnostic imaging. There have been a number of recent developments both in nuclear medicine and in magnetic resonance imaging (MRI) techniques, which may have potential to achieve this goal. This thesis describes the use of these techniques for the evaluation of focal pathophysiology in a rat model of model cerebral artery occlusion (MCAO).

Methods were described to use autoradiographic markers to study cerebral blood flow (^{99m}Tc-hexamethylpropylene amine oxime) and cerebral hypoxia (^{125}I-iodoazomycin arabinoside) simultaneously following MCAO in the rat. The uptake of these tracers was compared to MRI measurements of the apparent diffusion coefficient of water (ADC) and to histology. It was shown that the combined use of ^{125}I-IAZA or ADC imaging with perfusion imaging may allow differentiation between areas of oligaemic misery perfusion, ischaemic misery perfusion and ischaemic lesion core.

MRI was used to examine the effects of cerebral tissue anisotropy on calculation of the spatial distribution of ischaemia in the rat using ADC measurements. Demonstration of grey matter anisotropy led to the use of rotationally invariant ADC measurements which were shown to improve stroke lesion delineation.

To investigate the acute changes in NMR parameters of diffusion, perfusion, T1 and T2 a remote controlled MCAO model in the rat was refined for a vertical 8.5T high field magnet. Combined perfusion and diffusion data distinguish between a "moderately affected area", with reduced perfusion but normal diffusion; and a "severely affected area", in which both perfusion and diffusion were significantly reduced. Two novel MRI observations were reported, namely a decrease in T2 and an increase in T1, both within the first few minutes of ischaemia.

A rat model of oligaemic misery perfusion was developed in which a large region of homogeneously reduced blood flow was produced without cytotoxic oedema forming. Early NMR changes in CBF, T1 and T2 were noted without reduction in the ADC value. This approach may provide a model of penumbral flow, which may be of value in studying and evaluating neuroprotection

Contents

Figures

Tables

ADC	apparent diffusion coefficient
ADP	adenosine diphosphate
ATP	adenosine triphosphate
BBB	blood brain barrier
BOLD	blood oxygen level-dependent
CBF	cerebral blood flow
CBV	cerebral blood volume
CCA	common carotid artery
DSCI	dynamic susceptibility contrast imaging
DWI	diffusion weighted imaging
EAA	excitatory amino acid
ECA	external carotid artery
EEG	electroencephalogram
FID	free induction decay
FOV	field of view
HLV	hemispheric lesion volume
ICA	internal carotid artery
MCA	middle cerebral artery
MCAO	middle cerebral artery occlusion
MRI	magnetic resonance imaging
MRS	magnetic resonance spectroscopy
MTC	magnetisation transfer contrast
MTT	mean transit time
NA	number of acquisitions
NAA	N-acetylaspartate
NMDA	N-methyl-D-aspartate
NMR	nuclear magnetic resonance
PCr	phosphocreatine
Pi	inorganic phosphate
SD	spreading depression
TE	echo time
TR	repetition time

Acknowledgements

It is with great pleasure that I thank Dr. Isky Gordon, who initiated this project and provided me with the opportunity to undertake this work. I also thank my supervisor Professor Steve Williams and Professor David Gadian for their help and encouragement, and providing the scope for this work to evolve into its present form.

I am indebted to Albert Busza, especially in my former years, for helping me with the NMR and experimental work. My thanks are also to the people that I have met and have helped me while at the RCS Unit of Biophysics, these include: Nick van Bruggen, Simon Roussel, Jill Cremer, Nick Preece, Ted Proctor, Martin King, Neil Harris, Janel Le Belle, John Housemann, Alan Connelly and Sally Dowsett.

Many of the above that I have mentioned, have developed from colleagues to friends, and none more so than Fernando Calamante, David Thomas and Gaby Pell, whose constant support has made my Ph.D. student years an educational and enjoyable time.

Finally I would like to thank my family and friends, for their support and encouragement, which has brought me to the completion of this thesis.

' Our original zest had now quite gone
and it was turning more into a grim struggle.
I then realised that the ridge ahead, instead of still monotonously rising,
now dropped sharply away,
and far below I could see the North Col and the Rongbuk glacier.
I looked upwards to see a narrow snow ridge running up to a snowy summit.
A few more whacks of the ice-axe in the firm snow
and we stood on top.'

First ascent of Everest by Edmund Hillary and Tenzing on the 29th May, 1953.

An extract from 'The Ascent of Everest' by John Hunt.

Preface

The objective of this thesis was to gain insight into the diagnosis and pathophysiology of cerebral ischaemia using several MRI parameters and nuclear medicine markers of cerebral blood flow and hypoxia.

Chapter 1 describes an overview of clinical stroke and the pathophysiology of cerebral ischaemia in both animals and humans. **Chapter 2** covers the various techniques used in this thesis to investigate experimental cerebral ischaemia. The application of both MRI and nuclear medicine in the field of human and animal stroke, are described in **Chapter 3**.

Chapters 4-7 include the experimental work undertaken for this thesis and follow the developmental evolution of the animal models from the classical '*on the bench*' occlusion of the MCA in the rat, to a novel animal model of oligaemic misery perfusion. In **Chapter 4** I compare the nuclear medicine markers of CBF (^{99m}Tc-HMPAO) and hypoxia (^{125}I-IAZA) with diffusion-weighted imaging (DWI), T2 MRI and histology, using conventional '*on the bench*' MCAO in the rat. In this study we observed anisotropic water diffusion changes in the cortex of the rat. This prompted a study to investigate the effect of brain tissue anisotropy on the delineation of a focal ischaemic lesion, the results of which are contained in **Chapter 5**. The animal model used in these initial chapters, does not allow the early changes during ischaemia to be observed. In **Chapter 6** I explain a method to remotely occlude the MCA of a rat in a vertical magnet (8.5T), which allowed the hyper-acute changes in CBF, T1, T2 and DWI to be observed. During this study, small regions of mismatch between DWI and

CBF were noted. In order to study these regions in greater depth, I produced an occluding device that would partially occlude the middle cerebral artery, and could be remotely manipulated from outside the vertical magnet. This technique, together with the MRI findings are described in **Chapter 7**.

Finally, the implications for the findings described in **Chapters 4-7** and the possible future role of these methodologies in the studies of experimental and clinical stroke are discussed in **Chapter 8**.

Publications

Lythgoe, M. F., Busza, A. L., Calamante, F., Sotak, C. H., King, M. D., Bingham, A. C., Williams, S. R., and Gadian, D. G.(1997). Effects of diffusion anisotropy on lesion delineation in a rat model of cerebral ischemia. *Magn. Reson. Med.* **38**, 662-668.

Lythgoe, M. F., Williams, S. R., Wiebe, L. I., McEwan, A. J. B., and Gordon, I.(1997). Autoradiographic imaging of cerebral ischaemia using a combination of blood flow and hypoxic markers in an animal model. *Eur. J. Nucl. Med.* **24**, 16-20.

Calamante, F., Lythgoe, M. F., Pell, G., Thomas, D. L., King, M. D., Busza, A. L., Sotak C. H., Williams, S. R., Ordidge, R. J., and Gadian, D. G.(1999). Early changes in water diffusion, perfusion, T1 and T2 during focal cerebral ischaemia in the rat studied at 8.5T. *Magn. Reson. Med.* 41: 479-485

Lythgoe, M. F., Williams, S. R., Busza, A. L., Wiebe, L. I., McEwan, A. J. B., Gadian, D. G., and Gordon, I.(1999). The relationship between magnetic resonance imaging and autoradiographic markers of cerebral blood flow and hypoxia in an animal stroke model. *Magn. Reson. Med.* 41: 706-714

Lythgoe, M. F., Thomas, D. L., Calamante, F., Pell, G., Busza, A. L., King, M. D., Sotak, C. H., Williams, S. R., Ordidge, R. J., and Gadian, D. G.(1999). A novel model of oligaemia using partial occlusion of the middle cerebral artery in a rat. *Stroke.* **Submitted**

Chapter 1

1. Overview of Cerebral Ischaemia

1.1 STROKE: A MODERN DEFINITION

Ischaemic stroke is the most common neurological disorder causing death or disability among adults living in industrialised nations. Stroke is a devastating condition and ranks third as a cause of death, surpassed only by heart disease and cancer (Mas and Zuber, 1991). Ischaemic events account for approximately 85% of all strokes. In any given year in Britain, 250,000 people suffered from some form of stroke, and in 1990, the Office of Population Census and Surveys for England and Wales reported a mortality of approximately 15,000 men and 26,000 women. Despite substantial declines in incidents during the last two decades (Mas and Zuber, 1991), stroke is still a leading neurological reason for hospitalisation and one of the most common causes of long term disability.

A clear definition of stroke is difficult to give because one of the principal features, its sudden onset, is shared by other neurological diseases. The National Survey of Stroke in the USA used the following definition:

Stroke is a clinical syndrome (collection of symptoms and signs) consisting of a constellation of neurological findings, sudden in onset, which persist for more than 24 hours, and whose vascular origins are limited to:

- Thrombotic or embolic occlusion of the cerebral artery resulting in infarction.
- Spontaneous rupture of a vessel resulting in intracerebral or subarachnoid haemorrhoid.

The WHO diagnostic criteria for stroke is defined as:

'rapidly developing clinical signs of focal (at times global) disturbances of cerebral function, lasting more than 24 hours, or leading to death with no apparent cause other than that of vascular origin' (Hatano, 1976).

Within the above definitions, ischaemic cerebrovascular disease is clinically divided into several syndromes, although in reality they are components of the continuum of brain ischaemia (Adams and Biller, 1995). *Transient ischaemic attacks* (TIA) and reversible ischaemic neurological deficit are ischaemic events from which the person completely recovers over a designated period (24 hours and 3 weeks, respectively). A cerebral infarction with transient symptoms is an episode of ischaemia that completely resolves clinically, but imaging of the brain demonstrates a small stroke. *Acute ischaemic stroke* is diagnosed in a patient who reaches medical attention within the first hours after the onset of symptoms and includes patients who may be deteriorating. These patients may have complete resolution of their deficits or may be left with permanent sequelae; most show some degree of incomplete recovery. Stroke patients may have a wide selection of symptoms, including weakness and sensory loss, but there are two features which are common to all types of stroke. The first is its sudden onset arising from the abrupt disturbance of blood supply and the second is the focal disturbance of function occurring at the site of ischaemic insult within the brain.

1.2 PATHOPHYSIOLOGY OF CEREBRAL ISCHAEMIA

1.2.1 Definitions of cerebral ischaemia

The term ischaemia is composed of the Greek words *"ischein"* (to suppress) and *"haima"* (blood). Cerebral ischaemia, i.e. lack of blood supply to the brain, can be classified according to its distribution (global or focal) and duration (permanent or transient). Some workers, for example Siesjo in 1978, have used the term ischaemia to denote complete interruption of flow, and oligaemia to characterise a reduction of cerebral blood flow (CBF) below normal (Siesjo, 1978). Currently there are several terms used to classify a reduction in flow. These are broadly used and may depend on a technique used to measure the degree of insult. I have defined the terms and origins used within this thesis to reduce the possibility of misunderstanding a represented region within a lesion (Figure 1.1).

- *Ischaemia* may be defined as a reduction of cerebral blood flow to levels insufficient to maintain normal cerebral function, metabolism or structure.
- *Oligaemic misery perfusion*, is a combination of the term 'misery perfusion', originally used by Baron et al. to indicate a region of increased oxygen extraction (Baron *et al.* 1981), and 'oligaemia' used by Lassen and Astrup to characterise the interval of moderately reduced flow that is fully compensated for by increased oxygen extraction fraction (OEF) (Lassen and Astrup, 1987). These two terms were latter combined by Baron (1991) to give the term 'oligaemic misery perfusion' which indicated an increased OEF and normal oxygen consumption ($CMRO_2$) (Baron, 1991) and remained consistent with the definition of Lassen et al. (Lassen and Astrup, 1987). In the literature the term oligaemic misery perfusion is often seen shortened to 'misery perfusion', which by definition, is a very broad CBF concept.

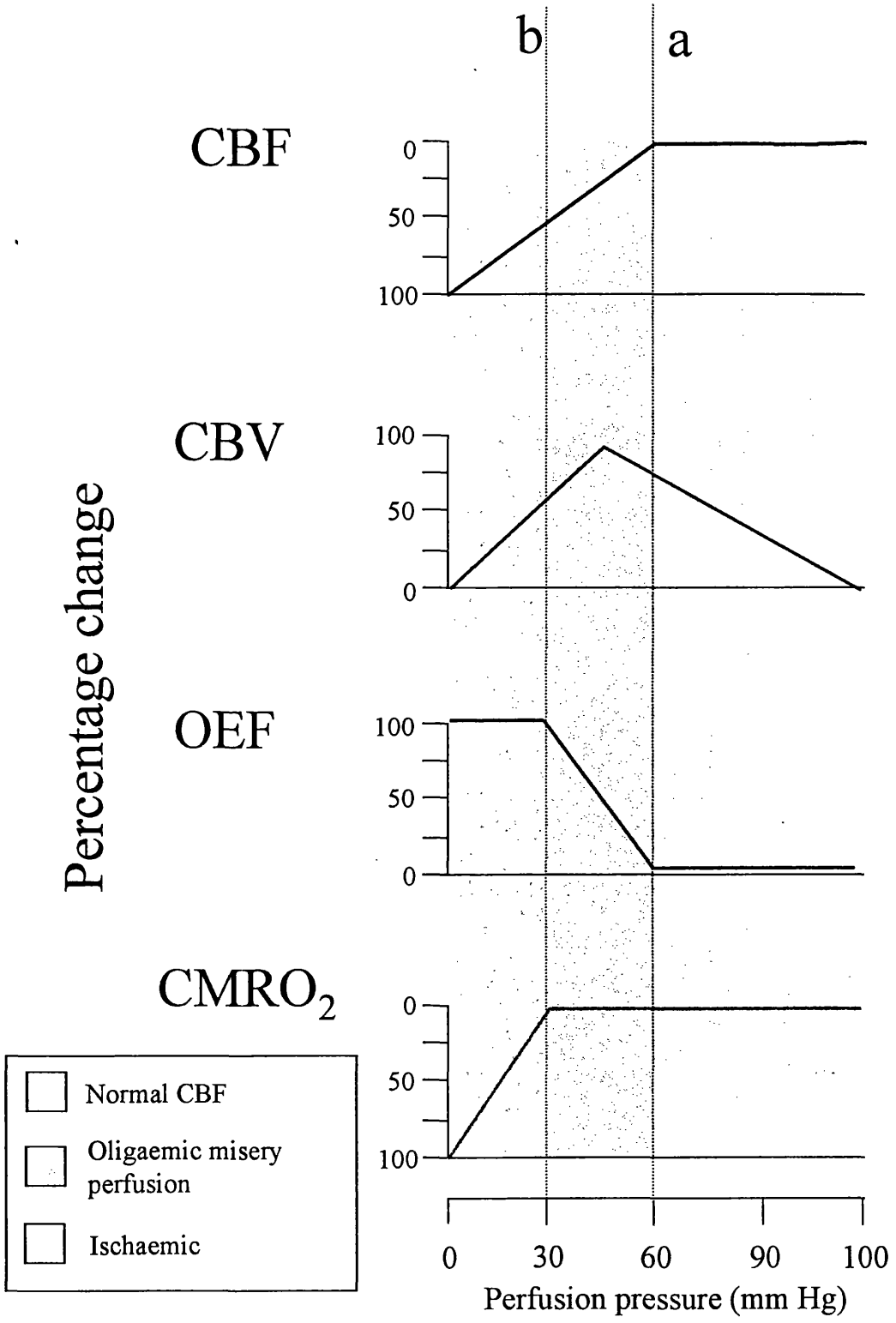

Figure 1.1 *As cerebral perfusion pressure falls, cerebral blood flow (CBF) is initially maintained by dilation of precapillary resistance vessels. As a result, both cerebral blood volume (CBV) and the CBV/CBF ratio (not shown) increase. When vasodilation can no longer compensate, cerebral autoregulation fails and blood flow begins to fall (a). (This occurs prior to maximal vasolidation). As perfusion pressure continues to fall. CBV may decrease as vessels collapse but the CBV/CBF ration remains elevated. A progressive increase in the oxygen extraction fraction (OEF) now maintains cerebral oxygen metabolism ($CMRO_2$). Once this mechanism becomes maximal (b), further declines in blood flow cause disruption of normal cellular metabolism and function.*

1.2.2 Autoregulation

The autoregulation of CBF is a mechanism to ensure a constant supply of blood and substrates, within a large spectrum of perfusion pressures, to the brain (Figure 1.1). The immediate consequence of arterial occlusion is a decrease of the blood pressure distal to the occlusion. The adequacy of alternative arterial routes of collateral flow, is one of the main determining factors for the level of distal blood pressure. Two homeostatic mechanisms, autoregulation and perfusion reserve, exist that tend to compensate for the reduced perfusion pressure so that tissue oxygen uptake and neuronal function can remain normal (Powers, 1991).

A moderate drop in distal arterial pressure in the normotensive human being, from the usual level of approximately 90mmHg (mean pressure) to 60mmHg, is fully compensated by the autoregulation of CBF by dilation of the down stream resistance vessels, the smaller arteries, arterioles and possibly veins. Below the lower level of autoregulation (60mmHg), the vasodilatation is inadequate as compensation and a pressure-passive fall in flow results. It should be noted that this pressure-passive flow dependence does not imply that vasodilatation is maximum.

When the compensatory mechanism of autoregulation is exhausted, CBF falls. As perfusion pressure falls below 60mmHg and the flow decreases, this fall is compensated by an increase in oxygen extraction fraction. Under normal conditions, the brain tissue only extracts about 35% of the delivered amount of oxygen, a value that can be increased to about double before hypoxic symptoms develop and is known as the perfusion reserve. Flows at this level will fulfil the criteria for regions of 'oligaemic misery perfusion' and below this level fall into the category of ischaemic flows.

When distal blood pressure falls below 35mmHg the two compensatory mechanisms, autoregulation and perfusion reserve, are inadequate to prevent failure of oxygen delivery. As the flow drops below the ischaemic threshold of 23ml/100g/min in humans, symptoms of tissue hypoxia develop (Lassen and Astrup, 1987).

1.2.3 Relationship between CBF and cerebral function

1.2.3.1 Vulnerability of the brain to ischaemia

The brain is especially vulnerable to interference with its blood supply and on the basis of both clinical and experimental evidence, it is generally accepted that brain tissue can survive between 5 and 10 minutes of ischaemia before permanent neurological deficits occur (Lust *et al.* 1985). Certain facts about the brain explain why ischaemia has such a profound effect on its function. The adult human brain, although weighing approximately 1,400g, and representing about 2% of total body weight, receives 15% of cardiac output and requires 20% of the total body oxygen. Thus the brains receives 25 times as much blood and oxygen as an equivalent weight of resting skeletal muscle. It is set apart from other organs by its unique sensitivity to ischaemia and its luxuriant blood supply which enables the venous return from the brain to be 64% oxygen saturated. The supply of glucose is even more luxuriant amounting to 34 μmol/100g/min and with a consumption averaging 0.31 μmol/100g/min. Under normal circumstances the brain relies solely on the oxidative metabolism of glucose to maintain its high metabolic rate and normal brain function. Essentially brain tissue has no oxygen stores and comparatively meagre reserves of high energy phosphates and carbohydrates. These energy reserves are only capable of sustaining ATP for about 1 minute in the absence of blood flow (Lust *et al.* 1985). Thus there is a delicate balance

between a continual supply of nutrients from the blood and energy demands from the brain.

1.2.3.2 Cerebral blood flow thresholds

Specific CBF levels exist below which particular brain functions deteriorate or certain processes start (Hossmann, 1994) (Figure 1.2). In rat and gerbils, protein synthesis starts to decline at CBF values approximately 55 ml/100g/min and is completely suppressed below 35 ml/100g/min (Mies *et al.* 1991). Glucose utilisation transiently increases at CBF values of about 35 ml/100g/min before it sharply declines below 25 ml/100g/min (Paschen *et al.* 1992). Lactate accumulation and tissue acidosis as well as excitatory amino acids also begin to develop at these lower CBF values (Obrenovitch *et al.* 1988). When CBF has dropped below 25 ml/100g/min to 20 ml/100g/min in gerbils, the concentration of high energy phosphates, phosphocreatine and ATP decline (Allen *et al.* 1993). Finally a loss of ion homeostasis (Harris and Symon, 1984) and abolished electrical activity (suppressed EEG activity) (Astrup *et al.* 1981) and disappearance of evoked potentials appear beneath 20-15 ml/100g/min (Astrup *et al.* 1977). It is important to note that most of these threshold values differ between species and may increase with time of ischaemia. In conclusion, the exact pattern, rate and potential reversibility of the pathogenic cascade in cerebral ischaemia, will depend on both the degree and duration of the CBF reduction.

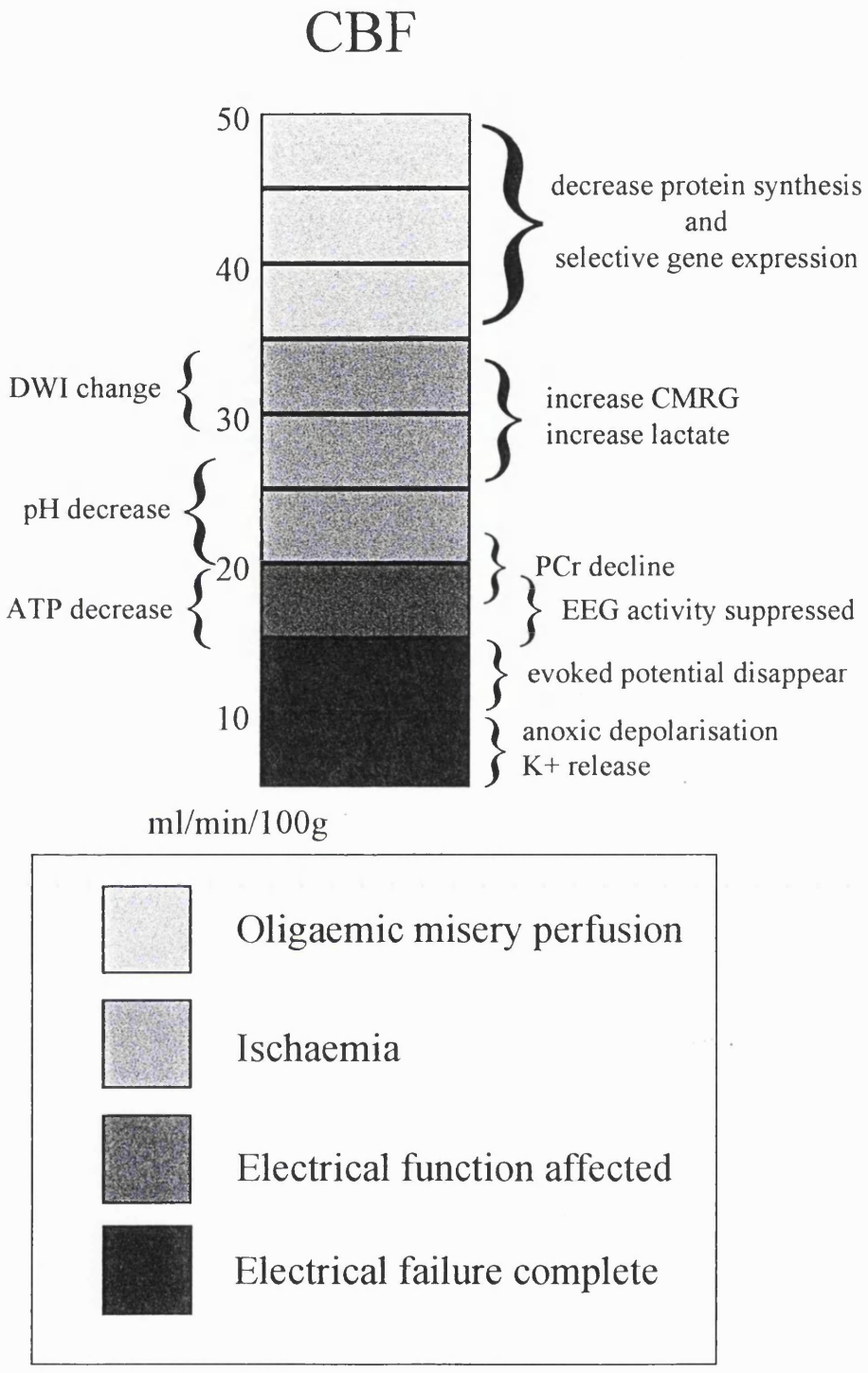

Figure 1.2 *Cerebral blood flows thresholds for metabolic and functional disturbances, and diffusion-weighted imaging (DWI) changes. These CBF thresholds are dependent upon both animal species and technique used to induce ischaemia.*

1.2.4 Energy failure and cytotoxic oedema

1.2.4.1 Energy failure

Energy is produced in the brain almost entirely from the oxidative metabolism of glucose, which is oxidised to CO_2 and water. Cell energy production relies on the manufacture of adenosine triphosphate (ATP) from adenosine diphosphate (ADP). A constant supply of ATP is required to maintain ionic homeostasis through the Na^+/K^+-ATPase system. During ischaemia, with an absent or extremely reduced oxygen supply available to produce ATP, there is a rapid depletion of available energy reserves in the brain. As phosphocreatine (PCr) and ATP decline, anaerobic glycolysis is stimulated, leading to an increase in the concentration of anaerobic glycolytic products. During aerobic metabolism oxidative phosphorylation produces 38 mol of ATP per glucose molecule. In an aim to maintain ATP during ischaemia, glucose may be converted to lactate and ATP, although only 2 mol of ATP per glucose molecule is synthesized in the absence of oxygen. In the event of limited oxygen supply lactic acid will accumulate leading to acidosis. Despite ATP production from anaerobic glycolysis, PCr and ATP are rapidly consumed under severely ischaemic conditions and are depleted within 1 to 2 minutes after complete ischaemia, leading to a rapid failure of the energy requiring process (Siesjo, 1992b).

1.2.4.2 Cytotoxic oedema

Usually ion concentration gradients across cell membranes are maintained by the energy dependant pump mechanisms. ATP provides energy to pump Na^+ out and K^+ into the cell to maintain ionic homeostasis. Approximate intracellular-to-extracellular ratios of ion concentration in mmol/l are: K^+,100/3; Na^+,30/150; Cl^-,5/130; Ca^{2+},0.0001/1.3; Mg^{2+},0.8/1; HCO_3^-,12/24; pH;7.0/7.3 (Hanson, 1985). Normally, the glucose and

oxygen supplied in the blood flow to the brain can provide this energy; however if the flow is severely reduced below the critical level, electrical activity abruptly ceases, followed at further reduction in flow by failure of the Na^+/K^+ pump and an accumulation of intracellular Na^+. Loss of control of Na^+ and K^+ levels is associated with an influx of Ca^{2+}, Cl^- and osmotically obliged water, which leads to cell swelling or *cytotoxic oedema* (Hanson, 1985).

1.2.4.3 Excitotoxic hypothesis and Ca^{2+} homeostasis

During ischaemia there is a large flux of calcium into the intracellular space. This influx is largely due to the so-called glutamate cascade, which begins after terminals of ischaemic neurons release excessive amounts of excitatory neurotransmitter glutamate into the extracellular space. The cells are prompted to release glutamate due to the failure of the ATP-driven ionic membrane pumps, causing depolarisation of the outer membrane. Glutamate activates membrane bound receptors which are linked to ion channels (i.e. ionotropic receptors) or activate secondary messenger systems (i.e. metabotropic receptors). Following depolarisation, the glutamate binds to N-methyl-D-aspartate (NMDA) receptors on neighbouring neurons inducing an influx of Ca^{2+} into the cell directly via NMDA receptors or indirectly through voltage-gate Ca^{2+} channels. Finally, activation of metabotropic receptors results in a rise of intracellular Ca^{2+} from either intracellular stores or from Ca^{2+} binding proteins (Siesjo, 1992b).

The non-physiological rise in Ca^{2+} induces over activation of lipases and proteases and possibly also endonucleases. These processes directly affect cell integrity via degeneration of cytoskeletal proteins, degradation of membranes, deoxyribonucleic acid destruction, and free radical production. Phospholipid hydrolysis leads to accumulation of free fatty acids, including arachidonic acid, a substrate for free radicals. Further

more, increased intracellular Ca^{2+} indirectly causes cell damage by alterations of protein phosphorylation, which secondarily affects protein synthesis and gene expression (Siesjo, 1992a).

1.3 MECHANISMS OF TISSUE DAMAGE

1.3.1 Penumbra

Penumbra means 'almost shadow', and the word is used in astronomy to indicate a zone between total darkness and full light, as occurs in a solar eclipse. In physiology, the term was introduced by Symon and his co-workers to designate a zone of brain tissue with moderate ischaemia paralysing neuronal function, the paralysis being fully reversed upon reperfusion (Astrup *et al.* 1977; Symon, 1980; Astrup *et al.* 1981) (Figure 1.3). The concept is based on a report that massive K^+ efflux into the extracellular space occurs at blood flow thresholds that are significantly lower than those required to abolish the cortical evoked responses and close to the levels that subsequently produce infarction (Astrup *et al.* 1977). Currently the term is used to describe a region of ischaemic tissue peripheral to the core where viable neurons may be found, and thus potentially salvageable with suitable intervention (Kinouchi *et al.* 1993; Hossmann, 1994). Thus, the penumbra is an important target for acute stroke therapy. Since the penumbra can be considered as a temporary phase of potential viability through which ischaemic tissue progresses into infarction, the therapeutic time-window is limited, possibly to a few hours (Hossmann, 1994; Obrenovitch, 1995).

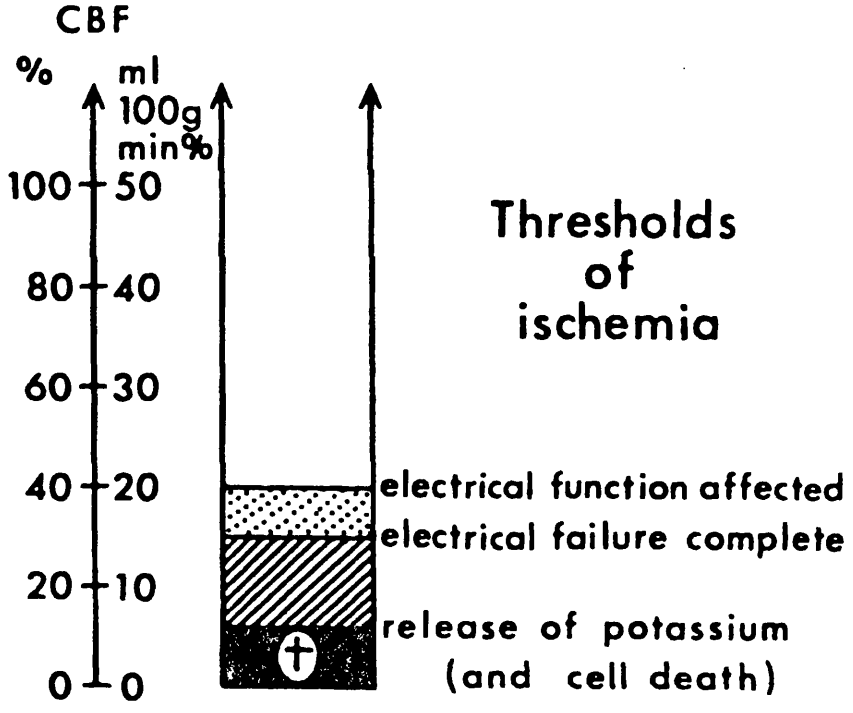

Figure 1.3 *Early definition of the penumbra based on ischaemic thresholds for electrical failure and for release of cellular potassium ion (K^+). Adapted from Astrup and Symon et al. 1977.*

1.3.1.1 Imaging methods to define the penumbra

Penumbral zones can be delineated using several different imaging modalities, all of which have definitions that rely on the underlying mechanisms of that technique. Thus, the penumbra has been described by the uncoupling between regional cerebral blood flow (rCBF) and the cerebral metabolic rate of oxygen ($CMRO_2$) in humans using positron emission tomography (PET) (Marchal *et al.* 1996). Autoradiographic and bioluminescence studies in the rat middle cerebral artery occlusion (MCAO) model, demonstrated a penumbra via uncoupling between rCBF and cerebral glucose utilisation (Back *et al.* 1995) and via differences in the lesion areas delineated using regions of ATP depletion and pH change (Hossmann, 1994). A suggested non-invasive MRI approach to define the penumbra is diffusion-weighted imaging (DWI). During ischaemia, the region of signal intensity change in DWI corresponds closely to the region of periinfarct acidosis, but also encompasses the area of ATP depletion (infarct core). Therefore it was postulated that the outer margin of the DWI visible lesion corresponds with that of the penumbra (Kohno *et al.* 1995b). To identify both inner and outer margins of the penumbra, quantitative measures of the diffusion of water, known as the apparent diffusion coefficient of water (ADC), have been combined with a MRI measure of CBF in a multispectral analysis in an attempt to extract both inner and outer limits for the penumbra in a rat model; although this technique has not predicted the recoverable tissue with complete certainty (Carano *et al.* 1998).

1.3.1.2 Spreading depression and the penumbra

The occurrence of transient waves of membrane depolarisation known as *spreading depression* (SD), emanating from an infarct core have been suggested as one mechanism for the expansion of tissue injury into the penumbral zone (Nedergaard and

Astrup, 1986). In a normal rat, SD can be induced via the application of KCl to the cerebral cortex, subsequently a wave of cell depolarisation progresses at a rate of 3 mm/s across the cortex with a concomitant blood flow and cell volume change. During SD, the metabolic rate of the tissue increases in response to the greatly enhanced energy demands of the activated ion exchange pumps (Kocher, 1990). In the penumbra flows are suppressed, and as a result, the increased metabolic demand is not compensated by an increase in oxygen and glucose (Back *et al.* 1994). Eventually ATP stores will be depleted, followed by the cascade of pathophysiological events leading to tissue infarction. Using diffusion-weighted imaging (DWI) and ADC maps to monitor cell volume change, (Latour *et al.* 1994) and gradient-echo imaging to following apparent changes in blood flow, both of these consequences can be imaged (Gardner Medwin *et al.* 1994). The first observation during focal ischaemia of transient abnormalities on DWI, coincident with transient depolarisations, was described by Gyngell et al. (Gyngell *et al.* 1994). The change in ADC associated with SD has been used to study the pathological basis by which SD leads to infarct growth and the mechanism whereby neuroprotective drugs have their therapeutic effect (Hasegawa *et al.* 1995; Rother *et al.* 1996; Takano *et al.* 1996).

1.3.2 Reperfusion injury

Following reperfusion to a previously ischaemic region, restoration of oxygen and glucose supply reinstates the oxidative phosphorylation process that helps to normalise energy demand. However, a parallel cascade of deleterious biochemical processes can be triggered that may paradoxically antagonise the beneficial effect of reperfusion. This phenomenon has been demonstrated in various tissue and is termed *reperfusion injury* (Aronowski *et al.* 1997). The understanding and treatment of reperfusion injury is an

important objective especially in the era of reperfusion therapy for stroke. In 1994, Yang and Betz demonstrated that 3 hours of focal ischaemia followed by 3 hours of reperfusion in the rat produced more damage than 6 hours of continuous ischaemia without reperfusion (Yang and Betz, 1994). The causes of early reperfusion injury may be multifactorial and include:

- secondary wave of excitatory amino acid release
- Ca^{2+} influx producing further elevation of cytosolic Ca^{2+} concentration
- free radical formation
- disaggregation of polyribosomes and depression of protein synthesis
- blood brain barrier injury
- elevation of leukotrienes and prostoglandins
- expression of endothelial adhesion molecules

These mechanism have been discussed in the previous section or will be covered in the following paragraphs.

1.3.3 Selective vulnerability and delayed tissue damage

1.3.3.1 Selective vulnerability

Some cell types in the brain are more vulnerable to ischaemia than others. Neurons are the most sensitive cells in the brain, followed in order by oligodendroglia, astroglia and finally endothelia cells (Pulsinelli, 1985). Further, certain regions of the brain have been shown to be more susceptible to ischaemia than others. This *selective vulnerability* leading to *selective neuronal death* has predominately been described in an experimental model of transient global ischaemia. Following 30 minutes of ischaemia and reperfusion, the CA1 neurons of the hippocampus and the Purkinje cells appear to be the most vulnerable neurons, followed in order by medium sized striatal

neurons and then neocortical neurons in layers 3, 5, and 6 (Pulsinelli *et al.* 1982). Vascular architecture is one of the factors which influence the distribution of neuronal necrosis that develops after transient periods of ischaemia. Boundary or watershed lesions are examples of brain injury caused by vascular anatomy. In such lesions, ischaemic necrosis occurs in the watershed zones between major arterial territories and is exemplified by infarction of the boundary zone between the anterior and middle cerebral arteries (Pulsinelli, 1985). Micro-watershed lesions were reported in immature rats subject to unilateral common carotid artery ligation and simultaneous hypoxia. The pathogenesis of these lesions was thought to reflect the boundary zone between the arteries and veins which penetrate the neocortex (Rice *et al.* 1981).

1.3.3.2 Delayed neuronal death

If the ischaemia is transient or brief in duration, typically global or forebrain ischaemia, the appearance of damaged tissue can be postponed by hours or even days. In 1982, Kirino (Kirino, 1982) and Pulsinelli et al. (Pulsinelli *et al.* 1982), using different animal models, described the process of *delayed neuronal necrosis,* in which CA1 neurons did not show light or electron microscopic evidence of damage until 24 hours after the initial insult. In these animal models of global ischaemia, an occlusion period of 5 minutes is long enough to induce delayed neuronal death (Kirino, 1982). More recently, both selective neuronal necrosis and delayed neuronal death have been observed in a reversible MCAO rat model (Garcia *et al.* 1995). In this study, Garcia et al. made the clear distinction between infarction or pannecrosis, which appears in prolonged arterial occlusion, and selective necrosis characteristic of incomplete infarctions due to transient (<25 minutes) occlusion. Although the exact mechanism for the *delayed damage* is still unknown, several mechanisms have been proposed.

- Post-ischaemic hypoperfusion, which can last for several hours after reperfusion, in combination with high metabolic activity, could lead to a mismatch between energy demand and supply (Hossmann, 1985), and as a consequence energy failure.
- A gradual rise in intracellular calcium may lead to a slow triggering of destructive events (White *et al.* 1993).
- The depression of protein synthesis, which can persist over a long period during post-ischaemic reperfusion (Thilmann *et al.* 1986).
- Ischaemic-induced DNA damage in apoptosis-like cell death may produce a late manifestation of cell injury (Nitatori *et al.* 1995; Du *et al.* 1996).
- An increase of intracellular calcium concentration damages so-called motor proteins, such as cytoplasmic dynein and kinesin, which convert the energy from ATP hydrolysis into mechanical work and move mitochondria along tubules. Dysfunction of this mitochondrial shuttle system may cause progressive failure of energy production that eventually result in cell death (Abe *et al.* 1995).

1.3.3.3 Reperfusion following ischaemia: No-reflow and hypoperfusion

Following a period of ischaemia two types of recirculation disturbances can be distinguished: the no-reflow phenomenon or post-ischaemic hypoperfusion. In 1968, Ames et al. observed that in rabbits periods of cerebral ischaemia of more than five minutes were followed by multifocal deficits in brain reperfusion, which was described as the *no-reflow phenomenon* (Ames *et al.* 1968). The cause of this probably involves the combination of increased blood viscosity, microcirculatory compression by swollen perivascular glia cells, formation of endothelial microvilli, increased intracrainal pressure, post ischaemic hypotension and disseminated intravascular coagulopathy (Hossmann, 1985). The extent of the no-reflow depends on the type and duration of the

ischaemia. It increases with time (Kagstrom *et al.* 1983), and seems to be most pronounced when the vessels are filled with blood, i.e. after incomplete ischaemia or when the outflow is obstructed. This is the reason that after only 15 minutes of tourniquet ischaemia, reperfusion may fail in up to 95% of brain tissue (Ames *et al.* 1968). However, even without venous obstruction, small areas of no-reflow are a consistent finding when global ischaemia is longer than 10 minutes (Kagstrom *et al.* 1983). Despite this potentially serious complication of ischaemia, it is noted that prevention of the no-reflow promotes tissue recovery only in the resistant but not selectively vulnerable areas of the brain (Levy *et al.* 1975). Further, with correct management of the arterial blood pressure during reperfusion the areas of no-reflow may be eliminated (Ito *et al.* 1980).

The *post-ischaemia hypoperfusion* syndrome is a usual complication of reperfusion even under those conditions when the regions of no-reflow are absent, and commonly develops after a period of reactive hyperaemia (Figure 1.4). It has been suggested that, paradoxically, shorter periods of ischaemia result in a more pronounced degree of post-ischaemic hypoperfusion (Hossmann, 1985). For example, 1 hour of forebrain ischaemia in the gerbil resulted in a delayed drop in flow that represents approximately 50% of the control level (Levy *et al.* 1979), while 4 or 5 minutes of ischaemia in a similar gerbil model, the CBF fell to a value of approximately 15% of the pre-occlusion flow (Tomida *et al.* 1987b; Pell *et al.* 1999b) (Figure 1.4). Hypoperfusion has also been reported to occur after only 2 minutes of forebrain ischaemia in the gerbil, and became most pronounced at 1 hour and returned to normal after 4 hours (Kato *et al.* 1990). It is well documented that five minutes of ischaemia will damage only neurons in the hippocampus (Kirino, 1982), whereas 10-15 minutes of ischaemia causes

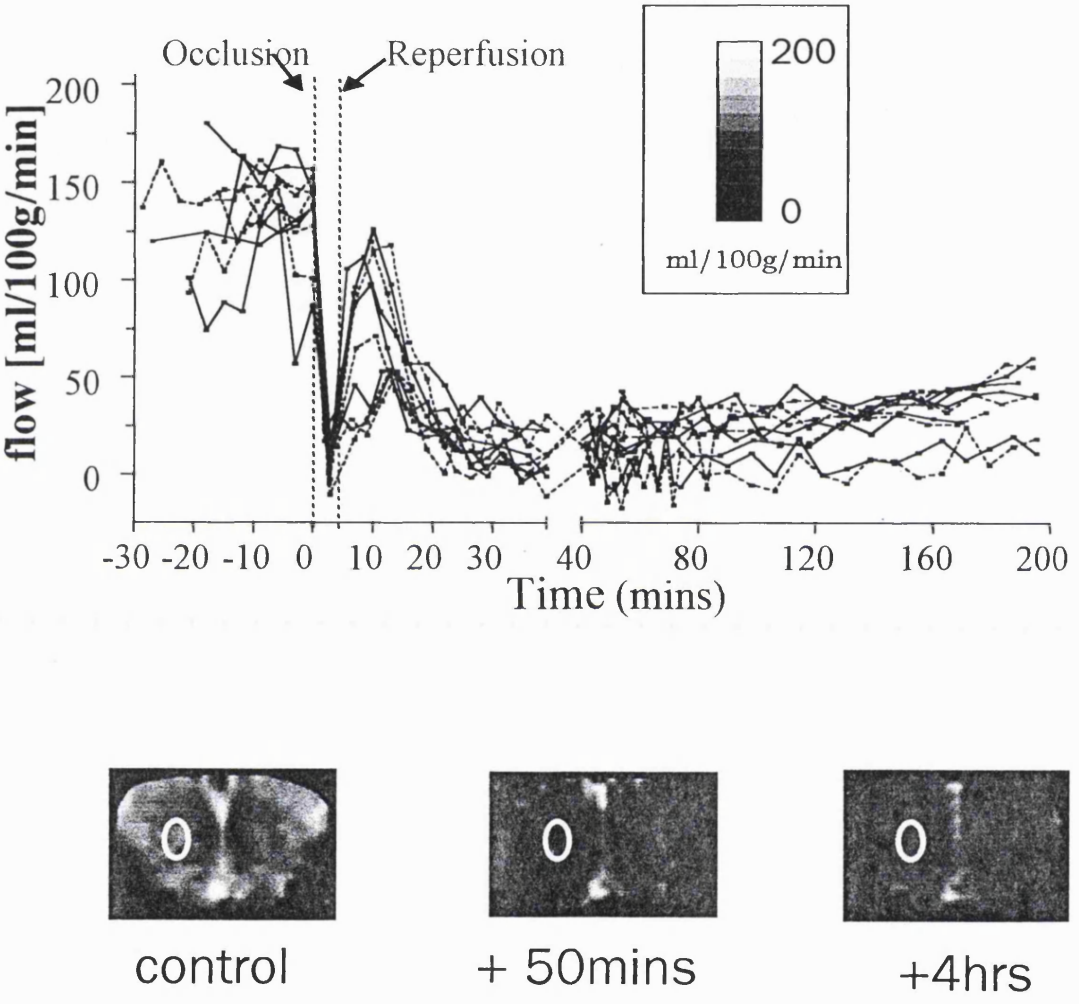

Figure 1.4 *Demonstration of the time-course of hypoperfusion following 4 minutes of forebrain ischaemia in a gerbil model. CBF measured using the FAIR pulsed arterial spin labelling technique. Images represent CBF at selected times points. (Pell et al. 1999a).*

extensive damage to other selectively vulnerable regions (Pulsinelli *et al.* 1982). Interestingly, even though hypoperfusion was present in the former study using 2 minutes of ischaemia (Kato *et al.* 1990), there was no evidence of morphological tissue damage. Therefore hypoperfusion per se, may not be directly associated with selective neuronal necrosis (Kato *et al.* 1990). On the other hand, 2 minutes of ischaemia in gerbils decreases cerebral metabolism and cerebral protein synthesis for several hours after reperfusion (Araki *et al.* 1990).

A hypoperfusion region may be characterised by a dissociation between suppressed CO_2 reactivity and maintained autoregulation (Hossmann, 1985), or by uncoupling of blood flow from metabolic activity (Hossmann *et al.* 1976; Suzuki *et al.* 1983). The uncoupling of CBF from metabolism results in increased levels of brain glucose uptake combined with low oxygen availability, which in turn can lead to anaerobic glycolysis with tissue acidosis and subsequent metabolic disturbances (Hossmann *et al.* 1976; Hossmann, 1979). An example of this is observed in borderzone infarcts, in which oxygen delivery is limited during hypoperfusion, and results in depletion of ATP and cell damage. These observations would suggest that if the hypoperfusion period could be avoided by reducing the extent or period of time, then tissue damage may be limited. The effect of reducing the hypoperfusion is demonstrated in an elegant study in which gerbils subjected to locomotion activity, which increases the quality of post-ischaemic blood flow, showed improved metabolic normalisation when compared to gerbils without pre-ischaemic activity (Stummer *et al.* 1995). However, other studies have shown evidence that calcium antagonists, which inhibit post-ischaemic brain hypoperfusion, had little or no effect on neurological outcome; questioning the significance of the hypoperfusion phase (White *et al.* 1993).

Although it is suggested that post-ischaemic hypoperfusion limits the progression of global recovery after ischaemia, it is less clear whether it is also of importance for the maturation of lesions in selectively vulnerable areas. Further, the reasons for delayed hypoperfusion are still unclear and may involve:

- local tissue alkalosis producing vasoconstriction and decreased blood flow (Levy *et al.* 1979)
- increased blood viscosity (Stummer *et al.* 1995)
- reduction of vascular lumen by endothelial and perivascular swelling (Ames *et al.* 1968)
- endothelial blebs protruding into the capillary lumen (Stummer *et al.* 1995)
- platelet aggregation / thrombotic phenomenon (Tomida *et al.* 1987)
- vessel obstruction by leukocyte attachment to endothelial surface (Stummer *et al.* 1995)
- compression of the microvascular bed by cerebral oedema (Tomida *et al.* 1987)

Finally, hypoperfusion appears to be a phenomenon that is reliably produced following global ischaemia and reperfusion. However, in focal rat models of ischaemia and reperfusion the pattern is predominated by hyperperfusion in the core, with hypoperfused areas in the penumbra (Tsuchidate *et al.* 1997). This pattern was seen after 2 hours of occlusion and is yet to be confirmed at other periods of ischaemia.

1.3.3.4 Effects of repeated ischaemic episodes

Five minutes of ischaemia damages only neurons in the hippocampus, whereas 10-15 minutes of ischaemia causes extensive neuronal damage to selectively vulnerable regions. Intestingly, Tomida et al. found that damage following three 5-minute

ischaemia insults at 1 hour intervals, was greater than that following a single 15-minute insult and concluded that post-ischaemic hypoperfusion plays an important role (Tomida *et al.* 1987). Further, Kato et al. demonstrated that a single 2-minute ischaemic insult caused no morphological neuronal damage. However a moderate number of neurons of the hippocampus were destroyed after two 2-minute ischaemic insults with 1 hour intervals, and almost all CA1 neurons were destroyed following 3 or 5 insults at 1 hour intervals (Kato and Kogure, 1990). Hossmann has noted that repetitive ischaemic insults in the cat caused accumulation of electrophysiological dysfunction (Hossmann *et al.* 1990). The duration of the post-ischaemic EEG suppression distinctly lengthened when the ischaemic episodes were repeated, which suggest that the brain tries to compensate for the increased metabolic stress by shutting down its electrical activity. Finally, Hossmann et al. reported that following repeated occlusions in a cat model, accumulation of oedema did not correlate with post-ischaemic hypoperfusion, as oedema developed in both cortex and caudate nucleus, although only the latter exhibited hypoperfusion (Hossmann *et al.* 1990).

The possible mechanisms that may explain the cumulative effect of neuronal damage produced by repeated ischaemic insults are as follows:

- Tomida et al. reported that damage was most prominent when repeated insults were at one hour, at which time hypoperfusion was at the lowest value, possibly indicating a microcirculatory rationale.
- In 1990 it was suggested that 'no evidence exists that this hypoperfusion impedes microcirculation to such an extent that secondary energy failure occurs' (Kato and Kogure, 1990). This is now questioned and secondary effects are observed in MRI diffusion-weighted images changes during hypoperfusion (Pell *et al.* 1999a), and

may point to the accumulation of products from anaerobic metabolism and formation of cytotoxic oedema.

- Post-ischaemic metabolic disturbances may contribute to this cumulative effect. Protein synthesis is depressed and amino acid incorporation into proteins decreased (Araki *et al.* 1990).
- Excitatory neurotransmitter release (section 1.2.4.3)

1.3.4 Blood brain barrier and vasogenic oedema

The blood brain barrier is of key importance in regulating the internal environment of the brain. In 1885 it was first demonstrated that intravascular dyes injected into animals affected all organs except the brain (Ehrlich, 1885). The actual concept of a barrier to the passage of substances from the blood to the brain originated in 1913, when it was demonstrated that trypan blue injected into the cerebrospinal fluid coloured the brain a deep blue, whereas intravenously injected trypan blue did not affect the brain (Goldmann, 1913).

Brain endothelial cells are connected to each other via tight junctions that effectively prevent passive diffusion of most molecules across the capillary walls. This forms the blood brain barrier, which exerts an important control with respect to the exchange of compounds between blood and tissue in the brain. Ischaemia induces a variety of processes which can have an effect on the blood brain barrier integrity. Necrosis of the endothelial cells and separation of the tight junctions will result in a disruption of the microvascular endothelial organisation and a leaky blood brain barrier. As a consequence the blood brain barrier allows the extravasation of plasma proteins, which is followed by hydrostatically and osmotially obliged water and therefore leads to the

accumulation of fluid in the interstitial space. The unnatural accumulation of water in the extracellular space is called *vasogenic oedema* (Klatza, 1967). Vasogenic oedema may lead to a detrimental swelling of brain tissue and concomitant increased intracranial pressure.

1.4 ANIMAL MODELS OF CEREBRAL ISCHAEMIA

The investigation of the pathophysiology of cerebral ischaemia requires animal experimental models in which an ischaemic insult can be produced under controlled conditions. The animal model should be relevant to the clinical situation, highly reproducible, avoid extra cerebral complications and should be technically easy to perform. This goal is not easy to achieve in the view of the diversity of scientific issues related to brain ischaemia research. Due to such diversity, several species of animal and different methods for producing ischaemia have been employed. The most widely used animal for ischaemia studies is the rat. Rats are relatively inexpensive, reproduce fairly easily, require minimal husbandry and their cerebral organisation is sufficiently homologous to humans. The experimental models of ischaemia may be classified into four groups: global, focal, permanent and transient.

In this section I will provide a brief overview of the fours categories of experimental models which are applicable to both large and small animals. Following this, there is an account of the methods for producing ischaemia in small animals, which is more pertinent to the MRI studies described in this thesis.

1.4.1 Overview of animal models

Global ischaemia of the brain is the reduction or cessation of the total cerebral blood flow. One of the clinical interests of global ischaemia is the study of the vulnerability of the brain to cardiac failure and the reperfusion of the central nervous system following such an incident. There are several animal models which involve cardiac arrest, such as: intravenous administration of potassium chloride, ventricular fibrillation, exsanguination, or drowning (Hossmann, 1991). However, cardiac failure affects not only the brain, but all organs of the body which, in turn, may interfere with the metabolic recovery of the brain. For this reason a number of models have been developed which induce a reduction or cessation of CBF with little interference of peripheral organs. Examples of complete cerebral global ischaemia are the compression of blood vessels in the neck by strangulation or inflation of a pneumatic cuff (Nemoto *et al.* 1977); the intrathoracic occlusion of the brachiocephalic and left subclavian and common carotid arteries which results in interruption of blood supply to both carotid and vertebral arteries (Hossmann and Zimmermann, 1974); or the increase of intracranial pressure above blood pressure by infusing fluids into the cisterna magna (Marshall *et al.* 1975). For certain purposes, isolated head or brain preparations are used for the production of complete ischaemia (Kriegelstein *et al.* 1972).

Incomplete global ischaemia (oligaemia) is produced by reducing cerebral perfusion pressure, i.e. by lowering arterial blood pressure, using extracranial ligation of the carotid and vertebral arteries or by increasing intracranial pressure slightly below blood pressure (Marshall *et al.* 1975). Various degrees of global hypoperfusion may be introduced using a combination of vascular occlusion and ganglionic blocking agents or postural hypotension (Hekmatpanah, 1970). The main pathophysiological peculiarity of

incomplete global ischaemia is the fact that the critical perfusion pressure necessary for the maintenance of CBF in the brain is compromised at first in peripheral regions of the supplying territories of the cerebral arteries. Since these regions are located in the border zones between these territories, the resulting decrease in blood flow is referred as border zone ischaemia (Brierley *et al.* 1969).

Focal ischaemia cannot be induced via *extracranial* occlusion of a carotid or vertebral artery without further surgical intervention because the circle of Willis provides sufficient collateral blood supply via the non-affected vessels. The only exceptions to this are the Mongolian gerbil in which the circle of Wills is incomplete, the sheep in which the vertebral arteries do not unite to form a basilar artery, and the stroke-prone spontaneously hypertensive rat in which the collateral system is compromised. However, even in these species, infarcts do not develop in all animals. Extracranial occlusion will develop a focal lesion when combined with other interventions such as: intracranial hypertension, or anastomosing the contralateral carotid artery with the jugular vein (Busto and Ginsberg, 1985).

Focal ischaemia may be induced using *intracranial* occlusion of a major cerebral artery, most commonly the middle cerebral artery (MCA). This vessel can be exposed by a retroorbital, postorbital or transorbital approach, and can be clipped or ligated. The transorbital approach requires removal of the eyeball, but is otherwise considered to be atraumatic because it is not necessary to retract the brain for exposure of the vessel (O'Brien and Waltz, 1973). Intracranial vessels have been occluded by injecting *macroemboli*, such as: aged blood clots, silicon rubber, or metal balls (Turner, 1975). The advantage of this method is that craniotomy is not required for the exposure of the

intracerebral arteries. Recently, retractable emboli have been developed which can be removed by the use of a fine thread attached to an embolus. Under favourable conditions, ischaemia may develop in the total distribution of the occluded vessel (maximal area of infarction), but the ischaemic region may also be very small when collateral supply is optimal (minimal infarct). For this reason, a great variety of modifications for MCA occlusion have been described to improve reproducibility of the final lesion size. This type of model will be discussed in the next section in greater detail, as it is similar to the type used in this thesis.

Another particular type of focal ischaemia is that produced by *microembolism,* for example, fat emboli, platelet aggregates or air embolism, by means of which arterioles or capillaries are reversibly or irreversibly occluded (Vise *et al.* 1977). Other experimental models are the intracarotid infusion of adenosine diphosphate or arachidonic acid in order to induce platelet aggregation (Fieschi *et al.* 1975). An important physiological difference between microembolism and other forms of ischaemia is the fact that following microembolism, the blood brain barrier instantaneously breaks down (Vise *et al.* 1977). Barrier damage presumably is the consequence of an 'irritation' of the vascular wall and not of the ischaemic event itself, because, under pure ischaemic conditions, the blood brain barrier breaks down only after several hours.

1.4.2 Focal Ischaemia

1.4.2.1 Permanent occlusion

Rats with *permanent* occlusion of the MCA are frequently used for exploring the pathogenesis of infarction and for the evaluation of new therapeutic agents. In 1975,

Robinson et al. developed a model of MCA occlusion in the rat, in which the MCA was coagulated distal to the rhinal fissure performed through a craniotomy (Robinson *et al.* 1975). To improve the reproducibly of this model, a subtemporal approach was introduced by Tamura et al. (Tamura *et al.* 1981). This method resulted in a reproducible ischaemic model following occlusion of the proximal MCA between the rhinal branch and the lateral striate arteries in Sprague-Dawley rats. Several modifications of the above model have been described in conjunction with occlusion of the MCA to increase reproducibility, such as MCAO following a brief period of hypotension or permanent occlusion of the ipsilateral CCA (Brint *et al.* 1988). Other methods of inducing focal ischaemia have included injection of homologous blood clot fragments or microspheres (Takaizawa and Hakim, 1991). These methods avoid a craniotomy but the location of infarcts is not predictable a priori. Further methods for producing focal infarction include injection of rose bengal dye, which is followed by photochemical activation to induce focal thrombosis and cerebral ischaemia (Van Bruggen *et al.* 1992). This model has the advantage of being relatively non-invasive, as well as providing several cerebral locations for the placement of the lesion, although it does result in microvascular injury.

1.4.2.2 Reversible occlusion

In 1985, Shigeno et al. placed a snare ligature around the stem of the MCA just distal to the lenticulostriate branches, and by pulling and releasing the thread, occluded then reperfused the MCA (Shigeno *et al.* 1985). Many of the above techniques, including the latter, are complex and invasive, requiring craniotomy, durotomy, and archnoid incision, with an associated cerebrospinal fluid drainage, air influx, local temperature change and altered intracranial pressure. Although some of these techniques allow

reperfusion, most do not. The next section describes a rat model of *reversible* MCA occlusion which avoids many of the above disadvantages.

In 1986, Koizumi et al. developed a unique reversible focal ischaemic model (Koizumi *et al.* 1986). The MCA was occluded by a silicone rubber cylinder attached to a thread inserted through the internal carotid artery in Wistar rats. Recirculation was accomplished by pulling the thread out of the artery. This model has the advantage of avoiding craniotomy and has an important use in MRI investigation of ischaemia. The intraluminal thread method of occlusion was later modified by Zea Longa et al. (Zea Longa *et al.* 1989) using a blunted nylon monofilament in an aim to increase reproducibility (Figure 1.5). One study has compared these two techniques, suggesting that there were differences in the levels of reduced CBF on occlusion, and that the Koizumi method was more reliable than that of Zea Longa et al. (Laing *et al.* 1993). However, other investigators have not supported these conclusions and the discussions for these variations were focused on degree of silicone coating of the thread, 3-0 or 4-0 filament size, length of the filament, and body weight of animals (Garcia, 1993; Holland *et al.* 1993). It is interesting to note that when comparing two uncoated 4-0 nylon monofilaments from different manufacturers, that subtle differences in material and diameter resulted in variations in the final infarct size following MCAO (Kuge *et al.* 1995). Two recent studies have investigated, at some length, the intraluminal suture model. Li at al. using a silicone coated 4-0 nylon occluder adapted for remote

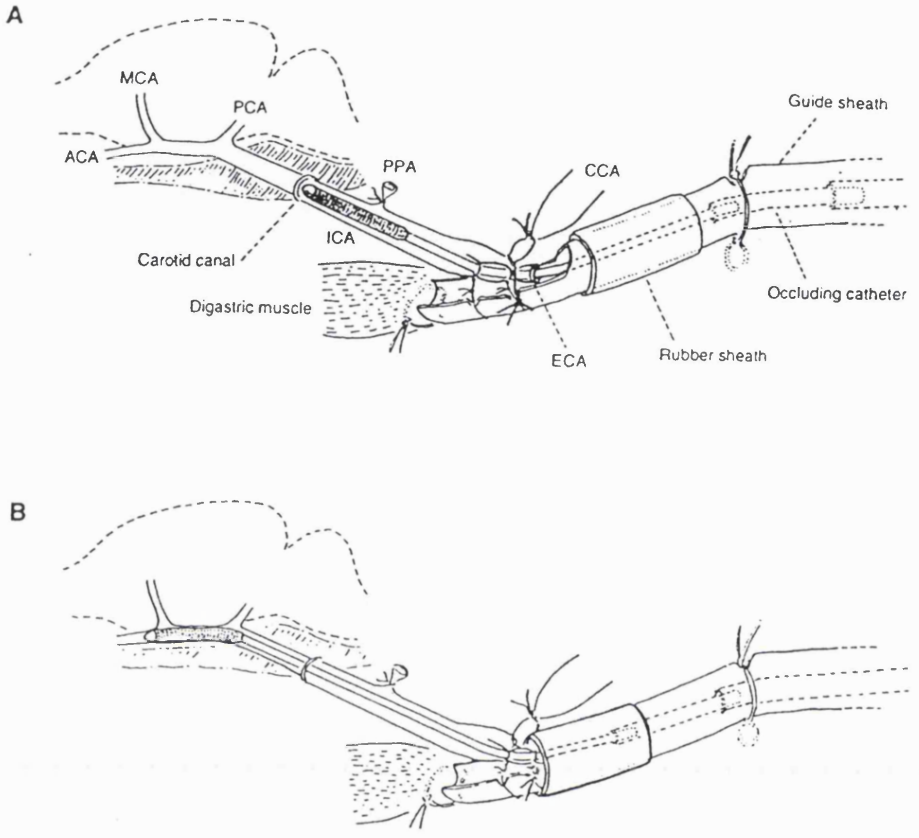

Figure 1.5 *Schematic drawing of the modified MCA thread occlusion used in both conventional and partial occlusion models. (A) Pre-occlusion. The tip of the occluding suture is placed under microscopic control at the carotid canal of the skull base. (B) Post-occlusion. The occluder is advanced by 8 - 11mm; this corresponds to the position of the tip at the origin of the anterior cerebral artery.*

ACA, anterior cerebral artery; MCA, middle cerebral artery; PCA, posterior cerebral artery; PPA, pterygopalatine artery; ICA, internal carotid artery; CCA, common carotid artery; ECA, external carotid artery.
(Adapted from Kohno et al., 1995)

occlusion during MRI (see section 1.3.4), achieved successful occlusions in 88% of animals without subarachnoid haemorrhage (Li *et al.* 1998). The failures include pre-occlusion damage (1/67), occluding device sliding out of the outer holding catheter (1/67), no occlusion (2/67), and arterial perforation (4/67). The other critical evaluation of the suture method by Schmid-Elsaesser et al., indicated that a 4-0 silicone coated suture, when compared with a 3-0 uncoated suture, produced less subarachnoid haemorrhage, 8% as opposed to 30% (Schmid-Elsaesser *et al.* 1989). However in both these types of sutures, there was premature reperfusion occurring in the first minutes of MCAO in approximately 25% of studies, which contributes to variability in the lesion size. Therefore as we have seen, institutions using equivalent methods observe different lesion variability, which indicates the difficulty with these methods. Further, the lengths one must go to in order to standardise the intraluminal MCAO technique, cannot be over estimated.

1.4.2.3 Incomplete or partial occlusion

Models of *focal oligaemia* are not common, although they are finding increasing use in the investigation of the pathophysiology of penumbra, in which regions of oligaemic misery perfusion are present. The aim of these experimental models is to produce a large focal lesion, in which the CBF is moderately reduced throughout the MCA territory. The degree of reduction in CBF is dependant upon the method used and the degree of stenosis or partial occlusion. In 1994, Derugin et al. developed a reversible MCA stenosis in the cat (Derugin and Roberts, 1994). The right eye was enucleated, the MCA dissected and a suture looped around the vessel. A thicker suture was placed on the MCA and the looped suture tied. The thick suture was then removed, resulting in partial stenosis of the MCA. The knot was untied and the suture removed to restore blood flow. A hypoperfusion rat model was developed by Grohn et al., in 1998, in

which they used a combination of hypotension induced by placing the rat vertical and electrocoagulation of the distal MCA. Only one of these models allows reperfusion to take place and neither can be occluded from outside an MRI scanner to observe the hyper-acute phase following occlusion.

1.4.3 Global ischaemia

Decapitation is the simplest technique to produce global ischaemia without recirculation and has been employed for the study of biochemical mechanisms in global ischaemia, but does not lend itself to any modulations. Global ischaemia by a neck tourniquet has also been used in rats, but complicating factors such as venous congestion cause variable ischaemic outcomes (Seimkowicz and Hanson, 1978). Essentially there are three commonly used small animal models of global cerebral ischaemia, two in the rat and one in the gerbil. The four-vessel occlusion model in the rat produces a complete global ischaemia and the other two models induced a bilateral forebrain ischaemia.

1.4.3.1 Four-vessel occlusion model

In 1979, Pulsinelli and Brierley introduced the four-vessel occlusion model to provide reversible forebrain ischaemia in rats (Pulsinelli and Brierley, 1979). Modifications by their group allowed an increase in the percentage of successful studies (Mima, 1995). Briefly, on the day before the experiment, atraumatic clasps are placed loosely around both CCAs. A silk ligature is passed posteriorly around the cervical and vertebral muscles, which may be tightened in the event of collateral supply. The rat's head is tilted downwards and the vertebral arteries are electrocauterised thorough the foramen alar in the first cervical vertebra. Global ischaemia is induced by tightening the sutures around the CCAs. A period of between 10 and 30 minutes of ischaemia followed by

reperfusion, produces cell changes that are consistent with selective vulnerability and delayed neuronal damage (Pulsinelli *et al.* 1982).

1.4.3.2 Rat Two-vessel occlusion model

Bilateral occlusion of the CCAs combined with systemic hypotension produces reversible ischaemia (Takaizawa and Hakim, 1991). Arterial blood pressure is lowered to approximately 20 mmHg by bleeding (Eklof and Siesjo, 1972) or with the administration of trimethaphan or phentramine (Smith *et al.* 1985). This model is influenced by the need to maintain anaesthesia during the study and the alterations in systemic hypotension, and may result in post-ischaemic seizures.

1.4.3.3 Gerbil bilateral common carotid occlusion model

In most animals, as in man, occlusion of the common carotid arteries will not produce ischaemia. Since the gerbil has an absence of the posterior communicating arteries, which connect the anterior and posterior circulation to the brain, occlusion of the CCAs produces forebrain ischaemia. In 1966, Levin and Payen demonstrated that there was an anomaly in the Circle of Willis, such that unilateral occlusion of the CCAs resulted in ipsilateral forebrain ischaemia in 40% of gerbils (Levine and Payne, 1966). Subsequently, it was demonstrated that almost all gerbils exhibited neurological signs of ischaemia if both CCAs were ligated.

1.4.3.4 Graded global ischaemia

On occlusion, the degree of ischaemia is dependent on the vessel occluded and the collateral supply to that region. Most types of intervention give little or no control over the level of the induced ischaemia. Controllable graded ischaemia however, allows investigation of cerebral tissue at the desired level of CBF. Using a gerbil model, Allen et al. have placed adjustable snares around the CCAs which can be tightened to

decrease the internal diameter of the CCAs, thereby reducing the flow to the forebrain (Allen *et al.* 1993). Bilateral forebrain blood flows ranging from 80 to 8 ml/100g/min are attainable with this method.

1.4.4 Animal models and MRI

Animal models of stroke have been combined with MRI to investigate not only pathophysiology, but also stroke therapies and develop new diagnostic techniques (Van Bruggen *et al.* 1994; Hoehn-Berlage, 1995). There are two commonly used methods of production of ischaemia for NMR studies. One technique induces the ischaemia with the animal outside the magnet, which is sometimes known as 'on the bench' occlusion. The other is a remote occlusion of the vasculature from outside the magnet. Remote occlusion is essential to investigate the hyperacute MRI changes post-occlusion, and also to allow a direct comparison of pre- and post-occlusion image data (Roussel *et al.* 1994; Li *et al.* 1998). The NMR magnet, which has a limited internal bore diameter, invariably restricts the size of the animal used in NMR studies. Experimental studies of cerebral ischaemia use cats, rats, gerbils or mice and occasionally piglets or rabbits. The most commonly performed techniques are the intraluminal or permanent MCAO in the rat. The first remote occlusion of the MCA in a rat was performed by Roussel et al. (Roussel *et al.* 1994) using a 2×0.25 mm silicon embolus on a nylon thread and by Kohno et al., (Kohno *et al.* 1995a) using a 3-0 monofilament coated with glue, and more recently by Li et al. (Li *et al.* 1998) using a silicon coated 4-0 monofilament (Figure 1.5). In *Chapters 4 and 5*, MCA occlusion is performed using an 'on the bench' intraluminal suture approach. The animal model used in *Chapters 6 and 7*, was based on the earlier work of Roussel et al. (Roussel *et al.* 1994) and Kohno et al., (Kohno *et al.* 1995a) and was designed to facilitate remote controlled occlusion and

reperfusion of the MCA from outside the bore of a vertical imaging magnet. Thus providing the opportunity to document the early changes in the areas of ischaemia and oligaemic misery perfusion.

Chapter 2

2. Nuclear Magnetic Resonance and Autoradiography

2.1 BASIC PRINCIPLES OF MAGNETIC RESONANCE

Nuclear magnetic resonance (NMR) is now widely used as a non-invasive means of obtaining clinical images and of studying tissue metabolism in vivo. In 1944, the American physicist I.I. Rabi was awarded a Nobel prize for his method of measuring the nuclear magnetic moment. Independently, two scientists discovered the phenomenon of nuclear magnetic resonance in condensed matter, Edward Purcell at Harvard and Felix Bloch at Stanford. Both were awarded the Nobel Prize in 1952. The theory of chemical shift was described by Norman Ramsey in 1949, and experimental proof came in 1950, when W.C. Dickenson at MIT, and W.G. Procot and F.C. Yu at Stanford, described their observation of resonant-frequency shifts that occurred when identical nuclei occupied different chemical environments. In 1950, Erwin Hahn submitted a paper on the discovery of spin echoes, which became a fundamental tool both in NMR chemical analysis and NMR imaging (Hahn, 1950).

NMR imaging developments, based largely on the detection of ^{1}H signal of water, began in the 1970s. In 1972, Lauterbur demonstrated that by superimposing linear field gradients on the main field, projections of an object can be generated from which an image can be reconstructed. At about the same time, Mansfield and Granell were working on NMR diffraction studies in Nottingham University. Both had realised that, since the resonant frequency of a nuclear spin is proportional to the strength of the applied field gradient, a magnetic field gradient would give rise to a range of resonant frequencies which reflected the spatial distribution of the contributing spins.

In the following years many imaging techniques were proposed, but with the help of increasing power of computers, Fourier Transform techniques soon became the method of choice. The imaging techniques used at present are generally based on two types of sequence. Two Dimensional Fourier Transform (2DFT), or more accurately spin-warp imaging, developed by Edelstein from an initial demonstration by Ernst, is one of the most prevalent imaging sequences available on commercial scanners. Whilst producing images of extremely high quality, it requires long scanning times and subject motion can lead to degradation of the image. The second sequence, proposed in 1977 by Mansfield and called Echo Planar Imaging (EPI), has become increasingly popular over recent years because it offers the ability to acquire an image in as little as tens of milliseconds. This technique, however, requires specialised gradient hardware, which has limited its widespread availability. In general 2DFT methods are less prone to image artefacts and are capable of higher spatial resolution than EPI imaging. Presently, commercially available magnetic resonance imaging (MRI) scanners have progressed up to 5T in field strength and there is even a whole body system at 8T.

Initial use of imaging techniques revealed images of the nuclear spin density. Presently, images can be weighted according to the properties of the nuclei (e.g. T_1- and T_2 weighting), and also according to various physiological parameters. Diffusion-weighted images have been shown to highlight regions affected by an ischaemic event (Moseley *et al.* 1990) and methods are currently being developed to generate quantitative images of blood flow and perfusion. Another approach to image contrast uses the dependence of an NMR parameter (T_2*) on the state of blood oxygenation and is used to investigate functional activation in regions of the brain.

2.1.1 NMR Theory

NMR may be explained using either a quantum mechanical or classical approach. The quantum mechanical description employs the concept that individual atoms and molecules have discrete energy levels. The classical approach assumes a system which contains a very large number of nuclei and uses the concept of the bulk magnetisation vector. Certain aspects of NMR may only be described using the quantum approach. However, classical physics describes NMR theory surprisingly adequately and for this reason the classical approach will predominate in the next section.

2.1.1.1 Nuclear Spin and Angular Momentum - Quantum approach

In order to detect an atom via NMR, the atomic nuclei must posses the property known as spin. Atomic nuclei are characterised by discrete values determined by the quantum number *I*, known as the spin of the nucleus. The spin quantum number may only have integral or half integral values, for example:

1. Nuclei with an even mass number and an odd charge number have an integral value of I, e.g. deuterium-2, nitrogen-14
2. Nuclei with an even mass number and an even charge number have zero spin (e.g. carbon-12, oxygen-16) and therefore do not produce NMR signals.
3. Nuclei with an odd mass number have half integral spin, e.g. hydrogen-1, carbon-13, phosphorus-31

The nuclei with spin also posses angular momentum (p) which is related to the spin number by:

$$p = \hbar\sqrt{I(I+1)} \qquad (2.1)$$

Where $\hbar$ = h(plank's constant)/2π. Angular momentum is a vector and therefore requires specification of both its magnitude and its direction. Quantum theory demands that the directional component of angular momentum can only have discrete values with respect to any given direction, and these directions are defined by the introduction of another quantum number *m*. The component p_z of angular momentum along the (arbitrarily defined) z-direction is:

$$p_z = m\hbar \qquad (2.2)$$

where *m* may have any of the $2I + 1$ values $I, I - 1, ..., -I$. For a nucleus with spin ½ (such as hydrogen-1), *m* can be +½ or -½, and therefore $p_z = \pm ½ \hbar$.

The existence of such angular momentum, in combination with the internal charge distributions associated with the nucleons, leads to the generation of a magnetic moment, μ_z, where:

$$\mu_z = \gamma p_z = \gamma \hbar m \qquad (2.3)$$

γ is the gyromagnetic ratio, which depends on the exact structure of the nucleus and therefore varies for different nuclei. For the hydrogen-1 nucleus, it has a value of 2.675 $\times 10^8$ radians/second/Tesla.

2.1.1.2 The nucleus within a magnetic field

If a static magnetic field[1] B_0 is applied along the z-axis, a nucleus will acquire energy E as a result of the interaction between the field B_0 and the nuclear moment, given by:

$$E = -\mu_z B_0 \qquad (2.4)$$

or equivalently (from equation (2.3)):

$$E = -\gamma\hbar m B_0 \qquad (2.5)$$

Since m can have any of the values I, I - 1, ..., -I, the nuclear energy levels are split into $2I + 1$ states by the application of the magnetic field. For a nucleus of spin I = ½, there are two possible energy states, corresponding to m = +½ and m = -½ , and the difference between these two energy levels is (figure 2.1.1):

$$\Delta E = \gamma\hbar B_0 \qquad (2.6)$$

The lower energy nuclei have their magnetic moment pointing in the direction of the magnetic field and are said to be in the parallel state, whilst the remainder are said to be anti-parallel.

[1] A magnetic field can be described in terms of its flux density B_0 which determines the force exerted on other magnets. Henceforth, for simplicity, I will refer to B_0 as the magnetic field rather than the magnetic flux density. The unit of B_0 is the Tesla (T).

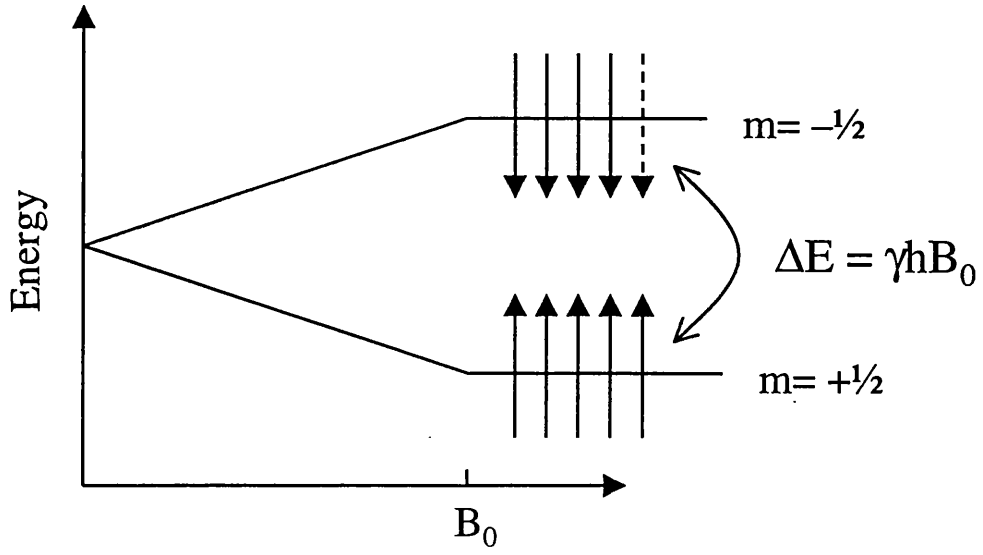

Figure 2.1.1 *Nuclear energy levels in a magnetic field B_0 for a spin ½ nucleus. Arrows represent nuclear spins at each energy level; transitions between energy levels are induced by supplying photons with an energy ΔE*

2.1.1.3 Transition of energy state

In order to obtain an NMR signal, it is necessary to induce transitions between the different energy states. A nucleus can transfer between energy levels when a quantum of energy exactly equal to the energy difference is supplied or removed from the system. This energy must be in the form of an oscillating magnetic field (termed B_1) in the *xy*-plane, and the field should oscillate with a frequency ν_0 that satisfies the fundamental relationship:

$$\Delta E = h\nu_0 \qquad (2.7)$$

Using equation (2.6), this means that

$$\nu_0 = \gamma B_0 / 2\pi \qquad (2.8)$$

or equivalently, since ω is equal to $2\pi\nu$,

$$\omega_0 = \gamma B_0 \qquad (2.9)$$

Equation (2.9) is the principle equation of nuclear magnetic resonance describing the resonance condition for magnetic nuclei, and the resonant frequency at which transitions occur is called the Larmor frequency. Since γ differs for each nuclear isotope, different nuclei resonate at widely different frequencies in a given field B_0. At conventional values of B_0 the frequencies occur in a convenient radio frequency band, and the oscillating field B_1 is commonly referred to as the radio frequency (RF) field.

2.1.1.4 The population distribution of the nuclear energy states

The populations of nuclei in each of the energy states are determined by the Boltzmann distribution. The larger the separation of energies and the lower the thermal energy, the larger is the proportion of spins in the lower state. At a thermal equilibrium characteristic of the temperature *T*, the relative numbers n^+ and n^- of nuclei in the spin +½ and -½ states are given by

$$\frac{n^-}{n^+} = \exp(-\Delta E/kT) = \exp(-\gamma\hbar B_0/kT) \qquad (2.10)$$

where k is the Boltzmann constant. For protons at a magnetic field of 8.5T, n^-/n^+=0.99994. This means that at 8.5T there is a population difference of only six in every hundred thousand nuclei between the two energy states. The similarity of the occupancy of the energy states means that net signal absorption is only seen from a very small proportion of the nuclei, and thus the inherent sensitivity of the technique is quite low. It is worth noting that an increase in the magnetic field B_0 increases the difference between adjacent states (equation(2.6)) and hence their population difference (equation(2.10)). This considerably enhances the net absorption of energy. As a result, a high magnetic field is generally desirable to improve the signal to noise ratio.

2.1.1.5 Nuclear Magnetism -Classical approach

The nucleus of an atom may be envisaged to spin around its own axis and therefore posses the property of angular momentum. Since the nucleus is charged, this circulating charge generates a magnetic field. In an NMR experiment, we study a sample containing a very large number of magnetic nuclei. The sum of their magnetisation vectors is called the net magnetisation vector. When placed in a external magnetic field the magnetisation vector aligns itself parallel to the field and due to its angular momentum will precess about the field at an angular frequency known as the Lamour frequency = $\omega_0 = \gamma B_0$; this is identical to equation (2.9) from the quantum description. The gyromagnetic ratio is unique for each nucleus. Thus nuclei of ^{1}H and

^{31}P will resonate at 360MHz and 146MHz respectively at the same magnetic field strength of 8.5T.

Since there is no preferred orientation in the plane perpendicular to B_0 (the xy-plane), the net component of magnetic moment in the xy-plane is zero. However, there is a net magnetisation along the z-axis due to the unequal populations in the two energy states. In order to interrogate this net magnetisation, it is necessary to add energy to the system so that the state of equilibrium is upset, and a proportion of the magnetisation is tilted into the xy-plane. The next section explains how this can be achieved using the concept of the rotating frame of reference.

2.1.1.6 Rotating Frame

To understand the concepts of spin excitation more easily, it is convenient to deal with vectors in a frame of reference which is rotating about the z-axis at the Larmor frequency. If a nucleus precess with an angular frequency $\omega_0 = \gamma B_0$ within the frame of reference, which also rotates with the same frequency, then the net magnetisation vector does not appear to precess.

The rotating frame is especially useful for expressing the effects of a second field, B_1, in the transverse direction, also rotating at the frequency ω_0. This field will appear static in the rotating frame. In the same way that the application of B_0 causes the nuclei to precess about its direction with angular frequency γB_0, so the application of B_1 in the rotating frame causes the nuclear magnetisation to precess about B_1 with angular frequency γB_1. This is because the B_1 field is the only apparent field experienced in the

rotating frame. If the field B_1 is applied for a time t_p, the nuclei will rotate through an angle θ given by the product of angular frequency with time,

$$\theta = \gamma B_1 t_p \qquad (2.11)$$

The nuclei will rotate through an angle of 90° (corresponding to $\theta = \pi/2$ radians) if t_p is such that

$$\gamma B_1 t_p = \pi/2 \qquad (2.12)$$

A pulse of B_1 field that has this duration is known as a 90° pulse, and its effect is to tilt the net magnetisation away from the z-axis into the xy-plane of the rotating frame. Following a 90° pulse, the system relaxes to equilibrium.

2.1.1.7 Relaxation

The behaviour of the net magnetisation is best understood by considering two components separately: the longitudinal component in the direction of B_0 (M_z), and the transverse component in the perpendicular plane (M_{xy}). After a disturbance, M_z and M_{xy} return to their equilibrium values through spin-lattice (or longitudinal) and spin-spin (or transverse) relaxation respectively.

Spin-lattice relaxation is characterised by a time constant T_1 known as the spin-lattice, or longitudinal, relaxation time. This describes the return of the magnetisation M_z to its equilibrium value M_0 according to the Bloch equation:

$$\frac{dM_z}{dt} = \frac{M_0 - M_z}{T_1} \qquad (2.13)$$

The processes that are responsible for longitudinal relaxation are fluctuating magnetic fields that have a component in the xy-plane that oscillates at the resonant frequency. These fluctuations will induce transitions between the spin states of the nuclei, and if they are associated with the lattice (lattice is used in this context to mean the molecular framework in which the nuclei reside), there will be an exchange of energy until the nuclear spins are in thermal equilibrium with the lattice. The fluctuating magnetic fields are created by the random tumbling of neighbouring molecules, and the resulting time-dependant effect of their magnetic dipoles.

Spin-spin relaxation causes the return of M_{xy} to its equilibrium value, and is characterised by a time constant T_2 known as the spin-spin, or transverse, relaxation time. Since the equilibrium value of M_{xy} is zero, the Bloch equation for spin-spin relaxation is

$$\frac{dM_{xy}}{dt} = \frac{-M_{xy}}{T_2} \qquad (2.14)$$

T_2 relaxation involves interaction between neighbouring spins without exchange of energy to the lattice. The value of T_2 is limited by T_1 and is also determined by the spread of frequencies at which the spins are resonating. This depends on local B_0 field inhomogeneities caused by neighbouring spins (not necessarily rotating at the Larmor frequency), and means that for any biological sample, T_2 will be considerably shorter than T_1. In addition to these signal decay processes, the presence of magnetic field

inhomogeneities may also act to dephase spins around the precessionary orbit. This results in dephasing in the xy-plane and is called T_2' relaxation. The combined effect of T_2 and T_2' relaxation is called T_2^* relaxation, defined by:

$$\frac{1}{T_2^*} = \frac{1}{T_2} + \frac{1}{T_2'} \qquad (2.15)$$

T_2 relaxation is irreversible. However, dephasing caused by T_2' can be reversed by using a 180° refocussing pulse to produce a spin echo.

2.1.1.8 Free induction decay

Following a 90° RF pulse, the coherent rotation of the transverse magnetisation M_{xy} behaves according to:

$$M_x = \left[M_0 cos(\omega_0 t)\right] \times e^{-t/T_2^*} \qquad M_y = \left[M_0 sin(\omega_0 t)\right] \times e^{-t/T_2^*} \qquad (2.16)$$

where M_x and M_y are the components of magnetisation along the x- and y-axes respectively, and the exponential term describes the T_2^* decay of the signal. The voltage induced in a conducting wire placed near the sample (the receiver) oscillates at a frequency ω_0 and is called the free induction decay (FID) signal. The receiver is usually a coil which is designed to be as sensitive as possible to the FID, and can either be the same coil as that used to generate the B_1 excitation pulse or a separate device used only to receive.

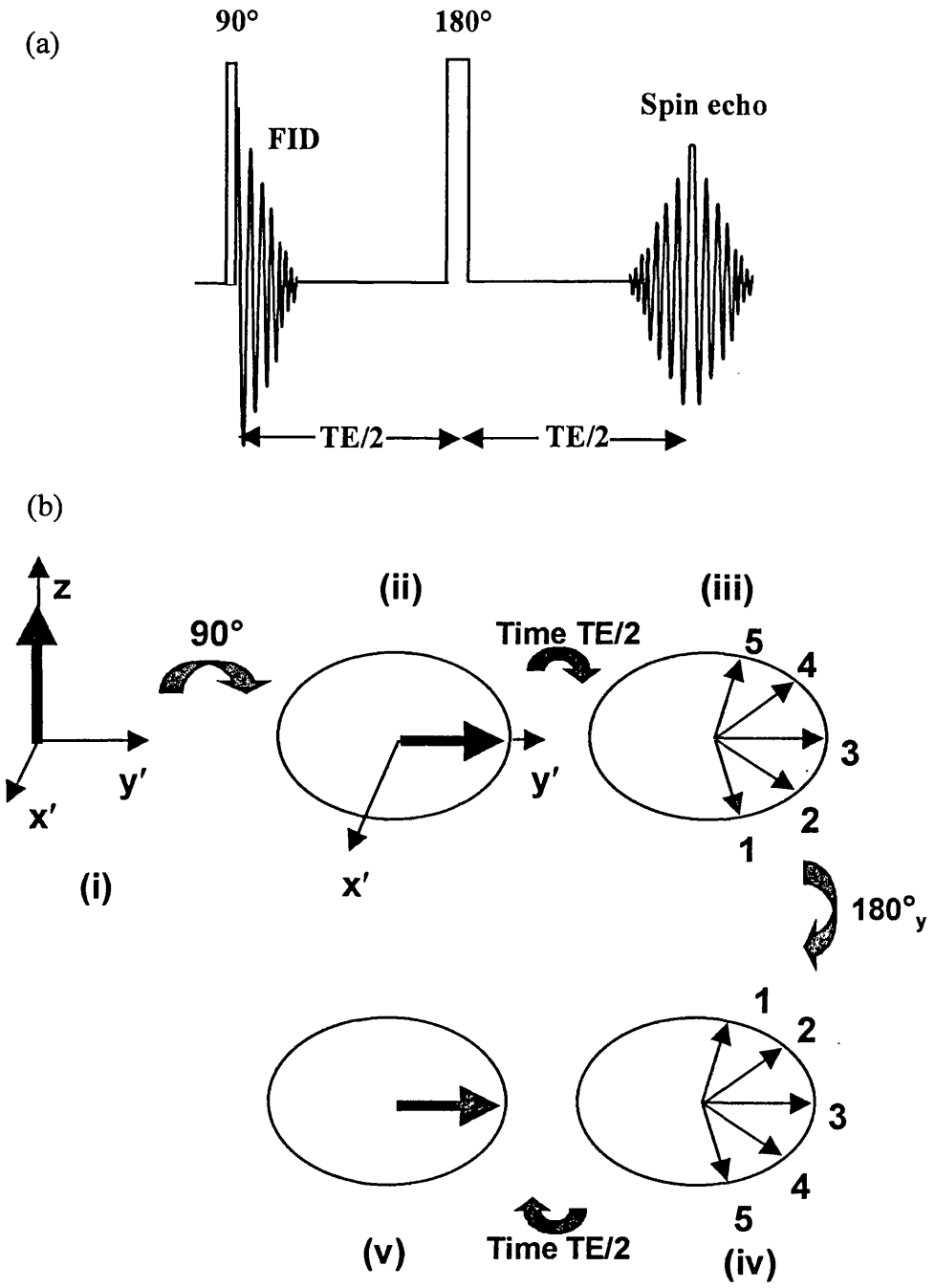

Figure 2.1.2 *Using a 180° refocusing pulse to create a spin echo (a) RF pulse sequence and observed signal (b) the process by which the spin echo is formed*

2.1.1.9 Fourier transformation

Once the FID has been detected, it can be transformed to give either spatial information for imaging (see later section) or the chemical information used in spectroscopy. The technique of Fourier transformation converts a waveform that is expressed as a function of time, into a signal that is a function of frequency. This technique allows a spectrum of frequencies to be detected simultaneously then separated in the frequency domain.

2.1.1.10 Spin echo

As shown by equation (2.16), following a 90° pulse the transverse magnetisation generated decays at a rate determined by T_2*. A 180° refocussing RF pulse can partially reverse this evolution to form a spin echo (figure 2.1.2). If a 180° pulse is applied at a time τ after the 90° pulse then the individual components of magnetisation remain in the xy-plane but their phase is inverted and their direction of precession reversed, so that those precessing at a faster rate now lag behind the slower ones. After another time τ the faster components will have caught up, resulting in phase coherence and thus producing a signal which is known as the spin echo (Hahn, 1950). The formation of an echo in this way counteracts only the dephasing caused by field inhomogeneity, and at the time of the echo the nuclei are still partly dephased because of the random effects of T_2 relaxation and molecular Brownian motion. The extent of this dephasing (or T_2-weighting, as it is known) depends on the value of τ which is used. This parameter is one of the most important methods used in MRI to generate different image contrast. If a series of measurements are taken at varying echo times (TE) then a relaxation curve may be built up, and a measurement of T_2 can be made.

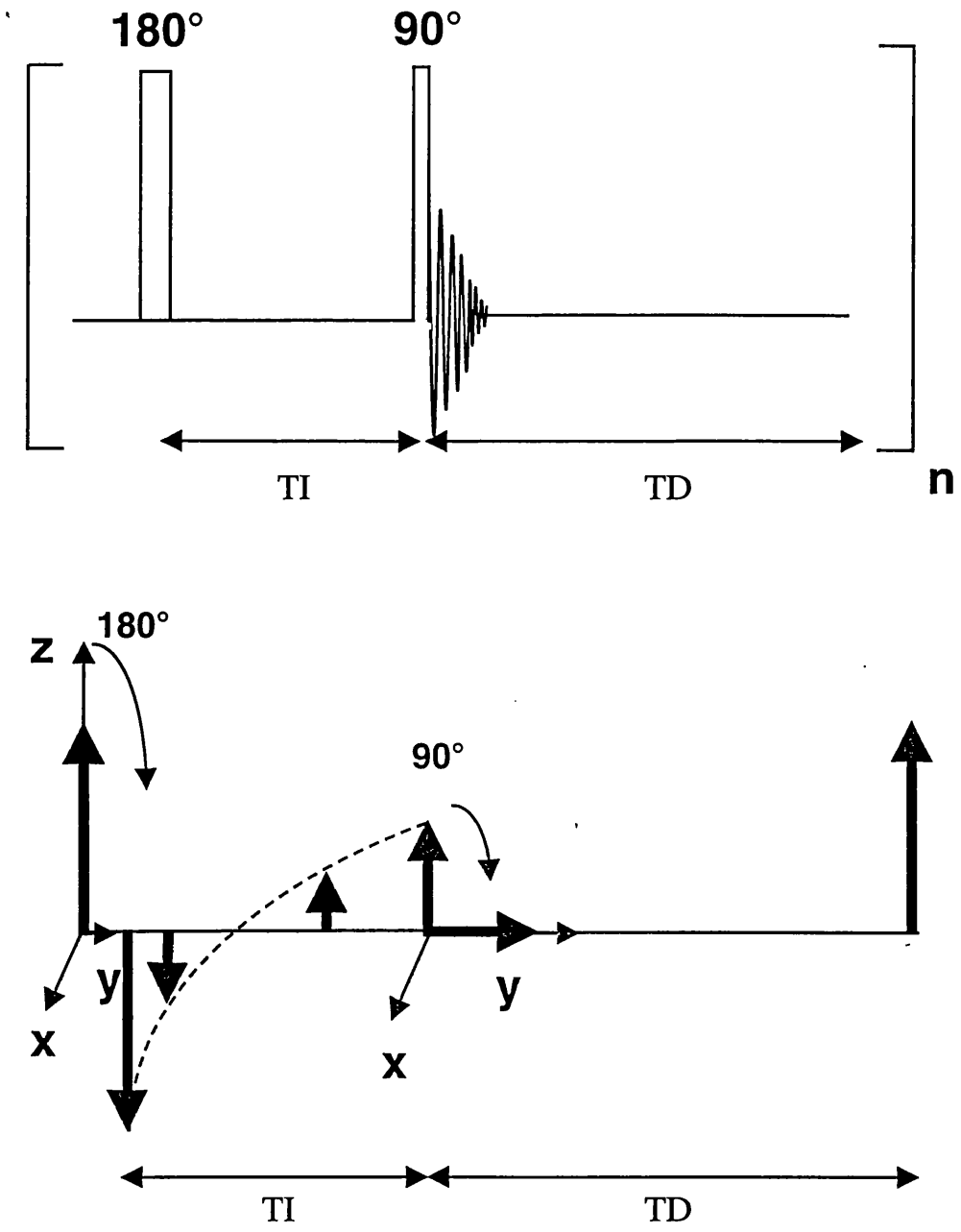

Figure 2.1.3 *The inversion recovery sequence. (a) the RF pulse sequence and observed signal (b) behaviour of the magnetisation. The magnetisation is initially inverted by a 180° pulse, and undergoes an amount of T_1 relaxation determined by the choice of TI. It is then tipped into the xy-plane using a 90° pulse and the resulting FID sampled*

2.1.1.11 Inversion recovery

Figure 2.1.3 shows a sequence which is commonly used to weight the NMR signal according to the longitudinal relaxation time (T_1) of the sample under study. A 180° pulse is first applied to tip the magnetisation anti-parallel to the z-axis, or to 'invert' the magnetisation. The spins then relax back toward equilibrium at a rate determined by T_1. As this relaxation is occurring, a 90° pulse is applied to rotate any longitudinal magnetisation M_z into the xy-plane so that it gives a FID signal. The amplitude of the signal depends on the size of M_z at the time of the 90° pulse, and so T_1 dependence is introduced by appropriate choice of timing in the sequence. If a series of measurements are taken at varying inversion times (TI) then an inversion recovery curve may be built up, and a measurement of T_1 can be made.

2.1.2 Image formation using NMR

The aim of magnetic resonance imaging (MRI) is to produce representations of objects containing NMR sensitive nuclei with good spatial accuracy. This is done nowadays almost exclusively by the use of Fourier analysis techniques, in which spins are spatially encoded by manipulating their resonant frequency using magnetic field gradients. For a standard two dimensional Fourier transform (2DFT) image pulse sequence (figure 2.1.4), the main features for consideration are:

1) the use of a frequency selective pulse (a 'shaped' 90° pulse) to excite a single slice from the three dimensional region
2) the use of phase-encoding gradients, G_y, to provide information along one direction (the y-direction) within the slice
3) the use of the read gradient, G_x, to provide information along the x-direction within the slice

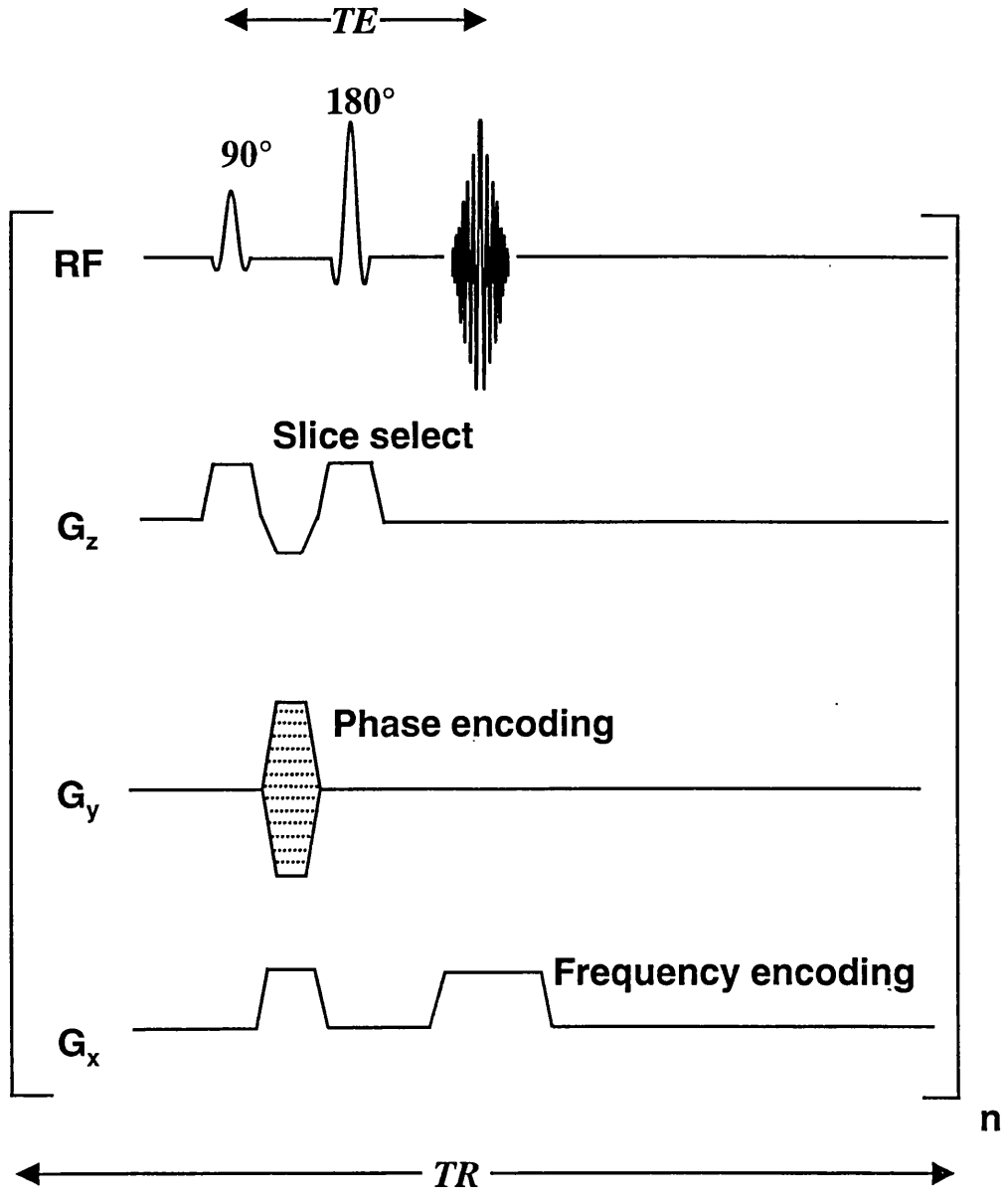

Figure 2.1.4 *A standard spin echo 2DFT imaging sequence. Magnetic field gradients applied along the three perpendicular directions x, y and z allow spatial encoding of the signal. The sequence is repeated for incrementally changing magnitudes of the phase encoding gradient; an image can be created by 2D Fourier transformation of the resulting echo set.*

2.1.2.1 Slice selection

Protons in the slice of interest can be selectively excited by the combination of a frequency-selective RF pulse and a magnetic field gradient applied perpendicular to the imaging plane. The bandwidth of the RF pulse and the amplitude of the slice-selection gradient determine the thickness of the slice (figure 2.1.5). In order to excite the material within the slice evenly the RF pulse must be of a certain shape e.g. a sinc function. Also, because the slice is of finite thickness, the slice selection gradient, as well as enabling the slice to be selected, causes nuclei through the slice to be dephased. A negative gradient after the RF pulse compensates for this by rephasing the nuclei.

2.1.2.2 Frequency encoding or read gradient

Following a slice selective 90° pulse, nuclei precess about B_0 at the Larmor frequency ω_0. Ignoring field inhomogeneity effects, all spins resonate at the same frequency. A magnetic field gradient applied along the x-direction causes neighbouring spins within the gradient to precess at different frequencies. Frequency encoding involves acquisition of an echo in the presence of a linear field gradient. Frequency analysis of the echo by Fourier transformation produces a profile of the sample.

2.1.2.3 Phase encoding

To obtain a further axis of spatial information, spins are subjected to a third magnetic field gradient G_y perpendicular to both the slice select and frequency encoding gradients. This causes the nuclei to precess at different rates according to their position along the y-axis, and if the gradient is applied for a period of time Δt the nuclei at a point y will have accumulated a phase shift $\Delta\phi$ equal to

$$\Delta\phi = \gamma G_y y \Delta t \qquad (2.17)$$

It can be seen that the gradient G_y causes the nuclei to acquire a phase shift that is proportional to their y-co-ordinate. If the size of the gradient is increased in a stepwise manner, the signal will be modulated with a frequency that is determined by the y-co-ordinate of the nuclei generating the signal. Fourier analysis of how the signal varies from one scan to another provides the means of disentangling the frequency modulations and hence yielding the y-distribution of the nuclei that give rise to the signals. This provides the second dimension for the image, and the combination of phase and frequency encoding enables the reconstruction of a two dimensional image.

2.1.3 K-space

K-space is a graphical representation of imaging techniques, based on the received signal being a Fourier transform, which helps to visualise the effects of applied gradients. A K-space representation of a spin echo sequence is show in figure 2.1.6. In the 2D-FT experiment, one line of k-space in the read direction is acquired per excitation of the spin system, and k-space is stepped through in the other direction by incrementally increasing the phase encode gradient for successive acquisitions. This means that the scan time for a spin warp image tends to be on the order of a few minutes, and is the reason why this type of image acquisition is rather prone to motion artefacts. In an effort to reduce the motion sensitivity of MRI, techniques have been proposed which reduce the length of the imaging period, such as echo planar imaging.

2.1.4 Gradient echo imaging

Just as T_2 can be measured from a series of spin-echo measurements, so T_2^* can be measured by means of gradient echoes. In spin-echo sequences, the 180° pulse reverses the effects of the local field inhomogenities and hence generates a T_2-weighted spin-echo signal. An alternative means of generating an echo is by reversal of an applied

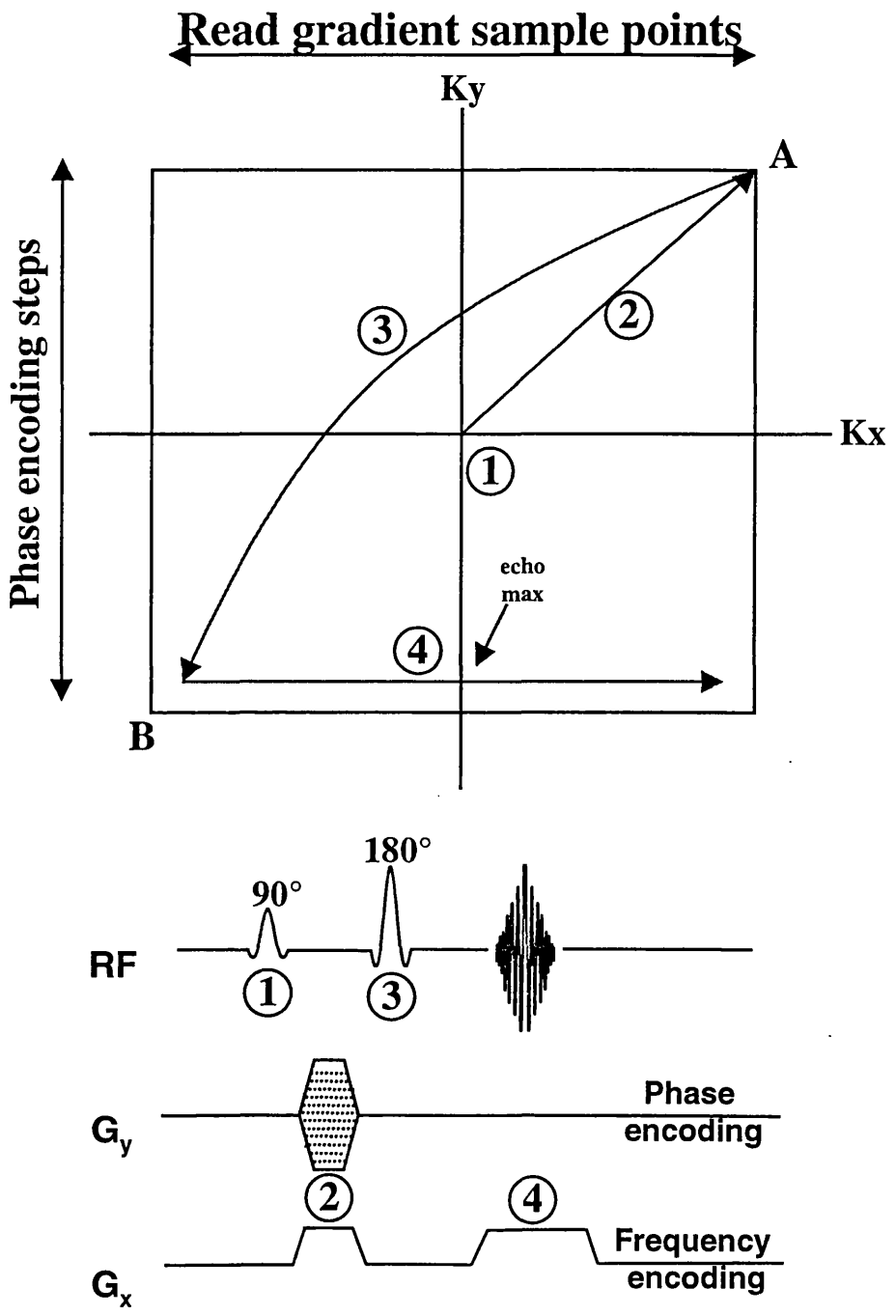

Figure 2.1.6 *K-space representation of a spin echo sequence.*
1) A 90° RF pulse initiates signal evolution at the origin of K-space.
2) Positive frequency and phase encoding gradients are indicated by a diagional movement through K-space.
3) A 180° RF pulse causes movement from A to B.
4) Finally, a positive frequency encoding gradient is applied and the signal is sampled

field gradient. The first negative gradient dephases the magnetisation, by an amount that is dependent upon the integral of the gradient over time. On reversal of the gradient, the magnetisation rephases, the maximum rephasing occurring when the integral is fully reversed. At this time the signal is partially regenerated, producing a so called gradient echo. The main difference between a spin echo and a gradient echo is that the gradient echo does not refocus the dephasing effects of the intrinsic field inhomogenities, and therefore generates a signal that is weighted according to T_2^* rather than T_2.

2.1.5 Fast low angle shot (FLASH) imaging

The Fast Low Angle Shot (FLASH) sequence is an example of a gradient echo sequence, in which a 180° refocussing pulse is not used and the sampled data comes from the FID of a single excitation pulse. The read gradients immediately follow the excitation pulse, thus reducing the echo time of the sequence. The scan time can also be reduced by making the time between successive excitations much less than the T_1 of the sample (the value typically used in spin echo imaging). This leads to loss in the signal to noise ratio (SNR) of the resulting image, but for a given repetition time, the SNR can be optimised by adjusting the flip angle of the excitation pulse according to the Ernst equation:

$$\cos\alpha = \exp(-TR / T_1) \qquad (2.18)$$

where α is the pulse flip angle and TR is the sequence repetition time. FLASH imaging therefore offers the possibility of a greatly reduced scan time at the cost of a degradation of image quality.

2.1.6 Diffusion-weighted imaging

Measuring molecular diffusion has brought several useful new approaches to tissue characterisation and functional studies, from the determination of cell geometry to the early clinical evaluation of cerebrovascular accidents (or strokes). This interest in diffusion results from the unique feature of this parameter; diffusion directly reflects molecular mobility. Molecular mobility also affects T_1 and T_2 relaxation times, but diffusion refers only to *translational* molecular motion, whereas T_1 and T_2 reflect complex molecular interactions involving *rotational* motion and exchanges. Moreover, T_1 and T_2 are MR parameters affected by MR experimental conditions, such as the magnetic field strength. By contrast, diffusion is defined entirely outside the MR context and does not depend on the MR environment. However, MRI is the only *in vivo* technique available today to measure diffusion directly from molecular displacements. Thus diffusion has not been used previously in the clinical domain and represents a new parameter. Over recent years, it has been shown to be a parameter which holds much useful information.

2.1.6.1 Molecular Diffusion

Molecular diffusion results from a random, microscopic, translational motion of molecules known as Brownian motion. Because of thermal agitation, molecules are constantly moving and colliding with each other. Diffusion was originally described in non-uniform systems, where a macroscopic flux of differing species of particles could be observed. Fick's first law states that this flux density depends linearly on the concentration gradient of this particle species. The proportionality constant is known as the *diffusion coefficient* (*D*). A typical experiment is to monitor the diffusion of a substance between two compartments separated by a semi-permeable membrane. The

diffusion coefficient can be determined, for instance, by measuring the concentration of the substance at different times, using either chemical or physical methods. The principle of Fick's law is currently being applied, for example, in haemodialysis.

2.1.6.2 Random walk and Einstein's equation

For a particular molecule, the random molecular walk produces net displacements over time, which are randomly distributed if we consider large molecular populations. The probability that a molecule travels a distance r in a time interval t can be calculated. For a simple liquid, one finds a Gaussian distribution, the mean of which is zero because the probability of motion in one direction is the same as that in the opposite direction. The variance of the distance travelled is proportional to the time interval t according to the Einstein equation:

$$\langle r^2 \rangle = 2Dt \quad \text{(or } 6Dt\text{, for displacements in three dimensions)} \qquad (2.19)$$

The proportionality constant D, the diffusion coefficient, characterises the mobility of molecules within and relative to the diffusing medium. The D of water at 25°C is about 2.2×10^{-3} mm^2/s. This means that, during 100ms, the standard deviation for water molecular displacements is 20μm. In complex systems such as biological ones, the distribution of molecular displacements may deviate from the Gaussian model because of the presence of obstacles.

2.1.6.3 Boundaries and restriction

Restricted diffusion occurs when molecules are confined in a limited medium by borders. When the molecules reach these borders they are reflected back into the medium. Therefore the diffusion distance is not found to increase indefinitely with the

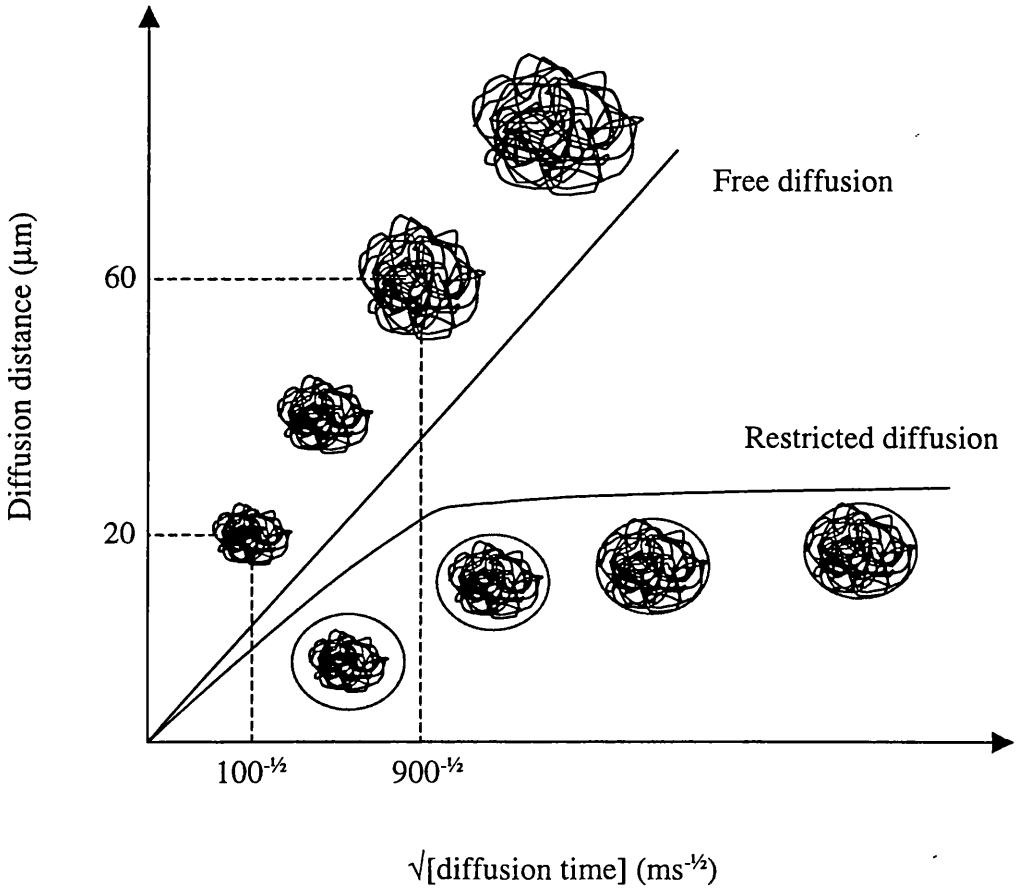

Figure 2.1.7 *Diffusion behaviour of molecules in free and restricted media. For free diffusion, the diffusion distance $\langle r^2 \rangle^{-½}$ increases linearly with the square root of the diffusion time. The constant of proportionality is the diffusion coefficient D. If diffusing molecules are restricted to a closed system, the relationship is no longer linear, and the 'apparent' diffusion coefficient (ADC) depends on the diffusion time used.*

diffusion time, as seen with free diffusion: rather, this distance 'saturates' when all the molecules have reached the boundaries (figure 2.1.7). By comparing this saturation diffusion value and the free diffusion coefficient, which can be measured using very short diffusion times so that molecules do not experience any restriction, it is theoretically possible to evaluate the dimensions of the restrictive boundaries. This is of great interest for tissue characterisation if the media in question are, for example, cells. In practice, the situation is complicated by the shape and permeability of the medium, and diffusion measurements can be used to estimate the permeability of cell membranes.

The dependence of the measured diffusion coefficient on diffusion time means that equation (2.19) does not hold true, and the definition of the diffusion coefficient needs to modified. Le Bihan *et al.* (Le Bihan *et al.* 1986) introduced the concept of the 'apparent' diffusion coefficient (ADC) to recognise the fact that in biological systems there is always some degree of restriction, and therefore some departure from the Gaussian model. When presenting diffusion measurements, it is important to state the diffusion time used to enable comparison with other reported values.

2.1.6.4 Effects of diffusion on the spin echo MR signal

As seen in this chapter, a linear magnetic field gradient in the z direction G_z causes the effective field B seen by nuclei at location z to be:

$$B = B_0 + G_z z \qquad (2.20)$$

and the corresponding precession (Larmor) frequency is:

$$\omega = \gamma B = \gamma B_0 + \gamma G_z z \qquad (2.21)$$

where γ is the gyromagnetic ratio (see chapter 2). The phase accumulated by the transverse magnetisation of spins at any location r in the presence of any gradient G over a time interval t will then be

$$\phi = \int_0^t \omega \, dt = \int_0^t (\gamma B_0 + \gamma G \cdot r) dt = \phi_0 + \gamma \int_0^t (G \cdot r) dt \qquad (2.22)$$

where ϕ_0 is the phase accumulated by spins at location r = 0. Spins moving in the presence of a magnetic field gradient (or any field gradient inhomogeneity) have the phase of their transverse magnetisation shifted compared to that of static spins. This phase shift results from changes in the magnetic field, and the associated frequency, seen with spins that translate along the direction of the field gradient. In the situation where many molecules are moving with different velocities, the sum of the phase shifts results in destructive interference of the MR signal and an associated loss in signal amplitude.

2.1.7 Calculation of the apparent diffusion coefficient

2.1.7.1 Single echo and constant gradient

The effects of molecular diffusion have been studied since the early days of NMR (*e.g.* see Stejskal and Tanner, 1965). Because the probability distribution of diffusion displacements has a Gaussian shape, the attenuation of the spin echo has an exponential dependence:

$$S = S_0 \exp(-bD) \tag{2.23}$$

D is the diffusion coefficient and b is a factor that depends on the magnetic field gradients. If a constant gradient G is applied during the echo delay TE of a spin echo sequence, one has

$$b = \gamma^2 G^2 TE^3 / 12 \tag{2.24}$$

and the echo signal is

$$S = S_0(N, T_1)\exp(-TE/T_2)\exp(-\gamma^2 G^2 TE^3 D/12) \tag{2.25}$$

where N refers to spin density. Although b depends on the square of G and the cube of TE, diffusion effects can only be observed with strong gradients and/or quite long diffusion measurement times, since D is generally small in biological tissue.

2.1.7.2 Pulsed gradients and Stejskal-Tanner sequence

A significant improvement in diffusion measurements using a single spin echo was introduced by Stejskal and Tanner (Stejskal and Tanner, 1965). By using very large but short gradient pulses placed on each side of the 180° pulse of the spin echo sequence, which are balanced and therefore have no effect on static spins, accurate measurements of low diffusion can be made. In the *Stejskal-Tanner sequence* the expression for b becomes:

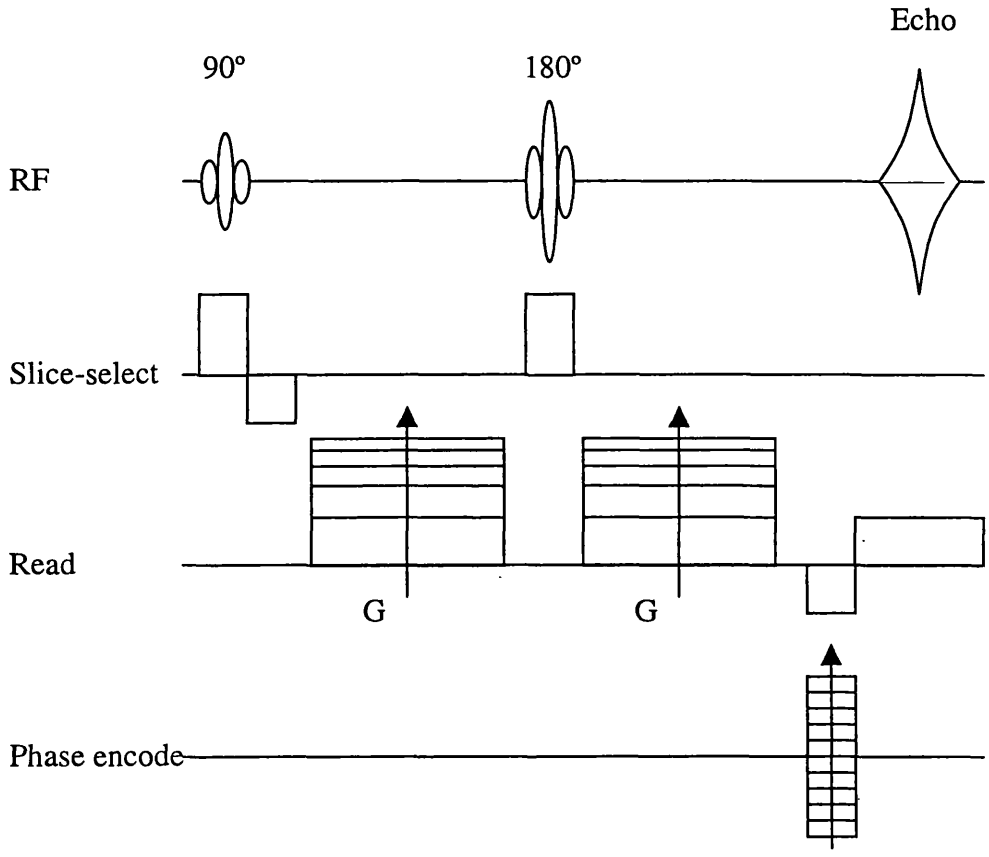

Figure 2.1.8 *2DFT spin echo diffusion-weighted imaging sequence. Sensitisation to diffusion is obtained by inserting a pair of Stejskal-Tanner gradients, shown here along the read axis. By changing the amplitude G of these gradients, one can modulate the degree of diffusion-weighting of the echo. Diffusion maps are directly obtainable from the resulting set of images.*

$$b = \gamma^2 G^2 \delta^2 (\Delta - \delta/3) \qquad (2.26)$$

where δ is the duration of each gradient pulse and Δ is the time interval separating their onset (figure 2.1.8). The Stejskal-Tanner sequence offers the following advantage: when $\delta << \Delta$, the time during which the diffusion effect forms is exactly known and is controllable independently of TE. The diffusion measurement time in this sequence is $\Delta - \delta/3$ and can be made variable. This is particularly useful for restricted diffusion studies in which the diffusion time is a critical parameter.

2.1.7.3 Apparent diffusion coefficient maps

The computation of diffusion images, *i.e.* maps where the diffusion coefficient is displayed for each pixel, is possible by using two or more MRI sequences that are differently sensitised ('weighted') to diffusion but otherwise identical (same T_1 and T_2 dependence) (figure 2.1.8). For a typical 2DFT spin echo imaging sequence that contains multiple but low-amplitude gradient pulses, the b factor of the imaging gradients remains low (typically less than 1s/mm^2) so that the diffusion effect is completely negligible (for D = 2.2 $\times$ 10^{-3} mm^2/s the attenuation is less than 1%). To increase the sensitivity of the imaging sequence to diffusion, one must incorporate additional gradient pulses in the sequence. These gradients can be applied along any axis.

For instance, in the case of two images S_1 and S_0 obtained with gradient factors b_1 and b_0, the diffusion coefficient D can be determined in each pixel from the relative signal intensities $S_0(x,y)$ and $S_1(x,y)$ by rearranging equation (2.23):

$$D(x,y) = \ln[A(x,y)]/(b_1-b_0) \quad (2.27)$$

with $$A(x,y,) = S_0(x,y)/S_1(x,y) \quad (2.28)$$

Diffusion coefficients can also be determined from more than two images obtained with different known b values by fitting the signal attenuation with equation (2.23).

2.1.7.4 Anisotropic diffusion and the diffusion tensor

So far this description has concentrated on isotropic diffusion i.e., diffusion that exhibits no directional dependence, but it needs to be modified for anisotropic systems. The directional dependence of diffusion is known as diffusion anisotropy and is especially apparent in brain white matter in which diffusion mobility is greater along the nerve axon fibres. Along the other directions, diffusion is considered as being restricted. Studies have also indicated that even grey matter displays a certain degree of anisotropy (Chapter 5). The diffusion coefficient is therefore better represented within brain tissue by a second rank tensor that takes into account molecular displacements in x, y, and z directions (diagonal terms) and also their possible coupling terms (non-diagonal terms). The elements of the tensor are denoted by the notation Dij, where D is the diffusion coefficient and, i and j can take any of the three gradients directions x, y, and z. The trace of the tensor (Trace (**D**)) contains the diagonal elements D_{xx}, D_{yy} and D_{zz} and the image formed from these elements is rotationally invariant. The Trace (**D**) is described as:

$$\text{Trace}(\mathbf{D}) = D_{xx} + D_{yy} + D_{zz} = 3D_{av} \quad (2.29)$$

Where D_{xx} is the ADC along the x-axis and **D** is the diffusion tensor.

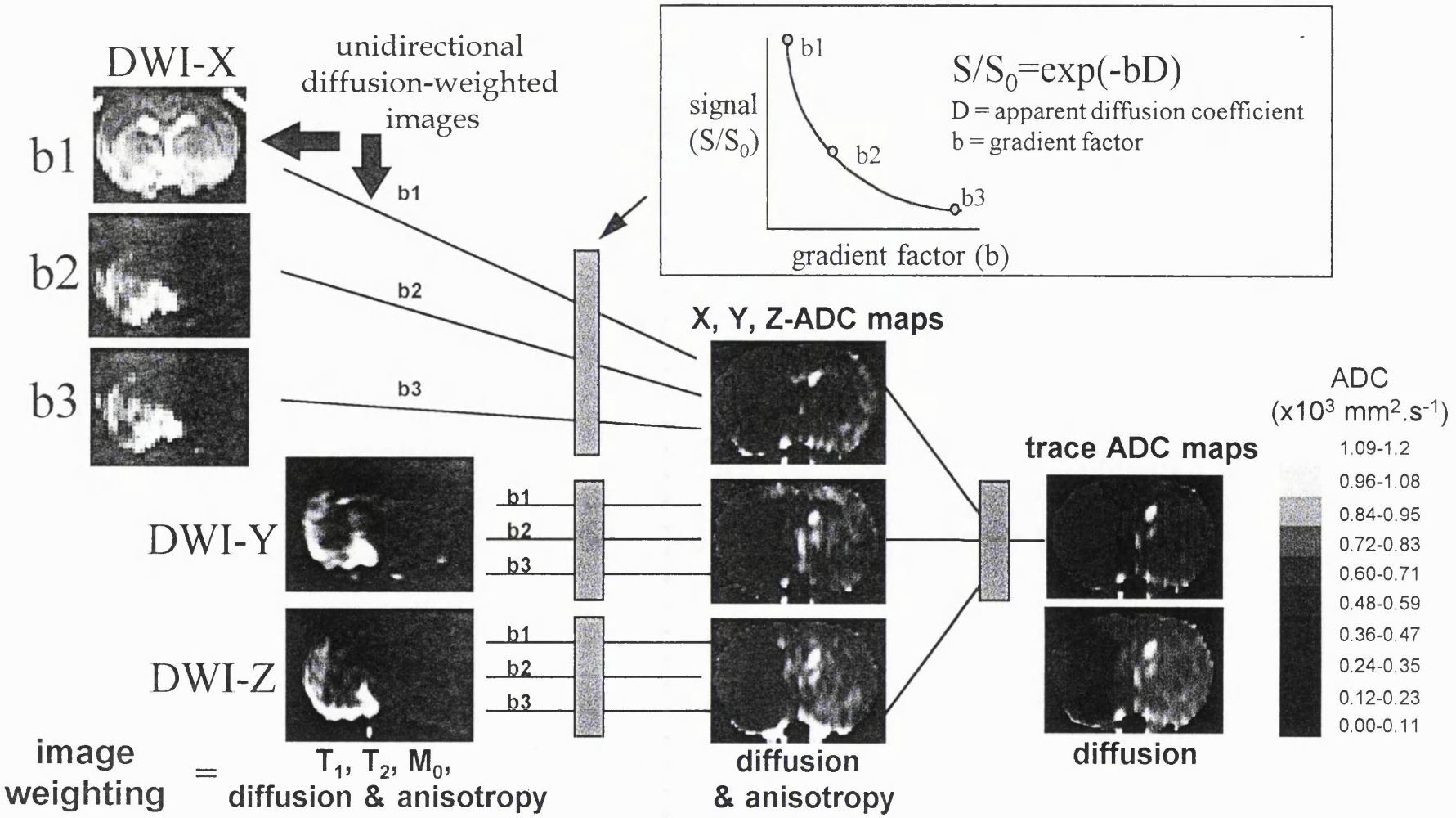

Figure 2.1.9 Calculation of unidirectional (X, Y, Z) ADC maps and maps of the trace of the diffusion tensor, from 3 single-axis (X,Y,Z) diffusion-weighted images at different b-values. All images acquired 2 hours following MCAO in a rat model. The effect of tissue anisotropy on lesion delineation is observed in the X, Y and Z -ADC maps.

A third of the tracer of the tensor, 1/3Trace (**D**) (D_{av}), can be most easily determined by obtained separate diffusion-weighted measurements with the diffusion encoding placed along orthogonal directions and by averaging the result (Figure 2.1.9). Application of this technique to biological systems is discussed in Chapter 5.

2.1.8 Perfusion imaging

Over recent years, methods for measuring perfusion using NMR techniques have been proposed. These techniques have been made practically feasible by the development of ultrafast technology, which greatly increases MRI's efficiency in data collection and allows images to be acquired on the time scale required for the measurement of rapid physiological changes. Several different methods have been suggested, most of which are based on one of two approaches: (i) the use of contrast agents (exogenous and endogenous), or (ii) arterial spin labelling.

2.1.8.1 Non-invasive Perfusion MR Imaging using Spin Labelling of Arterial Water

An MR image can be made sensitive to the effect of inflowing blood spins if those spins are in a different magnetic state to that of the static tissue. The family of techniques known as arterial spin labelling (ASL) techniques uses this idea by magnetically labelling blood flowing into the slice(s) of interest. Blood flowing into the imaging slice exchanges with tissue water, altering the tissue magnetisation (figure 2.1.10). A perfusion-weighted image can be generated by the subtraction of an image in which inflowing spins have been labelled from an image in which spin labelling has not been performed. Quantitative perfusion maps can be calculated if other parameters (such as tissue T_1 and the efficiency of spin labelling) are also measured. Since exogenous contrast agents are not required for these techniques, the perfusion

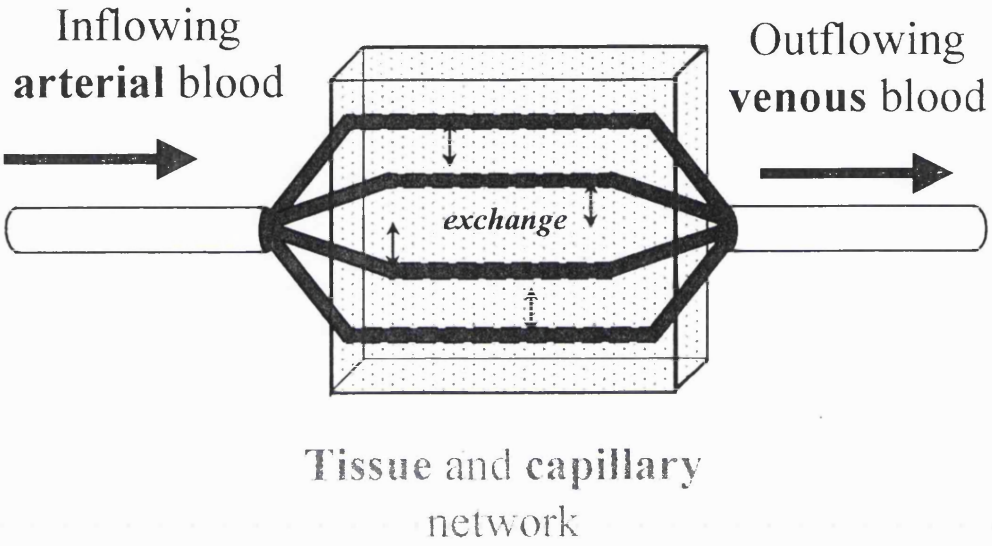

Figure 2.1.10 Schematic diagram of tissue perfusion.

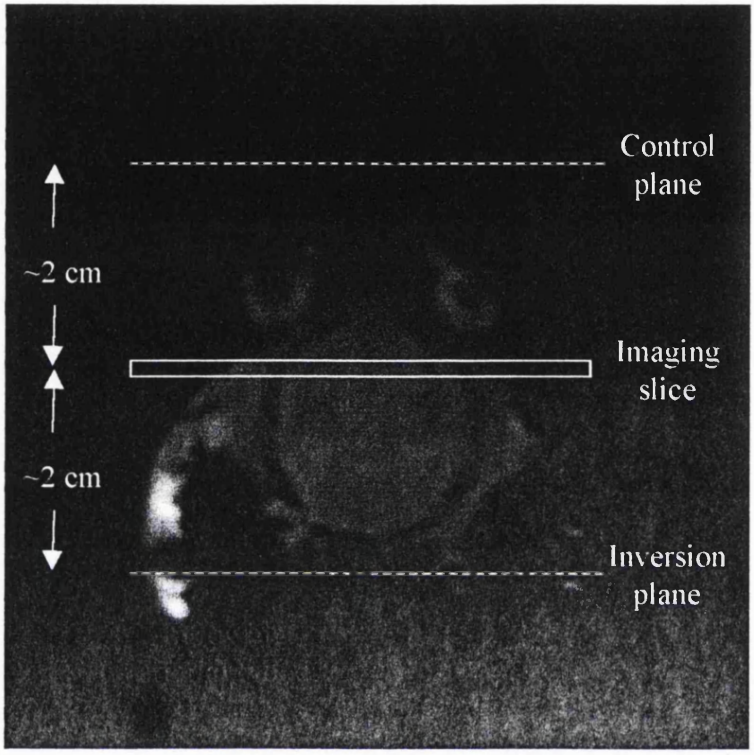

Figure 2.11 *Coronal scout image of the rat brain, showing the position of the imaging slice and approximate control and inversion planes. The offset for the inversion pulse was chosen for each animal by altering the slice select gradient until the plane of inversion was 2mm proximal to the rear of the brain in this image; this corresponded on average to a 20mm offset from the imaging slice. The control plane was then chosen by default to be symmetrically opposite by reversing the polarity of the slice-select gradient*

measurement is completely non-invasive. Under the general heading of arterial spin labelling, two distinct sub-groups exist: continuous ASL and pulsed ASL. The technique of continuous ASL is discussed in the next section, as this was the method used for the MR quantitation of cerebral blood flow in this thesis.

2.1.8.2 Continuous Arterial Spin Labelling techniques

The first arterial spin labelling (ASL) technique, proposed by Detre *et al.* in 1992 (Detre *et al.* 1992), is known as continuous ASL (CASL). In the initial implementation, blood water spins were repeatedly saturated as they flowed through a slice in the neck by the use of a train of RF pulses, applied over a period of several seconds (figure 2.1.11). The labelled spins flow into the brain and, assuming water is a freely diffusible tracer, exchange completely with brain tissue water, thus reducing the overall tissue magnetisation. A steady state develops where the regional magnetisation in the brain is directly related to cerebral blood flow. Modifying the Bloch equation for longitudinal relaxation to include flow leads to the following equation for flow quantitation:

$$f = \frac{\lambda}{T_{1app}}\left(1 - \frac{M_b^{ss}}{M_b^0}\right) \qquad (2.30)$$

where f is blood flow (perfusion) in ml/100g/min, λ is the blood:brain partition coefficient for water, M_b^{ss} is the steady state magnetisation per unit mass of brain tissue, M_b^0 is the fully relaxed tissue magnetisation per unit mass, and T_{1app} is the constant which describes the exponential decay to the steady state magnetisation and is defined by:

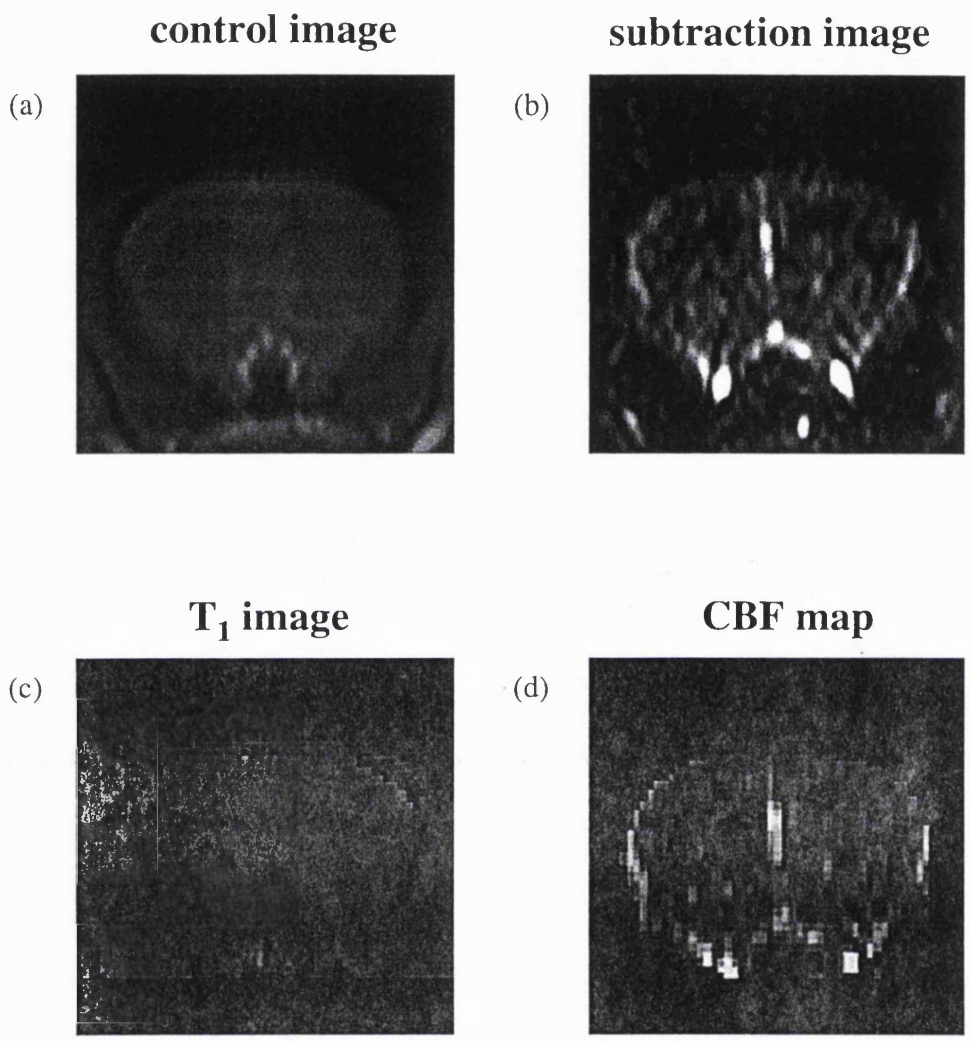

Figure 2.1.12 *An example of the images which are used to create a perfusion map. (a) shows the control image of the perfusion image pair and (b) shows the result of subtracting the spin labelled image from this control image. A T_1 map (c) is then combined with these images according to produce a quantitative perfusion map (d).*

$$\frac{1}{T_{1app}} = \frac{1}{T_1} + \frac{f}{\lambda} \qquad (2.31)$$

By measuring T_{1app} and the ratio of magnetisation with and without arterial spin saturation, a value for flow can be calculated (figure 2.1.12). The values for cerebral perfusion in the rat brain reported by Detre *et al* (Detre *et al.* 1992) were in reasonable agreement with previously published values using other techniques.

2.2 BASIC PRINCIPALS OF AUTORADIOGRAPHY

Autoradiography is the determination of the spatial distribution of a radioactive tracer via production of an image on a photographic emulsion. There are two types of autoradiography, one is macroautoradiography with a spatial resolution of about 50μm and is the primary modality for radiographic determination of tissue tracer concentrations in kinetic studies. The other is microautoradiography, which is primarily used to determine either cellular or intracellular location of tracers and a resolution of 0.05μm can be achieved. The type of autoradiography that is presented in this thesis is macroautoradiography and will be referred to as autoradiography.

2.2.1 History of autoradiography

Autoradiographs were actually produced before the discovery of radiation, although their cause was misunderstood. In 1867, Niepce de St. Voctor observed that uranium nitrate blackened emulsions of silver iodide and silver chloride through sheets of coloured glass and attributed the effect to fluorescence (Niepce de St.Victor, 1867). Becquerel repeated the experiment in 1896 and showed that the darkening would occur even through two layers of black paper, and thus ruled out fluorescence as the cause (Becquerel, 1896). The first biological research specifically using autoradiography was performed in 1924 in the study of the distribution of polonium in biological specimens (Lacassagne *et al.* 1925). In 1943 autoradiographs were prepared by placing sections of thyroid containing ^{131}I in contact with lantern slides to determine the location of iodine in the glands (Leblond, 1934). The technique was improved in 1946 by painting emulsions, which had been removed by melting from lantern slides, onto specimens. Later this technique was modified for use with ultra-high-resolution emulsions and was

finally improved by dipping slides in molten emulsions, thus developing the basis for present day liquid emulsion microradiography.

Macroautoradiographic studies of the brain began in the late 1950s. ^{131}I-labelled trifluoroiodomethane was used as a tracer to measure cerebral blood flow (CBF) in the rat (Landau *et al.* 1955). In these experiments rats were given intravenous injections of the tracer and then sacrificed. Thick sections (5mm) were placed on Kodak SB54 film, and beta radiation from the section was allowed to expose the film for 10 days while it was kept in a dry ice freezer. Although reasonable CBF values were obtained, the technique did not gain widespread use because of the volatility of the compound and the low resolution of the thick sections. This prompted a search for suitable compounds to measure CBF and better sectioning technology. In 1977, ^{14}C-labelled iodoantipyrine was used to measure CBF in rats (Sakurada *et al.* 1978). Following this study, autoradiography using [^{14}C] iodoantipyrine, became the reference technique for the measurement of CBF in animals. Since this work, a large number of autoradiographic studies have been performed to measure the radiopharmaceutical distribution within the whole body or other organs than the brain. Diffusible and non-diffusible tracers have been used to measure rates of amino acid incorporation into proteins using ^{14}C- or ^{3}H-labelled leucine. Other compounds measure parameters such as ligand binding, receptor distribution and drug interaction.

2.2.2 Radionuclides

2.2.2.1 Technetium-99^{m}

Technetium-99^{m} (^{99m}Tc) is the most commonly used radionuclide in clinical gamma camera scintigraphy. The reasons for the prolific use in clinical studies are because of

the low radiation dose to the patient due to the short half-life and limited charged particle emission; the ease of availability from most hospital radiopharmacies; and the compatibility of the gamma-ray emission energy (141 keV) to the Anger gamma camera. Commercially available kits of HMPAO, the blood flow tracer, are easily labelled with ^{99m}Tc in just a few minutes. Hence the use of this radionuclide with HMPAO in these studies.

To produce an image on a film emulsion, the radiotracer must emit charged particles during the radioactive decay process. Some radionuclides, such as Technetium-99^{m}, are known as metastable products and have desirable emission characteristics for human use. To reach the metastable state a nucleus must undergo several specific stages. After an initial radioactive decay from the parent nuclide, a daughter nuclide is often left in an excited state and emits gamma radiation in order to reach the ground state (figure 2.2.1). In most cases this happens virtually instantaneously, but in a number of cases the nuclide has an excited level with a relatively long half-life, minutes or hours. These long-lived excited states are called "metastable levels" and are designated by use of the suffix or superscript m. Thus, there is a long lived excited level of technetium-99, designated technetium-99m which has a half-life of six hours (T½=6h). When a metastable level decays, the radiation emitted is only in the form of gamma radiation - being just an excited state of the decay product, and in the case of ^{99}Tc^{m}, the gamma energy is 141 keV. Particulate radiation is only emitted in the form of electrons (mean energy = 120 keV) as the result of internal conversion[1] of the gamma radiation.

[1] When a nucleus makes the transition to the ground state the energy is given off as gamma radiation. This energy may be transferred to one of the bound electrons which is ejected from the atom.

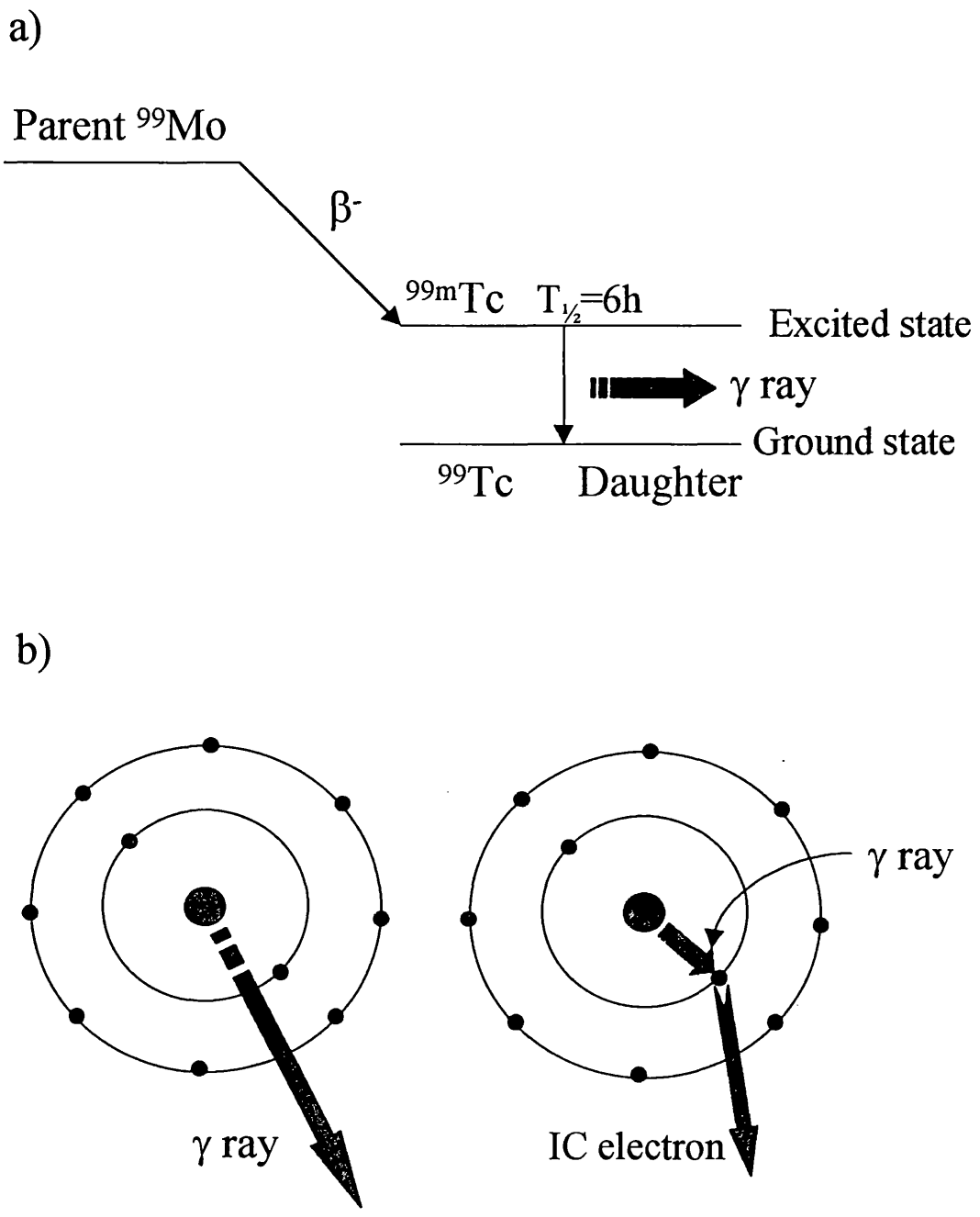

Figure 2.2.1 *a) Shows the decay of molybdenum-99 via beta emission to the metastable daughter technetium-99m, which decays with a half-life of 6 hours and the emission of gamma radiation. b) The emitted gamma radiation can eject one of the orbiting electrons. The emitted electron is called the internal conversion electron and all of the energy of the gamma radiation is transferred to the electron to overcome the binding energy.*

Importantly, it is these electrons that form the autoradiographic image on the film (figure 2.2.1).

2.2.2.2 Iodine-125

When the nucleus of an ^{125}I atom decays both gamma rays and electrons are emitted as a result of the nucleus achieving the ground state. The half-life for this decay process is 60 days, which provided a suitable period of time to perform dual autoradiography (section 2.2.5). As in the case of $^{99}Tc^{m}$, it is the emission of electrons during the decay process that cause the resultant image on the autoradiographic emulsion. The principal gamma emission is 27 keV with a approximate mean electron energy of 31 keV.

2.2.3 Image formation

The emulsions of the film can be exposed by light, X-rays, gamma-rays or moving charged particles. Typically in autoradiography, it is the moving charged particles that result in exposure. The understanding of the interaction of charged particles and film stems from the theory on the interaction of light with crystals in emulsions known as the Gurney-Mott hypothesis, first proposed in 1948 (Gurney and Mott, 1948). This theory states that when a light photon interacts with a silver halide crystal (silver bromide:silver iodine, 10:1) in the emulsion, a bromide ion is oxidised to atomic bromine with the concurrent release of an electron. Released electrons tend to drift toward sites of crystal imperfections, such as areas where the strain in the crystal has caused a silver ion to migrate out of the lattice or to the silver sulphide sensitivity speck. The electron attracts one of the mobile interstitial silver ions and atomic silver is formed. The atomic silver then acts as temporary trap for additional electrons that are released from other photon interactions with the crystal. When the additional electrons are released from interactions with light and drift toward the silver atoms, additional

silver ions are then attracted to form more atomic silver. These small clumps of silver are known as "latent image centres". Charged particles interact with grains of silver halide in a different manner from that of light photons. When an electron or positron strikes a crystal, the interaction produces many areas of lattice distortion, with the subsequent release of many electrons. Thus, a single interaction of a charged particle with a grain can render the grain developable. Also a single, charged particle can interact with many grains as it passes through the emulsion.

2.2.4 Single radionuclide autoradiographic studies

In macroautoradiography, the resolution does not approach the cellular level, and therefore tissue fixation to preserve cellular morphology is generally not needed. After removal from the animal, the tissue is frozen to prevent diffusion of the tracer. The necessary rate of freezing is a function of the diffusion rate of the tracer. For highly diffusible tracers such as iodoantipyrine, the tissue is usually immersed in liquid nitrogen or freon to achieve very rapid (less than 1 min) freezing. For less mobile tracers such as deoxyglucose or isopropyliodoamphetamine, it is adequate to bury the tissue in powered dry ice for several minutes. After the tissue is frozen, it is transferred to a microtome kept at - 20°C. The tissue is allowed to equilibrate for at least 1 hour and is then sectioned into thin slices, usually 20 to 40 μm. Thinner slices require longer exposure durations without significant improvements in resolution, and thicker slices have decreased resolution and problems of variation in internal absorption of the beta emissions. The cut brain sections are placed on glass cover slips and dried rapidly by placing the cover slips on a hot plates. The cover slips are then placed on the film with the tissue in contact with the emulsion side. It is very important to have close contact to achieve maximum resolution.

2.2.4.1 Quantitation using long-lived radionuclides

The most common long-lived radionuclides used in macroautoradiography are ^{3}H and ^{14}C, with half-lives of 12 and 5,700 years, respectively. Quantitation is performed by comparing the amount of darkening produced by the exposure from tissue sections containing either ^{14}C or ^{3}H, to that produced by calibrated standards. Methylmethacrylate standards containing 8 to 12 different levels of ^{14}C activity are available commercially. However, before they can be used for quantitative autoradiography, they must be calibrated to units of activity per gram of ^{14}C for a standard tissue thickness. This latter process is sometimes performed by the manufacturer.

2.2.4.2 Quantitation using short-lived radionuclides

Standards are not commercially available for short-lived radionuclides, which therefore must be produced in-house. To manufacture a standard, different concentrations of the nuclide being used are added to homogenates of tissue (figure 2.2.2). The tissue is sectioned to produce autoradiographic standards and a portion of it is weighed and counted to give the equivalent activity per gram. These standards are placed onto every autoradiographic film to convert the optical density of the image to activity. Although this is the most straight forward method of quantitation, its use is limited with nuclides of very short half-life, because standards must be produced for every experiment, which is a tedious process. To avoid producing a new set of standards for each experiment, I cross calibrated a standard of ^{99m}Tc against a commercially available standard of ^{14}C. Thus by placing the cross calibrated ^{14}C standard onto the film with brain sections containing ^{99m}Tc-HMPAO, the optical density on the film could be converted to ^{14}C activity and finally to ^{99m}Tc activity through the cross calibration curve (Chapter 4).

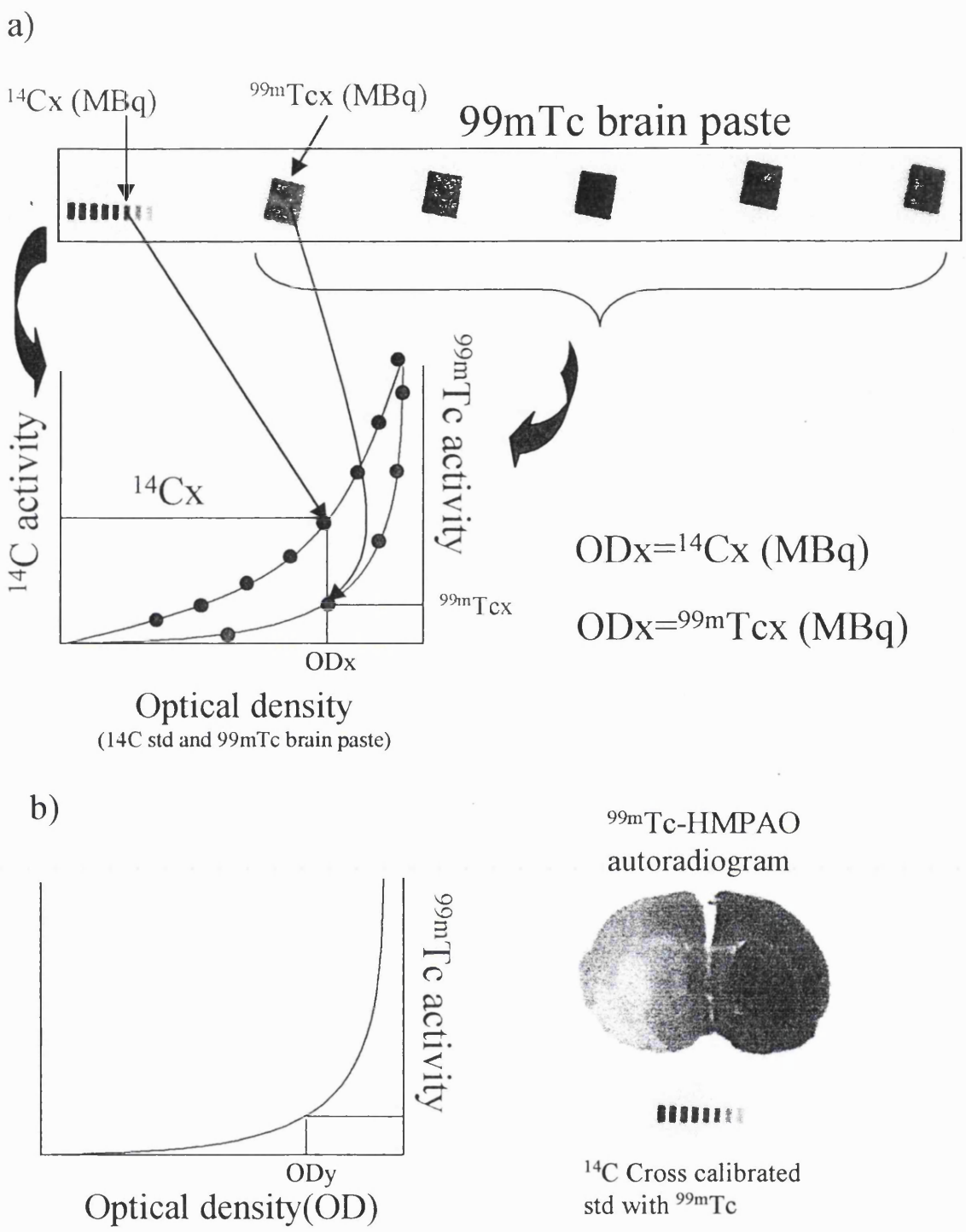

Figure 2.2.2 *a) ^{99m}Tc was added to homogenate of rat brain tissue and cut sections were placed in contact with the film to give a range of activities and therefore optical densities (OD). ^{14}C standards are placed on the same film and a graph of OD vs activity was plotted. From the two standard curves, the ^{99m}Tc activity required to produce a given OD can be related to the ^{14}C activity which gives the same OD. Thus in (b) the ^{14}C standard curve can be used to calculate the ^{14}C equivalent activity of any region in the ^{99m}Tc autoradiogram, and the cross-calibration can be used to convert this into ^{99m}Tc activity (see Chapter 4 for further details).*

2.2.5 Dual radionuclide autoradiographic studies

In this thesis, two images are produced from a single tissue section containing both ^{99m}Tc-HMPAO and ^{125}I-IAZA (figure 2.2.3). Using the properties of the half-lives ($T_{½}(^{99m}Tc)$ =6hrs, $T_{½}(^{125}I)$ =60d) and varying levels of administered activity, it is possible to obtain images of CBF and hypoxia without cross-contamination. The first image, which was that of ^{99m}Tc-HMPAO, was produced after the brain section has been in contact with the film for a period of 7-8 hours. During this time the low level of activity from the ^{125}I-IAZA was not sufficient to create any exposure on the film, therefore the first image contains information from the distribution of ^{99m}Tc-HMPAO in the brain section[2]. Subsequently, the section was removed from the film for approximately 4 days, during which time the ^{99m}Tc decayed to a negligible level (0.0015% of original activity). The section was then placed back in contact with another film and a second exposure for 1 week was then produced, which resulted from the ^{125}I emission. The timings and administered activity were chosen to optimised the purity of each image and optical density (methodology in Chapter 4). Finally a ^{14}C standard cross-calibrated against ^{99m}Tc was placed on the film with the ^{99m}Tc-HMPAO images for quantitation of CBF, and commercially available ^{125}I standards were placed on the film to calibrate the hypoxic images.

---

[2] To test whether the exposure from the ^{125}I cross-contaminated ^{99m}Tc-HMPAO image, sections of tissue containing only ^{125}I-IAZA were place on a film for the same length of time necessary to produce the CBF image (7-8 hours). During this period of time, the ^{125}I-IAZA did not produce any detectable image.

a) ^{99m}Tc-HMPAO autoradiograms and cross calibrated ^{14}C standard

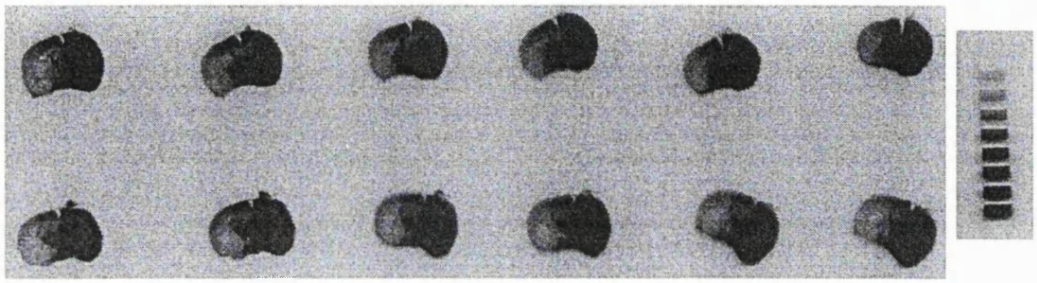

b) ^{125}I-IAZA autoradiograms and ^{125}I standard

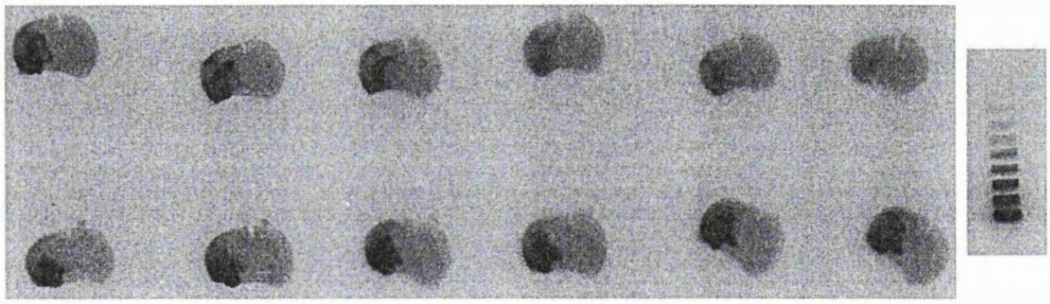

Figure 2.2.3 *a) sections containing both ^{99m}Tc-HMPAO and ^{125}I-IAZA are placed on a film for approximately 7 hours, to obtain the image of ^{99m}Tc-HMPAO (CBF). b) subsequently the sections are removed and 4 days later placed in contact with a second film to obtain the image of ^{125}I-IAZA (hypoxia) for approximately 1 week. Cross calibrated ^{14}C standards are placed in contact with film containing the ^{99m}Tc-HMPAO images and ^{125}I standards are placed in contact with film containing the ^{125}I-IAZA images.*

2.2.6 Hexamethyl-propylene-amine-oxime (^{99m}Tc-HMPAO)

For the past decade ^{99m}Tc-HMPAO has been used as the clinical marker for CBF in single photon emission computed tomography studies (SPECT) (figure 2.2.4). The imaging of CBF using ^{99m}Tc-HMPAO has a wide variety of uses in both neurological and psychiatric disease including, cerebrovascular disease, schizophrenia, epilepsy, Parkinson's disease, Alzheimer's disease, as well as functional imaging (Messa *et al.* 1995). Hexamethyl-propylene-amine-oxime is a lipophilic ligand that is extracted by the brain on its first pass through the cerebral circulation. Thereafter, the molecule is rapidly converted to a hydrophilic form, causing entrapment in the brain proportional to regional CBF (Bullock *et al.* 1991). Autoradiographic investigations using ^{99m}Tc-HMPAO are limited in number and are mostly confined to biodistribution studies (Hoffman *et al.* 1988a; Lear, 1988a) or validation as marker for CBF (Lear, 1988; Bullock *et al.* 1991). Although ^{99m}Tc-HMPAO is widely used clinically, it has found limited use as a marker to investigate CBF in autoradiographic studies. This is mainly due to the difficulties of absolute quantitation, so that only relative (% change from a selected region) values of CBF can be calculated, which are accurate for flows less than 120 ml/100g/min (Bullock *et al.* 1991). However the main advantage for this study is that ^{99m}Tc-HMPAO does not redistribute in the brain and therefore provides a 'snapshot' of CBF at the time of the injection (Sharp *et al.* 1986).

The first clinical studies using ^{99m}Tc-HMPAO were performed at the Middlesex Hospital Medical School (Ell *et al.* 1985), which were subsequently extended by the university of Aberdeen (Sharp *et al.* 1986) and confirmed that ^{99m}Tc-HMPAO and in particular the d,l isomer was well retained in the brain with a washout less than 1% per

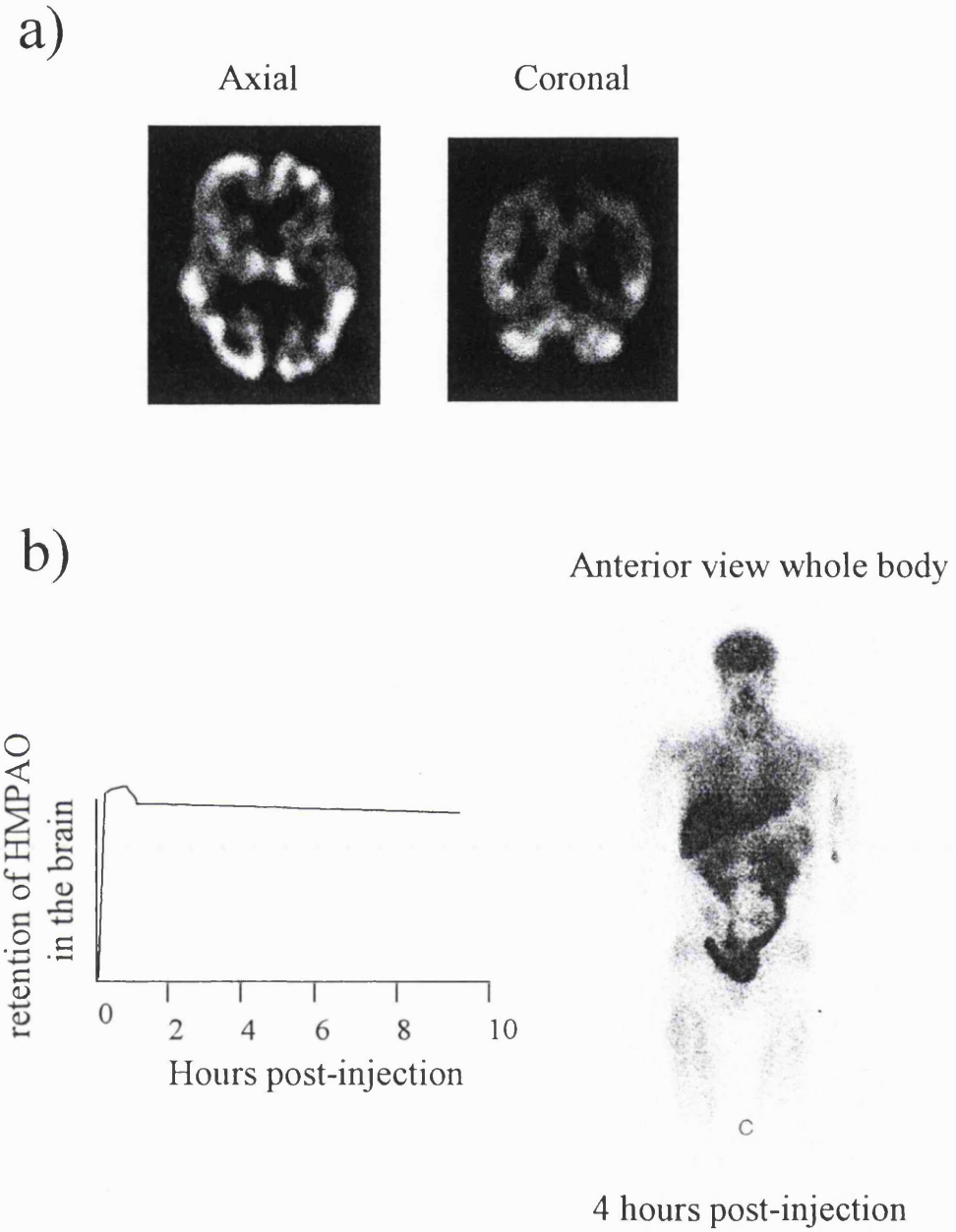

Figure 2.2.4 *a) SPECT images of CBF from a normal patient using ^{99m}Tc-HMPAO b) time course of the retention of ^{99m}Tc-HMPAO in the brain indicates minimal redistribution of ^{99m}Tc-HMPAO during the first 10 hours. The whole body images shows the biodistribution of ^{99m}Tc-HMPAO 4 hours post-injection. 5% of the injected ^{99m}Tc-HMPAO localises in the brain.*

hour (figure 2.2.4). The human distribution reflected the findings in rats (Costa *et al.* 1986; Sharp *et al.* 1986) and indicated that in man, approximately 5% of the injected dose localises in the brain, and about 86% of this activity remains 24 hours after injection.

2.2.7 Iodoazomycin arabinoside (^{125}I-IAZA)

A class of compounds that are known to undergo hypoxia-dependent binding are nitroimidazoles, and in 1979 Chapman (Chapman, 1979) demonstrated the use of a radiosensitising agent, misonidazole, for the non-invasive detection of hypoxic tissue. This agent is preferentially retained within hypoxic cells, following reduction of the 2-nitroimidazole group by cellular reductase enzymes, and binding to cellular components. However, in the presence of normal oxygen the molecule is immediately reoxidised and is not available for further reduction and trapping. Nor is the tracer retained in severely damaged tissue in which the enzymes necessary for the initial reduction are compromised. Uptake of this tracer during cerebral ischaemia was first investigated in a gerbil model (Hoffman *et al.* 1987), where it was demonstrated that misonidazole would cross the intact blood brain barrier and distribute within ischaemic tissue. Further development of this tracer led to another nitroimidazole derivative, 99mTc0 (PnAO-1-(2-nitroimidazole)) (BMS-18132), which was tested in the rat middle cerebral artery occlusion (MCAO) model (Di Rocco *et al.* 1993). Uptake was observed in regions which had a reduction in blood flow below 50 ml/min/100g, although not in the infarct region, suggesting that retention of the tracer delineated tissue at risk of infarction. A recent preliminary clinical study, using this marker in three stroke patients, has been shown to have a similar pattern of uptake as in the animal study (Baron *et al.* 1998). Another clinical study investigating patients with

stroke using a hypoxic marker was performed by Yeh et al. (Yeh *et al.* 1994) using ^{18}F-fluoromisonidazole and PET, which confirmed uptake in three out of the six patients they imaged within 2 hours of the insult.

Mannan et al. (Mannan *et al.* 1991) developed a further 2-nitroimidazole derivative for imaging hypoxia that may be labelled to a single photon emitter, the iodinated sugar iodoazomycin arabinoside (IAZA). Initial studies of this compound have demonstrated hypoxia-dependent binding in EMT-6 cells (Mannan *et al.* 1991). Clinically, increased uptake of IAZA has been observed in areas of decreased perfusion (measured by 99mTc-HMPAO) in patients with various carcinomas including brain metastases from small-cell lung carcinoma (Groshar *et al.* 1993) and patients with diabetes mellitus (Al-Arafaj *et al.* 1994). It is the use of this compound which is described in this thesis.

Chapter 3

3. Application of Magnetic Resonance Imaging and the Radiopharmaceuticals ^{99m}Tc-HMPAO and ^{125}I-IAZA in Cerebral Ischaemia

3.1 MAGNETIC RESONANCE IMAGING

3.1.1 Proton density, T_1 and T_2 relaxation

Proton density, T_1-weighted and T_2-weighted MRI are conventional MRI methods used in the assessment of cerebral ischaemia. An increase in any of these parameters, during ischaemia, has been attributed to an increase in interstitial water due to the development of vasogenic oedema (Van Bruggen *et al.* 1994). In animals studies of focal ischaemia, T_1 and T_2 changes are not regularly detected during the first 2-4 hours after an ischaemic insult (Knight *et al.* 1994; Loubinoux *et al.* 1997) and a distinct increase in proton density is only detected after 48 hours (Knight *et al.* 1994). In 1975, using in vitro spectroscopy studies of excised tissue, NMR was clearly shown to detect the formation of vasogenic oedema (Bakay *et al.* 1975). Since this time, several studies have demonstrated that regions depicted on T_1 and T_2 images are oedematous, and correlate well with regions of tissue damage defined on post-mortem histology (Brant-Zawadzki *et al.* 1986; Pierpaoli *et al.* 1993). Further, ischaemia induced changes in T_2 appear to be more profound than changes in T_1 (Van Bruggen *et al.* 1994). This was apparent during 7 hours of MCAO in rats, in which the T_2 increased by 51% in the ischaemic lesion, whereas T_1 increased 29% above the pre-occluded value (Hoehn-Berlage *et al.* 1995a).

T_1 and T_2 images are acknowledged to provide information about cerebral vasogenic oedema several hours following a stroke. A possibility that an early increase (1-2 hours post-occlusion) in T_1 and T_2 is not due to vasogenic oedema, was suggested by Hoehn-Berlage et al. using a MCAO rat model, in which it was observed that an increase in T_1 and T_2 occurred at 1.5 hours following occlusion, although blood brain barrier breakdown was not detected (Hoehn-Berlage *et al.* 1995a).

3.1.2 Magnetisation transfer

Macromolecular protons (those attached to proteins) have resonance linewidths which are too broad to detect directly using conventional MRI. However, if these signals are selectively saturated using irradiation which is several kHz off-resonance with respect to the free water signal, a perturbation of the steady-state magnetisation of the free water protons is observed. This is caused by magnetisation transfer and cross-relaxation between the two coupled spin systems. Magnetisation transfer contrast (MTC) can be used to investigate the rate of exchange of magnetisation between the free and bound states, and the relative populations of the two states (Wolff and Balaban, 1989).

MTC imaging has been successfully applied in pathologies that alter structural integrity and relative macromolecular water composition in brain tissue, such as multiple sclerosis and other white mater lesions (Mehta *et al.* 1996). MTC imaging of ischaemic brain has not found wide application as yet. A few years ago Ordidge et al. (Ordidge *et al.* 1991) performed MRI of MTC following cerebral ischaemia in rats. They found a reduction in the magnetisation exchange rate between 'free' and 'bound' water protons, which was maximum after approximate 24 hours, however there was a reduction after

only 2 hours of ischaemia, which occurred before the onset of vasogenic oedema (Ordidge *et al.* 1991). More recent work demonstrated a decrease in MTC within 45 minutes of ischaemia (Ewing *et al.* 1998). This latter study suggests that a change in MTC may indicate more than vasogenic oedema.

3.1.3 Diffusion-weighted imaging

During the past 13 years, diffusion-weighted imaging (DWI) sequences have been developed that are sensitive to the self-diffusion of water (Le Bihan *et al.* 1986) and can detect ischaemic lesions at the earliest periods studied (Moseley *et al.* 1990) (figure 3.1). A widely accepted refinement of DWI is the measurement of the apparent diffusion coefficient of water (ADC), which provides a quantitative assessment of water diffusion (Van Bruggen *et al.* 1994). What follows is a description of DWI in the context of the mechanisms of change during ischaemia, CBF thresholds, metabolic correlations, time course in experimental and human stroke, and reperfusion.

3.1.3.1 Mechanisms of DWI decrease in stroke

Moseley et al. observed the first DWI changes in cerebral ischaemia and attributed this reduction of tissue water diffusion to an osmotically obliged shift of extracellular water to intracellular compartments as a result of a disruption of ion homeostasis and formation of cytotoxic oedema (Moseley *et al.* 1990). Later work by Benveniste et al. supported this hypothesis with studies in which the ADC decreased during induction of cytotoxic oedema by ouabain (a specific inhibitor of Na^+, K^+-ATPase) administration (Benveniste *et al.* 1992). It was suggested that the reduction of ADC is indeed caused by an influx of extracellular water, which has a high intrinsic diffusion, to intracellular compartments, where the water diffusion would be retarded due to various intracellular obstacles and the relatively high cytoplasmic viscosity. Consequently, it is now

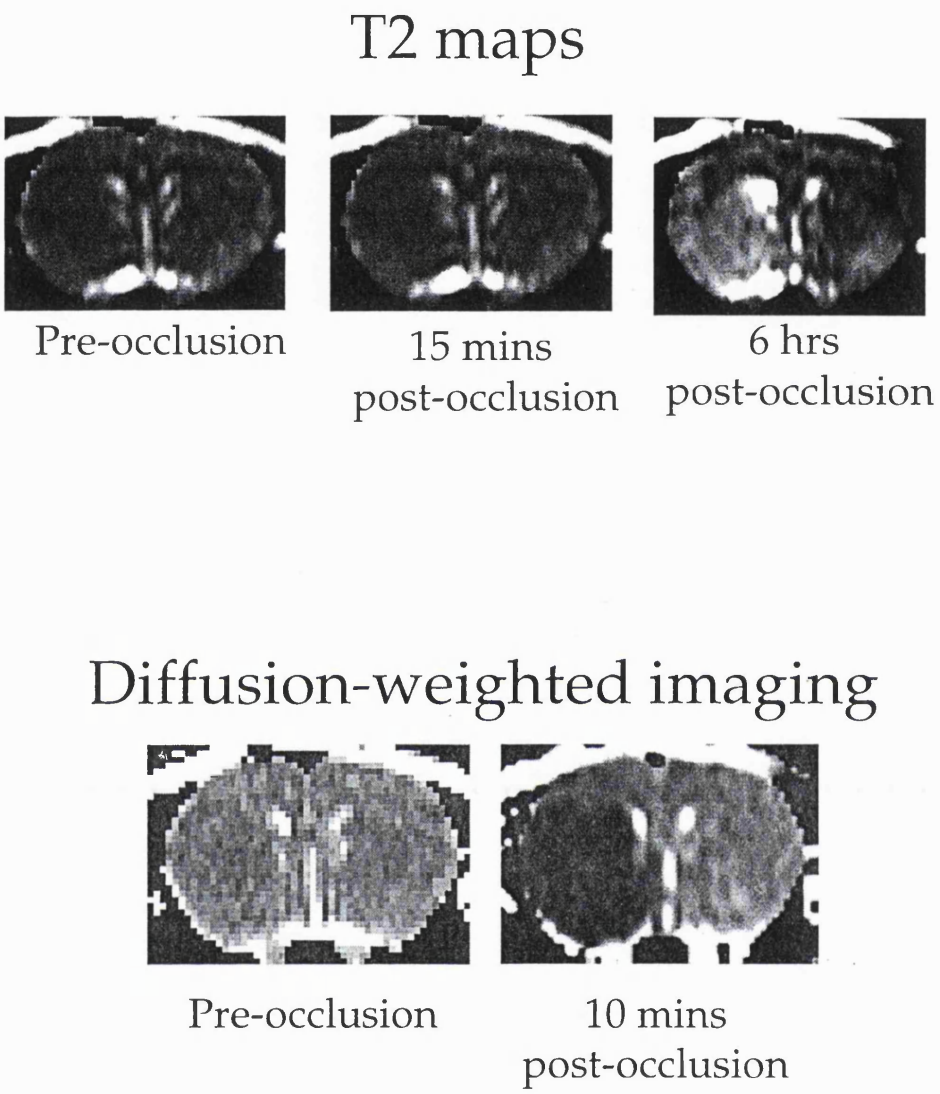

Figure 3.1 *T2 and ADC maps following MCA occlusion in the rat. Acquired at 8.5T using remote controlled occlusion of MCA. Note that at 10 minutes post-occlusion the ADC value has decreased yet at 15 minutes post-occlusion the T2 map is the same as pre-occlusion. T2 changes are very noticeable at 6 hours post-occlusion.*

accepted that an ischaemia induced drop of the tissue water ADC is associated with the development of cytotoxic oedema.

However the exact biophysical mechanisms of water ADC reduction are still unclear. Several hypothesis have been advanced to account for the biophysical mechanisms underlying the ADC changes in ischaemia. Latour et al. have suggested , for example, that DWI changes are caused by a reduction in extracellular diffusion due to an increase in the tortuosity of the extracellular space that occurs after cell swelling (Latour *et al.* 1994; Hasegawa *et al.* 1996). Alternatively, Helpern et al. suggested that a reduction in cell membrane permeability is the cause (Helpern *et al.* 1992), whereas DWI of intracellular metabolites indicate that a decrease in intracellular diffusivity might be involved (van der Toorn *et al.* 1994; Duong *et al.* 1998).

3.1.3.2 Relation of diffusion-weighted imaging to cerebral blood flow

In 1992, using a gerbil model of forebrain ischaemia, Busza et al. found that DWI signal enhancement only occurred when the CBF fell below 20ml/100g/min (Busza *et al.* 1992). Interestingly, this is similar to the flow threshold for the maintenance of tissue high-energy metabolism necessary for cellular ion homeostasis (Crockard *et al.* 1987; Verheul *et al.* 1992). These results differ to those achieved for the CBF threshold in a rat model of focal ischaemia, which was approximately 35 ml/100g/min (Kohno *et al.* 1995; Perez Trepichio *et al.* 1995). This discrepancy may be due to the species difference, or to the different properties of global and focal lesions. Further work, using a MCAO rat model, has shown a time dependent increase in CBF threshold from 34 ml/100g/min (30 minutes) to 41 ml/100g/min (120 minutes) over a 4 hours period, indicating the growing sensitivity of the tissue to perfusion deficits (Kohno *et al.* 1995). This work was confirmed by Mancuso et al., who demonstrated that after 30 minutes

the area occupied by more than 15% reduction in ADC corresponded to CBF levels below 25 ml/100g/min, and after 90 minutes this threshold had increased to 30 - 35 ml/100g/min (Mancuso *et al.* 1995).

3.1.3.3 Relationship of diffusion-weighted imaging to metabolic alterations

Mintorovitch et al. correlated DWI signal change with tissue water content, ATPase activity, and electrolyte content (Mintorovitch *et al.* 1994). Within 30 minutes of ischaemia DWI changes had occurred with a concomitant decrease of 30% to 40% in ATPase activity, while tissue water content and electrolyte concentrations were normal. By 60 minutes the ATPase activity had decreased further, the water and sodium content had increased, and the potassium concentration was lowered. These data indicate that DWI monitors very early disturbances of ion pumps, at times when such changes are thought to be potentially reversible. Autoradiographic techniques for measuring CBF, ATP, glucose, lactate and pH have been used to study the spatial relationship between DWI changes and metabolism following MCAO in the rat (Kohno *et al.* 1995). In contrast to diffusion-weighted changes observed in global ischaemia (Busza *et al.* 1992; Verheul *et al.* 1992), Kohno et al. reported that during the early phase of cerebral ischaemia (30 minutes) the area of hyperintensity seen on DWI was significantly larger than the region of ATP depletion, although it matched the area exhibiting tissue acidosis (Kohno *et al.* 1995). This difference became progressively smaller with the evolution of the lesion, such that by 7 hours the area of tissue damage, as indicated by DWI, was identical to the region of ATP depletion and histological infarction. If in fact DWI changes result from an alteration in compartmentation of tissue water, then the latter observations indicate that water redistribution occurs prior to the loss of high energy metabolism. These observations do not necessarily contradict the former statements, since the anaerobic production of metabolites, including lactate, can also

give rise to redistribution of water, which might be expected to result in DWI changes. Consistent with this, there is good agreement between lactate production and signal intensity changes seen with DWI following cardiac arrest in experimental animals (Decanniere *et al.* 1995). As mentioned, several studies have shown that cytotoxic oedema related changes in brain tissue water ADC, are paralleled by lactate accumulation, decrease in high energy phosphates and intracellular pH, and an increase in inorganic phosphate. A recent study showed that administration of the neurotoxin *N*-methyl-D-aspartate (NMDA) results in a ADC reduction, which is interesting as the NMDA mediated excitotoxicity neither leads to profound energy failure nor to a significant lactate accumulation, but does promote depolarisation, ion movements and cell swelling. Therefore the metabolic basis underlying the acute reduction in brain water ADC is different in an excitotoxic insult as compared to cerebral ischaemia (Dijkhuizen *et al.* 1996).

3.1.3.4 Lesion development and DWI change in animals and humans

It was first demonstrated, by the use of DWI, that the ischaemic lesion in both rat and cat expands primarily during the first 2 hours after MCAO (Roussel *et al.* 1994b; Hoehn-Berlage *et al.* 1995b) (figure 3.2). Although the lesion size has nearly fully evolved at 2 hours, the ADC value continues to decrease for a period of up to 4-6 hours following MCAO (40% of control) (Knight *et al.* 1994) (figure 3.2), with some studies indicating lowest ADC values at 24 to 48 hours (40-50% of control) (Hoehn-Berlage *et al.* 1995; Kohno *et al.* 1995). In the chronic stages of cerebral ischaemia, the ADC of water exhibits a different pattern. At approximately 24 - 48 hours after a vessel occlusion, the ADC rises and slowly returns to normal at 7 days (Knight *et al.* 1991; Helpern *et al.* 1993). Following this, a subsequent increase in the diffusion of water above the ischaemic control can be observed after 1 week (Verheul *et al.* 1992; Knight

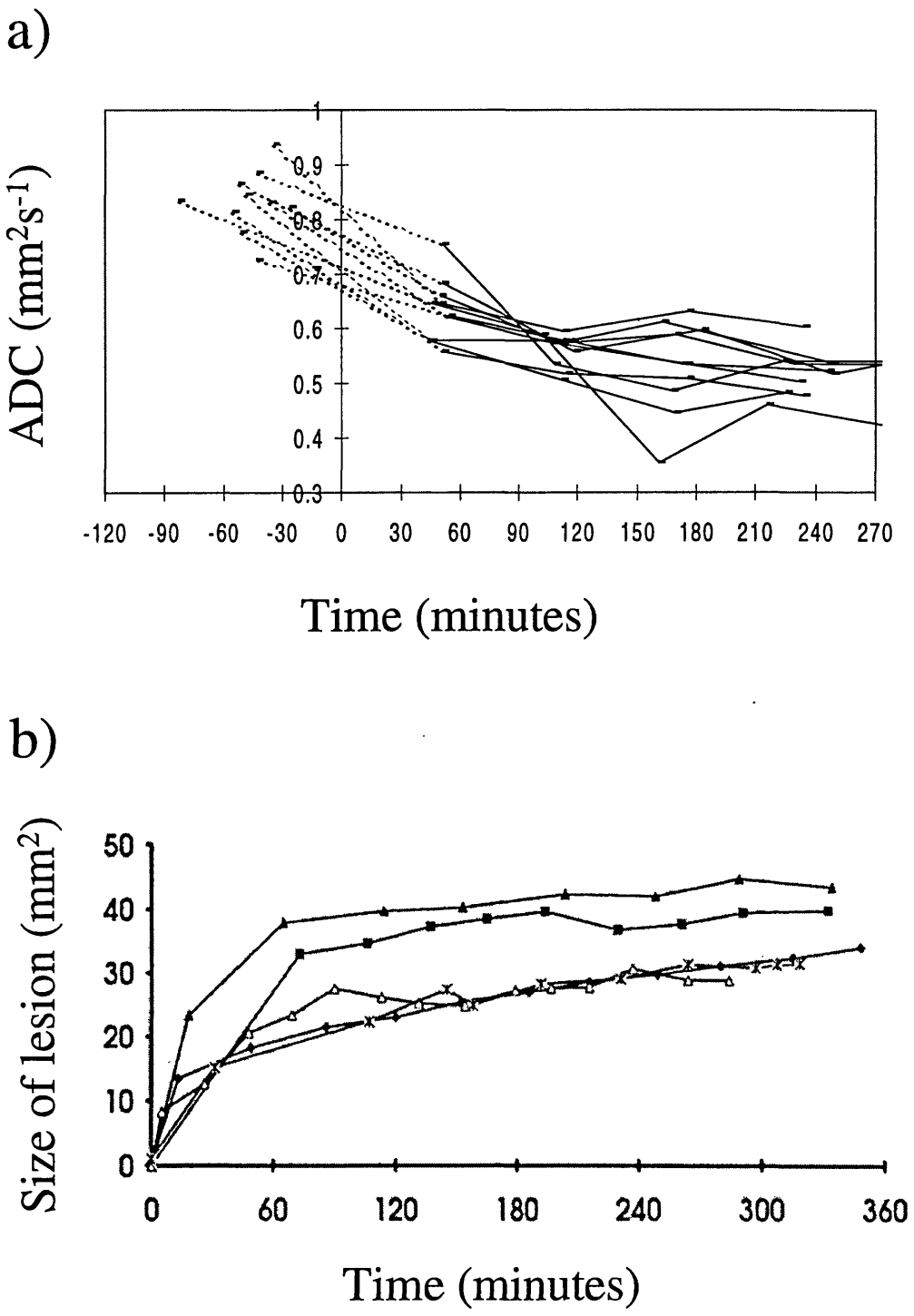

Figure 3.2 *a) ADC values from ten studies pre- and post-occlusion in a rat MCAO model. b) Lesion expansion monitored with diffusion-weighted imaging in five rats. (adapted from Roussel et al. 1994)*

et al. 1994)). The elevated ADC of tissue water, above control values, is associated with cellular lysis, the loss of cellular barriers, combined with excessive accumulation of oedematous water (Pierpaoli *et al.* 1993).

Following a stroke in man, a reduced ADC has been observed as early as 105 minutes after the initial onset (Warach *et al.* 1992) and as with the animal studies, a pseudo normalisation occurs at between 4 and 10 days (Baird and Warach, 1998). The large variation in human results may depend on the proposed method for the calculation of ADC with respect to diffusion anisotropy (Chapter 5). For diagnostic purposes, temporal evolution of ADC following a stroke provides information to discriminate between acute and chronic lesion, based on the low or high ADC value, provided the insult is imaged at the appropriate time (Baird and Warach, 1998).

3.1.3.5 Diffusion-weighted imaging during reperfusion

There are four ADC patterns that occur on reperfusion:

- The ADC remains decreased at the ischaemic level (Busza *et al.* 1992)
- The ADC normalises and remains normal (Mintorovitch *et al.* 1991)
- The ADC normalises followed by a secondary decline at approximately 24 hours (Thornton *et al.* 1997)
- The ADC normalises for a short period, then gradually declines (figure 3.3) (Pell *et al.* 1999a)

In 1991, Mintorovitch et al. first demonstrated that the hyperintense regions of the ischaemic brain seen on DWI could be reversed if the occlusion was removed 33 minutes after the MCAO in the rat (Mintorovitch *et al.* 1991). More recently it was

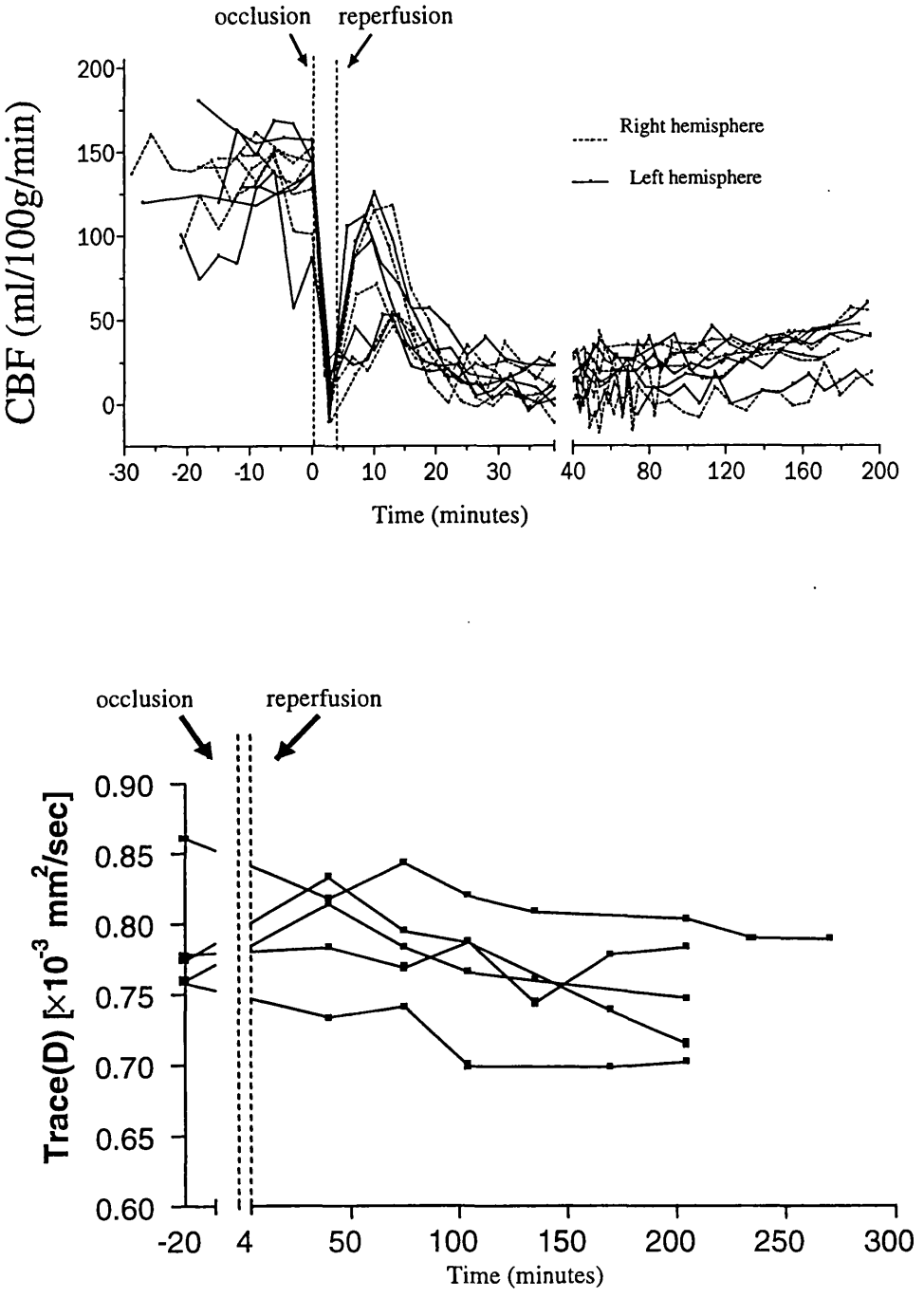

Figure 3.3 *CBF and ADC values pre- and post-four minutes of forebrain ischaemia in the gerbil. Note the slow decline in ADC values after reperfusion, subsequent to only four minutes of occlusion*

shown that the size of the lesion on the diffusion-weighted images declined if the flow was restored 1 hour following occlusion, but not after 2 hours (Minematsu *et al.* 1992). Even a 15 minute period of cardiac arrest in cats, which resulted in a decline of water ADC values, subsequently normalised within 30 minutes of successful cardiac resuscitation (Fisher *et al.* 1995). At this period in time, DWI furnished the observer with information about regions of reversibility within the area of DWI change, provided that time of ischaemia was considered. In the quest for better prognostic information, the DWI data were further refined using quantitative measures of the ADC of water. ADC thresholds for reversibility of the lesion in a rat MCAO model have been estimated to be either less than 0.55 $\times 10^{-3} mm^2 sec^{-1}$ (Dardzinski *et al.* 1993) or a reduction of greater than 0.25 $\times 10^{-3} mm^2 sec^{-1}$ relative to the contralateral hemisphere (Hasegawa *et al.* 1994). During MCAO in cats, lesions were reversible if reperfusion occurred before the ADC decreased to less than 70% of the control. These data may point to a prognostic role for the measurement of ADC values, although the temporal component cannot be ignored.

After reperfusion of a previously ischaemic region, the low ADC values can return to normal levels. However some studies are now reporting a secondary decline in ADC, which, as yet, is little understood. The secondary decline had been termed 'secondary' or 'delayed' energy failure and initial reports using MRS in infants suffering an hypoxic-ischaemia insult during birth, demonstrated a delayed fall in [PCr]/[Pi] (phosphocreatine/inorganic phosphate) at 24-48 hours (Azzopardi *et al.* 1989). This hypoxic-ischaemic condition has been recently modelled in piglets and a secondary decline has also been observed in ADC values (Thornton *et al.* 1997). This effect is not limited to a hypoxic-ischaemia insult, since a delayed ADC decrease, following

normalisation, has been observed at 24 hours post-reperfusion in a rat MCAO model (Van Bruggen *et al.* 1998). In another rat model, Dijkhuizen et al. using 20 minutes of hypoxic-ischaemia in adult rats, demonstrated secondary reductions of ADC at 24 hours (Dijkhuizen *et al.* 1998). This delayed effect has also been confirmed in the immature rat and may be suggestive of delayed neuronal death (Tuor *et al.* 1998). The underlying reasons for this process are still unclear, however hypoperfusion following reperfusion, produces gradual changes in ADC which could result from a mismatch between CBF and metabolic rate in the hypermetabolic post-ischaemic brain, giving rise to a delayed ADC decrease (figure 3.3) (Pell *et al.* 1999a).

3.1.4 Perfusion imaging

Over recent years, methods for measuring perfusion using NMR techniques have been proposed. These techniques have been made practically feasible by the development of ultrafast technology, which greatly increases MRI's efficiency in data collection and allows images to be acquired on the time scale required for the measurement of rapid physiological changes. Several different methods have been suggested, which are based on one of two approaches: (i) the use of contrast agents, or (ii) arterial spin labelling.

3.1.4.1 Contrast agents

Dynamic susceptibility contrast imaging (DSCI) is well suited to haemodynamic studies in the CNS. Gadolinium-DTPA (Gd-DTPA) enhanced T_1-weighted contrast is useful when the blood-brain barrier (BBB) is grossly disrupted. However when the BBB is intact, it has little impact on most brain regions since the intravascular space is small and T_1 effects occur locally. Unlike T_1 contrast, magnetic susceptibility (T_2 or T_2*) contrast results from microscopic variations produced by the heterogeneous distribution of high magnetic susceptibility contrast agents within a tissue's magnetic field. The

concept of susceptibility contrast was introduced by Villringer *et al.* (Villringer *et al.* 1988). Early studies reported that the injection of agents such as Gd-DTPA or $Dy(DTPA)^2$ led to a significant decrease in brain signal intensity on spin or gradient echo images (Villringer *et al.* 1988). This magnetic susceptibility effect results from local field gradients induced by intravascular compartmentalisation of the contrast agent. There are several parameters that can in principle be derived from DSCI and include: ΔR_2*, the change in effective transverse relaxation rate; CBV, cerebral blood volume; MTT, mean transit time; t_{peak}, the time between bolus injection and maximal ΔR_2*; and CBF, cerebral blood flow.

3.1.4.2 Arterial spin labelling

There are two distinct groups of methods: continuous and pulsed arterial spin labelling (ASL). Continuous ASL has been covered in Chapter 2 and is the technique for the assessment of perfusion in this thesis. Briefly, measurement of CBF using pulsed ASL is based on the observed changes in T_1 if a slice selective inversion is used to invert spins within the imaging slice. The entry of fully relaxed blood spins into the imaging slice increases the apparent relaxation rate, with the increase being directly proportional to flow.

3.1.4.3 MRI perfusion measurements in ischaemia

While DWI may provide unique information about the effect of an ischaemic insult as early as minutes postictus, it is clearly desirable to obtain information regarding the integrity of the vascular bed. Experimentally, Morawetz et al. showed that in a primate model, a reduction of CBF below 12 ml/100g/min for > 2 hours produces focal infarction, demonstrating a link between degree and duration of ischaemia and eventual tissue injury (Morawetz *et al.* 1974). Loss of perfusion during cerebral ischaemia was

demonstrated by Quast et al., who described absence of contrast agent passage on DSCI in the ischaemic core of a focal lesion in the rat (Quast *et al.* 1993). Interestingly, in the periphery of the lesion, they detected marginal perfusion without DWI changes. This was similar to a study using DWI and DSCI in a unilateral MCAO cat model, in which perfusion deficits not great enough to cause energy failure may go unnoticed on DWI (Morawetz *et al.* 1974; Roberts *et al.* 1993). The sensitivity of perfusion measurements to minor alterations in blood flow is illustrated in a cat model of hypoperfusion (Derugin and Roberts, 1994). The diffusion-weighted images show no evidence of abnormality in the territory of the occluded MCA, whereas the DSCI blood flow measurements show decreased CBF throughout the MCA region. DSCI may also be applied to examine haemodynamic alterations following reperfusion of the brain. A study into the effects of reperfusion after MCAO in cats revealed three types of reflow outcome: complete reperfusion (normalised t_{peak}); initial hyperaemia (short t_{peak}) and persistent hypoperfusion (longer t_{peak}). These three CBF patterns have now been quantified (ml/100g/min) using a pulsed ASL technique (Pell *et al.* 1999b). In addition, in studies of transient ischaemia or hypoxic ischaemia, DSCI has been used to detect the change in CBV during and after the insult (D'Arceuil *et al.* 1998). These data illustrate that CBF measured with either contrast agent or arterial spin labelling techniques, can explicitly measure responses of various haemodynamic parameters under conditions of ischaemia and reperfusion, and provided additional information to that of DWI alone.

In addition to animals models of cerebral ischaemia, DSCI and ASL have now been applied to the study of cerebral perfusion in humans. In patients studied with acute stroke, enlargement of the ischaemic lesion occurred when there was a larger perfusion

deficit (measured with relative MTT) but not when the perfusion abnormality was equivalent to or smaller than the DWI lesion (Baird and Warach, 1998). In addition to the MTT and DWI volumes, Sorensen et al. have studied the CBF and CBV perfusion parameters in acute stroke lesions. In 19 cases studied within 10 hours of onset, the volume of MTT abnormality (mean=119cm^3) and CBF abnormality (mean= 112cm^3) were larger than the mean CBV (47 cm^3) and the mean DWI volume (35 cm^3). The final infarct volume (mean 67 cm^3) was between the DWI/CBV and the MTT/CBF volumes (Sorensen *et al.* 1997). These data indicated the importance of measuring multiple parameters during the investigation of stroke.

*3.1.5 Blood oxygenation level-dependent MRI - T_2 and T_2**

Blood oxygenation level-dependent (BOLD) MRI is based on the magnetic properties of blood which is dependent on the oxygenation state of haemoglobin (Thulborn *et al.* 1982; Ogawa *et al.* 1990). Because deoxygenated haemoglobin is more paramagnetic than oxygenated blood and normal tissue, it can act as an endogenous intravascular paramagnetic contrast agent. This phenomenon is now widely used for MR functional neuroimaging, in which local increases of image intensity have been observed in association with specific brain activation tasks. However, the most elementary analysis of the biophysical and haemodynamic events relating to brain activation lead to the conclusion that many factors can affect the MR signal in such studies. The list includes blood volume, blood flow, arterial and venous haemoglobin saturation, oxygen extraction rate, blood viscosity and haematocrit. Deoxygenation results in an increased magnetic susceptibility difference (due to an increase of paramagnetic deoxyhaemoglobin) in and around the vascular compartment, and thereby is expected to cause signal loss in both T_2*- and T_2-weighted images.

Since BOLD MRI is sensitive to changes in regional tissue oxygenation status, it can be used to monitor acute deoxygenation following induction of ischaemia as well as reoxygenation after reperfusion (De Crispigny *et al.* 1992; Roussel *et al.* 1995). Bold MR signal intensity, measured by T_2*-weighted MRI, drops immediately upon the onset of ischaemia, and rises when reflow occurs. A transient overshoot in signal intensity during reperfusion has been described and may reflect post-reperfusion hyperaemia (De Crispigny *et al.* 1992). These haemodynamic responses indirectly report on local changes in CBF, CBV and oxygen extraction fraction and their individual contributions cannot easily be distinguished. More recently, early changes in T_2 values have been reported in conditions of ischaemia (Busza *et al.* 1994; Grohn *et al.* 1998) and oligaemia (>25 minutes post-occlusion) (Grohn *et al.* 1998). In the latter studies of cerebral ischaemia, two patterns were observed following an initial T_2 decrease:

(i) T_2 values remained depressed throughout the study without an ADC change- indicating a mild hypoperfusion condition (Grohn *et al.* 1998).

(ii) T_2 and ADC values are decreased throughout the study, indicating a severe hypoperfusion condition (Roussel *et al.* 1995).

The combination of T_2* or T_2 and ADC measurements may provide MRI tissue signatures for the status of the tissue. These data highlight that changes in T_2 are not always related to vasogenic oedema and early changes in T_2 may provide information as to the pathophysiological nature of ischaemia or oligaemia, which is investigated further in Chapters 6 and 7.

3.2 RADIOPHARMACEUTICALS OF CBF (^{99m}Tc-HMPAO) AND HYPOXIA (^{125}I-IAZA)

3.2.1 ^{99m}Tc-HMPAO

3.2.1.1 Autoradiographic use of ^{99m}Tc-HMPAO

^{99m}Tc-HMPAO was the first commercially available ^{99m}Tc-labelled radiotracer to study regional brain perfusion in patients with single photon emission computerised tomography (SPECT) (Ell *et al.* 1985a). Since its introduction, ^{99m}Tc-HMPAO has become widely accepted as the clinical marker for measurement of CBF with SPECT gamma cameras (Messa *et al.* 1995). Autoradiographic investigations using ^{99m}Tc-HMPAO are limited in number and are mainly confined to biodistribution studies (Hoffman *et al.* 1988b; Lear, 1988b) or validation as a marker for CBF (Lear, 1988; Bullock *et al.* 1991). Chapter 4 reports on two studies investigating the pathophysiology of cerebral ischaemia, used HMPAO as a CBF marker to compare with a hypoxic tracer and various MRI parameters in a rat MCAO model. The rapid trapping of HMPAO was well suited to these studies and allowed an image of blood flow at 2 hours post-occlusion to be compared with MRI at various time points before sacrifice in the same animal.

3.2.1.2 Clinical use of ^{99m}Tc-HMPAO

The clinical utility of ^{99m}Tc-HMPAO in the investigation of cerebrovascular disease was first demonstrated in 1985 (Ell *et al.* 1985b). Following this work, stroke patients imaged using ^{99m}Tc-HMPAO, demonstrated perfusion deficits without abnormality in X-ray CT (De Roo *et al.* 1989; Feldmann *et al.* 1990) and thus raised the question of additional information from CBF maps (figure 3.4). More recently, studies have shown

^{99m}Tc-HMPAO CT scan

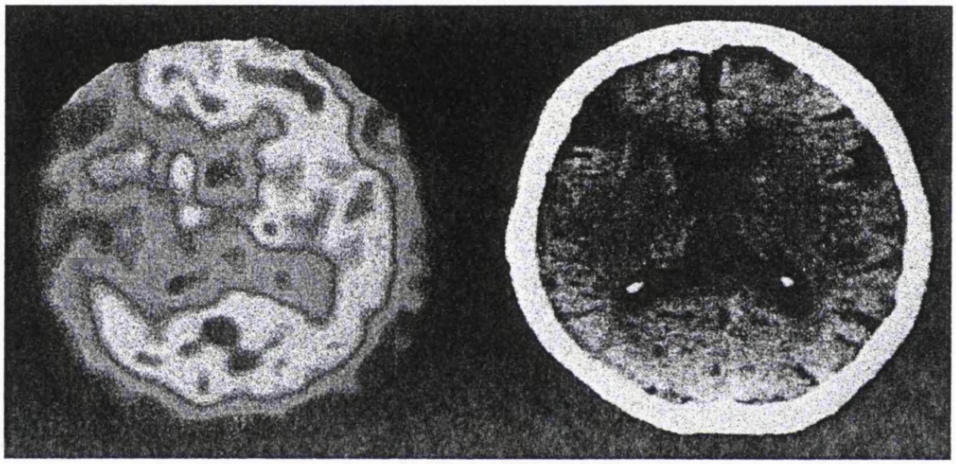

Figure 3.4 *84 year old subject with a thrombotic embolism of the right middle cerebral artery. Acute ^{99m}Tc-HMPAO SPECT imaging demonstrated a large perfusion deficit with minimal change on the CT scan. (Feldmann et al. 1990)*

the prognostic value of ^{99m}Tc-HMPAO SPECT images in predicting stroke outcome (Alexandrov *et al.* 1996; Bowler *et al.* 1996), although the additional clinical contribution, over and above neurological scoring is still unclear. Following reperfusion of an ischaemic insult, a marked increase in blood flow may be observed and is known as luxury perfusion (Lassen, 1966). Jorgensen et al. (Jorgensen *et al.* 1994) showed that patients displaying early (<1 week) reperfusion in the site of previously absent perfusion, recovered better than those with late (>1 week) reperfusion. In a large population study, Barber et al., using ^{99m}Tc-HMPAO SPECT imaging, observed spontaneous reperfusion following stroke, which was shown to be relatively common (55% of patients), although full reperfusion was never apparent. In this latter study, a pattern of spontaneous reperfusion and luxury perfusion was correlated with clinical improvement and better patient outcome (Barber *et al.* 1998). This work emphasised the prognostic value of measuring hypoperfusion deficit volumes, although did not state the advantage over neurological measures (Barber *et al.* 1998). Even though several studies have investigated the luxury perfusion syndrome, the exact prognostic value appears to be still unclear and may need to be combined with further information for a complete clinical picture (Barber *et al.* 1998). The phenomenon of diaschisis (a matched depression of CBF and metabolism in the contralateral hemisphere to the insult), both in the cerebellum and the cortex, can be observed using ^{99m}Tc-HMPAO, and may be a suitable technique to monitor treatment of this secondary effect (Infeld *et al.* 1995). The clinical availability of ^{99m}Tc-HMPAO encourages the use of this tracer to monitor and stratify patients for therapeutic trials, and has been used by several institutions (Hanson *et al.* 1993; Baird *et al.* 1994). There have been many reports of the wide use of ^{99m}Tc-HMPAO (Messa *et al.* 1995),

although it is important to remember that one imaging modality, will not as yet, produce an accurate clinical diagnosis and prognosis of stroke

3.2.2 ^{125}I-IAZA

There has only been one reported study using ^{125}I-IAZA to image cerebral hypoxia.. This was a clinical investigation in which uptake of ^{123}I-IAZA was observed in brain metastases with low perfusion (Groshar *et al.* 1993). In chapter 4 I report on two further autoradiographic studies which compare ^{125}I-IAZA with the autoradiographic tracer ^{99m}Tc-HMPAO and several NMR parameters.

Chapter 4

4. The Relationship between Magnetic Resonance Diffusion Imaging and Autoradiographic Markers of Cerebral Blood Flow and Hypoxia in an Animal Stroke Model

In this chapter I report on the combination of MRI and the nuclear medicine markers of cerebral blood flow and cerebral hypoxia in ischaemia. The aim of this study was to examine the relationship between the MRI parameters of diffusion and T_2, and the nuclear medicine markers ^{99m}Tc-hexamethylpropylene amine oxime (^{99m}Tc-HMPAO) and ^{125}I-IAZA, together with histology in a rat MCA occlusion model. The main findings of this investigation were as follows:

- The hypoxic marker (^{125}I-IAZA) accmulates in cerebral tissue when the blood flow decreases to a level of 34 ± 7% of the normal flow.
- Two hours following middle cerebral artery occlusion the lesion distributions from the diffusion maps and hypoxic autoradiographs were comparable, indicating similar blood flow thresholds.
- The combination of diffusion or hypoxic images with perfusion maps allowed differentiation between four regions:

  i) normal tissue;

  ii) a region *oligaemic misery perfusion* - moderately decreased perfusion but normal diffusion and normal uptake of hypoxic marker;

  iii) a region of i*schaemia* - severely decreased perfusion, decreased diffusion and increased uptake of hypoxic marker;

  iv) a region lesion core - of decreased perfusion, decreased diffusion and low uptake of hypoxic marker.

4.1 INTRODUCTION

Following a stroke, the ability to discriminate between areas of non-recoverable tissue and potentially salvageable tissue remains a goal of diagnostic imaging (Fisher, 1997). Currently there is no single investigation that allows a complete diagnosis and prognosis, and it therefore remains important to utilize information from a variety of imaging methods with differing sensitivities to normal and abnormal physiology. There have been a number of relevant developments both in nuclear medicine and in magnetic resonance imaging (MRI) techniques, and in this work I report on the combined use of these techniques for the evaluation of focal pathophysiology in the rat model of middle cerebral artery occlusion (MCAO).

The nuclear medicine protocol combined two autoradiographic markers, the cerebral blood flow (CBF) tracer ^{99m}Tc-hexamethylpropylene amine oxime (^{99m}Tc-HMPAO), and the hypoxic marker ^{125}I-iodoazomycin arabinoside (^{125}I-IAZA). For the past decade ^{99m}Tc-HMPAO has been used as a clinical marker for CBF in single photon emission computerised tomography (SPECT) gamma camera studies, both in adults and in children (Messa *et al.* 1995). The hypoxic marker (^{125}I-IAZA) not been used to image cerebral ischameia before, although there is one report of uptake in a hypoperfused region of brain metasteses (Groshar *et al.* 1993).

The present study combines the use of two autoradiographic markers - the blood flow tracer ^{99m}Tc-HMPAO, and the hypoxic marker ^{125}I-IAZA - with apparent diffusion coefficient (trace) imaging (van Gelderen *et al.* 1994; Miyabe *et al.* 1996) and histology, with a view to providing a better definition of pathophysiology than can be obtained with either nuclear medicine or magnetic resonance techniques alone.

4.2 MATERIALS AND METHODS

4.2.1 Animal preparation

Experiments were performed under a protocol in accordance with national animal studies legislation. Five male Wistar rats (120-130g) underwent occlusion of the MCA using a modified intraluminal suture approach (Koizumi *et al.* 1986; Zea Longa *et al.* 1989; Roussel *et al.* 1994). Anaesthesia was induced using 3% halothane/O_2, while surgery was carried out using a concentration of 1.5% halothane/O_2. Following the surgery the halothane was reduced to 0.8% with a change to N_2O/O_2 (70/30%). Venous catheters were introduced into the femoral vessel for injection of radiopharmaceuticals. Occlusion of the MCA was carried out before introduction into the vertical magnet. Using an operating microscope, the right CCA was exposed by longitudinal midline incision from the submandibular triangle to the supraclavicular notch. The internal carotid artery (ICA) was isolated up to the carotid canal at the base of the skull. Both vagus and hypoglossal nerves were carefully dissected from both the ICA and CCA. A microvascular clip was placed on the common carotid artery at the junction of the external and internal carotid arteries. A blunted 3/0 nylon thread occluder was introduced into the common carotid artery via a small incision, a suture was placed around the common carotid artery to prevent bleeding, and the clip was then removed. The occluder was advanced under visual inspection to the internal carotid artery in the carotid canal, and MCAO was completed by advancing the thread 8 mm into the circle of Willis (Roussel *et al.* 1995).

To minimise motion artefacts during imaging, the skin was reflected from the dorsal aspect of the skull and connective subcutaneous tissue removed between the lambda

and bregma. A strip of clear plastic, securely fixed onto the animal probe, was glued to the area of cleaned skull using an epoxy resin. No discernible image artefacts were produced from the epoxy glue.

Following arterial occlusion the animal was placed in the magnet and the radionuclides were injected at 2 hours post-occlusion, at which time the diffusion-weighted images were acquired. T_2-weighted data were acquired 7 hours post-occlusion, after which animals were decapitated and brains removed and frozen for autoradiography and histology.

4.2.2 Magnetic Resonance Imaging

Rats were imaged in an 8.5T vertical magnet (Oxford Instruments, Oxford, UK.) interfaced to a SMIS (Surrey Medical Imaging Systems, UK.) console. A 38 mm birdcage coil was used as a transmitter/receiver. A 2 mm thick coronal slice 6 mm from the interaural line was studied. This image slice varied slightly depending upon the position of the animal on the imaging probe. Conventional DWI was performed using a pulsed-gradient spin-echo sequence with trapezoidal diffusion gradients along each of the X- (sagittal),Y- (axial) or Z- (coronal) axes in turn, at three 'b' values: 4 s/mm^2, 900 s/mm^2 and 1800 s/mm^2 (δ = 10 ms; Δ = 28 ms; diffusion gradient ramp = 1 ms). In order to minimise cross terms, the slice-rephase and read dephase gradients were applied immediately after and before the respective imaging gradients. Imaging parameters were: TR/TE = 1000/80 ms; slice thickness = 2 mm; FOV = 40 mm; data matrix = 128 × 64 views; 4 signal averages; imaging time = 12 min. Imaging was started 2 hours following MCAO. T_2-weighted data were acquired using a multi-spin-

echo sequence: TR/TE =1000/35,70,105,140; slice thickness = 2 mm; FOV = 40 mm; data matrix = 128 × 64 views; 4 signal averages.

4.2.3 Data processing

Apparent diffusion coefficient maps and T_2 maps were generated using routines written in the IDL software package (RSI, Boulder, Colorado). To obtain the ADC value (D), non-linear curve fitting of signal intensity (S) *vs.* gradient factor (b) was performed on a pixel-by-pixel basis according to the function (Le Bihan *et al.* 1986):

$$S = S_0 e^{-b D}$$

where S_0 represents the signal amplitude that would be obtained in the absence of diffusion sensitisation. Maps were generated with diffusion sensitisation applied along each axis (X-,Y- and Z-ADC), and then the diffusion tensor trace (ADC_{av}) images were calculated from the average of these three ADC maps (ADC_{av} = 1/3 Trace(D) $=1/3(D_{xx}+D_{yy}+D_{zz})$) (van Gelderen *et al.* 1994; Miyabe *et al.* 1996). T_2 maps were generated using a two-parameter (single exponential) fit on a pixel by pixel basis.

4.2.4 Autoradiography and Histology

Two hours following MCAO, 5 MBq of ^{125}I-IAZA in 0.4 ml of 0.9% NaCl and 100 MBq of ^{99m}Tc-HMPAO in 0.3 ml of 0.9% NaCl were injected via the femoral vein. The MCA remained occluded for a further 5 hours, at which time the brain was removed rapidly from the skull and placed in liquid hexane at -40°C. The frozen brain was sliced at -20°C into 20 μm sections, using a cryostat microtome. Tissue sections were thawed onto coverslips and immediately dried on a hot plate. Adjacent tissue sections were stained with haematoxylin and eosin to demarcate the area of infarct.

Double-labelled $^{99m}Tc/^{125}I$ autoradiography allows separate images of the distribution of the hypoxic marker and CBF from the same tissue section. Approximately 20 sections per brain were placed on autoradiographic film (Hyperfilm, Amersham) for 7-8 hours to acquire the CBF images; five autoradiographs per animal were used in the final analysis. This exposure time varied and was calculated from the initial activity and the time after injection at which sections were placed onto the film. Thus, each set of autoradiographs had a similar optical density range. Once these sections had been removed, eight precalibrated ^{14}C standards ranging from 39-1075 nCi/g (Amersham International, Amersham, UK), which had previously been cross calibrated with known amounts ^{99m}Tc activity, were placed on the film for 8 days and were used to calculate the ^{99m}Tc tissue concentrations. The ^{14}C standards had to be left on the film for this length of time due to their relatively low activity. Cross-contamination from the ^{125}I activity to the ^{99m}Tc-HMPAO optical density was confirmed to be negligible (<0.1%) after placing brain slice sections containing only ^{125}I-IAZA onto the autoradiographic film for the same length of time as the ^{99m}Tc-HMPAO sections.

To obtain the ^{125}I-IAZA autoradiographs (^{125}I $T_{½}$ = 60 days), the brain sections were placed on autoradiographic film (Biomax, Kodak) together with calibrated ^{125}I standards ranging from 1.3-640 nCi/mg (Amersham International, Amersham, UK) for 7 days; this procedure began 3 days after the completion of the ^{99m}Tc-HMPAO autoradiography to allow for complete decay of the ^{99m}Tc activity ($T_{½}$ = 6 hr), thereby avoiding cross-contamination of the hypoxic image.

4.2.5 Quantification

To calibrate the ^{99m}Tc-HMPAO autoradiographs in terms of relative activity, a ^{99m}Tc precalibrated standard with known activities must be placed onto the film with the cryostat sections. Due to the short half-life of ^{99m}Tc ($T_{½}$=6 hr) these standards are not commercially available and must be made for each experiment. Therefore I carried out a cross-calibration of ^{99m}Tc against ^{14}C standards. Brain paste sections, 20μm thick, were prepared with known amounts of activity (0.5-10 MBq). These were then exposed for 7-8 hr on autoradiographic film (Hyperfilm, Amersham). The ^{14}C standards ranging from 39-1075 nCi/g (Amersham International, Amersham, UK) were then exposed to the same film for 8 days. This extended period of exposure was required because of the low activity of the ^{14}C standards. After processing and digitisation of the film, optical density (OD) vs activity curves were constructed for both ^{99m}Tc and ^{14}C. Using the information from both these curves, ^{99m}Tc OD can be related to activity through the OD of the calibrated ^{14}C standards present on the film.

Both standards and autoradiographs were digitised using a CCD camera (KP-M1, Hitachi Denshi, Ltd.). The digitised autoradiographs were converted from units of optical density to activity (nCi/g) using the calibration function in the public domain program "Image" (NIH, Bethesda, MD, USA). No attempt was made to quantify the images in units of ml/100g/min. In this study I normalised the ^{99m}Tc-HMPAO autoradiograph activity to a region in the contralateral cortex, and the image was finally displayed as a percentage of that region. The ^{125}I-IAZA autoradiographs and precalibrated ^{125}I standards were similarly digitised and calibrated. Hypoxic images are displayed in terms of relative activity (RA) using a reference region in the contralateral cortex. ^{125}I-IAZA autoradiographs are subsequently displayed as relative activity.

4.2.6 Calculation of Lesion Areas

A histogram of the distribution of activities from the ^{125}I-IAZA autoradiograph was used to define the area of increased hypoxic marker uptake. The threshold for differentiating ischaemic from normal pixels was set at the minimum between the modes of the bimodal distribution (see Chapter 5). Using this threshold, areas of hypoxia were calculated from the ^{125}I-IAZA images as regions enclosed within the threshold value. These areas were expressed as a percentage of the area of the ipsilateral hemisphere (HLA%) to allow comparison with the diffusion ADC_{av} (trace) maps.

The area of ischaemic ADC_{av} decrease was defined from the ADC_{av} maps acquired 2 hours post occlusion. Using a histogram of the ADC_{av} map, a threshold for determining the area of ADC_{av} decrease was calculated from the minimum between the modes of the bimodal distribution. These areas were expressed as a percentage of the area of the ipsilateral hemisphere (HLA%) to allow comparison with the ^{125}I-IAZA images.

Cerebral blood flow was expressed as the percentage change from a reference region in the contralateral hemisphere of the ^{99m}Tc-HMPAO autoradiograph. The normal distribution of ^{99m}Tc-HMPAO uptake was calculated from a region in the contralateral hemisphere. Uptake more than 2SD below the mean was classified as decreased perfusion. Using this relative activity value an area for the decreased perfusion was calculated.

Areas of infarction defined from the haematoxylin and eosin stained sections were easily demarcated at 7 hours (Back *et al.* 1994; Hoehn-Berlage *et al.* 1995). Similarly,

regions of T_2 increase 7 hours post occlusion were readily delineated manually using "Image".

4.2.7 Blood Flow Thresholds

Four regions were discriminated on the basis of blood flow and hypoxic marker uptake: 1) a region of normal ^{125}I-IAZA and normal ^{99m}Tc-HMPAO uptake; 2) an area of decreased perfusion and normal ^{125}I-IAZA uptake; 3) an area of decreased perfusion and increased ^{125}I-IAZA uptake; 4) an area of decreased perfusion and low ^{125}I-IAZA uptake. Normal flow was calculated from the mean ± 2SD of a region in the contralateral hemisphere (region 1). The lower limit of normal flow (mean - 2SD) was used to define the threshold for decreased perfusion (region 2). The flow threshold for increased uptake of ^{125}I-IAZA (region 3) was calculated from the outline of the area of ^{125}I-IAZA uptake superimposed on a coregistered blood flow image. This was performed on five coregistered ^{125}I-IAZA and ^{99m}Tc-HMPAO autoradiographs from each animal, ranging from 3-8mm anterior to the interaural line. The flow threshold for low uptake of ^{125}I-IAZA (region 4) was calculated in a similar fashion.

The relationship between blood flow and hypoxia was further investigated using a pixel by pixel comparison of the coregistered autoradiographs of blood flow and hypoxia. A scatter plot of this relationship was constructed, in which the intensity of each point indicates the number of pixels in the autoradiographs with a discrete blood flow and ^{125}I-IAZA uptake.

A pixel by pixel comparison of a ADC_{av} map and blood flow image was not performed due to differences in spatial orientation of ADC_{av} images and autoradiographs.

Instead, the blood flow thresholds for the ADC_{av} images and comparison of lesion areas from autoradiographs were compared using HLA% (Back *et al.* 1994; Kohno *et al.* 1995).

4.2.8 Statistics

All values are given as means ± SD. Statistical comparison between groups was assessed by one-way analysis of variance, and the differences determined by a Tukey's test. Statistical significance was taken as $P < 0.05$.

4.3 RESULTS

Figure 4.1 shows typical ^{99m}Tc-HMPAO and ^{125}I-IAZA autoradiographs, together with a diffusion (ADC_{av}) map obtained from the same animal 2 hours after occlusion. For comparison, Figure 4.1 also shows a T_2 map acquired from this animal 7 hr after occlusion, and the results of histology corresponding to the 7 hr time point.

In all five slices from five animals the ^{99m}Tc-HMPAO images demonstrated a decrease in CBF in the area supplied by the middle cerebral artery. The spatial extent of the reduced CBF was similar but not identical in all animals. Each brain demonstrated an area of normal perfusion on the affected side compared to the opposite hemisphere, as well as areas of reduced uptake of tracer to varying degrees. There was also a small area of severely decreased CBF in the affected hemisphere in all animals. However, this region was not visible on all autoradiograph sections and was mainly confined to the preoptic region.

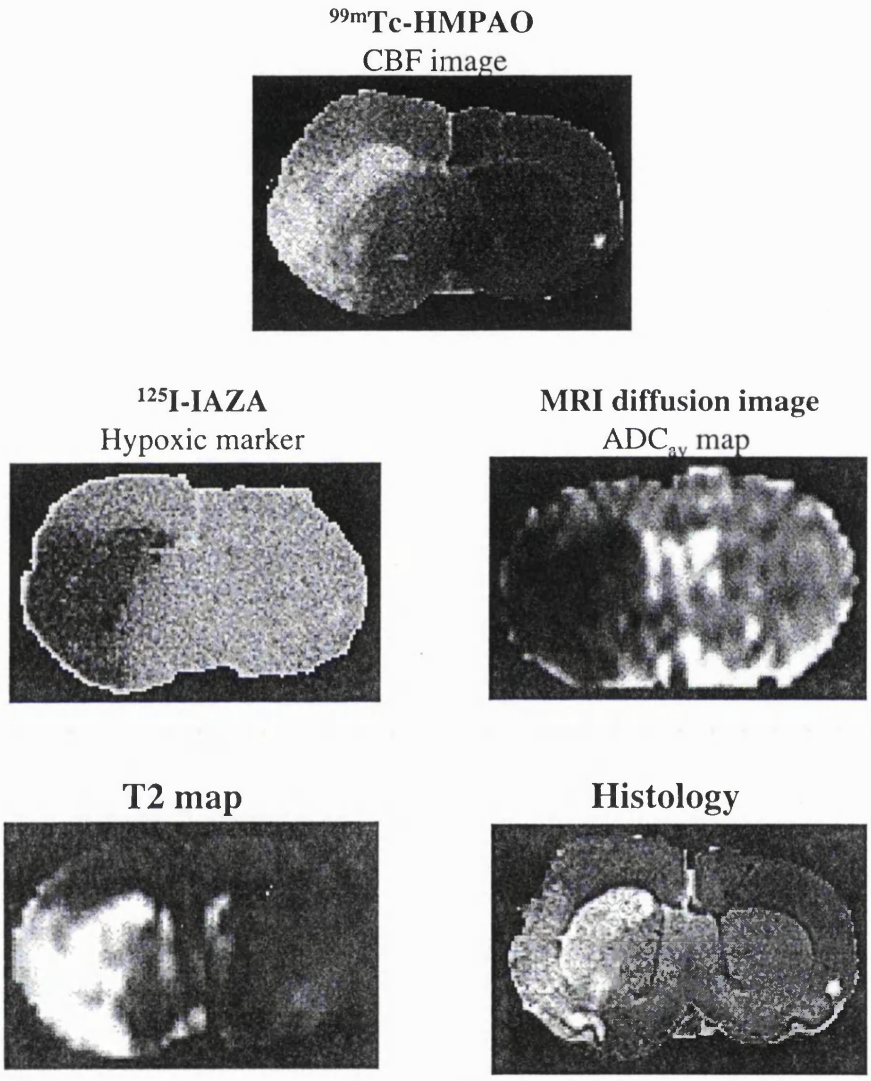

Figure 4.1 Images of blood flow, hypoxia and ADC 2 hours post-occlusion, and T2 and histology 7 hours post-occlusion.

Heterogeneous uptake of the hypoxic marker ^{125}I-IAZA was also seen in all five sections from the five animals. The ipsilateral hemisphere showed areas of normal uptake, varying degrees of increased uptake, as well as severely impaired uptake in comparison to the contralateral hemisphere. The area of severely impaired uptake was not visible on all five slices but was sited within the area of severely decreased CBF.

Diffusion-weighted imaging, performed 2 hours following occlusion, yielded mean ADC_{av} values of $0.69\pm0.02\times10^{-3}mm^2/s$ in the contralateral hemisphere and $0.41\pm0.03\times10^{-3}mm^2/s$ from the ischaemic lesion. Within the ischaemic lesion the ADC_{av} values were not homogeneous and tended to increase in value towards the boundary of the lesion.

4.3.1 Comparison of lesion sizes

Quantitative delineation of lesion areas was carried out as described in the Methods section and as illustrated in Figure 4.2. The figure shows a ^{125}I-IAZA autoradiograph, together with a histogram of the distribution of activities that was used to define the area of increased uptake (shown in red). Figure 4.2 also shows a CBF map that was used to calculate the flow threshold for increased uptake of the hypoxic marker (see below).

Lesion areas calculated from the autoradiography, DWI, T_2 and histology are presented for individual animals in Table 4.1. The lesion areas are calculated as a percentage of the area of the ipsilateral hemisphere (hemispheric lesion area=HLA %) to allow comparison of all the imaging modalities. Five areas were calculated: 1) an area of decreased ADC_{av} values; 2) an area of increased hypoxic marker uptake; 3) an area of decreased CBF; 4) a region of T_2 increase at 7 hours; and 5) an area of infarction at 7

Table 4.1: Calculated lesion areas

Lesion areas calculated from ADC_{av} maps, ^{125}I-IAZA and ^{99m}Tc-HMPAO autoradiographs (2 hours post-occlusion), T_2 images and histology (7 hours post-occlusion)

	ADC_{av}†	IAZA†	HMPAO	T_2†	Histology†
Study	**HLA (%)**	**HLA (%)**	**HLA (%)**	**HLA (%)**	**HLA (%)**
1	52	52	93	53	54
2	65	64	77	58	60
3	45	46	84	45	42
4	26	32	86	29	27
5	48	51	81	52	49

HLA indicates hemispheric lesion area.

†significantly different from HMPAO - all other lesion areas were of similar size.

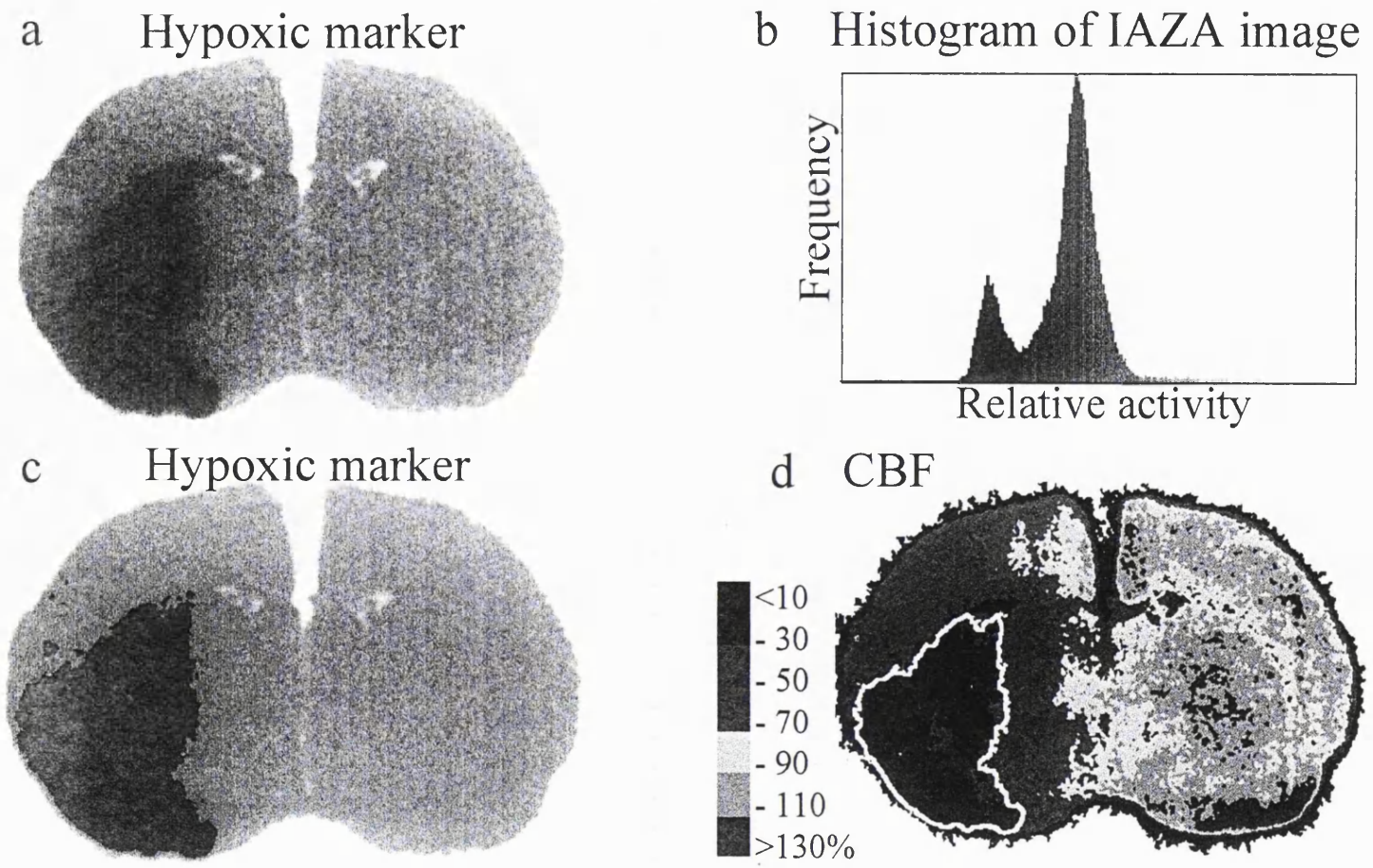

Figure 4.2 (a) ^{125}I-IAZA autoradiograph 2 hours following MCAO; (b) histogram of ^{125}I-IAZA autoradiograph activity used for the calculation of region of hypoxia; (c) area of increased hypoxic marker uptake (shown in red); (d) CBF image (%) (CBF relative to ROI in contralateral cortex) with the coregistered outline of the area of increased hypoxic maker uptake (shown in white) used for the calculation of the CBF threshold for hypoxic marker uptake

hours post-occlusion. The largest area was that of decreased perfusion, which was significantly larger than the areas of ADC_{av} decrease, hypoxic marker uptake, T_2 increase and infarction ($p<0.001$). However the lesion areas from the DWI, ^{125}I-IAZA autoradiographs (2 hr post MCAO) T_2 and histology (7 hr post MCAO) were similar to each other in both size ($p>0.05$) and distribution.

4.3.2 Relationship between the autoradiographic markers of flow and hypoxia

Paired ^{99m}Tc-HMPAO and the ^{125}I-IAZA autoradiographs demonstrated a similar pattern of distribution in all rats. Up to four distinct territories could be delineated (Fig 4.3): region 1 was an area of normal flow and normal ^{125}I-IAZA uptake; region 2 a territory of slightly reduced blood flow (CBF more than 2SD below mean) with normal uptake of the hypoxic marker; region 3 a further decrease in CBF with a concomitant increase in the uptake of the hypoxic marker; and region 4 where there was severely reduced blood flow with a concomitant low uptake of the hypoxic marker.

Table 4.2 shows the blood flow thresholds for regions 2, 3 and 4. The thresholds are expressed as a percentage of the normal flow, which was calculated from a region in the contralateral hemisphere. The lower limit of normal flow (mean - 2SD) was 66 ± 4%, which defines the threshold for decreased perfusion. By superimposing the outline of the area of increased ^{125}I-IAZA uptake on the ^{99m}Tc-HMPAO image (Fig 4.2), the blood flow threshold for ^{125}I-IAZA uptake (region 3) was calculated to be 34 ± 7%. A similar value was obtained from the scatter plots (Fig 4.3). Similarly, the flow threshold for region 4 was calculated to be 7 ± 5 %. The flow threshold for increased ^{125}I-IAZA

Table 4.2: CBF thresholds for ADC and hypoxia

Blood flow thresholds for selected territories, together with ADC_{av} values and IAZA uptake from within the regions

Regions 1-4	CBF threshold (%)	ADC_{av} ($10^{-3}mm^2/s$)	IAZA (relative activity)
1) normal CBF normal IAZA	NA	0.69 ± 0.02	1.0 ± 0.4
2) decreased CBF+ normal IAZA	66 ± 4 *	0.68 ± 0.03	1.1 ± 0.5
3) decreased CBF++ increased IAZA	34 ± 7 *†	0.41 ± 0.03*†	2.1 ± 0.6 *†
4) decreased CBF+++ low or absent IAZA	7 ± 5 *†‡	0.35 ± 0.02*†‡	0.8 ± 0.4 *†‡

* = significantly different from normal values $p<0.05$

† = significantly different from the values in region 2 $p<0.05$

‡ = significantly different from the values in region 3 $p<0.05$

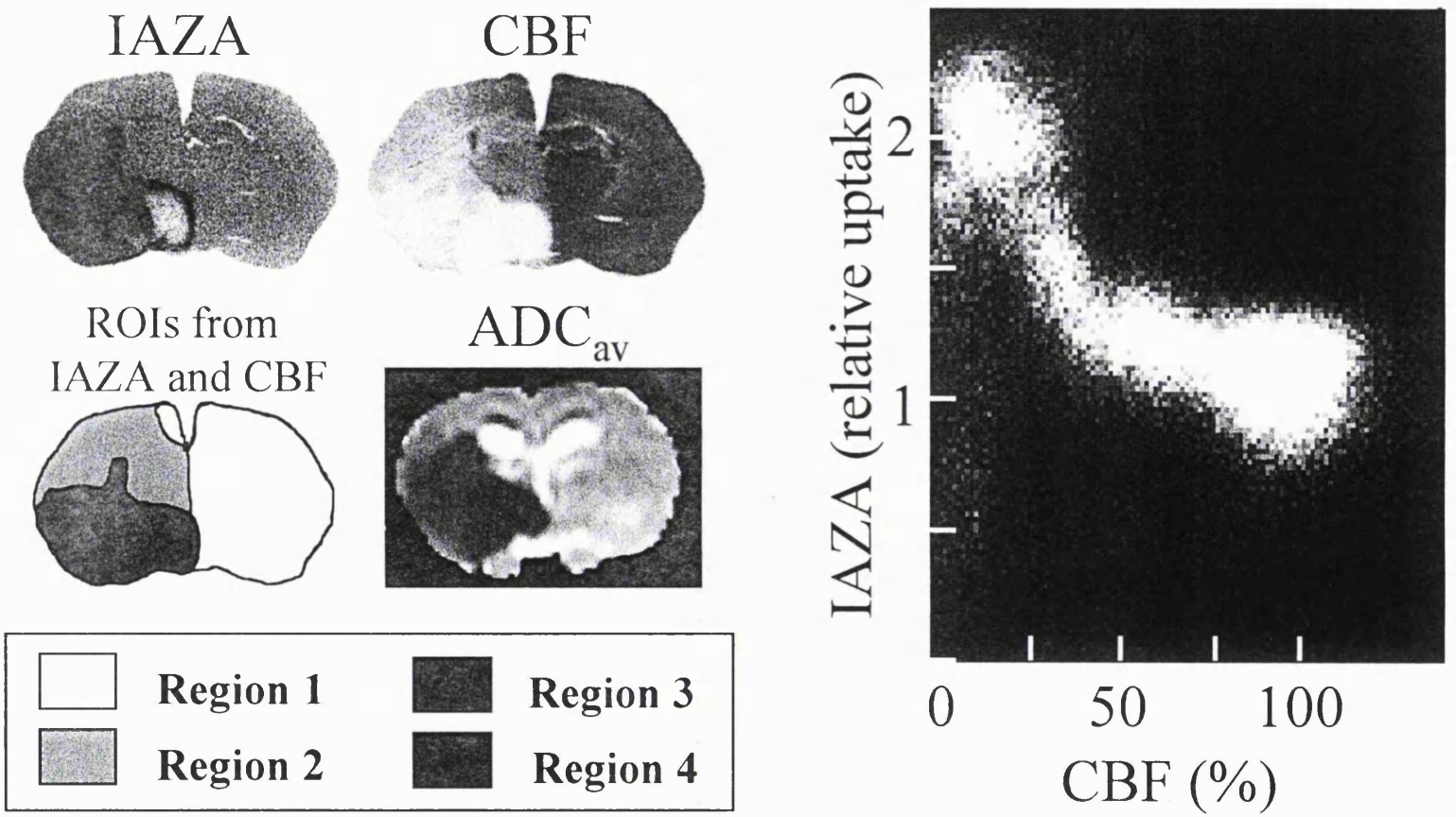

Figure 4.3 Scatter plot of ^{99m}Tc-HMPAO and ^{125}I-IAZA data, derived from the displayed autoradiographs, together with the associated 2 hour ADC map and a diagram of the 4 regions referred to in the text.

uptake was significantly less ($p<0.001$) than that of the decreased perfusion territory 66 ± 4%, yet was greater than the upper limit of 7 ± 5 % for low uptake of hypoxic marker.

4.3.3 Relationship between MR and autoradiography

Table 4.2 shows the ADC_{av} and relative ^{125}I-IAZA uptake values (mean ± SD) from within the four regions as defined above. In regions 1 and 2 (normal and reduced CBF with normal ^{125}I-IAZA uptake) the ADC_{av} values were not significantly different from the values in the contralateral hemisphere. In region 3 (reduced CBF, increased ^{125}I-IAZA uptake) the ADC_{av} was significantly reduced below normal to $0.41\pm 0.03\times10^{-3}mm^2/s$ while in region 4 (severely reduced blood flow, low IAZA uptake) the ADC_{av} was further reduced ($0.35 \pm 0.02\times10^{-3}mm^2/s$). Region 4 had the lowest blood flow range (<7%) and was associated with the lowest ADC_{av} and ^{125}I-IAZA uptake values. Both ADC_{av} and ^{125}I-IAZA values in region 4 were significantly different from their values in all other regions.

4.4 DISCUSSION

There are four major findings in this Chapter:

- ^{125}I-IAZA accmulates in the brain during reduced blood flow and hypoxia;
- during cerebral ischaemia the spatial distribution of ^{125}I-IAZA uptake and ADC_{av} decrease are equivalent - indicating similar CBF thresholds;
- following occlusion of the MCA the combination of ADC_{av} decrease or ^{125}I-IAZA uptake with CBF allows differentiation between normal tissue and three regions of affected tissue ranging from mildly hypoperfused to infarcted, which, as I argue below correspond to areas of oligaemic misery perfusion, ischaemic misery perfusion and lesion core;

- the infarct size at 7 hr was similar to both ADC_{av} and ^{125}I-IAZA lesion sizes at 2 hr.

4.4.1 Time points of images post-occlusion

Cerebral blood flow and hypoxic markers were injected 2 hours post-occlusion, at which time DWI images were acquired for calculation of the ADC_{av} maps. ^{99m}Tc-HMPAO is a ligand that is extracted into brain on its first pass through the cerebral circulation and does not redistribute in the brain with time; thus provides a 'snapshot' image at the time of injection (Sharp *et al.* 1986; Matsuda *et al.* 1988). ^{125}I-IAZA has a rapid blood clearance and decreases to 95% of the initial activity within the first 2 hours, indicating the brief period of time over which the uptake ^{125}I-IAZA is likely to occur. Again, the image of hypoxia is likely to reflect a 'snapshot' image at the time of administration (Mannan *et al.* 1991). The short time for conversion and trapping of these markers allows comparison of CBF, hypoxia and ADC_{av} at approximately 2 hours following MCAO and a further comparison with T_2 maps and histology at 7 hours post-occlusion because of the lack of redistribution of the tracers.

4.4.2 Quantitation of relative cerebral blood flow

In this study I have normalised the ^{99m}Tc-HMPAO autoradiograph to the activity within a normal region in the contralateral cortex, and the activity from the image was displayed as a percentage of normal values. No attempt has been made to quantify CBF absolutely. It is noted that because ^{99m}Tc-HMPAO is not trapped instantaneously but with an exponential half time of 40 seconds due to back diffusion (Matsuda *et al.* 1988), the uptake of ^{99m}Tc-HMPAO is not linearly related to flow at values above 120 ml/100g/min (Bullock *et al.* 1991). I have not corrected for these effects (Lassen *et al.* 1988) as the maximum flow rates that I encountered with the animal in the vertical position during ischaemia (133 ml/100g/min - measured with hydrogen clearance, data

not shown), are approximately within the linear portion of the relationship and the maximum calculated error would be <6%.

4.4.3 Uptake of ^{125}I-IAZA

The retention of ^{125}I-IAZA was highest (approximately double normal tissue) in regions of moderately decreased blood flow (<34% of normal flow), in which levels of cellular oxygenation are sufficiently low for uptake of the tracer. This CBF limit is consistent with that found with another hypoxic marker ^{99m}TcO(PnAO)-1-(1-2-nitroimidazole)) (BMS-18132) (Di Rocco *et al.* 1993), where uptake was observed in regions which had a reduction in blood flow below 50ml/100g/min. In these regions of moderately decreased blood flow, the hypoxic marker enters the cell via diffusion, followed by reduction to a potentially reactive free radical, which in the presence of inadequate supplies of oxygen is further reduced to a relatively inactive species and retained within the cell.

4.4.4 Lesion areas and CBF thresholds: DWI and hypoxic marker

Following MCA occlusion, the differences in ischaemic effects between animals were presumably dependent upon the degree of occlusion and vascular anatomy. Despite this variation in lesion size, the area of ADC_{av} decrease spatially agreed with the region of ^{125}I-IAZA uptake in all animals and any small variation between lesion areas may be attributed to different slice position or partial volume effects due to slice thickness of the ADC_{av} map. This concordance suggests that the CBF threshold necessary for ADC_{av} change is equivalent to that required for binding of the hypoxic marker, which was approximately 34 ± 7% of the normal flow, and agrees with previous results for ADC_{av} blood flow thresholds (Kohno *et al.* 1995). The reduction in ADC_{av} relative to

ipsilateral hemisphere was approximately 40%, similar to values reported by van Gelderen et al. (van Gelderen *et al.* 1994) and Miyabe et al. (Miyabe *et al.* 1996) (36 and 35% respectively) despite the differences in diffusion time and animal model.

There are considerable data in the literature to support a relationship between reduced CBF, impaired energy metabolism and ADC change in cerebral ischaemia, though the precise association appears to be model-dependent, and there are varying interpretations as to whether ATP, phosphocreatine, lactate or pH best correlate with ADC (Busza *et al.* 1992; Decanniere *et al.* 1995; Kohno *et al.* 1995). Nevertheless, it seems clear that once oxygen delivery drops below a certain threshold, ADC changes will ensue. Studies of IAZA retention in isolated cells in culture have shown that the hypoxic marker is known to be retained in cells when oxygen saturation drops below 1% and maximal retention is observed at 0.03% (Mannan, 1991). These in vitro thresholds are consistent with oxygen saturation levels which induce complete energy failure in vitro in brain slice preparations (oxygen < 1%) (Kauppinen and Williams, 1990). Thus if changes in ADC are related to failure of aerobic metabolism, a close relationship between ^{125}I-IAZA uptake and ADC decrease in ischaemia may be envisaged. The region where I observe decreased blood flow, increased IAZA uptake and a decrease in ADC_{av}, is likely to represent an area of 'ischaemic misery perfusion', that is, a territory which has a reduced blood flow, increased oxygen extraction fraction (OEF) together with depressed cerebral metabolic rate of oxygen consumption ($CMRO_2$) (Baron, 1991). The issue as to whether this region represents 'penumbra', by which I mean a region of ischaemic tissue peripheral to the core where viable neurones may be found, and thus potentially salvageable with suitable intervention (Kinouchi *et al.* 1993; Hossmann, 1994), cannot be answered from the data alone. However I note that ADC

changes (and energy failure) are in principle reversible for at least 30 minutes if reperfusion occurs (Busza *et al.* 1992), though this itself does not mean the tissue has not suffered irreversible damage and will not go on to suffer secondary energy failure and neuronal loss (Hope and Reynolds, 1985; Busza *et al.* 1992; Lorek *et al.* 1994).

4.4.5 The region of oligaemic misery perfusion

A further territory of 'oligaemic misery perfusion' may also be discriminated within the region of perfusion deficit, that is, an oligaemic area where the oxygen extraction fraction has increased due to the reduced blood flow yet the $CMRO_2$ remains normal. The combination of blood flow and DWI or the hypoxic marker in this study discriminates a region in which CBF is decreased without ADC_{av} change or ^{125}I-IAZA uptake, thus defining the area of oligaemic misery perfusion. This uncoupling between flow and metabolism has been demonstrated using positron emission tomography (PET) both in humans (Baron, 1991) and animals (Young *et al.* 1996). Misery perfusion (oligaemic) areas have also been identified by MRI in both animals and man from the mismatch between areas of either increased O_2 extraction (increased levels of deoxyhaemoglobin) or decreased perfusion and areas of cytotoxic oedema (decreased diffusion) (Van Bruggen *et al.* 1994; Roussel *et al.* 1995; Copen *et al.* 1997; Grohn *et al.* 1998; van Zijl *et al.* 1998; Calamante *et al.* 1999). The metabolic and haemodynamic changes occurring in this region may play an important role in the final outcome of the patient following stroke, yet have received relatively little attention. PET studies in humans have indicated that, up to 17 hours following a stroke, areas of normal $CMRO_2$ and decreased CBF (oligaemic misery perfusion regions) spontaneously evolved toward infarction (Marchal *et al.* 1996). However, in a reperfusion animal stroke model PET data indicate that it is not always the region with

the highest OEF that will go on to infarction (Young *et al.* 1996). If areas of oligaemic misery perfusion reflect compromised tissue that could proceed onto infarction (as indicated in PET studies (Marchal *et al.* 1996)) yet are possibly salvageable, then these regions may be classified as penumbra and require identification. I note that in this study the oligaemic misery perfusion area identified at 2 hours does not become recruited into the histologically defined infarct measured at 7 hours post occlusion. Nevertheless, the full extent of the area of misery perfusion needs to be delineated following a stroke, if a complete assessment of the condition is to be made.

4.4.6 Determination of the ischaemic core

The final area distinguished in this study is that of low ^{125}I-IAZA uptake with a concomitant severely decreased ADC_{av} ($0.35 \pm 0.02 \times 10^{-3} mm^2/s$) and low CBF ($<7 \pm 5$ %). These characteristics may be explained in one of several ways. If the regional flow is zero, then the delivery of the tracer will be impaired to such an extent that, despite decreased cellular oxygen, uptake of the marker would not be seen. However in this model it is unusual that the flows reach zero (Kohno *et al.* 1995) and it is unlikely that the ^{125}I-IAZA could not reach its target. Alternatively, ^{125}I-IAZA may not be retained within the hypoxic tissue if damage has occurred to the enzymes necessary for the initial reduction and retention of ^{125}I-IAZA. This would allow the nitroimidazole to diffuse in and out of the cell freely and not to be preferentially bound due to reduced levels of oxygen. Finally it has been shown that a nitroimidazole will not bind to regions of infarcted cerebral tissue (Di Rocco *et al.* 1993), although I cannot state whether the tissue had infarcted when the ^{125}I-IAZA was administered since the animals were sacrificed 5 hours after the administration of the tracers. The lowest ADC_{av} values were within this region of low ^{125}I-IAZA binding; however the ability to

discriminate the ischaemic core was more obvious in the ^{125}I-IAZA image due to the greater contrast to noise ratio. Either of these two techniques may prove useful in detecting areas of non-recoverable ischaemic tissue, using threshold values of ADC_{av} or ^{125}I-IAZA uptake. Previous studies have suggested that ADC thresholds may be used as an indicator of recoverable tissue (Dardzinski *et al.* 1993; Helpern *et al.* 1993; Hasegawa *et al.* 1994). However, the use of ADC thresholds is reliant upon the time from occlusion (Pierpaoli *et al.* 1996), and calculated ADC values are dependent upon the parameters used for the acquisition of the images (Latour *et al.* 1994; Norris and Niendorf, 1995).

The area of ischaemic tissue necrosis at 7 hr indicated by histological staining was similar in size to the region of ADC_{av} decrease and ^{125}I-IAZA uptake at 2 hr. This finding is perhaps not unexpected as DWI lesion size expands little from 2 to 7 hr in the rat (Roussel *et al.* 1994) and the DWI lesion area at 7 hours has been shown to be equivalent to the histological lesion area (Back *et al.* 1994). Further, my work agrees with a previous study which performed MCAO in the cat, and showed excellent agreement between area of infarction and reduced ADC_{av} at 2 hours post-occlusion (Miyabe *et al.* 1996). It is important to note that regions of misery perfusion were not recruited into the infarct area within this 7 hr period.

4.4.7 Conclusion

In conclusion, it remains important to be able to differentiate areas of recoverable and non-recoverable tissue within the area of perfusion deficit, if one is to give an accurate diagnosis and prognosis. The areas of hypoxic marker (^{125}I-IAZA) uptake and ADC_{av} change that I have observed following an ischaemic insult are similar to each other,

indicating that these markers have comparable blood flow thresholds and may reflect regions of ischaemic misery perfusion. I have suggested that the combined use of ^{125}I-IAZA or DWI and perfusion imaging will allow differentiation between areas of oligaemic misery perfusion, ischaemic misery perfusion and ischaemic core. This combination of CBF and ^{125}I-IAZA or DWI should prove invaluable in the early detection of stroke for both nuclear medicine and magnetic resonance imaging modalities and warrants further evaluation in humans.

Chapter 5

5. Effects of diffusion anisotropy on lesion delineation in a rat model of cerebral ischaemia

During my initial diffusion-weighted imaging (DWI) experiments using a control rat model, I observed a change in intensity throughout both the white and grey matter when the diffusion-gradients were applied in a single axis. The change in intensity appeared to be dependent upon the direction of the diffusion gradient and thus prompted the hypothesis that both grey and white cerebral tissue possess anisotropic properties, that is, water will preferentially diffuse in one direction. The aim of this study was to test this hypothesis and investigate the implication of cerebral tissue anisotropy on lesion delineation using DWI, following middle cerebral artery occlusion in the rat.

5.1 INTRODUCTION

As described previously, measurements of the apparent diffusion coefficient (ADC) are being used more frequently in the investigation of cerebral ischaemia (Van Bruggen *et al.* 1994). It has been proposed that additional information will be available from measurements of the diffusion tensor, which provides a full description of the anisotropic properties of diffusion (Basser *et al.* 1994a). A simpler approach than measuring the full tensor is to use diffusion-weighting gradients independently along three orthogonal axes in order to generate maps of the trace of the diffusion tensor which is rotationally invariant (Basser *et al.* 1994b). Van Gelderen et al. (van Gelderen *et al.* 1994) have proposed that using the trace of the tensor may improve definition of ischaemic lesion contrast, by removing the effects of diffusion anisotropy. Diffusion anisotropy, most notably in white matter (Moseley *et al.* 1990), leads to ADC values

which differ according to the axis along which the diffusion-weighting is applied, and this can confound the interpretation of ADC maps.

Pulsed-gradient spin-echo DWI (PGSE-DWI) may be performed with diffusion-sensitising gradients applied separately along each of the X-,Y-, and Z-axes to produce ADC maps in three orthogonal directions. Diffusion tensor trace images may be calculated from the average of these three ADC maps (ADC_{av}=1/3 Trace(D) = 1/3(D_{XX}+D_{yy}+D_{ZZ})), when the contribution of imaging gradients (cross terms) is negligible. Alternatively, the trace of the diffusion tensor may be obtained by using a single scan (ADC_{SS}) technique in which the diagonal elements add constructively, while off-diagonal tensor elements cancel (Mori and van Zijl, 1995). Moreover, with this technique the cross terms are eliminated and it therefore provides a true estimate of the trace.

The effects of grey and white matter anisotropy upon lesion delineation have not been investigated in the rat. In this Chapter, I compare the effect of diffusion anisotropy on ADC determination in the investigation of cerebral ischaemia in a rat model of middle cerebral occlusion (MCAO). I show that grey matter, as well as white matter, displays anisotropic diffusion, and demonstrate the advantage of trace measurements for the delineation of lesion volumes.

5.2 METHODS

5.2.1 Animal preparation

I studied 11 male Wistar rats weighing 100-130g. Six animals were prepared for middle cerebral artery occlusion (MCAO) and were occluded using a modified Zea Longa approach (Longa *et al.* 1989) (see Chapter 4 - animal preparation). Five normal rats were studied without undergoing MCAO.

5.2.2 Imaging protocol

Rats were imaged in an 8.5T vertical magnet (Oxford Instruments, Oxford, UK.) interfaced to a SMIS (Surrey Medical Imaging Systems, UK.) console (see Chapter 4 - imaging protocol). Conventional DWI was performed using a pulsed-gradient spin-echo (figure 5.1a) (see Chapter 4). Images were also acquired using a single scan trace imaging sequence ((Mori and van Zijl, 1995), pulse gradient pattern III) at similar 'b' values (d = 5 ms; D = 5.4 ms; diffusion gradient ramp = 0.2 ms) (figure 5.1b). Imaging parameters were: TR/TE = 1000/80 ms; slice thickness = 2 mm; FOV = 40 mm; data matrix = 128 × 64 views; 4 signal averages; imaging time = 12 minutes. Imaging was started 2 hours or more after MCAO.

5.2.3 Data processing

Apparent diffusion coefficient maps were calculated as in Chapter 4. In addition, trace maps were calculated directly from sets of single scan trace-weighted images (ADC_{SS}).

5.2.4 Image processing for calculation of lesion areas

Before the calculation of lesion areas all extracerebral pixels were removed. This procedure was performed in three stages: (1) a rectangular region of interest (ROI) was

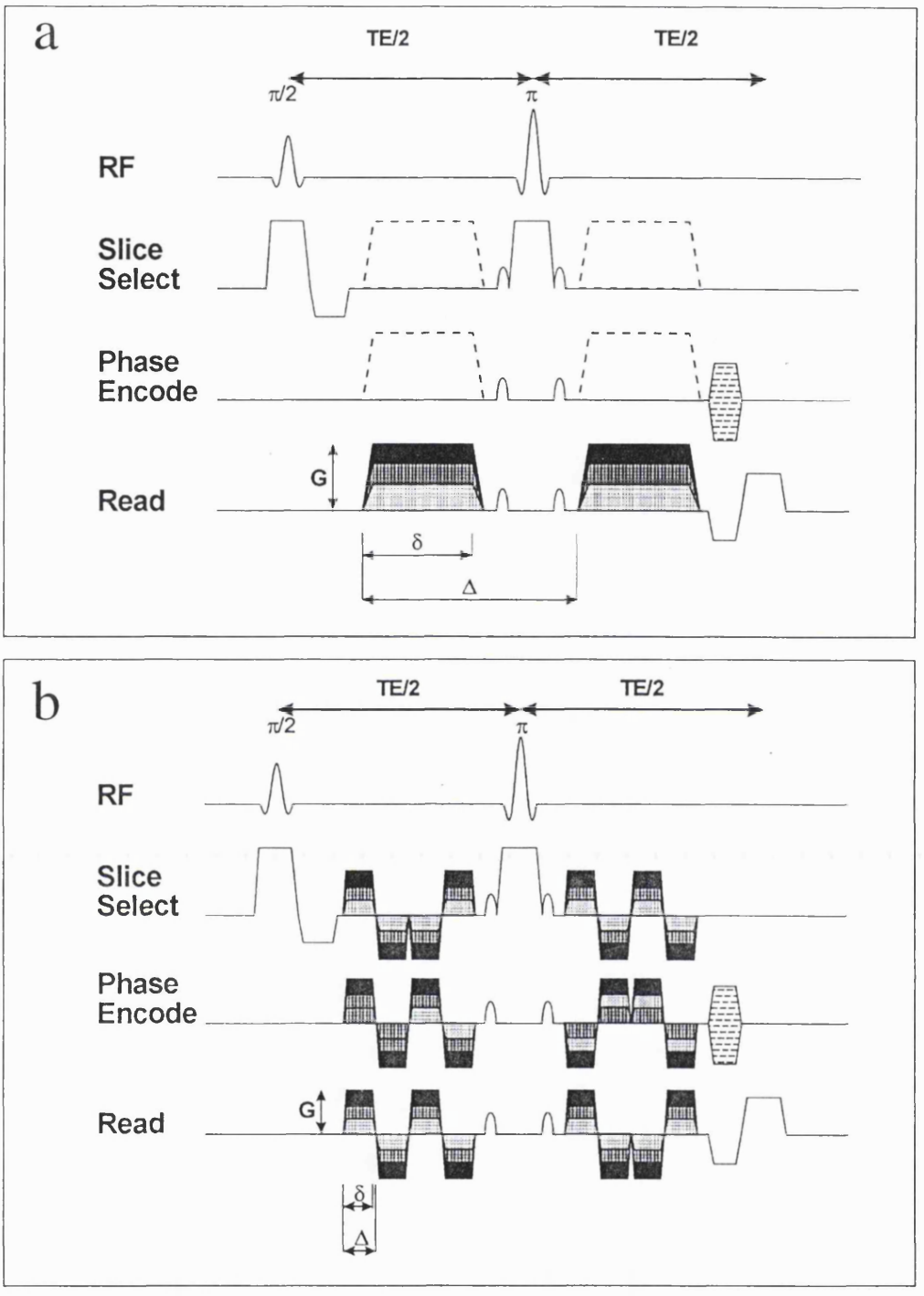

Figure 5.1 *The two imaging sequences used in these experiments were based on a standard spin echo sequence. a) shows the incorporation of pulsed-field diffusion-weighting gradients (shaded) either side of the π refocusing pulse. In separate experiments, these diffusion-weighting gradients are applied along the X,Y and Z-axes (δ=11ms, Δ=28ms). b) shows the incorporation of bipolar gradient pairs (shaded) around the π refocusing pulse to produce a trace imaging sequence (δ=5.2ms, Δ=5.4ms).*

placed around the brain, located three pixels outside the lateral margins, and this ROI was extracted and used for all subsequent ADC maps; (2) using the lowest 'b' value image, a threshold was determined to reject pixels which were below the lowest signal intensity of the brain (rejected pixels assigned a value of 0); (3) following this process, no extracerebral pixels were left in contact with the brain in the ADC image, and any remaining pixels outside the brain were assigned a value of 0. This image was designated as the ADC_{raw} map.

To compare ischaemic regions among studies, lesion areas are quoted as a percentage of the ADC_{av} lesion size for each animal, as not all the animals had lesions of equal size. I compared three methods for the delineation of lesion areas:

1) *Method A*: The resolution of the ADC_{raw} map was changed from 128×128 to 512×512, and the values of the new pixels were calculated using a bilinear interpolation algorithm (NIH image v1.59) (referred to as the ADC_{int} map). A histogram of the distribution of ADC values from the final interpolated ADC map (ADC_{int} map) was calculated. The threshold for differentiating ischaemic from normal pixels was set at the minimum between the modes of the bimodal distribution. Histograms were produced from the ADC_{int} map rather then the ADC_{raw} map, as the former allowed better definition of the minimum between the two distributions. Using this threshold, lesion areas were then calculated from the ADC_{raw} map. The ADC_{int} maps were not used for the delineation of lesion areas because artefacts confounded the area calculation due to the method of interpolation. These artefacts were produced around the outside of the brain due to interpolation between cerebral ADC pixels and the background of pixel value 0; interpolated values then fell into the range of ischaemic

ADC values. Using ADC_{raw} maps, all ADC values that fell below the threshold were highlighted. In certain images a small number of unhighlighted pixels were present in the centre of the lesion, and these were deemed lesion and included in the final area calculation. Also, isolated clusters of highlighted pixels were sometimes found in the contralateral hemisphere (but only in the unidirectional PGSE-DWI images); these were not included in the final ischaemic area calculation. The final lesion area was calculated from the number of highlighted pixels that were below the threshold and met the above criteria.

2) *Method B:* Calculation of the lesion area was performed using a ROI in the normal hemisphere, which was used to define a threshold based on the standard deviation of the distribution within that ROI. The threshold was calculated as:

Ischaemic ADC upper threshold = mean - (2 or 3 SD).

3) *Method C:* A histogram of ADC values from a ROI in the contralateral normal area was calculated. The ADC value below which 0.5% of the pixel values fell (equivalent to 2.6 SD if normally distributed) was used as the threshold.

5.3 RESULTS

5.3.1 Normal animals

5.3.1.1 Grey and white matter anisotropy

Figure 5.2 shows typical ADC maps for a normal rat obtained with diffusion gradients applied along the X- and Y-axes. Regions of interest were placed in two grey matter

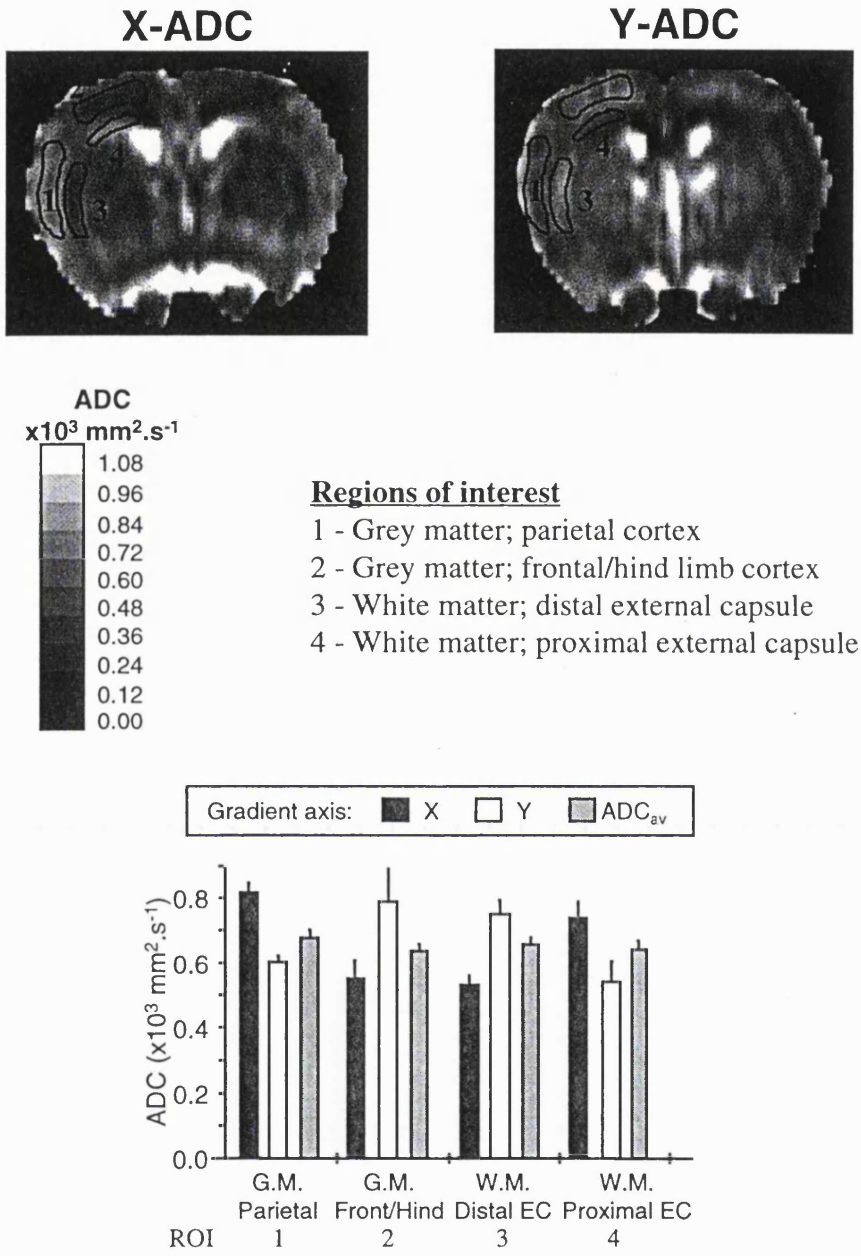

Figure 5.2 *ADC maps from a normal rat with sensitising gradients in the X and Y directions (arrowed). The bar chart indicates mean (±1 SD) ADC values from regions of interest in both grey and white matter, in five normal rats. Marked anisotropy is demonstrated in both grey and white matter.*

areas: the parietal cortex, and frontal/hind limb cortex. Two regions of white matter were also examined: proximal and distal external capsule. The bar chart in Figure 5.2 shows mean ADC values derived from the four labelled ROIs in five normal rats. All regions exhibited a marked degree of anisotropy. In the white matter regions, the ADC values were significantly higher when the sensitising gradient was along the predominant fibre axis (region 3,Y; region 4,X). Moreover, in region 1- a grey matter area in the parietal cortex - the ADC value along X (0.82×10^{-3} mm^2s^{-1}) was significantly higher (t-test p=0.001) than that along Y (0.60×10^{-3} mm^2s^{-1}). Conversely, in a ROI of grey matter from the frontal cortex (region 2) the ADC value along X (0.55×10^{-3} mm^2s^{-1}) was lower (p=0.004) than that along Y (0.79×10^{-3} mm^2s^{1}).

5.3.1.2 Diffusion-weighted trace image - normal animal

Maps of 1/3 trace of the tensor (ADC_{av}) yielded values of 0.67×10^{-3} and 0.63×10^{-3} mm^2s^{-1} for region 1 and 2 (grey matter cortex) respectively, which were not significantly different from each other (p=0.21). Similar results were obtained from the white matter tracts in regions 3 and 4 (0.66×10^{-3} and 0.64×10^{-3} mm^2s^{-1}).

5.3.2 MCA occluded animals

5.3.2.1 Methods for lesion delineation

Figure 5.3 shows ADC maps obtained from a rat following MCAO. In order to differentiate the ischaemic from non-ischaemic tissue, three methods of analysis were investigated. The calculated threshold using *Method B* was dependent upon the position of the ROI and the resulting distribution of the pixel ADC values; these values were found to be non-normally distributed and the distribution changed with the direction of the sensitising gradient. The effects of this can be seen in Figure 5.3, where

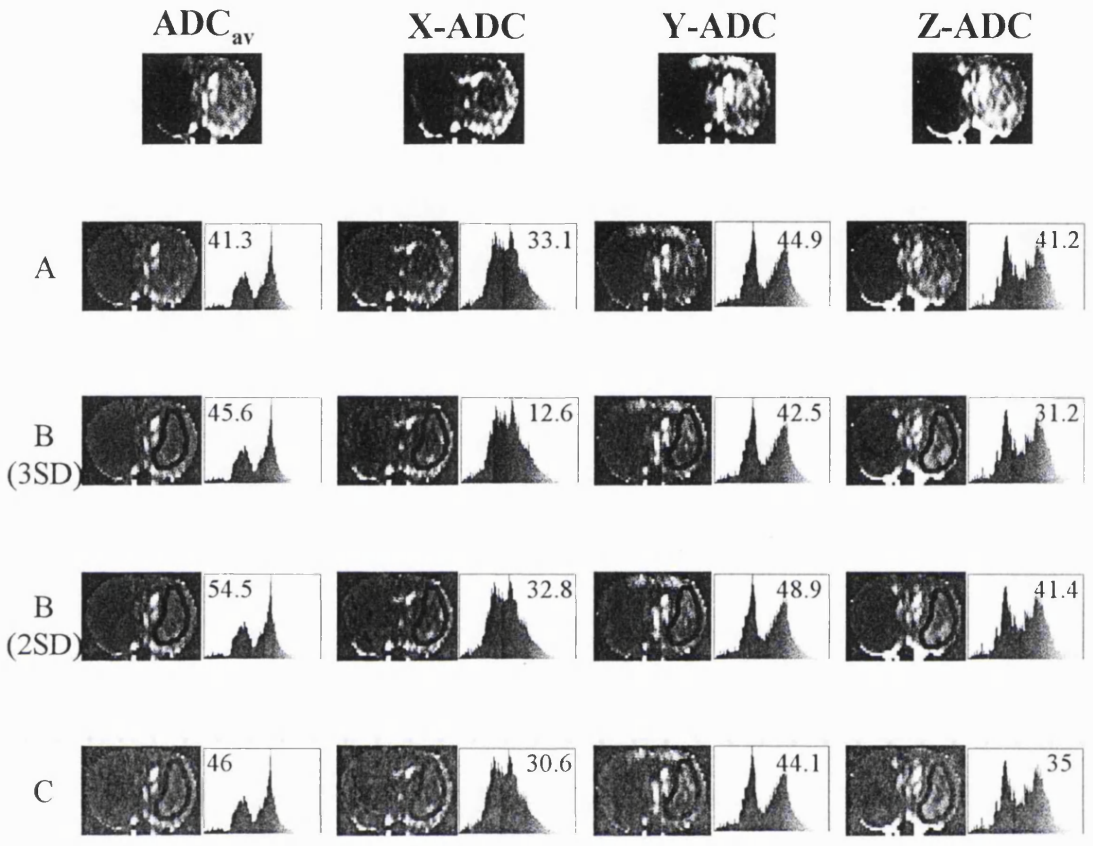

Figure 5.3 *ADC maps from PGSE-DWI with sensitising-gradients in the X, Y, and Z axes, together with the generated ADCav image. Lesion areas have been calculated from ADCraw map using the three methods described in the text (A, B, C) and displayed together with the histogram distribution of ADC values from the ADCint map. Method A: minimum between modes. Method B: mean - (2 or 3 SD) of non-ischaemic distribution. Method C: ½ percentile low-ADC rejection of non-ischaemic distribution. The value inside the histogram represents the corresponding lesion area in mm^2. ROI are included in the images when required by that method.*

the use of 2 or 3 standard deviations incorrectly classified non-ischaemic pixels from the contralateral hemisphere as ischaemic. This is due not only to the overlap between distributions, but also to the difficulty in characterising the non-ischaemic distribution. Consequently *Method B* failed to differentiate correctly between normal and ischaemic tissue and was not used for any further calculation of lesion areas.

Like Method B, *Method C* calculates an ADC threshold on the basis of pixel values in the non-ischaemic ROI, but using a threshold corresponding to the ½ percentile (see Methods). Although this method was not dependent upon the shape of the pixel distribution, some pixels in the contralateral hemisphere were classified as ischaemic, and this method therefore failed to differentiate accurately between the ischaemic and non-ischaemic ADC values (figure 5.3). However, the performance of this method will depend upon the particular percentile that is chosen.

The method used in this study for the final comparison of lesion areas was *Method A*, which calculated the ADC threshold from the minimum between the two modes of the ischaemic and non-ischaemic distributions. This technique allowed differentiation between the two distributions (figure 5.3), which although empirical, provided a reproducible method which did not rely upon a selection of a particular ROI or critical value, or on a specific pixel distribution.

5.3.2.2 PGSE-DWI ADC maps

In the occluded animals, unidirectional PGSE-DWI ADC maps showed areas of reduced ADC within the affected hemisphere which varied according to the direction of the sensitising gradient. One animal study was omitted from the following analysis as this lesion did not fully evolve until 6 h post occlusion and only occupied an area within

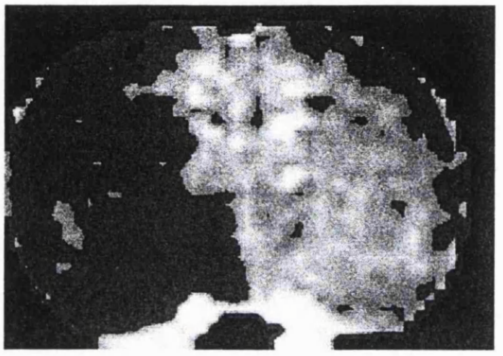

Z-ADC 45 mm^2

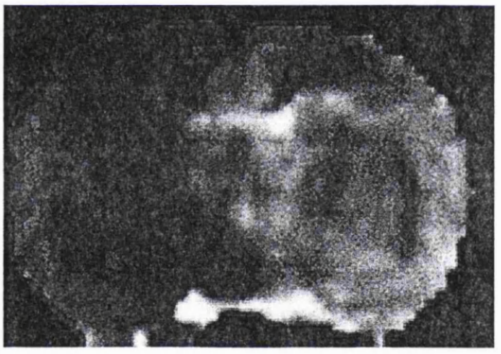

X-ADC 43mm^2

Figure 5.4 *Z- and X-ADC maps from the same animal. Lesion areas calculated using Method A. Calculated lesion areas are similar but have different spatial distributions.*

the basal ganglia. For each remaining animal (n=5), Method A was used to calculate the lesion size from the X-, Y- and Z-ADC maps and from the ADC_{av} and ADC_{ss} maps. The mean lesion sizes (expressed as a percentage of the lesion area from the ADC_{av}) for these X-, Y- and Z-ADC maps were 86 ± 4 %, 109 ± 4 % and 99 ± 4%, respectively. One-way ANOVA demonstrated that these means were significantly different ($p< 0.001$). Further, it was noted that in those cases where lesion areas were similar, the spatial distribution of the lesion varied depending upon the direction of the diffusion-weighting gradient (figure 5.4). In contrast, the ADC_{av} and ADC_{ss} maps gave lesion sizes that were not significantly different from each other ($p>0.05$), with similar lesion distributions (Table 1), despite the diffusion times being different. The mean differences between the normal and ischaemic ADC values for each of the X-, Y- and Z-ADC maps were 0.3×10^{-3} mm^2s^{-1}, and was not dependent upon the direction of the diffusion sensitising gradient.

5.3.2.3 Diffusion-weighted trace images

Mean ADC values in the ADC_{av} and ADC_{ss} maps were $0.41 \pm 0.03 \times 10^{-3} mm^2s^{-1}$ and $0.54 \pm 0.05 \times 10^{-3}$ mm^2s^{-1}, respectively in the ischaemic lesion, and $0.69 \pm 0.02 \times 10^{-3}$ mm^2s^{-1} and $0.82 \pm 0.04 \times 10^{-3}$ mm^2s^{-1} respectively in the normal hemisphere. The ADC values in both normal and ischaemic regions differed significantly between the two techniques. However, the differences in ADC between the normal and ischaemic regions were the same for both methods, and very similar to the single axis ADC values.

Finally, the animal that was excluded from the statistical analysis highlights a further consideration that needs to be made during evaluation of the single axis PGSE-DWI

Table 5.1: Calculated lesion areas

Lesion areas calculated using Method A, from PGSE-DWI images and diffusion tensor ADC maps. These are expressed in mm^2 and percentage of the area from the ADC_{av} image. Mean ± 2SD of the percentages of the ADC_{av} lesion areas from studies 1-5.

Study	1 mm^2 (%)	2 mm^2 (%)	3 mm^2 (%)	4 mm^2 (%)	5 mm^2 (%)	6 mm^2 (%)	% of ADC_{av} mean ± 2SD
X-ADC	42.5 (90)	33.7 (87)	24.7 (84)	33.1 (81)	19.9 (89)	16.5 (125)	86±8
Y-ADC	49.1 (104)	42.7 (110)	34.1 (116)	44.9 (110)	23.8 (106)	15.1 (114)	109±8
Z-ADC	45.2 (96)	39.7 (102)	28.0 (95)	41.2 (100)	22.9 (102)	20.0 (152)	99±7
ADC_{ss}	46.4 (99)	37.1 (95)	29.4 (100)	37.3 (91)	21.9 (98)	12.7 (96)	96±7
ADC_{av}	47.1	38.9	29.5	41.0	22.4	13.2	

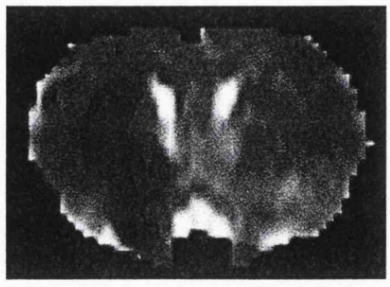

ADC_{av} $13mm^2$

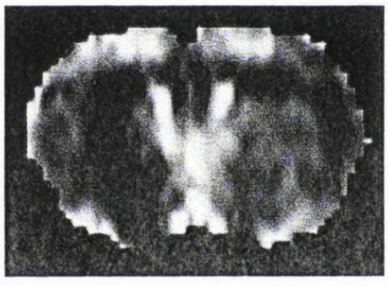

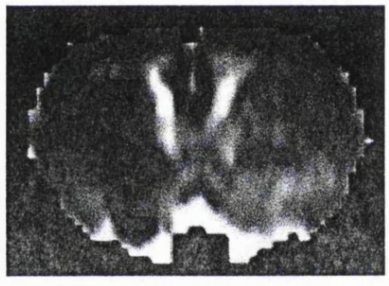

Y-ADC $15mm^2$ Z-ADC $20mm^2$

Figure 5.5 *ADC maps from the PGSE-DWI with sensitising-gradients in the Y and Z axes and the corresponding ADCav image in the same animal. The ischaemic region calculated from the Y-ADC map corresponded most closely with the ADCav in both area and distribution.*

maps. In all the other animals, the Z-ADC map corresponded most closely to the ADC_{av} map; this was not the case in the excluded animal, where it was found that the Y-ADC map corresponded most closely (figure 5.5). This difference is likely to be due to the unusual nature of the lesion which in this animal occupied only the basal ganglia.

5.4 DISCUSSION

5.4.1.1 Grey and white matter anisotropy

If the diffusion of water in the central nervous system were essentially isotropic, then ischaemic lesion delineation would be independent of the direction of the applied sensitising gradient using unidirectional PGSE-DWI. However, directional dependence of the diffusion of water in the brain is influenced by the structural properties of the tissue, and it is well understood that white matter is anisotropic (Doran *et al.* 1990; Moseley *et al.* 1990), although grey matter has received less attention. Grey matter anisotropy has been recognised in a small number of studies (Dardzinski *et al.* 1993; Kajima *et al.* 1994; Hoehn-Berlage *et al.* 1995; Thornton *et al.* 1996), although its effects upon ischaemic lesion delineation have not been investigated and one study has suggested that it may be small enough to be ignored (Back *et al.* 1994).

I have shown that, in the normal rat brain, ADC values from areas of both grey and white matter are dependent upon the direction of the sensitising gradient, and this has prompted my investigation into the effect of grey and white matter anisotropy upon lesion delineation in the rat MCAO model.

5.4.1.2 Structure of grey matter: effects on lesion size

Following MCA occlusion in the rat, the areas of ischaemic lesions measured from X-, Y- and Z-ADC maps acquired in the same animal differed from each other not only in size, but also in spatial distribution. These differences may be attributed to the underlying anisotropy of the tissue, which will affect ADC values to a varying degree depending upon the direction of the diffusion-sensitising gradient. These effects may be explained when one considers the neuronal cell structure together with the direction of the diffusion-weighting gradients. The structure of the pyramidal cells in the rat cortex has a pattern, that is analogous to the spokes in a bicycle wheel, radiating out from the hub or, in the case of the rat brain, basal ganglia (Paxinos and Watson, 1986). It follows that the fibres parallel to the gradients would give higher ADC values than those perpendicular to the gradients. The ADC values from ROIs placed in the parietal cortex and the hind/forelimb cortex were found to exhibit the pattern appropriate for the direction of the fibres, indicating the anisotropic nature of both grey and white matter.

The ischaemic lesion in the model I have studied occupies, in part, the parietal cortex which itself demonstrates anisotropy. The X-ADC value in that region of the lesion will exceed the selected threshold for ischaemia (because diffusion is being measured along the direction of the fibres), and will therefore result in the underestimation of the lesion size. The Y-ADC map tends to overestimate the lesion size as it includes not only the region that was excluded on the X-ADC map, but also a region of white matter tracts (proximal external capsule) that run perpendicular to the Y-axis diffusion-weighting gradients and thus exhibit a low ADC value. This region is then below the ischaemic threshold, resulting in a concomitant increase in the lesion size. Other

regions may similarly be included or excluded in the final lesion area depending upon their degree and direction of anisotropy and the direction of the sensitising gradient.

Interestingly, in five animals, the area calculated from the Z-ADC map was equal to the area from the ADC_{av}, as previously reported (Dardzinski *et al.* 1993; Hasegawa *et al.* 1994). However, this will not necessarily be the case for all types of lesions. For example, when the lesion occupied only the basal ganglia, the area from the Z-ADC map was not equal to the ADC_{av} area (figure 5.5). Again, this is presumably a reflection of the particular anisotropy characteristics of the affected tissue.

5.4.1.3 Improved lesion delineation

The ability to differentiate between ischaemic and normal pixels lies in the separation of the two regions based on ADC values. It has previously been suggested that the removal of contrast due to anisotropy by imaging the trace of the diffusion tensor will provide a more accurate delineation of the lesion area (van Gelderen *et al.* 1994). In this study, the ADC_{av} and ADC_{ss} images were the only techniques that generated lesion areas in which the ischaemic pixels were contained within the ipsilateral hemisphere and corresponded to each other in both size and distribution. However, the ADC values from the ADC_{ss} were uniformly greater than those recorded from the ADC_{av} in both normal and ischaemic hemispheres. This can be attributed to the shorter diffusion time used in the ADC_{ss} sequence, since, in restricted systems, the ADC is a function of diffusion time. However, the difference in ADC values between normal and ischaemic regions was the same using both methods and is similar to results from a recent study using a single scan technique with equivalent diffusion times in a cat model (Miyabe *et al.* 1996). The spatial distribution of the lesion was very similar with the two methods, although there is some suggestion that ADC_{ss} yields an area

smaller than that given by ADC_{av}, however, the mean difference between the lesion areas obtained with the two methods does not achieve significance at the $p<0.05$ level.

The difference between the ischaemic and normal ADC was similar for each of the X-, Y- and Z-ADC maps, although this result may be at odds with the observation of Dardzinski et al. (Dardzinski *et al.* 1993), who observed that the greatest difference occurred when the sensitising gradients were in the Z direction. ADC values have been calculated for normal and ischaemic cerebral tissue in rats (Knight *et al.* 1991), cats (Moseley *et al.* 1990) and humans (Warach *et al.* 1992). In addition to defining ADC thresholds for the evaluation of ischaemic lesion areas, (Dardzinski *et al.* 1993; Hasegawa *et al.* 1994; Hoehn-Berlage *et al.* 1995; Kohno *et al.* 1995; Mancuso *et al.* 1995; Perez Trepichio *et al.* 1995) attempts have been made to establish an ADC threshold below which irreversible ischaemic damage will occur (Dardzinski *et al.* 1993; Helpern *et al.* 1993; Hasegawa *et al.* 1994). My data indicate that quantitative thresholding approaches based on diffusion sensitisation along a single axis may be prone to error due to the effects of the underlying anisotropy. Basser has previously emphasised the importance of dealing properly with anisotropy in diffusion-weighted imaging (Basser, 1995) and a complete quantitative analysis requires the estimation of the full diffusion tensor. The present study provides an example of the kind of errors that can occur when the effects of anisotropy are ignored.

5.4.2 Conclusion

In conclusion, the ability to make accurate measurements of lesion size and of ADC values is of prime importance in the investigation of cerebral ischaemia using DWI. This study has demonstrated the systematic effects of grey matter as well as white

matter anisotropy on both lesion area and ADC in the PGSE-DWI images, which can make delineation of ischaemic lesions inaccurate by this method. In contrast, lesion delineation was more consistent among ADC_{ss} and ADC_{av} maps, despite differing diffusion times. This demonstration that under the present experimental conditions, the presence of cross terms does not have an adverse effect on lesion delineation obtained using ADC_{av}. Therefore, imaging the trace of the diffusion tensor, either with the single-scan technique or by multiple directional PGSE-DWI, allows a more reproducible demarcation of the ischaemic lesion, and should be useful in defining critical thresholds in cerebral ischaemia.

Chapter 6

6. Early Changes in Water Diffusion, Perfusion, T_1 and T_2 During Focal Cerebral Ischaemia in the Rat Studied at 8.5T

In the last two chapters, I adopted an *on the bench* approach to the occlusion of the middle cerebral artery (MCA) in the rat. For the experiments in this chapter, I developed a method to *remotely* occlude the MCA while the rat was anaesthetised in vertical 5cm diameter bore of the 8.5T imaging magnet. This preparation permitted the measurement of the acute time evolution of water diffusion, perfusion, T_1 and T_2. The main observations in this Chapter are:

- the combination of perfusion- and diffusion-images to provide tissue signatures for regions of "moderately affected tissue", with reduced perfusion but normal diffusion; and "severely affected tissue", in which both perfusion and diffusion are significantly reduced.
- two novel MRI observations are also reported, namely a decrease in T_2 and an increase in T_1, both within the first few minutes of ischaemia. The rapid initial decrease in T_2 is believed to be associated with an increase in deoxyhaemoglobin levels, while the initial increase in T_1 may be related to several factors, such as flow effects, an alteration in tissue oxygenation and changes in water environment.

6.1 INTRODUCTION

In this study, I carried out investigations of water diffusion, perfusion, T_1 and T_2 during the first 4-6 hours following permanent middle cerebral artery (MCA) occlusion in the rat. I used a high magnetic field strength (8.5 T), which has well-recognised benefits for perfusion measurements (Detre *et al.* 1992), and which might also be expected to accentuate some of the effects that can influence relaxation times.

6.2 METHODS

6.2.1 Animal preparation

Ten male Wistar rats weighing 130-150g, were prepared for MCA occlusion, which was subsequently carried out remotely with the animal in the magnet. The surgical procedure was based on a modified Zea Longa approach (Longa *et al.* 1989) adapted for a vertical magnet. Anaesthesia was induced with 3% halothane/O_2 and continued via a nose cone at 1.25% halothane for the duration of the surgery. Rectal temperature was recorded and maintained at 37.5±0.5°C. The remote occluding device was a blunted 0.24 mm nylon thread occluder. Once the animal was inside the magnet, the halothane concentration was reduced to 0.8% in a gas mixture of 70% N_2O and 30% O_2.

6.2.2 Imaging protocol

The experimental protocol involved approximately 2 h for positioning, shimming and the acquisition of control data (pre-occlusion), followed by remote occlusion of the MCA, and subsequent continuous imaging for 4-6 h. The following imaging sequences were used to study the time-course of each parameter:

6.2.2.1 T_1 measurement

Series of 20 Snapshot-FLASH inversion recovery images (19) ($TE/TR/T_{image}$= 2.0/3.6/231 ms; inter-FLASH delay=2 ms; flip angle=5°; N_A=20). For efficient spin inversion, a slice-selective adiabatic frequency offset corrected inversion (FOCI) pulse (Ordidge *et al.* 1996) was used.

6.2.2.2 T_2 measurement

T_2 measurement: Four echo multi-spin-echo sequence ($TE_{[n=1,4]}$=35,70,105,140 ms; TR=1000 ms; N_A=4).

6.2.2.3 Measurement of the trace of the diffusion tensor (Tr(D))

Measurement of the trace of the diffusion tensor (Tr(**D**)): Single scan trace-weighted imaging sequence (Pattern III, (Mori and van Zijl, 1995)) (δ/Δ=5/5.4 ms; b-values=30,800,1700 s/mm^2), (TE/TR= 80/1000 ms; N_A=4).

6.2.2.4 Perfusion measurement

Perfusion measurement: Two different sequences were used: a) Sequence I: arterial spin tagging (AST) (Williams *et al.* 1992) was performed inverting the arterial spins using adiabatic fast passage (AFP). A 5 s continuous RF pulse was applied at a 9 kHz offset, in the presence of a field gradient (1.6 G/cm), and was immediately followed by a Snapshot-FLASH acquisition (centre-out phase encoding; $TE/TR/T_{image}$=2/5/320 ms; flip angle=14°; N_A=25). Control measurements were made by reversing the field gradient (Pekar *et al.* 1996). The degree of arterial spin water inversion (α) was estimated in normal rats using Zhang's technique (Zhang *et al.* 1993), and a value of 0.71 was obtained for the degree of inversion (data not shown). b) Sequence II: after most of these experiments were completed, an improved protocol for obtaining

quantitative perfusion maps was implemented (Alsop and Detre, 1996), in which a delay was introduced between the end of the tagging and image acquisition. More accurate quantification was obtained since the contribution of vascular blood to the perfusion signal was suppressed. A further two normal animals were studied in order to assess the effect of a significant vascular signal contribution. A 500 ms delay was found to be necessary in order to eliminate the vascular signal (as in figure 4 of (Alsop and Detre, 1996)). T_1 in the presence of saturation (T_{1s}) was measured as described in (Alsop and Detre, 1996), T_1 of arterial blood (T_{1a}) was assumed to be 2000 ms, and the transit time to tissue (δ in (Alsop and Detre, 1996)) was assumed to be 900 ms. Each sequence used a 128x64 acquisition matrix size, which was then zero filled to 128x128 points before Fourier transformation.

6.2.3 Data processing and analysis

Maps of T_1, T_2 and Tr(**D**) were generated using routines written with IDL software (RSI, Boulder, Colorado), by non-linear curve fitting on a pixel by pixel basis. Two-parameter fits (single exponential) were used with the T_2 and Tr(**D**) data, while a three-parameter fit, according to the equation given by Deichmann et al (Deichmann and Haase, 1992), was used with the T_1 data. The T_1 map was then used to calculate perfusion (Williams *et al.* 1992), assuming a brain-blood partition coefficient of 0.9 ml/g (Herscovitch and Raichle, 1985). For the calculation of perfusion using sequence II, the data were fitted to Eq. (9) in (Alsop and Detre, 1996).

A study of the time dependence of the various NMR parameters was performed by first defining three regions of interest (ROIs) in each animal using the combined information of the CBF and Tr(**D**) maps. One region was positioned in the contralateral normal

hemisphere, while the other two were in the affected hemisphere: one in the core, and the other in a border area of moderate ischaemia. The ROI in the core of the lesion was defined as the area with the largest change in diffusion, as seen on the Tr(**D**) maps at a late stage (4-6 h post-occlusion). It always lay within the thalamic and hypothalamic region, but its exact location was different in each animal. A border region (in the frontal parietal cortex, between the areas supplied by the middle and anterior cerebral arteries) was defined in 8 of the 10 animals as a region of moderately reduced blood flow with no change in Tr(**D**).

In order to analyse the time evolution of the different parameters and to examine regional differences, separate multiple linear regression calculations were used to fit polynomials to the data obtained from each animal. This was done independently for the pre- and post-occluded phases, and the regression coefficients, or parameters derived from them, were used as summary parameters in univariate analyses (Matthews *et al.* 1990). When a paired *t* test was used, the two animals that did not have a border region were excluded from the analysis. In order to document the absolute values of the various parameters, these are quoted as the mean ± SE over the total number of animals for each ROI (n=10 for the core and contralateral regions, and n=8 for the border region). It is important to note, however, that these standard errors were not used in any subsequent analysis of the within-subjects effects, which was performed using the paired *t* test and a selected summary parameter.

6.3 Results

Figure 6.1 shows calculated perfusion and Tr(**D**) maps 4 h after MCA occlusion, together with a schematic representation of the three main areas that were used for all

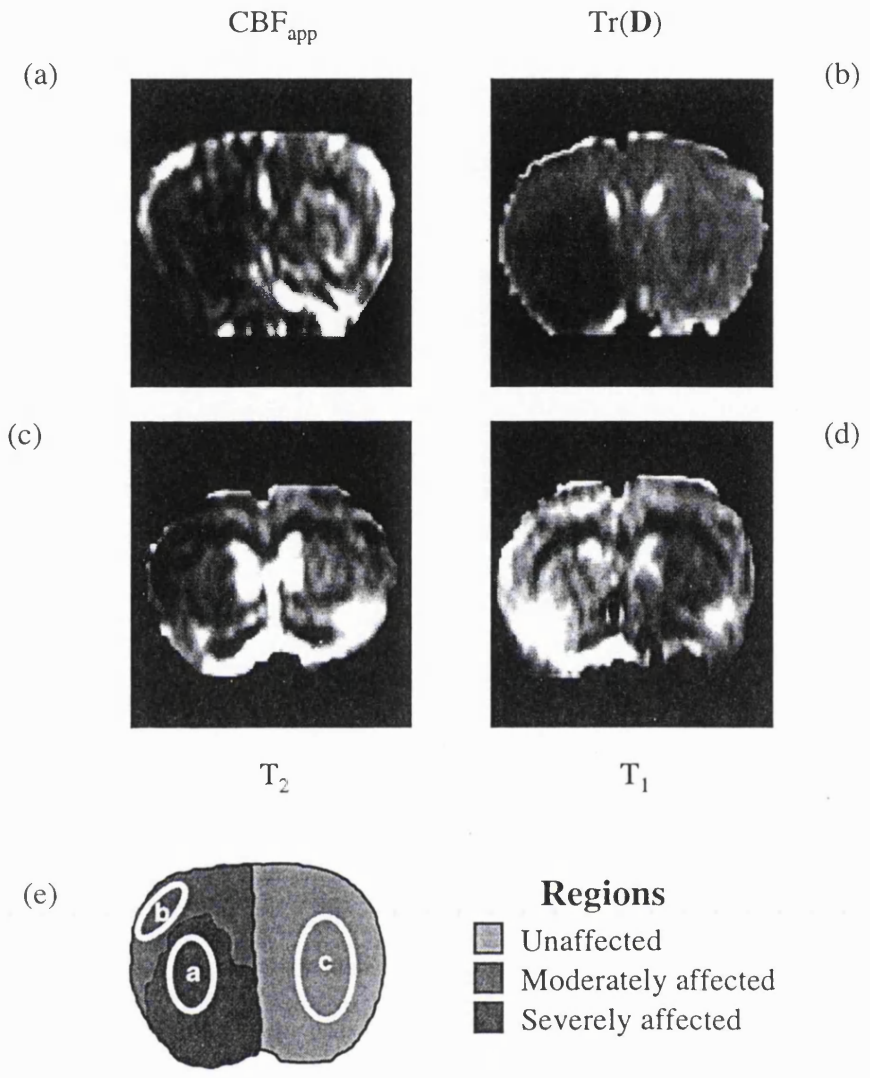

Figure 6.1 Typical maps obtained from a rat following MCAO. (a) shows a perfusion map with reduced flow in the occluded side (acquired 4 hours post-occlusion). (b) shows a trace map (4 hours post-occlusion) with a region of reduced diffusion indicating the area of cytotoxic oedema. (c) shows a T_2 map (1 minute post-occlusion) with a region of reduced T_2. (d) shows a T_1 map (5 minutes post-occlusion), with a region of increased T_1. The dark spot in the T_1 map is due to a DC artefact. (e) shows a schematic representation of the three main areas: "unaffected area", where a relatively small and transient reduction in flow was detected; "moderately affected area", with reduced CBF but normal Tr(**D**); and "severely affected area", in which both the CBF and Tr(**D**) were significantly reduced. The ROIs represent typical regions used for the time-course analysis: core region **(a)**, border region **(b)**, and contralateral region **(c)**.

the subsequent analyses. Region (A) is a "severely affected area" in the core of the lesion, with reduced diffusion; region (B) is a "moderately affected area", with reduced cerebral blood flow (CBF) but no reduction in diffusion; and region (C) is an "unaffected area", where a relatively small and transient reduction in flow was detected. Figure 6.1 shows perfusion, Tr(**D**), T_1 and T_2 maps from a single animal, and demonstrates regions of decreased CBF (≈4 h post-occlusion), reduced diffusion (≈4 h post-occlusion), increased T_1 (≈5 min post-occlusion) and decreased T_2 (≈1 min post-occlusion). In the following sections, I discuss in turn the time-course data for perfusion, diffusion, and the two relaxation times in the three selected regions of interest.

6.3.1 Perfusion (CBF)

Figure 6.1 show a typical perfusion map obtained 4 h after occlusion, and Figure 6.2 shows the time-course data for the three ROIs. The mean CBF before occlusion was 186 ± 11 ml/100g/min (range 144-244 ml/100g/min) in the core region (Figure 6.2a). Similarly, the mean CBF was 146 ± 8 ml/100g/min (range 111-175 ml/100g/min) in the border region (Figure 6.2b), and 205 ± 14 ml/100g/min (range 128-248 ml/100g/min) in the contralateral region (Figure 6.2c). I attribute the high CBF values and the large variability in the measurements, at least in part, to effects not accounted for in the quantification of perfusion, such as the contribution of vascular blood to the signal intensity (Alsop and Detre, 1996; Ye *et al.* 1997), and the effect of magnetization transfer (Zhang *et al.* 1995; McLaughlin *et al.* 1997). Both of these effects contribute to an overestimation of perfusion. The presence of a heterogeneous high vascular signal makes the measurement very dependent on the position of the ROI, and this could explain the large variability and the difference between regions prior to occlusion.

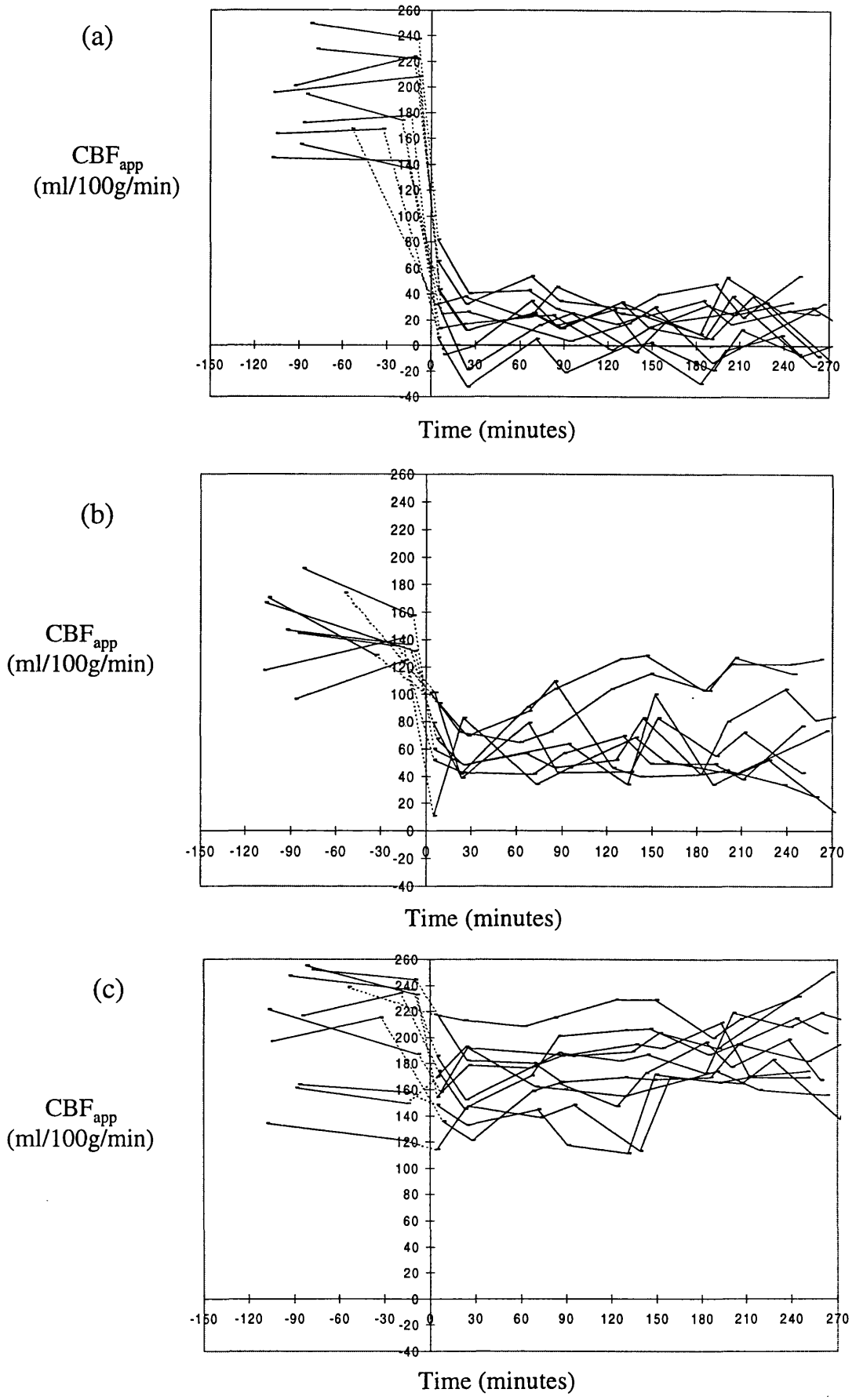

Figure 6.2 CBF time courses in (a) core, (b) border, and (c) contralateral regions of MCAO rat brain. Occlusion performed at time t = 0 minutes. The core experiences extreme an reduction in blood flow, the border zone a moderate reduction and the contralateral side a minimal reduction

Alsop et al (Alsop and Detre, 1996) and Ye et al (Ye *et al.* 1997) have recently shown that the flow rates are substantially overestimated when the vascular signal is not eliminated. Therefore, the values obtained in the present experiment with AST (sequence I) are referred to as apparent cerebral blood flows (CBF_{app}).

It may be seen from Figure 6.2a that, after the initial drop induced by occlusion, the CBF_{app} in the core remained approximately constant. When CBF_{app} was less than ≈20 ml/100g/min, the measured perfusion was within the noise level, which explains the negative data points. A decrease in CBF_{app} was also observed in the other two ROIs, with some of the rats showing a more variable flow in these two regions than in the core. Due to this variability, and the intrinsically low signal to noise ratio (SNR) in the measurement of perfusion using MRI, the difference ΔCBF_{app} between the mean pre-occluded measurement and the average of the first two post-occluded values was used as a summary variable to study the drop in CBF_{app}.

Although both ischaemic regions showed a highly significant reduction in CBF_{app} ($p<0.0001$ for both regions), ΔCBF_{app} was significantly larger (paired *t* test, $p<0.0001$) in the core (mean value=163±8 ml/100g/min) than in the border region (mean value=83±6 ml/100g/min). The relatively small initial flow change in the contralateral side (mean ΔCBF_{app}=39±11 ml/100g/min) was also statistically significant ($p=0.01$). After this initial drop, the perfusion in the contralateral hemisphere gradually returned to pre-occluded values.

As mentioned above, the absolute value of CBF was overestimated. A better estimation of the true perfusion values was obtained using sequence II, in which a delay is

introduced between the end of tagging and image acquisition. Measurements were made using ROIs similar to those used for the present time-course analyses. The mean CBF values from two normal rats were compared to the values obtained when no delay was introduced (as was the case for the rats that underwent MCA occlusion). When no delay was used (sequence I), the mean CBF values (CBF_{app}) were 185, 187, and 208 ml/100g/min, in the areas that correspond to core, border, and contralateral region, respectively. These values are similar to the pre-occlusion values obtained from the MCA occlusion group. In contrast, when the delay was added (sequence II), the calculated CBF were reduced to 85, 93, and 90 ml/100g/min in these three regions.

6.3.2 Water diffusion

Figure 6.1b shows a typical trace map obtained 4 h after occlusion, and Figure 6.3 shows the time-courses of Tr(**D**). The normal pre-occluded Tr(**D**) values were 0.83±0.02, 0.81±0.01 and 0.83±0.01 $x10^{-3}mm^2/s$, in the core, border, and contralateral regions, respectively. In the core region (Figure 6.3a), Tr(**D**) was reduced by ≈23% relative to pre-occlusion at the first time point (t≈50 min). Thereafter it showed a gradual decrease for 2-3h after occlusion, towards an asymptotic value of 0.51±0.02 $x10^{-3}mm^2/s$. The time-course was very different in the border region (Figure 6.3b), where no reduction in the Tr(**D**) was observed (p=0.9). Furthermore, a paired *t* test showed that there was no significant difference (p=0.1) between the asymptotic values in the border and contralateral regions, which remained unchanged throughout the experiment. The mean asymptotic values in these regions were: 0.80±0.01 $x10^{-3}mm^2/s$ in the border and 0.82±0.01 $x10^{-3}mm^2/s$ in the contralateral region.

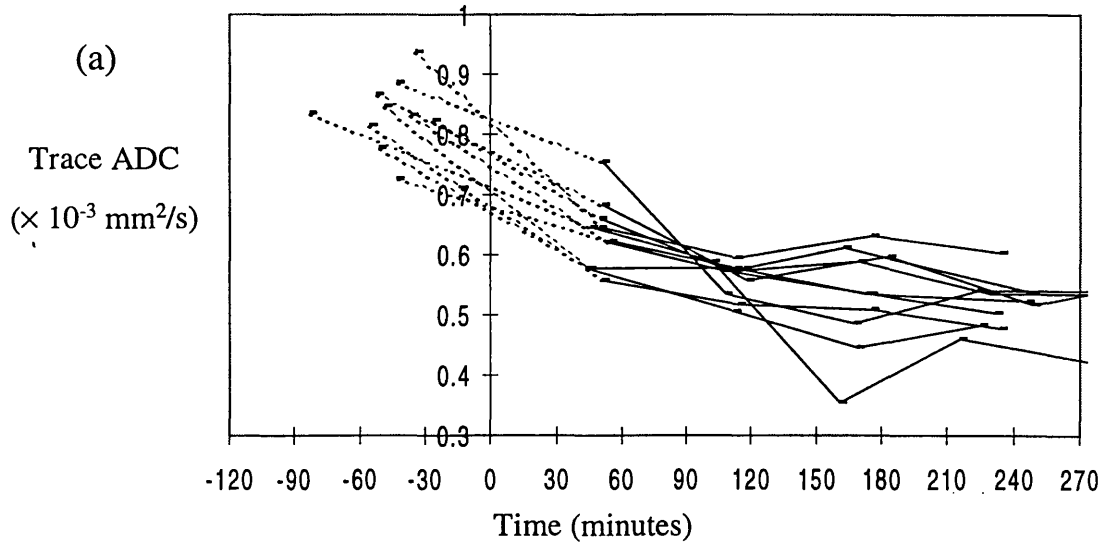

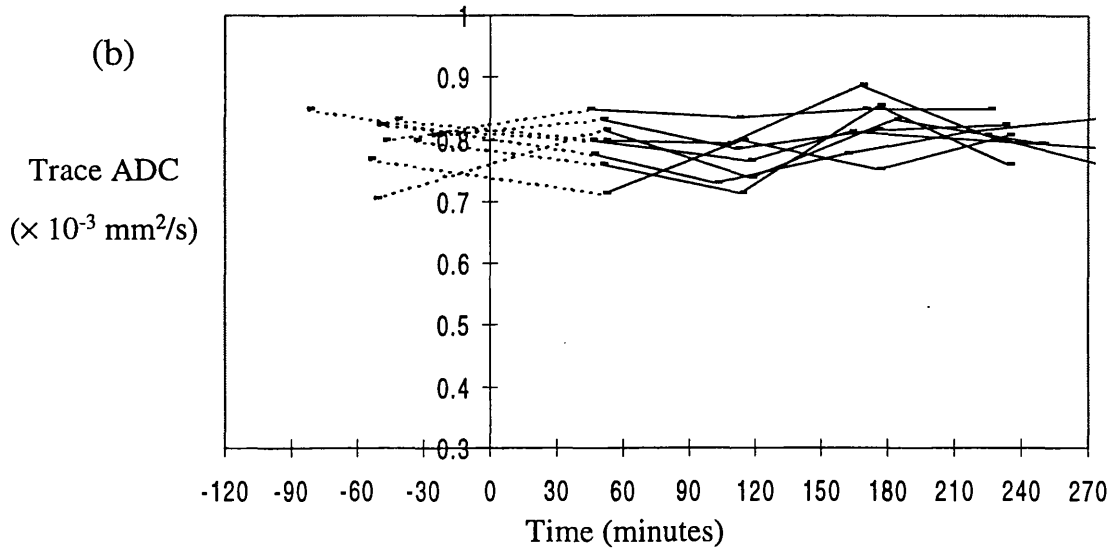

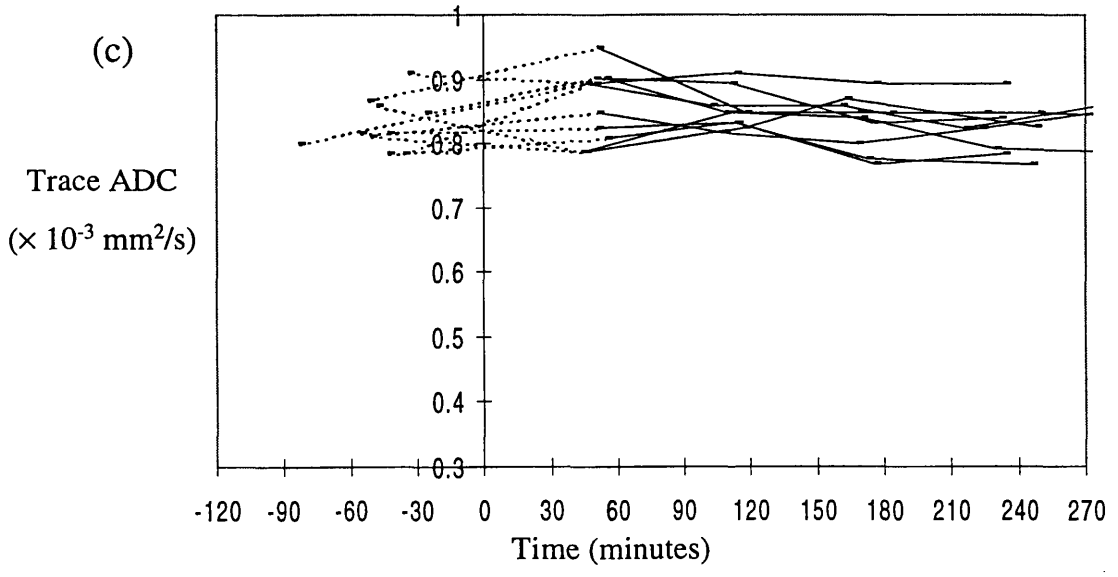

Figure 6.3 Trace ADC time courses in (a) core, (b) border, and (c) contralateral regions of MCAO rat brain. Occlusion performed at time t = 0 minutes. A reduced ADC in the core signifies cytotoxic oedema, whereas the ADC remains unchanged in the border and contralateral regions

6.3.3 Spin-spin relaxation time (T_2)

Figure 1c shows a T_2 map obtained 1 min following occlusion, and Figure 6.4 shows the time-course data for the core (Figure 6.4a), border (Figure 6.4b) and the contralateral (Figure 6.4c) regions. The mean pre-occluded T_2 values were 42.5±0.9 ms in the core, 40.7±0.5 ms in the border region, and 41.8±0.7 ms in the contralateral region. A very rapid decrease in T_2 from its pre-occluded value was seen in all rats in both the border and core regions at 1 min post-occlusion. After this early drop, the behaviour was different for each ROI. In the border region, T_2 returned to normal values (by 30-60 min after occlusion), thereafter increasing more slowly, while in the core region the T_2 values rose linearly for the duration of the measurements. An analysis of the T_2 changes for times >1 h was performed using the slopes obtained from linear regression analysis of the individual time-course data (a first order polynomial provided an adequate description of the data for times >1 h). Both the core and the border region exhibited a statistically significant slope ($p<0.0001$ and 0.002, respectively), with a mean value of 1.77±0.24 ms/h in the core, and 0.39±0.07 ms/h in the border region. A paired *t* test showed that these slopes were significantly different ($p=0.003$). In contrast, the slope in the contralateral region was not significantly different from zero ($p=0.7$), with a mean value of 0.08±0.17 ms/h.

The time resolution in the present study was insufficient to provide a detailed description of the time dependence of the rapid initial drop in T_2. Therefore, the difference between the average of the pre-occluded values and the first post-occluded measurement (time≈1 min) was used to characterise this initial decrease. Both the core (mean value= -2.19±0.29 ms) and the border region (-3.18±0.50 ms) yielded a

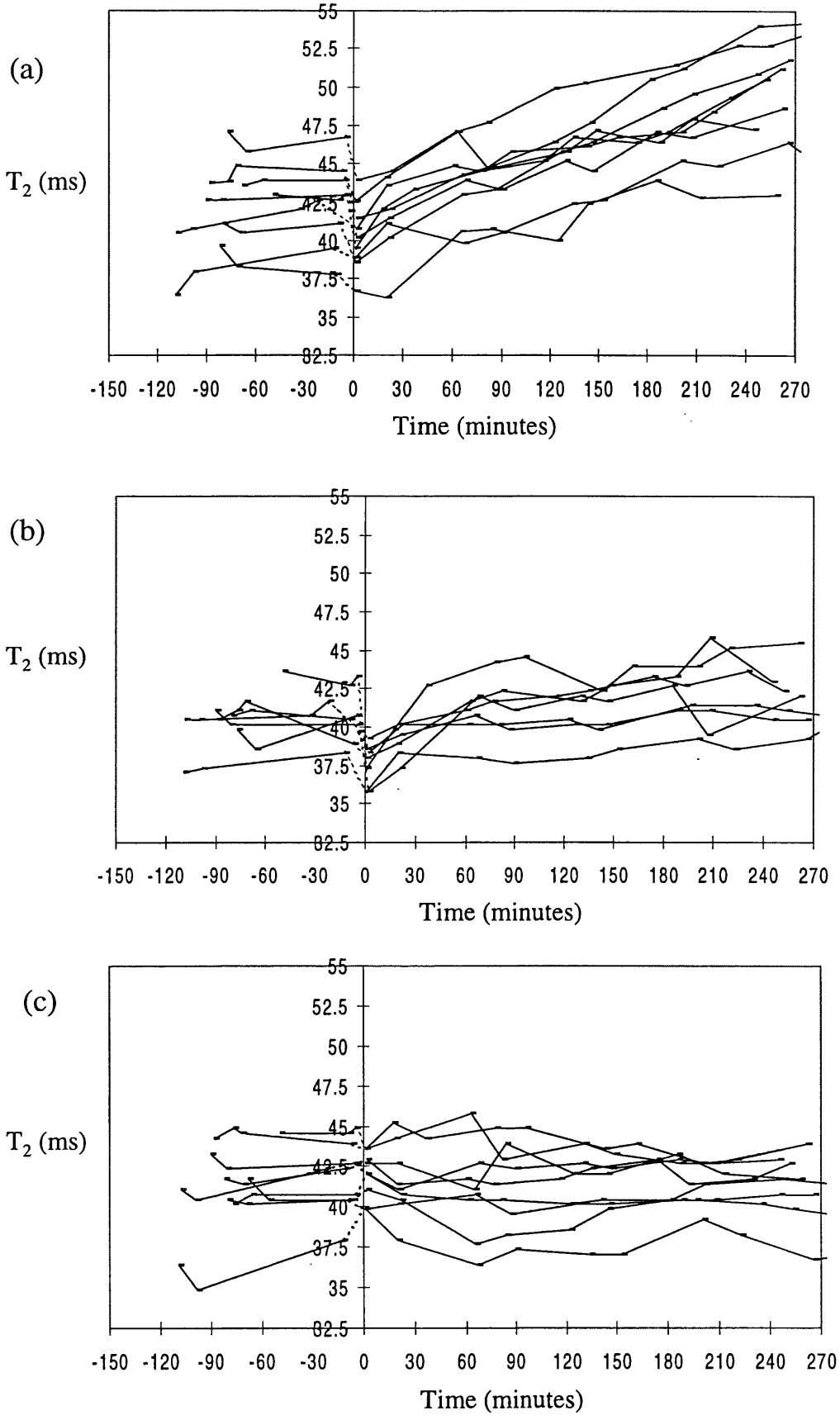

Figure 6.4 T_2 time courses in (a) core, (b) border, and (c) contralateral regions of MCAO rat brain. Occlusion performed at time t = 0 minutes. A rapid drop in T_2 is observed following occlusion in both the core and border regions, indicating increased levels of deoxyhaemoglobin. T_2 subsequently returns to normal in the border, and increases to values greater than the pre-occlusion levels in the core, indicating increased tissue water content

statistically significant initial decrease ($p < 0.0001$ and 0.001, respectively), while the change in the contralateral region (0.19±0.32 ms) was not significant ($p=0.6$).

6.3.4 Spin-lattice relaxation time (T_1)

Figure 1d shows a typical T_1 map obtained 5 min following occlusion, and Figure 6.5 shows the time-course data for the core (Figure 6.5a), border (Figure 6.5b) and the contralateral (Figure 6.5c) regions. The mean pre-occluded T_1 values were 1718±25 ms in the core, 1756±18 ms in the border region, and 1676±30 ms in the contralateral region. A rapid increase in T_1 occurred in the two ischaemic regions within 5 min of occlusion (first post-occluded measurement). The time evolution after this early increase was different in these two regions, progressively increasing at a slow rate in the core, while it remained approximately constant in the border region.

The initial change in T_1 was too rapid, relative to the time resolution of this study, for its time dependence to be analysed. Consequently, the rapid and slow-response phases of the time-course data were examined separately. An analysis of the slow-response phase (t>25min) was performed by fitting separate polynomials to the T_1 data obtained from each animal. The individual values predicted by the regression model at 45 and 240 min were then used to calculate the rate of change in T_1 during this interval. The 45 and 240 min time points were selected in preference to the 25 min and last measurement data because the confidence interval of the estimates increases at the extremities of the time interval. The mean rate of change of T_1 in the core was 46.1±5.5 ms/h, which is significantly different from zero ($p<0.0001$) while the mean value in the border region was -2.3±1.6 ms/h, which does not achieve significance ($p=0.2$). The value in the contralateral region was -5.6±1.9 ms/h, which is statistically significant

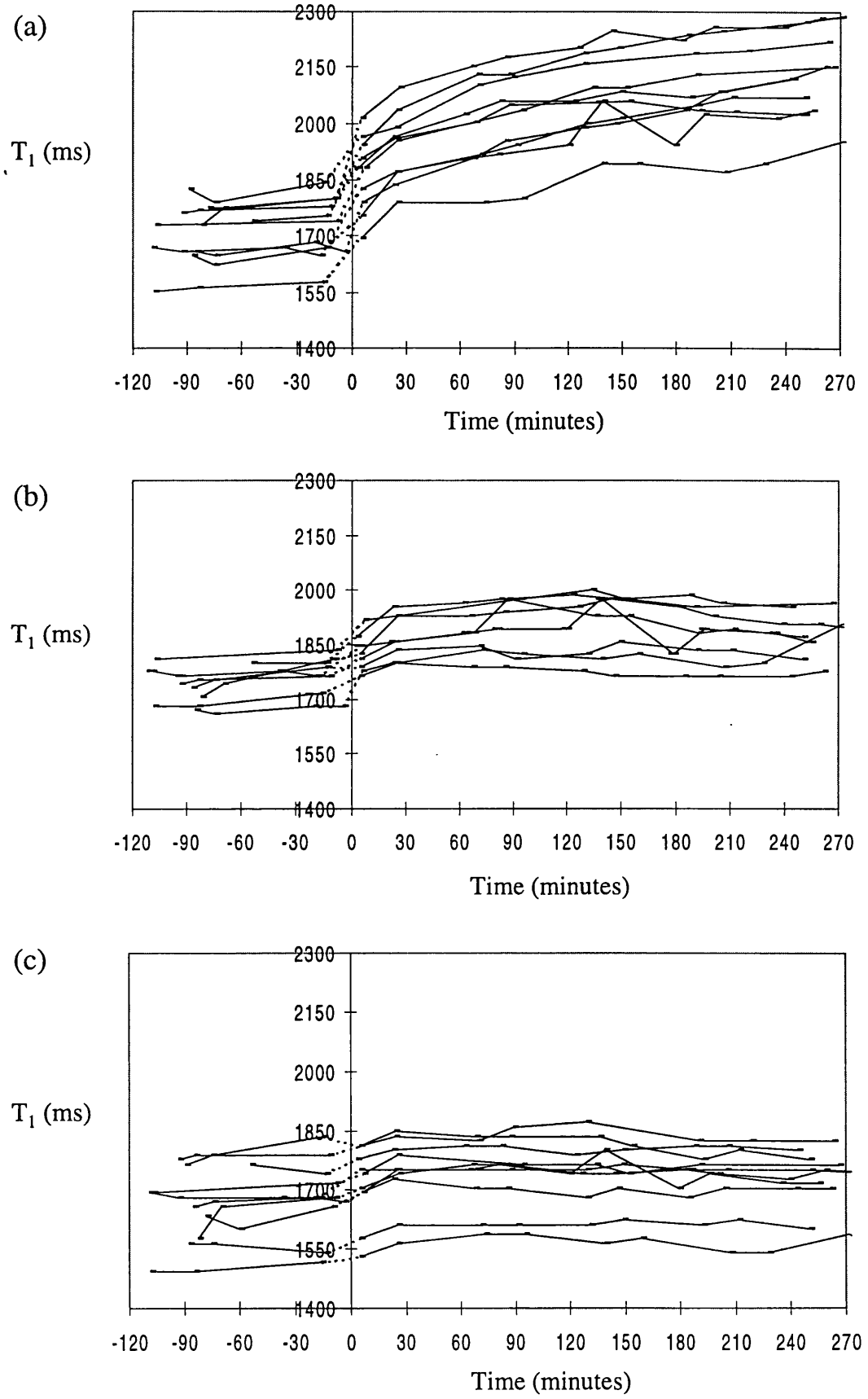

Figure 6.5 T_1 time courses in (a) core, (b) border, and (c) contralateral regions of MCAO rat brain. Occlusion performed at time t = 0 minutes. T_1 is elevated post- occlusion in the core and the border regions, and continues to rise over the next few hours in the core

compared with zero (p=0.02). This decrease in T_1 towards the pre-occluded values occurs simultaneously with the recovery in CBF in the contralateral ROI.

An additional characterisation of the differing T_1 behaviour in the three regions was obtained by examining the difference between the 45 min value predicted by the regression model and the average pre-occluded T_1 values. All three ROIs yielded differences that were significantly different from zero (mean values of 249±12 ms in the core, 126±10 ms in the border, and 68±7 ms in the contralateral region). The three pair-wise tests on the differences were also highly significant (paired *t* tests: core vs. border region, p<0.0001; core vs. contralateral region, p<0.0001; and border vs. contralateral region, p=0.0005).

Although I was unable to analyse the time dependence of the rapid, initial T_1 change, the difference between the average of the pre-occluded T_1 values and the first post-occluded measurement (t≈5 min) was used as a summary variable. The values obtained for the core (mean value=148±11 ms) and the border region (69±10 ms) were significantly different from the values obtained in the contralateral region (35±6 ms) (paired *t* test on the difference: p= 0.0001 and 0.01 respectively). The results demonstrate that high field MRI detects an immediate T_1 response to an ischaemic insult.

6.4 Discussion

6.4.1 Regional cerebral blood flow: MR perfusion imaging

In this rat model of middle cerebral artery occlusion, I have shown that T_1 and T_2 changes are observed at 8.5T in regions of reduced blood flow within a few minutes following occlusion. These changes occur not only in the core of the lesion, but also in a border region where there is a much less severe reduction in blood flow and no reduction in the apparent diffusion of water. In addition to the expected decrease in CBF in the occluded hemisphere there was also a small but significant decrease in the contralateral region. This phenomenon has been reported previously (Allergrini *et al.* 1996) and it was shown that an autoregulatory response to the ischaemic insult in one hemisphere was the cause of the CBF changes in the contralateral side.

The measurement of perfusion using MRI offers many advantages, including its non-invasive character, the possibility of continuous monitoring, and direct spatial registration to other MR images. However, great stability is demanded from the MR system, and reliable quantification of perfusion remains a major challenge. Recent improvements in methodology have led to more accurate quantification (Zhang *et al.* 1995; Alsop and Detre, 1996; McLaughlin *et al.* 1997; Ye *et al.* 1997). However, the very low CBF in the occluded regions introduces two main problems. Firstly, quantification of the resulting very small signal difference requires an extremely large SNR in the two images used to obtain the difference. Secondly, there is a much longer and heterogeneous distribution of transit times from the magnetically tagged region to the imaging slice, resulting in an underestimation of perfusion.

In the present study, a substantial reduction in the measured flow values was obtained in normal animals by using a recently proposed technique, in which a delay is introduced between the end of tagging and image acquisition (Alsop and Detre, 1996). The measured mean normal perfusion using a 500 ms delay (sequence II) was 50% of the value obtained without delay (sequence I). The quantification using sequence II should in principle be more accurate, because it reduces the signal contribution from vascular water spins. However, validation studies are needed to substantiate this. Furthermore, the improved accuracy of this technique for measurements in the occluded region remains to be established. Although the sensitivity to different transit times is reduced with this technique, the very long transit times present in the occluded regions may still be problematic. Any quantitative analysis of low CBF values (including, for example, flow thresholds for energy failure) must take these factors into account.

6.4.2 Diffusion-weighted imaging in acute cerebral ischaemia

The rather high Tr(**D**) values reported in this study are likely to reflect the short diffusion time (t_d) used in the diffusion sequence. This sequence was recently compared to one with the same TE but $t_d \approx 25$ ms. Although the measured Tr(**D**) values were different, the areas of the reduced diffusion were not significantly different. Consistent with previous studies(Van Bruggen *et al.* 1994; Hoehn-Berlage, 1995) the diffusion measurements have shown a decrease in ADC, with a reduction of ≈40% in the trace of the diffusion tensor in the ischaemic core region after 4 h of ischaemia. Moreover, the combined analysis of CBF and Tr(**D**) maps allowed us to define a region of moderate ischaemia (border region), where no reduction in diffusion was detected over a sustained period of 4-6 hours, despite the reduction in perfusion. Presumably, the flow remained above the threshold required to maintain the cellular energy status, so

that the ionic and osmotic balance of the cells remained normal. Further studies may reveal whether the low ADC region does expand into the border region, and whether this displays the same or higher flow thresholds when compared with the core region. It is interesting to note that the border region in the present work is similar to one of the border regions defined by Jones et al (BZM region in (Jones *et al.* 1989)) in their study of CO_2 reactivity. The latter region showed a much lower reactivity of CBF to $PaCO_2$, and they suggested that the tissue was haemodynamically compromised, and may become infarcted.

6.4.3 Relaxation times during acute cerebral ischaemia

The most striking finding is the observation of early changes (within a few minutes following occlusion) in the relaxation times T_1 and T_2, both in the border region as well as in the core region.

6.4.3.1 T_2 relaxation

A decrease in T_2 was observed immediately after a reduction in blood flow. Although a similar effect on T_2* has been observed previously using gradient-echo (GE) imaging (Roussel *et al.* 1995) and spectroscopic measurements of water relaxation (Busza *et al.* 1994; van der Toorn *et al.* 1994), there has been less emphasis on early T_2 changes in spin-echo images (Calamante *et al.* 1997). A hypointense region using spin-echo imaging has been reported previously (Quast *et al.* 1993; Mancuso *et al.* 1995) but although a relative long TR was used, complete separation of the T_2 from the T_1 contribution was not possible. The results shown in the present work clearly demonstrate the decrease in T_2 after ischaemia. I emphasise the contrast between this finding and the later increase in T_2 that is usually attributed to vasogenic oedema.

The similarity of the findings obtained with gradient-echo and spin-echo imaging suggests a mechanism common to the early decrease in T_2* and T_2 relaxation. One possibility is an increase in the amount of deoxyhaemoglobin (deoxyHb) in the ischaemic area. Our group have previously proposed (Busza *et al.* 1994) that the initial T_2 change was due to the dephasing of water spins as they diffuse through the local field gradients caused by the accumulation of deoxyHb. This effect would be greater at 8.5 T than at the lower field strengths typically used for NMR imaging, which may be the reason for the effect not being observed in investigations of cerebral ischaemia at lower field strengths. More recently van Zijl et al (van Zijl *et al.* 1998) have suggested a vascular mechanism for the reduction in T_2, with the vascular water relaxation enhanced through fast exchange across the red blood cell membrane. Based on a mild hypoxic hypoxia model, they were able to account for the observed changes in T_2 using only this vascular mechanism. However, the extension of this model to cerebral ischaemia remains to be shown. Whatever the mechanism (diffusion or exchange), the reduction in T_2 is larger for single echo than for multi-echo acquisition. However, the dependency on the inter-echo spacing is different for the two mechanisms, and further experiments characterising this dependency may differentiate between the two mechanisms.

It is notable that, although the reduction of CBF in the border region was less than in the core, there was no significance difference between these two regions with respect to the T_2 change (paired *t* test, p=0.09). Similar findings for T_2* were obtained using GE imaging (Roussel *et al.* 1995). However, interpretation of this regional similarity is difficult, for the levels of deoxyHb depend not only on CBF, but also on the cerebral blood volume (CBV), the oxygen extraction fraction (OEF) and the haematocrit levels.

Moreover, the effect of the deoxyHb on T_2 may depend in turn on the diffusional properties of the water, which also differ between the core and border regions. The subsequent T_2 increase in the core region may be related to the partial recovery of the OEF (Pappata *et al.* 1993), or the compression of capillaries due to cytotoxic oedema leading to CBV reduction (Roussel *et al.* 1995). It may also reflect the development of vasogenic oedema over the time-course followed.

6.4.3.2 T_1 relaxation

The increase in T_1 occurred prior to the onset of vasogenic oedema, which is thought to be responsible for the elevated T_1 values at later times (and which may, at least in part, account for the slow component of the T_1 increase seen in the core region). These early T_1 changes have not been reported at low field strengths and the phenomenon may therefore be field dependent.

Although the early T_2 decrease in the core and border regions were indistinguishable in magnitude, the initial increase in T_1 was smaller in the border region. Furthermore, the mean rate of change after ≈1h was significantly different from zero for T_2 but not for T_1. Therefore, in the present experiment, T_2 seems to be more sensitive than T_1 to the time dependent changes that occur in the border region. However, these observations may be sequence dependent, since it was shown that the T_2 measurements using multi-spin-echo sequence are dependent on the inter-echo interval (Thulborn *et al.* 1982).

One possible explanation for the observed initial increase in T_1 is its dependence on flow. Since selective inversion was used for the measurements of T_1, there is a flow contribution to the observed T_1 (Zhang *et al.* 1995):

$$\frac{1}{T_{1obs}} = \frac{1}{T_1} + \frac{f}{\lambda}$$

where T_{1obs} is the measured T_1, f is the flow, and λ is the brain-blood partition coefficient. Using the technique described by Alsop et al (Alsop and Detre, 1996), the mean CBF value in normal rats was measured to be approximately 90 ml/100g/min. Even in the extreme case of zero flow post-occlusion, a 90 ml/100g/min pre-occluded CBF would account for a change in T_1 of at most ≈3%. However, a larger initial (t≈5 min) increase in T_1 was observed in the core (≈9%). In order to explain the increase in T_1 as being solely a result of reduced tissue perfusion, a change of 260 ml/100g/min in blood flow would be required. Even in this situation, the subsequent progressive increase in T_1 could not be accounted by flow alone, since T_1 continues to increase, without a further decrease in CBF. Therefore, although changes in flow can account for part of the observed T_1 increase, it cannot be the only effect responsible for this change.

An effect associated with the paramagnetic properties of deoxyHb, as proposed for the early T_2 drop, is unlikely to play an important role since it has been shown that T_1 is much less affected by the levels of deoxyHb than T_2 (Thulborn *et al.* 1982; Gomori *et al.* 1987; Bryant *et al.* 1990). Another possibility is the loss of O_2, which acts as a relaxation agent in tissue due to the paramagnetic properties of molecular oxygen itself. It has been previously shown (Tadamura *et al.* 1997) that T_1 is modified by alterations in the dissolved O_2 concentration, although the response was dependent on the tissue type. After ischaemia, the amount of dissolved O_2 would be reduced, leading to an increase in the T_1.

Another possible cause of the increase in T_1 is a change in water environment during ischaemia. It is known that changes in the "bound" pool as well as changes in the exchange rate of magnetization between the different water pools have an influence on the observed relaxation times (Lynch, 1983; Wolff and Balaban, 1989). This effect has been previously suggested (Ordidge *et al.* 1991) as one of the possible explanations for the increases in T_1 and T_2 observed after 2 hours of ischaemia, which occur before the development of vasogenic oedema. It is possible that the same effect may be responsible for part of the early changes observed at high field. Ewing et al have recently reported (Ewing *et al.* 1998) a decrease in the exchange rate of magnetization between "bound" and "free" pools (k_f) as early as 45 min after infarction. However, further studies are needed in order to show that these changes are also present in the first few minutes of ischaemia.

6.4.4 Conclusion

In summary, using high field MRI, I report the novel observation of T_1 and T_2 imaging changes in the first few minutes after ischaemia. The T_1 and T_2 changes occurred not only in the core of the lesion, where there was a severe reduction in blood flow and a decrease in water diffusion, but also in a border region where the flow was only moderately reduced with no change in water diffusion. I have shown that the combined analysis of the T_1 and T_2 changes, together with perfusion and diffusion measurements, provides a means of distinguishing between "core" and "border" regions at high field strength, and may help to characterise tissue that is compromised but potentially salvageable.

Chapter 7

7. A Novel Rat Model of Oligaemic Misery Perfusion Using Partial Occlusion of the Middle Cerebral Artery: *Acute Changes in MRI Diffusion, Perfusion, T_1 and T_2*

The aim of this chapter was to develop a rat model of oligaemic misery perfusion, in which the cerebral blood flow was reduced throughout the middle cerebral artery territory, without disturbing energy metabolism. The model has been designed for remote controlled occlusion and reperfusion from outside an MRI scanner.

Following middle cerebral artery occlusion there was a decrease in CBF from 181 to 62 ml/100g/min throughout the middle cerebral artery territory, followed by a gradual rise to 115 ml/100g/min. During the entire period of the study there were no observed changes in the ADC. On occlusion, T_2 rapidly decreased in both cortex and basal ganglia, and then normalised to the pre-occlusion values. T_1 values rapidly increased (within approximately 7 minutes) on occlusion.

This study demonstrates the feasibility of partially occluding the middle cerebral artery to produce a large area of oligaemic misery perfusion. In this region we detect a rapid increase in T_1 and decrease in T_2. These changes occur before the onset of vasogenic oedema. We attribute the acute change in T_2 to increased amounts of deoxyhaemoglobin; the mechanisms underlying the change in T_1 require further investigation.

7.1 INTRODUCTION

During the past 20 years, middle cerebral artery occlusion (MCAO) in rats has been extensively used to model human stroke. This technique produces a focal area of cerebral ischaemia, which may be achieved in a variety of ways, including: permanent or reversible intraluminal MCAO (Koizumi *et al.* 1986; Zea Longa *et al.* 1989); remote controlled MCAO using an intraluminal suture for magnetic resonance imaging studies (Roussel *et al.* 1994; Kohno *et al.* 1995; Li *et al.* 1998); coagulation or ligation of the middle cerebral artery (MCA) after craniotomy (Tamura *et al.* 1981); and embolisation with blood clots (Kudo *et al.* 1992) or photochemically induced thrombosis (Watson *et al.* 1995).

Numerous MRI investigations of cerebral ischaemia in the rat have been performed by occluding the MCA, with the animal outside the magnet, using the intraluminal approach (Mintorovitch *et al.* 1991). Although this technique allows reperfusion of the MCA, the acute phase of the insult is lost during the time taken to introduce the animal into the magnet. This limitation has been overcome by remote-controlled occlusion of the MCA, in which occlusion is performed remotely from outside the bore of the imaging magnet (Roussel *et al.* 1994; Kohno *et al.* 1995; Li *et al.* 1998). Improvements such as this have allowed investigation of the pathological consequences of stroke immediately following occlusion, and have permitted direct comparison with control images without the need for image registration.

When occluding the MCA using an intraluminal approach, the area of decreased cerebral blood flow (CBF) is inhomogeneous (Laing *et al.* 1993; Roussel *et al.* 1995). There are broadly two territories of decreased perfusion: an area of ischaemic misery

perfusion, and a region of oligaemic misery perfusion. The region that is most familiar is the territory of ischaemic misery perfusion, which is produced in the conventionally occluded MCA studies and is distinguished by a severely reduced CBF, increased oxygen extraction fraction (OEF), decreased oxygen consumption ($CMRO_2$) (Baron, 1991). The territory of oligaemic misery perfusion, which is less frequently apparent after MCAO, is characterised by a reduced CBF, increased OEF, yet normal $CMRO_2$.

This regional classification, although originally defined in relation to positron emission tomography (PET) data, is also relevant to other imaging techniques such as MRI (Roussel *et al.* 1995) and autoradiography (Chapter 4). In previous studies using MCAO in the rat, small regions of oligaemic misery perfusion have been differentiated within the area of perfusion deficit using combinations of CBF and autoradiographic images of hypoxia (Chapter 4), MRI T_2* and ADC maps (Roussel *et al.* 1995), and MRI CBF and ADC images (Calamante *et al.* 1999).

The uncoupling between flow and metabolism in regions of oligaemic misery perfusion has been demonstrated using positron emission tomography (PET), both in humans(Baron, 1991) and animals (Young *et al.* 1996). PET studies in humans have indicated that, up to 17 hours following a stroke, oligaemic misery perfusion regions spontaneously evolved toward infarction (Marchal *et al.* 1996). Specifically important to the work reported here are the metabolic and haemodynamic changes occurring in these regions, which may play an important role in the final outcome of the patient following a stroke.

Conventional intraluminal suture occlusion of the MCA in the rat produces regions of oligaemic misery perfusion of limited spatial distribution and size (Calamante *et al.* 1999). As a result, this potentially important region has been difficult to investigate; indeed, in many animal studies it may not be detectable. The aim of the present study was to produce a region of oligaemic misery perfusion throughout the MCA territory using a remote-controlled intraluminal suture occlusion in the rat, and to use MRI to identify acute changes in CBF, ADC, and the water relaxation times T_1 and T_2 within this region.

7.2 METHODS

7.2.1 Animal preparation

Five male Wistar rats weighing 130-150g were prepared for MCA occlusion, which was subsequently carried out remotely with the animal in an 8.5T vertical magnet. Anaesthesia was induced with 3% halothane/O_2 and continued via a nose cone at 1.25% halothane for the duration of the surgery. Rectal temperature was recorded and maintained at 37.5±0.5°C. Respiration and heart rate were also monitored, as all animals were allowed to breath spontaneously throughout the experiment.

7.2.2 Occluding device

The occluding device was a 0.2 mm diameter (5.0 lb.) nylon monofilament (Perlon, Bayer). This was checked for irregularities along the length of the final 3 cm; if there was any tendency to bend due to its packaging or manufacture, it was straightened by applying mild tension to the length of the monofilament for approximately 24 hours prior to use. The nylon monofilament was carefully cut to maintain the external

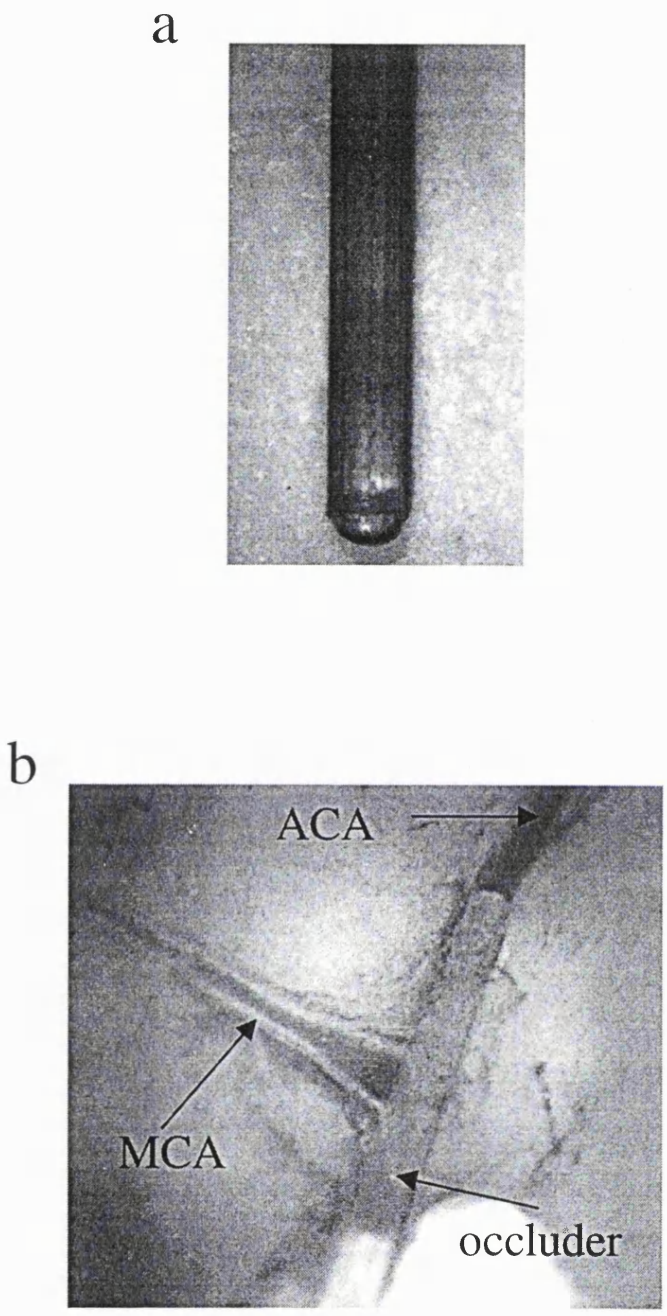

Figure 7.1. *(a) Embolus design for partial occlusion of the middle cerebral artery. Note the bullet-shaped tip formed with cyanoacrylate adhesive, 0.2 mm diameter. (b) Post-mortem examination of the ventral surface of the brain for the position of the occluding device. Anterior cerebral artery, ACA; middle cerebral artery, MCA.*

diameter, the end was dipped into cyanoacrylate adhesive and using the surface tension of the liquid a bullet-shaped tip was formed; care was taken not to exceed the external diameter of the thread (Figure 1a). The occluding thread was 50 cm long and moved freely in a Teflon guide (length: 45 cm, internal diameter 0.25 mm), which was inserted into the common carotid artery (CCA).

7.2.3 Animal surgery

The MCAO surgical procedure was based on a modified Zea Longa (Zea Longa *et al.* 1989) approach adapted for remote occlusion in a vertical magnet. The bore size of the 8.5T vertical magnet was 5 cm, which limits the weight of the rats to a maximum of 150g. Using an operating microscope, the right CCA was exposed by longitudinal midline incision from the submandibular triangle to the supraclavicular notch. The internal carotid artery (ICA) was isolated up to the carotid canal at the base of the skull. The vagus and hypoglossal nerves were carefully dissected away from the ICA and CCA.

Next, the rat was placed into the animal probe and the clear plastic strip attached to the skull was securely fixed to the probe. The surgery continued and a 6-0 silk suture was used to ligate the proximal CCA, and two further 6-0 silk sutures were placed around the distal end of the CCA. A microvascular clip was placed over the origin of both the ICA and the external carotid artery. The Teflon guide was inserted into the CCA via a small arteriotomy approximately 3 mm rostral to the carotid bifurcation. One of the 6-0 silk sutures was used to hold the CCA around the Teflon tube. The occluder was advanced under visual inspection until it reached the clip. At this time a second 6-0 suture was tied around the nylon monofilament to prevent bleeding into the guide once

the clip was removed. When the clip was removed, the occluder was advanced along the ICA past the patent pterygopalatine artery into the carotid canal. By advancing the occluder a further 9 mm from the tympanic bulla, the origin of the MCA could be occluded (Roussel *et al.* 1994). The Teflon guide was sutured to the sternomastoid muscle and the initial incision was closed. Once the animal was inside the magnet, the halothane concentration was reduced to 0.8% in a gas mixture of 70% N_2O and 30% O_2. Rectal temperature was recorded and maintained at 37.5±0.5°C by blowing warm air into the bore of the magnet. The final position of the occluder was visualised at post-mortem to ensure that the tip of the thread was past the origin of the MCA and that no haemorrhage had occurred (Figure 1b). The animal was fix to the probe as in Chapter 4.

7.2.4 Imaging protocol

See Chapter 6 for ADC, T_1 T_2 and CBF MRI measurements.

7.2.5 Data processing and analysis

For calculation of quantitative maps see Chapter 6. Data were analysed from 4 brain regions: in the cortex and basal ganglia both ipsilateral and contralateral to the side of MCAO. In order to analyse the temporal evolution of the different parameters and to examine regional differences, separate multiple linear regression calculations were used to fit polynomials to the data obtained from each animal. This was done independently for the post-occlusion phases, and the regression coefficients, or parameters derived from them, were used as summary parameters in univariate analyses (Matthews *et al.* 1990). In order to document the absolute values of the various parameters, these are quoted as the mean ± SE over the total number of animals for each ROI. It is important to note, however, that these standard errors were not used in any subsequent analysis of

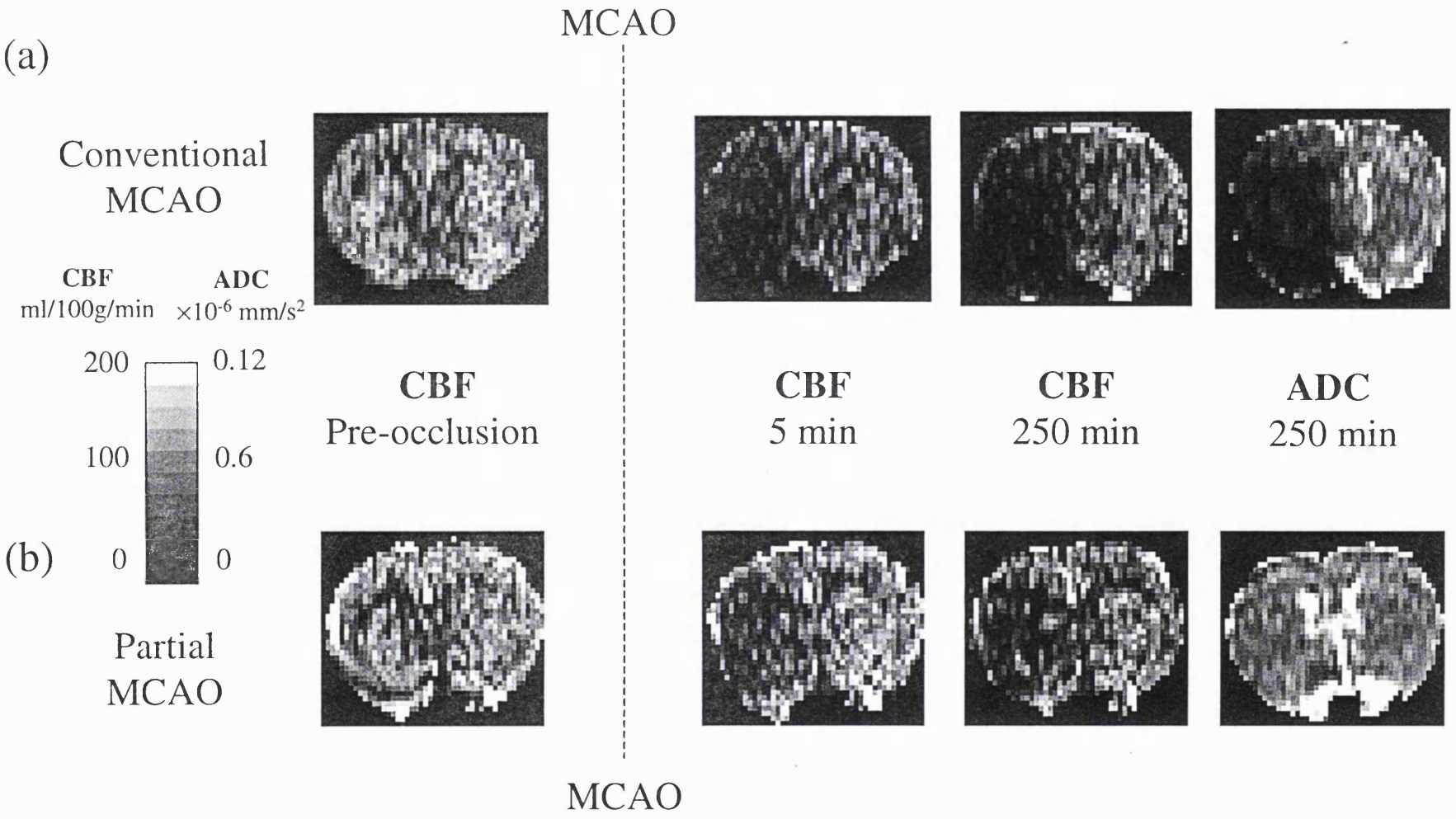

Figure 7.2 *(a) Conventional MCAO in the rat. Concomitant CBF and ADC decline. (b) Partial occlusion of the MCA. Moderate CBF decrease without energy failure, and therefore no ADC decrease.*

the within-subjects effects, which was performed using the paired *t* test and a selected summary parameter.

7.3 RESULTS

Figure 2 shows ADC and CBF maps obtained with both a conventional and partial MCAO (the model of oligaemic misery perfusion described here). In the conventional model, there is a severe decrease in CBF within the territory of the MCA, together with a concomitant decrease in ADC. However in the model of oligaemic misery perfusion, because of the partially occluded MCA, there is a less severe reduction in flow without any change in the ADC values. Complete analysis of the time course from the partial MCAO follows, together with the T_1 and T_2 relaxation findings.

7.3.1 Perfusion (CBF)

The mean CBF in the left and right hemispheres before occlusion was 198 ± 19 ml/100g/min in the basal ganglia and 177 ± 17 ml/100g/min in the cortex. Figure 3 shows the time course of the CBF changes. In the occluded hemisphere, it may be seen from Figure 3, that, within 5 minutes of partial occlusion, the CBF decreases significantly ($P<0.05$) to 105 and 72 ml/100g/min in the basal ganglia and cortex respectively. After 30 minutes of ischaemia, perfusion starts to increase towards the final values at approximately 270 minutes of 135 and 111 ml/100g/min in the two regions. These values are significantly different ($P<0.03$) from the pre-occlusion values, and the slope of the CBF data (after the first 25 minutes) is significantly different from zero ($P<0.03$). There were no statistically significant differences in flow between the two selected regions. The control hemisphere demonstrated a different pattern on initiation of ischaemia. There were initial small (but not significant) reductions in CBF

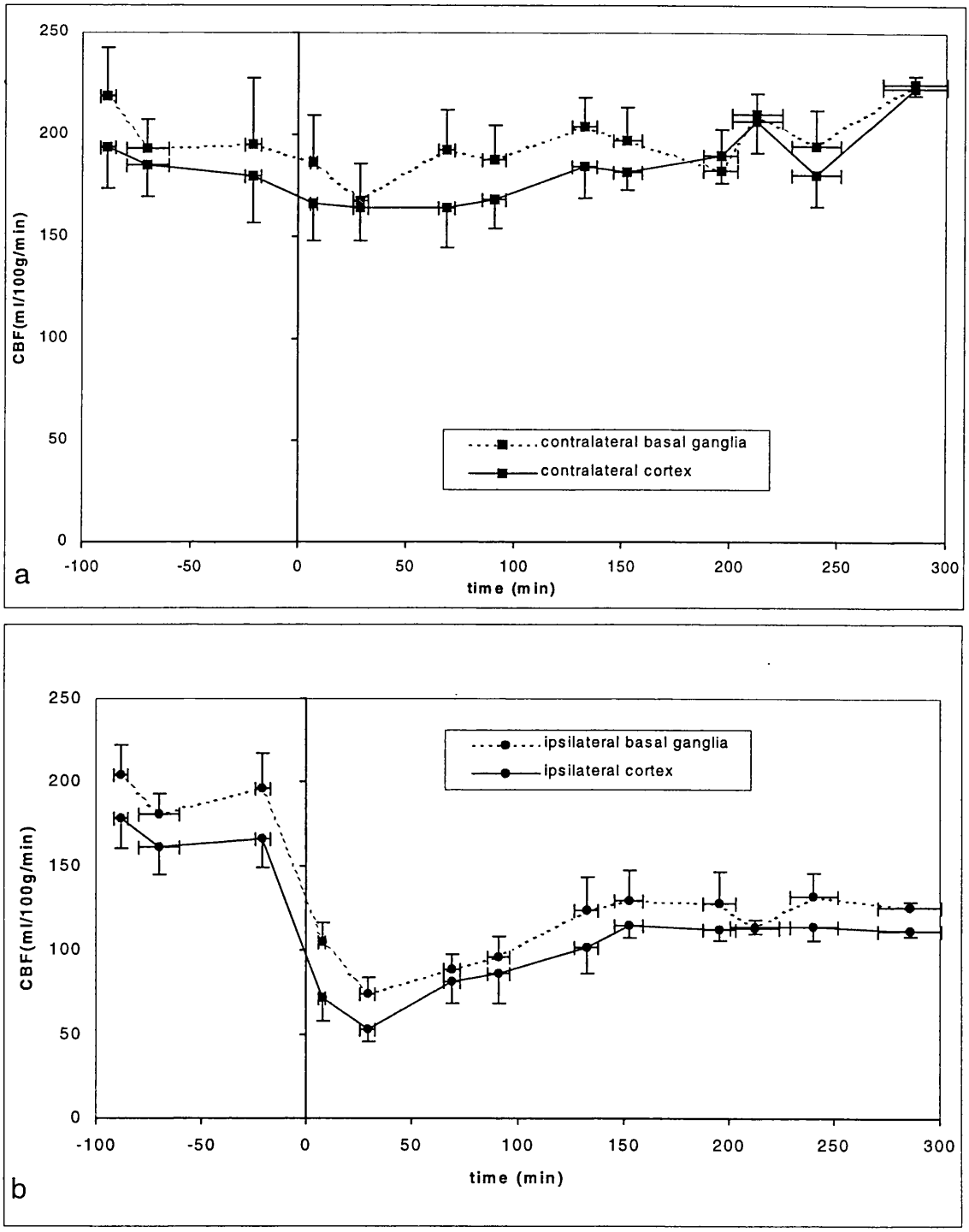

Figure 7.3 *Cerebral blood flow (CBF) time-course (mean ± SE, vertical error bars) from two ROIs in; (a) the contralateral hemisphere, and (b) the ipsilateral hemisphere. Time of occlusion was at t=0. Horizontal error bars represent the SE of the time at which the images were acquired.*

on occlusion of 23 and 26 ml/100g/min (basal ganglia and cortex respectively), followed by a gradual return towards pre-occlusion values.

7.3.2 Apparent Diffusion Coefficient (Tr(D)) of Water

Figure 2 shows typical trace maps obtained 4 hours after occlusion, and Figure 4 shows the time-courses of ADC data. The normal pre-occluded ADC values were 0.80±0.02 and 0.81±0.02 $x10^{-3}mm^2/s$ in basal ganglia and cortex respectively. There was no significant change in ADC for the duration of the experiment in either of the two regions (P=0.9, slope of the regression and t-test).

7.3.3 T_2 Relaxation Time

Figure 5 shows an image obtained on subtracting a T_2 map at approximately 2 minutes post-occlusion from a pre-occlusion T_2 map. Figure 6 shows the time course for the pre- and post-occlusion period. Pre-occlusion values in the ipsilateral basal ganglia and cortical regions were 41.3±0.4 and 40.7±0.3 respectively (P=0.7). Following occlusion there was an initial (≈2 minutes) rapid decrease in T_2 which then normalised to the control values at approximately 1 hour post-occlusion. T_2 values remained at the pre-occlusion level for the remainder of the study. There were no significant T_2 changes on the contralateral side.

The time resolution in the present study was insufficient to provide a detailed description of the time dependence of the rapid initial drop in T_2. Therefore the difference between the first post-occluded measurement (≈2 minutes) and the average of the pre-occluded values was used to characterise this initial decrease. The T_2 changes in both the basal ganglia (-1.9±0.5 ms) and the cortex (-2.2±0.3 ms) were statistically

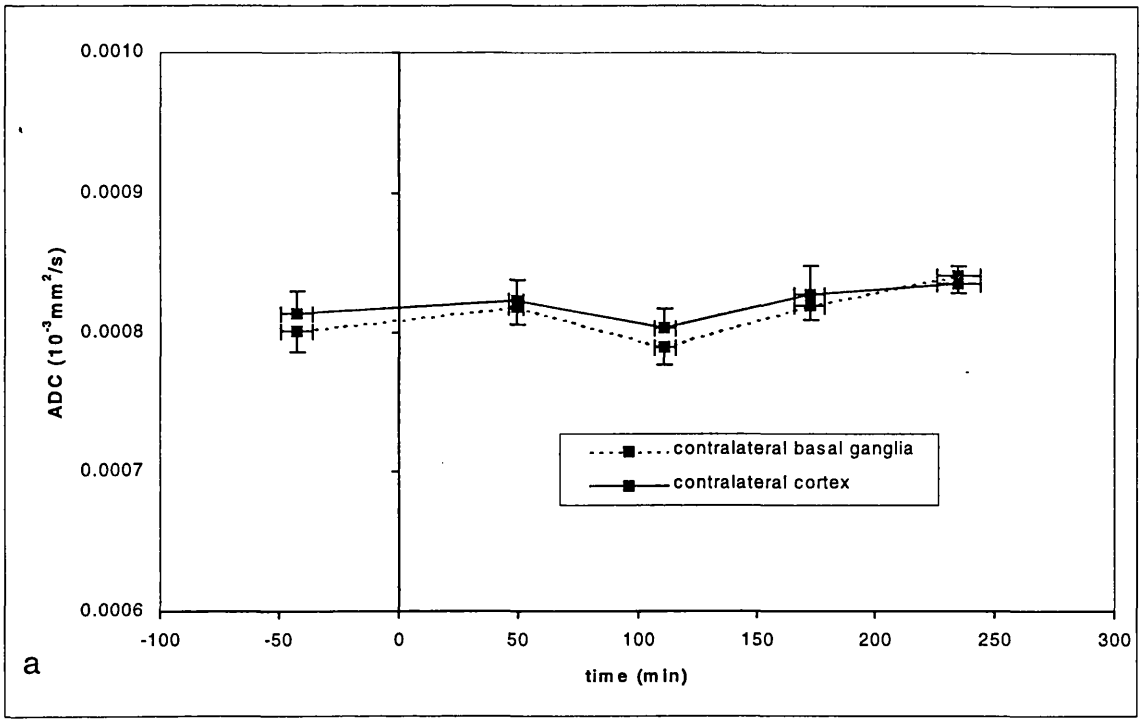

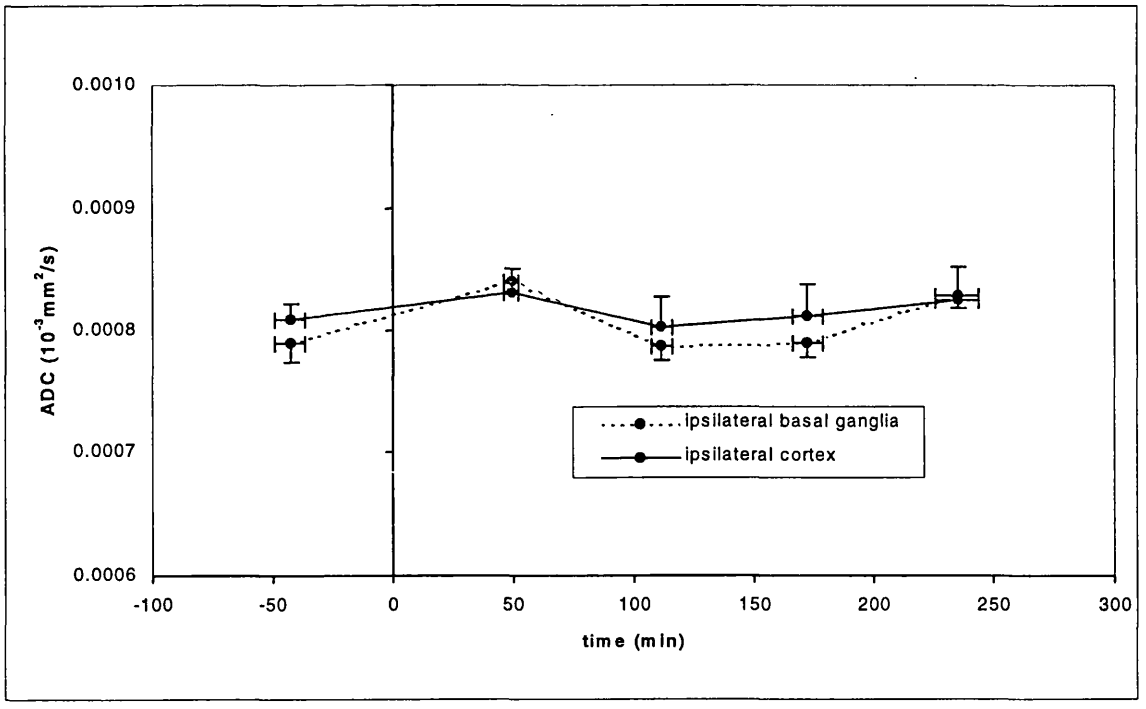

Figure 7.4 *ADC time-course (mean ± SE) from two ROIs in; (a) the contralateral hemisphere, and (b) the ipsilateral hemisphere. No significant change in ADC throughout the course of the study. Time of occlusion was at t=0.*

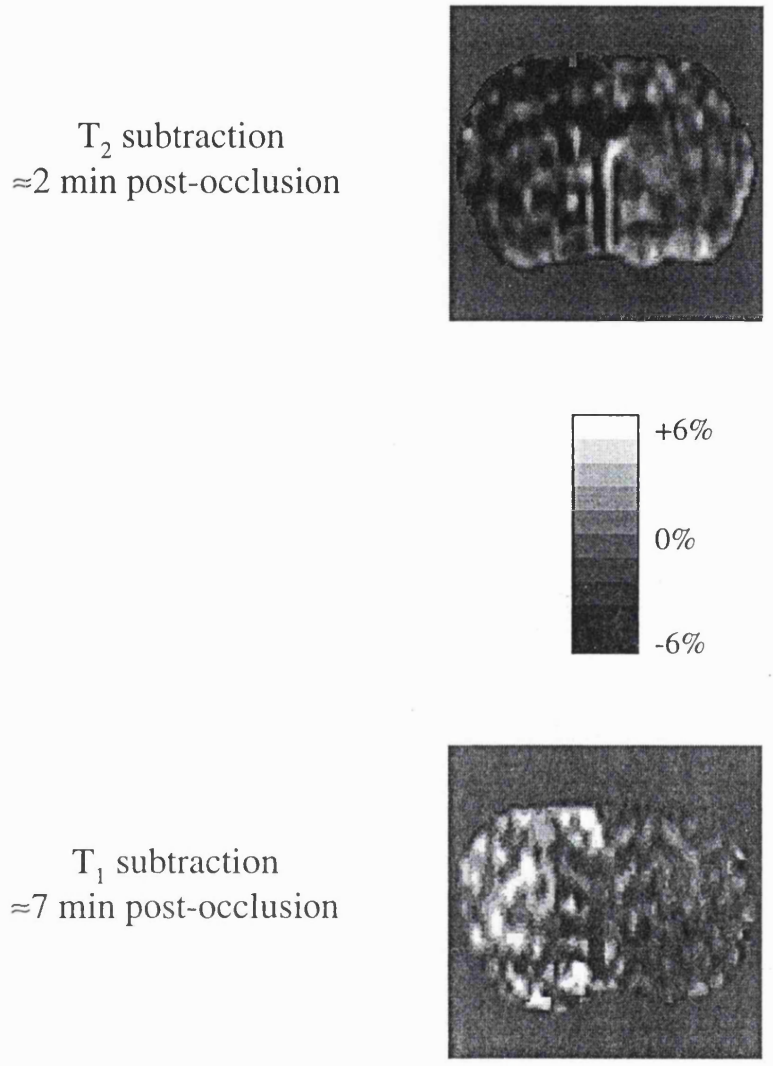

Figure 7.5 *T_1 and T_2 subtraction maps calculated from 1st post-occlusion time point minus pre-occlusion. An increase in T_1 and a decrease in T_2 is observed within minutes of occlusion.*

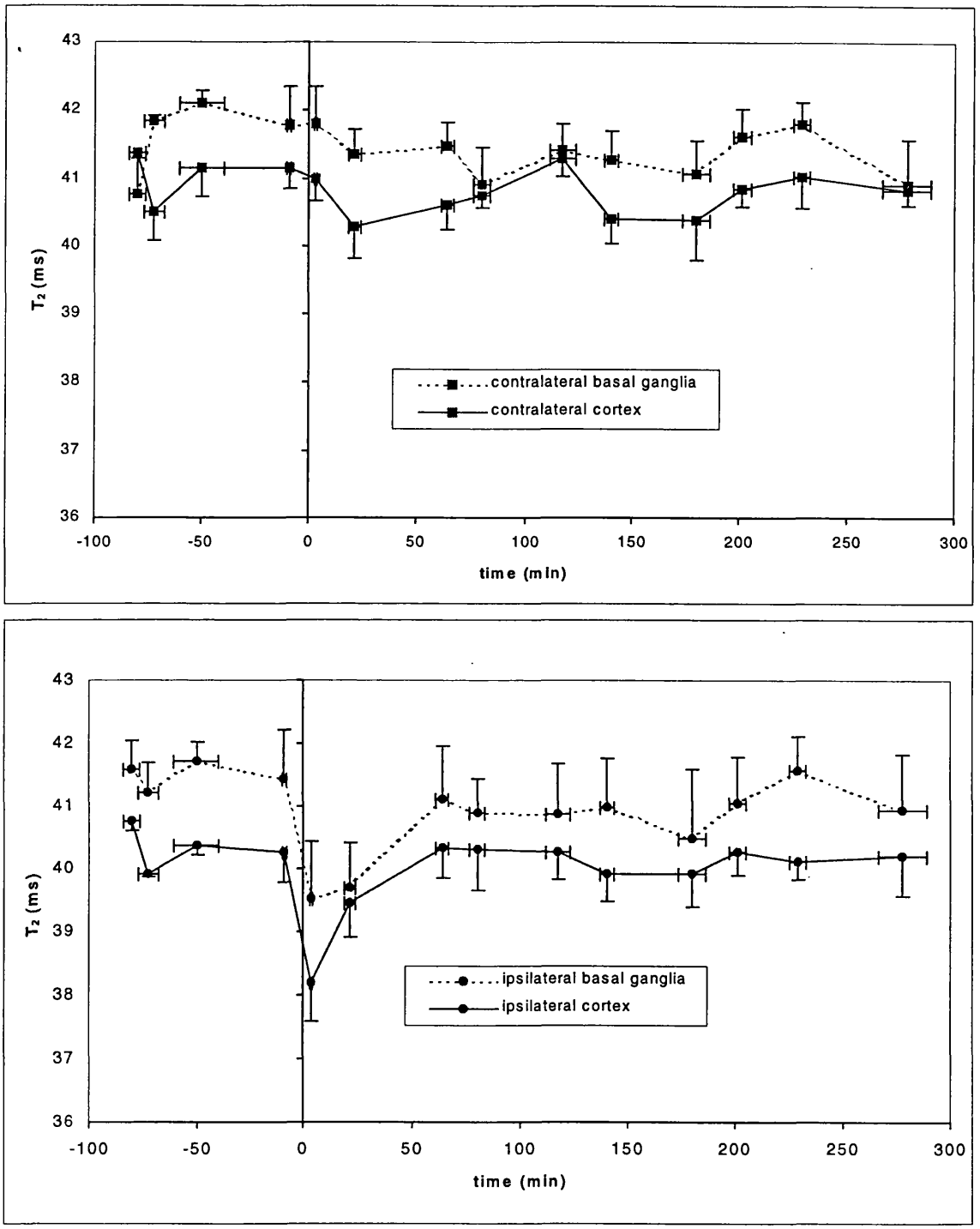

Figure 7.6 *T_2 time-course (mean ± SE) from two ROIs in; (a) the contralateral hemisphere, and (b) the ipsilateral hemisphere. Time of occlusion was at t=0.*

significant ($P<0.018$ and $P<0.009$ respectively). These initial decreases in T_2 were -4.6% and -5.5% of pre-occluded values in the two regions.

An analysis of the T_2 changes for times >1 hour was performed using the slopes obtained from linear regression analysis of the individual time-course data. Comparing a reduced model against a full model showed that a first order polynomial provided an adequate description of the data for times >1 hour. The slopes of the regions in the occluded and control hemispheres were not significantly different from zero ($P>0.3$). A paired *t* test showed that these slopes were not significantly different ($P=0.4$) from each other.

7.3.4 T_1 Relaxation Time

Figure 5 shows an image obtained on subtracting a T_1 map at approximately 7 minutes post-occlusion from a pre-occlusion T_1 map. Figure 7 shows the time-course and mean data for selected regions. The mean pre-occluded T_1 values were 1642±25 ms in the basal ganglia and 1717±16 ms in the cortex. A rapid increase in T_1 occurred in both regions of the occluded hemisphere within 7 minutes of occlusion (the time of the first post-occlusion measurement). After this rapid increase, a peak was reached at the second time point obtained at approximately 37 minutes post-occlusion, following which a slow decrease in T_1 to a limiting value was observed (slope of linear regression of the last 6 points (2hrs) was not significantly different from zero).

The initial change in T_1 was too rapid, relative to the time resolution of this study, for its time dependence to be analysed. Consequently, the rapid and slow-response phases of the time-course data were examined separately. An analysis of the slow-response phase

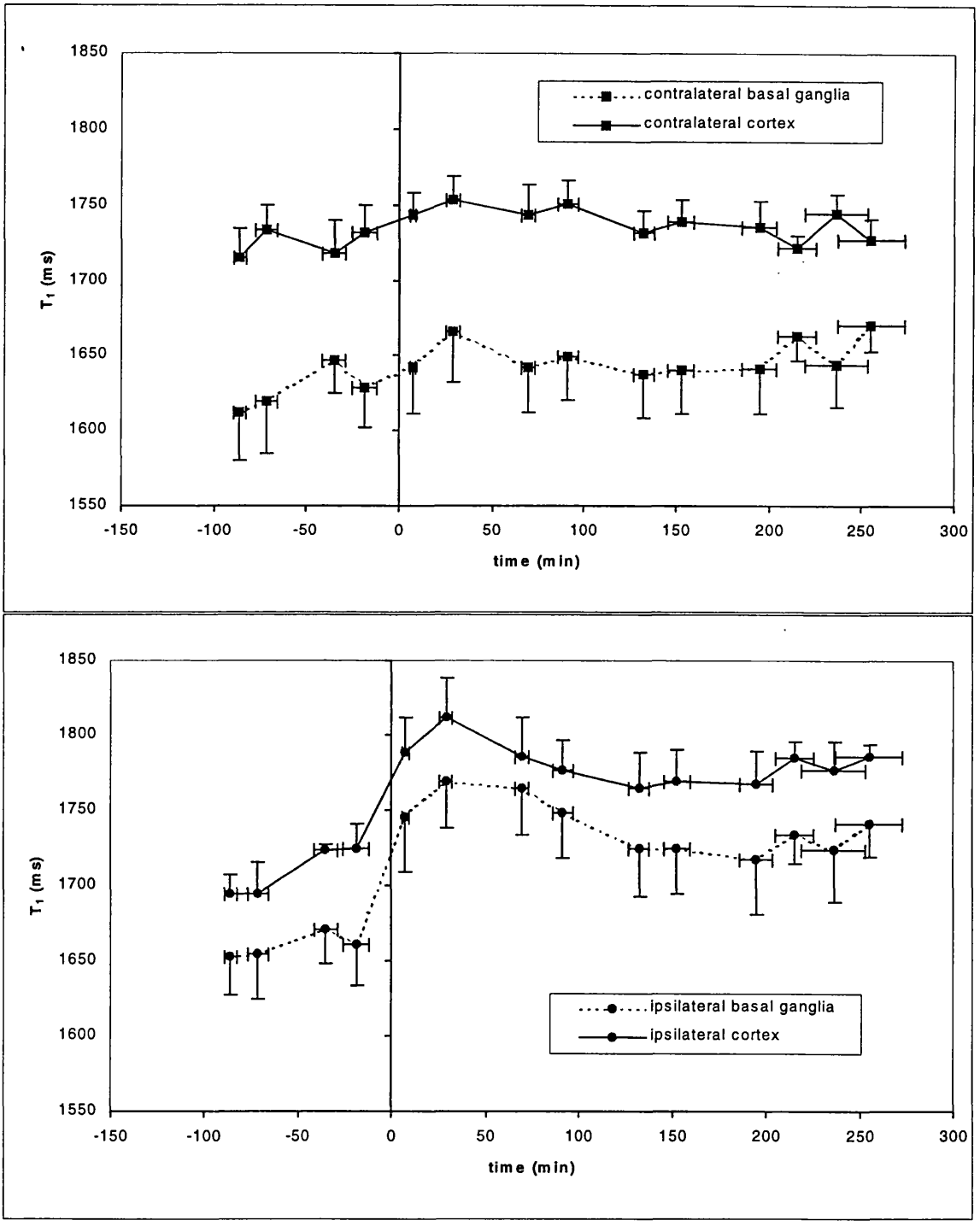

Figure 7.7 *T_1 time-course (mean ± SE) from two ROIs in; (a) the contralateral hemisphere, and (b) the ipsilateral hemisphere. Time of occlusion was at t=0.*

(t>25min) was performed by fitting a first order polynomial to the T_1 data obtained from each animal. The mean rate of change of T_1 was -15±1 ms/h in the basal ganglia and -8±3 ms/h in the cortex, which achieves significance (P<0.03). The values in the equivalent regions in the contralateral region were -2±3 ms/h and -5±3 ms/h respectively, which were not significantly different from zero (P>0.1). Further, the final values (at 255 min) were examined using the difference between the final and pre-occluded T_1 values to determine whether the T_1 were at the control levels. In the ipsilateral hemisphere, T_1 differences in both basal ganglia and cortex (72±8 and 63±9 respectively) were significantly different from pre-occluded T_1 values. In the contralateral hemisphere the T_1 differences were 33±7 ms (significantly different from zero, P=0.05) and 11±7 ms which was not significantly different from zero.

Although we were unable to analyse the time dependence of the rapid, initial T_1 change, the difference between the first post-occluded measurement (≈7 minutes) and the average of the pre-occluded T_1 values was used as a summary variable. The changes in T_1 values obtained in the ipsilateral basal ganglia and cortical regions were 98±18 ms and 79±19 ms respectively, i.e. 5.9% and 4.6% of pre-occluded values. The first post-occlusion measurements were found to be significantly different from the pre-occlusion T_1 values in both regions (P<0.05).

7.4 Discussion

To produce a new rat model of cerebral oligaemic misery perfusion, I have partially occluded the origin of the MCA using an intraluminal nylon monofilament. This technique differs from the conventional methods of MCAO by allowing a residual flow of blood through the partially occluded MCA. This residual level of perfusion appears

sufficient to prevent a decrease in the measured ADC, which we interpret as a marker of cytotoxic oedema resulting from impaired energy metabolism and consequent breakdown of ionic homeostasis (Busza *et al.* 1992). There are few animal models of oligaemic misery perfusion for use with MRI: one such study used partial stenosis of the MCA in a cat model (Derugin and Roberts, 1994), the other used coagulation of MCA combined with postural hypotension in the rat (Grohn *et al.* 1998). However, neither of these techniques permits remote occlusion for use with MRI and only one allows reperfusion (Derugin and Roberts, 1994).

7.4.1 Intraluminal thread occlusion

Conventional intraluminal thread occlusion was first developed by Koizumi (Koizumi *et al.* 1986) using a 4-0 silicone coated thread and was modified by Zea Longa (Zea Longa *et al.* 1989) using a blunted nylon monofilament. Comparison of these two techniques suggested that there were differences in the levels of CBF reduction, and that the Koizumi method was more reliable than that of Zea Longa (Laing *et al.* 1993). However, other investigators have not supported these conclusions. Discussion on the causes of these variations has focused on silicone coating, 3-0 or 4-0 filaments size, length of the filament, and bodyweight of animals (Garcia, 1993; Holland *et al.* 1993).

Ideally, a conventional MCAO should produce a brain lesion of reproducible spatial distribution, with a homogeneous decrease in CBF throughout the MCA territory. However, some studies using the intraluminal suture approach have produced variable lesion distributions and areas (Roussel *et al.* 1995; Li *et al.* 1998), presumably because the reduction in CBF is rarely homogeneous (Chapter 4). Fortuitously, this has led to the differentiation between regions of oligaemic misery perfusion and ischaemia (Li *et al.*

1998; Calamante *et al.* 1999), although there have still been difficulties in investigating the small areas of oligaemic misery perfusion even in larger animals such as cats (van der Toorn *et al.* 1994). I have overcome these difficulties by using a smaller embolus than in the conventionally occluded model, thereby partially obstructing the blood supply to the MCA. This produces a large region of decreased CBF without ADC change, which extends throughout the MCA territory. The embolus that I designed for this purpose was a 0.2 mm nylon monofilament with a small bullet-shaped tip fashioned from cyanoacrylate adhesive which allows a residual flow of blood into the origin of the MCA. For our model it is essential that a thrombus does not form near the end of the occluder blocking origin of the MCA, thereby maintaining a residual flow and permitting the possibility of reperfusion. Thrombi have been detected by others (Koizumi *et al.* 1986); however we did not observe any delayed decrease in flow after the initial drop in CBF upon occlusion, nor was there any evidence of coagulation around the tip of the embolus on post-mortem examination.

7.4.2 Remote MCA occlusion for MRI

MRI investigations of animal models of cerebral ischaemia are playing an increasingly important role in defining the underlying pathophysiology of stroke, in the evaluation of stroke therapies and in the development of new diagnostic techniques (Hoehn-Berlage, 1995). Remote occlusion is essential to investigate the hyperacute MRI changes post-occlusion, and also to allow a direct comparison of pre- and post-occlusion image data (Roussel *et al.* 1994; Li *et al.* 1998). Remote occlusions of the MCA in a rat were first reported by Roussel et al.(Roussel *et al.* 1994) using a silicone embolus (0.25mm diameter, 2mm long) on a nylon thread and by Kohno et al. (Kohno *et al.* 1995), using a 3-0 monofilament coated with glue, and more recently by Li et al.(Li *et al.* 1998) using a

silicone-coated 4-0 monofilament. Our model, based on the earlier work of Roussel et al.(Roussel *et al.* 1994) and Kohno et al. (Kohno *et al.* 1995), was designed to facilitate remote controlled occlusion and reperfusion of the MCA from outside the bore of the imaging magnet, thus allowing us to follow the early changes in an area of oligaemic misery perfusion.

7.4.3 Cerebral blood flow

Compared with other techniques for the investigation of CBF, our pre-occlusion values are rather higher than those typically measured (in the range 130 ml/100g/min) (Lacombe *et al.* 1980). This overestimation is dicussed in Chapter 6. Development of this model has enabled us to investigate acute changes in CBF, T_1 and T_2 in a region of oligaemic misery perfusion following partial MCAO. On occlusion, CBF rapidly decreased, the lowest recorded values being 54 and 71 ml/100g/min in the cortex and basal ganglia at approximately 27 minutes. After this, the blood flow gradually rose to reach a value of approximately 115 ml/100g/min at the end of the study. During the time frame of this study, there was no decrease in the ADC value, presumably because the flow threshold for the ADC changes associated with cytoxic oedema is below the CBF values attained in this study (Busza *et al.* 1992; Hoehn-Berlage, 1995).

7.4.4 T_2 relaxation

A finding of particular interest is the observation that both T_1 and T_2 relaxation times change immediately upon partial occlusion of the MCA, prior to the development of vasogenic oedema. We attribute the instantaneous decrease in T_2 upon occlusion to a local increase in the amount of deoxyhaemoglobin (Ogawa *et al.* 1990b), the level of which will depend upon the complex relationship of CBF, CBV, OEF and haematocrit.

Several groups have reported reductions in T_2* (De Crispigny *et al.* 1992; Roussel *et al.* 1995) and T_2 (Busza *et al.* 1994; van der Toorn *et al.* 1994; Grohn *et al.* 1998; Calamante *et al.* 1999) following the onset of cerebral ischaemia. Further studies have demonstrated strong relationships between the concentration of deoxyhaemoglobin and T_2* (Punwani *et al.* 1998) and between oxygen saturation and T_2 (van Zijl *et al.* 1998), in cases of hypoxic hypoxia. This phenomenon has similarities with the recognised blood oxygenation level dependent (BOLD) effect seen in functional MRI (Ogawa *et al.* 1990a). The reason for the reduction in signal intensity lies in the paramagnetic properties of deoxyhaemoglobin, which perturb the local field in and around the blood vessels, causing signal attenuation due to dephasing. This dephasing may occur as a result of exchange of water between plasma and erythrocytes (van Zijl *et al.* 1998), or diffusion of the water through magnetic field gradients surrounding the blood vessels (Busza *et al.* 1994).

Following the initial decrease in T_2, we observe a rise back to normal values at approximately 1 hour. There are two possible reasons for this normalisation of T_2, one indicating a deterioration of the tissue, the other a recovery. Following occlusion, perfusion pressure falls, and this reduction is compensated via vasodilatation in an attempt to maintain a normal flow. As perfusion pressure falls further, OEF starts to increase, raising levels of deoxyhaemoglobin and thus accounting for the initial decrease in T_2. When the capacity for vasodilation nears its limit, OEF increases to a maximum, following which CBV falls in parallel with perfusion pressure (Powers, 1991). At this stage the basic flow-volume haemodynamic relationships are not maintained and it is difficult to predict changes in T_2 (Grohn *et al.* 1998; van Zijl *et al.* 1998). However, we note that at 1 hour the CBF has not returned to normal and therefore the perfusion

pressure may be sufficiently low to cause a decrease in CBV (Powers, 1991) and a return of deoxyhaemoglobin concentration (per voxel), and thus a normalisation of the T_2 values. This could be analogous to an observation made in a hypoxic ischaemic rabbit model, in which an initial increase in CBV was followed by a delayed decrease, during which time the ADC did not change (D'Arceuil *et al.* 1998). Conversely the normalisation of T_2 may indicate a recovery of the CBV and OEF to normal values, although this is difficult to envisage with the CBF values at approximately 50% of control.

7.4.5 T_1 relaxation

Following occlusion, there was a rapid increase in T_1, followed by a slight decrease, after which T_1 values stabilise at a level approximately 4.5% above the pre-occlusion values. T_1 changes occur prior to the onset of vasogenic oedema and therefore must reflect a mechanism other than an increase in total water content (Van Bruggen *et al.* 1994). These early changes in T_1 have not been observed at low field strengths and the phenomenon may therefore be field-dependent. Early T_1 changes during ischaemia have been reported in a conventional model of MCAO at 5 minutes (Calamante *et al.* 1999) and 45 minutes (Ewing *et al.* 1998) post-occlusion. Possible explanations for the increase in T_1 include: its dependence on flow, decrease in dissolved O_2, a change in the environment of the water (discussed in Chapter 6).

7.5 Conclusion

In summary, I present a rat model of oligaemic misery perfusion in which we observe a decrease in perfusion, and an increase in T_1 throughout the occlusion period, together with T_2 values that are initially depressed then stabilise at the control value after 1 hour.

During the period of oligaemia, the ADC value does not change, indicating that the CBF remains above the threshold for cytotoxic oedema and energy failure. This model will allow further investigation of the pathophysiology of the regions of oligaemic misery perfusion, which have in the past been difficult to investigate.

Chapter 8

8. Discussion and conclusions

This thesis 'Studies of Experimental Cerebral Ischaemia using Magnetic Resonance Imaging and Autoradiography' deals with the potential of magnetic resonance imaging and nuclear medicine markers of cerebral blood flow and hypoxia, in the investigation of the pathophysiology of cerebral ischaemia.

Chapter 4 describes the combination of MRI and the nuclear medicine markers of cerebral blood flow and hypoxia in a rat model of middle cerebral artery occlusion. The regions defined by the hypoxic marker ^{125}I-IAZA and diffusion-weighted imaging (DWI) following ischaemia, are shown to progress onto histologically evident infarction by 7 hours. DWI and maps of the apparent diffusion coefficient are currently being used in the clinical environment, but as yet ^{125}I- IAZA has not entered clinical stroke trials. This must be a potential for future work, which may provide the nuclear medicine community with a marker for 'the penumbra'.

Accurate lesion delineation is essential if one is to assess the efficacy of therapy or monitor longitudinal studies. *Chapter 5* demonstrates that performing single axis diffusion-weighting experiments is inferior when compared with using the trace of the diffusion tensor in defining lesion sizes. Further, it is demonstrated that this improvement is due to the effects of grey matter anisotropy in the rat, which was previously ignored. Improved sequence implementation in MRI and especially DWI, will lead to a more accurate definition of the lesion size and therefore a more considered diagnosis and prognosis.

In *Chapter 6*, I demonstrate that a combination of perfusion and diffusion data provides tissue signatures to distinguish between "moderately affected tissue", with reduced perfusion but normal diffusion; and "severely affected tissue", in which both perfusion and diffusion are significantly reduced. Therefore, in order to characterise the territory effected following a stroke, it is not enough to have only the diffusion-weighted data, and a combination of diffusion and perfusion provides a more complete picture of the regional deficits.

One of the aims of this work was to investigate biophysical mechanisms which would produce MRI contrast following cerebral ischaemia. In *Chapter 6*, two novel MRI observations are reported, namely a decrease in T_2 and an increase in T_1, both within the first few minutes of ischaemia. Further, these changes are observed in regions of oligaemic misery perfusion presented in *Chapter 7*. The T_2 changes are likely to reflect an increase in the levels of deoxyhaemoglobin. However, it is still unclear whether there is a threshold associated with the T_2 decrease and if the T_2 values are able to discriminate between penumbra and ischaemic core. What is apparent, is that the T_2 change is sensitive to changes of blood flow, and occurs immediately following occlusion of a major cerebral artery in a rat. Characterisation of tissue status in patients may also be possible with T_2 values, for example, if the T_2 values were below normal then subsequently increased above the control level (vasogenic oedema), one can imagine that the CBF was severely compromised and the tissue was destined for infarction. However if the T_2 value remained depressed, then this may be indicative of a state of oligaemic misery perfusion and the opportunity for treatment still exists. The T_1 increase following reduced CBF is an unusual finding and the origins of this change

are still unclear. Again this contrast mechanism appears to be sensitive to changes in blood flow, however it does not offer the same opportunities as the T_2 changes to indicate tissue status as the T_1 only increases during ischaemia.

None of the latter findings, that is the early T_1 and T_2 changes, would have been observed unless novel animal models had been developed. This is a field which still requires much work to model human conditions and test therapeutic regimes. Throughout this thesis a strong emphasis has been placed on a combination of microsurgical techniques, the understanding of physiology related to NMR and last but not least, the magnetic resonance imaging.

Abe, K., Aoki, M., Kawagoe, J., Yoshida, T., Hattori, A., Kogure, K., and Itoyama, Y.(1995). Ischemia delayed neuronal death. A mitochondrial hypothesis. *Stroke* **26**, 1478-1489.

Adams, H. P. and Biller, J.(1995). *Neurology in clinical practice* (Bradley, W. G., Daroff, R. B., Fenichel, G. M., and Marsden, C. D. Eds.) 2nd edition. Butterworth-Heinemann, Boston. 993-1031.

Al-Arafaj, A., Ryan, E. A., and Hutchinson, K.(1994). An evaluation of iodine-123 iodoazymycinarabinoside as a marker of localised tissue hypoxia in patients with diabetes mellitus. *Eur. J. Nucl. Med.* **21**, 1338-1342.

Alexandrov, A. V., Black, S. E., Ehrlich, L. E., Bladin, C. F., Smurawska, L. T., Pirisi, A., and Caldwell, C. B.(1996). Simple visual analysis of brain perfusion on HMPAO SPECT predicts early outcome in acute stroke. *Stroke* **27**, 1537-1542.

Allen, K. L., Busza, A. L., Proctor, E., King, M. D., Williams, S. R., Crockard, H. A., and Gadian, D. G.(1993). Controllable graded cerebral ischaemia in the gerbil. Studies of cerebral blood flow and energy metabolism by hydrogen clearance and P-31 NMR spectroscopy. *NMR. Biomed.* **6**, 181-186.

Allergrini, P. R., Hoehn-Berlage, M., Busch, E., Kruger, K., and Kerskens, C. M.(1996). NMR imaging observations of rat brain perfusion changes during stroke: Interpretation based on combination of physiological parameters. *Proc. ISMRM 4th Annual Meeting, New York* 319

Alsop, D. C. and Detre, J. A.(1996). Reduced transit-time sensitivity in nonivasive magnetic resonance imaging of human cerebral blood flow. *J. Cereb. Blood Flow Metab.* **16**, 1236-1249.

Ames, A. I., Wright, R. L., Kowanda, M., Thurston, J. M., and Majno, G.(1968). Cerebral ischemia. II. The no-reflow phenomenon. *Am. J. Pathol.* **52**, 437-453.
Araki, T., Kato, H., Inoue, T., and Kogure, K.(1990). Regional impairment of protein synthesis following brief cerebral ischemia in the gerbil. *Acta. Neuropathol.* **79**, 501-505.

Aronowski, J., Strong, R., and Grotta, J. C.(1997). Reperfusion Injury: Demonstration of brain damage produced by reperfusion after transient focal ischaemia in rats. *J. Cereb. Blood Flow Metab.* **17**, 1048-1056.

Astrup, J., Siesjo, B. K., and Symon, L.(1981). Thresholds in cerebral ischemia - The ischaemic penumbra. *Stroke* **12**, 723-725.

Astrup, J., Symon, L., and Branston, N. M.(1977). Cortical evoked potentials and extracellular K^+ and H^+ at critical levels of brain ischemia. *Stroke* **8**, 51-57.

Azzopardi, D., Wyatt, J. S., Cady, E. B., Delpy, D. T., Baudin, J., Stewart, A. L., Hope, P. L., Hamilton, P. A., and Reynolds, E. O. R.(1989). Prognosis of newborn infants with hypoxic-ischaemic brain injury assessed by phosphorus magnetic resonance spectroscopy. *Pediat. Res* **25**, 445-451.

Back, T., Hoehn-Berlage, M., Kohno, K., and Hossmann, K. A.(1994). Diffusion nuclear magnetic resonance imaging in experimental stroke. Correlation with cerebral metabolites. *Stroke* **25**, 494-500.

Back, T., Kohno, K., and Hossmann, K. A.(1994). Cortical negative DC deflections following middle cerebral artery occlusion and KCl-induced spreading depression: Effect on blood flow, tissue oxygenation, and electroencephalogram. *J. Cereb. Blood Flow Metab.* **14**, 12-19.

Back, T., Zhao, W., and Ginsberg, M. D.(1995). Three-dimensional image analysis of brain glucose metabolism-blood flow uncoupling and its electrophysiological correlates in the acute ischaemic penumbra following middle cerebral artery occlusion. *J. Cereb. Blood Flow Metab.* **15**, 566-577.

Baird, A. E. and Warach, S.(1998). Magnetic resonance imaging of acute stroke. *J. Cereb. Blood Flow Metab.* **18**, 583-609.

Baird, A. E., Donnan, G. A., Austin, M. C., Fitt, G. J., Davis, S. M., and McKay, W. J.(1994). Reperfusion after thrombolytic therapy in ischemic stroke measured by single-photon emission computed tomography. *Stroke* **25**, 79-85.

Bakay, L., Kurland, R. J., Parrish, R. G., Lee, J. C., Peng, R. J., and Bartkowski, H. M.(1975). Nuclear magnetic resonance studies in normal and edematous brain tissue. *Exp. Brain Res.* **23**, 241-248.

Barber, P. A., Davis, S. M., Infeld, B., Baird, A. E., Donnan, G. A., Jolley, D., and Lichtenstein, M.(1998). Spontaneous reperfusion after ischemic stroke associated with improved outcome. *Stroke* **29**, 2522-2528.

Baron, B., Grotta, J., Lamki, L., Villar, C., Ephron, V., Patel, D., Linder, K. E., and Nunn, A. D.(1998). Preliminary experience with technetium-99m-181321, a nitroimadazole, in the detection of cerebral ischaemia associated with acute stroke. *J. Nucl. Med.* **37**, 272P

Baron, J. C.(1991). Pathophysiology of acute cerebral ischaemia: PET studies in humans. *Cerebrovasc Dis* **1(suppl 1)**, 22-31.

Baron, J. C., Bousser, M. G., Rey, A., Guillard, A., Comar, D., and Castaigne, P.(1981). Reversal of focal misery perfusion syndrome by EC-IC arterial bypass in hemodynamic cerebral ischemia: A case study with ^{15}O positron emission tomography. *Stroke* **12**, 454-459.

Basser, P. J.(1995). Inferring microstructural features and the physiological state of tissues from diffusion-weighted images. *NMR. Biomed.* **8**, 333-344.

Basser, P. J., Mattiello, J., and LeBihan, D.(1994a). MR diffusion tensor spectroscopy and imaging. *Biophys. J.* **66**, 259-267.

Basser, P. J., Mattiello, J., and LeBihan, D.(1994b). Estimation of the effective self-diffusion tensor from the NMR spin echo. *J. Magn. Reson. B.* **103**, 247-254.

Becquerel, H.(1896). *Comp. Rend.* **122**, 420

Benveniste, H., Hedlund, L. W., and Johnson, G. A.(1992). Mechanism of the detection of acute cerberal ischaemia in rats by diffusion-weighted magnetic resonance miscroscopy. *Stroke* **23**, 746-754.

Bowler, J. V., Wade, J. P. H., Jones, B. E., Nijran, K., and Steiner, T. J.(1996). Single-photon emission computed tomography using hexamethylpropyleneamine oxime in the prognosis of acute cerebral infarction. *Stroke* **27**, 82-86.

Brant-Zawadzki, M., Pereira, B., Weinstein, P., Moore, S., Kucharczyk, W., Berry, I., McNamara, M., and Derugin, N.(1986). MR imaging of acute experimental ischaemia in cats. *Am. J. Neuroradiol.* **7**, 7-11.

Brierley, J. B., Brown, A. W., Excell, B. J., and Meldrum, B. S.(1969). Brain drainage in the Rhesus monkey resulting from profound arterial hypotension I. Its nature, distribution and general physiological correlates. *Brain Res.* **13**, 68-100.

Brint, S., Jacewicz, M., Kiessling, M., Tanabe, J., and Pulsinelli, W. A.(1988). Foal brain ischemia in the rat: Methods for reproducible neocortical infarction using tandem occlusion of the distal middle cerebral artery and ipsilateral common carotid arteries. *J. Cereb. Blood Flow Metab.* **8**, 474-485.

Bryant, R. G., Marill, K., Blackmore, C., and Francis, C.(1990). Magnetic relaxation in blood and blood clots. *Magn. Reson. Med.* **13**, 133-144.

Bullock, R., Patterson, J., and Park, C.(1991). Evaluation of 99mTc-hexamethylpropyleneamine oxime cerbral blood flow mapping after acute focal ischemia in rats. *Stroke* **22**, 1284-1290.

Busto, R. and Ginsberg, M. D.(1985). Graded focal ischemia in the rat by unilateral carotid artery occlusion and elevated intracranial pressure: Hemodynamic and biochemical characterization. *Stroke* **16**, 466-476.

Busza, A. L., Allen, K. L., King, M. D., Van Bruggen, N., Williams, S. R., and Gadian, D. G.(1992). Diffusion-weighted imaging studies of cerebral ischemia in gerbils. Potential relevance to energy failure. *Stroke* **23**, 1602-1612.

Busza, A. L., Lythgoe, M. F., Allen, K. L., and Williams, S. R.(1994). T_2 decreases in acute global cerebral ischaemia in the gerbil - the contribution of magnetic suseptibility gradients. *Proc. SMR, 2nd Annual Meeting, San Francisco* 1389(Abstract)

Calamante, F., Lythgoe, M. F., Pell, G. S., Thomas, D. L., Busza, A. L., Gadian, D. G., and Ordidge, R. J.(1997). Comparison of early T1,T2,perfusion, diffusion and MTC changes during focal cerebral ischaemia in the rat at 8.5T. *Proc. ISMRM, 5th Annual Meeting, Vancouver* **2**, 600(Abstract)

Calamante, F., Lythgoe, M. F., Pell, G. S., Thomas, D. L., King, M. D., Sotak, C. H., Busza, A. L., Williams, S. R., Ordidge, R. J., and Gadian, D. G.(1999). Early changes in water diffusion, perfusion, T1 and T2 during focal cerebral ischaemia in the rat studied at 8.5T. *Magn. Reson. Med.* **In Press**,

Carano, R. A. D., Takano, K., Helmer, K. G., Tatlisumak, T., Irie, K., Petrucceli, J. D., Fisher, M., and Sotak, C. H.(1998). Estimation of the ischemic penumbra in the rat brain by multispectral analysis. *J. Magn. Reson. imaging* **8**, 1266-1278.

Chapman, J. D.(1979). Hypoxic sensitizers - implications for radiation therapy. *N. Engl. J. Med* **301**, 1429-1432.

Copen, W. A., Koroshetz, W. J., Ostergaard, L., Schwamm, L., Rordorf, G., Weisskoff, R. M., Gonzalez, R. G., Rosen, B. R., and Sorensen, A. G.(1997). Prediction of ischemic injury in acute human stroke with diffusion- and perfusion-weighted MRI. *Proc ISMRM* **1**, 272(Abstract)

Costa, D. C., Ell, P. J., Cullum, I. D., and Jarritt, P. H.(1986). The in-vivo distribution of ^{99m}Tc-HM-PAO in normal man. *Nuc. Med. Comm.* **7**, 647-658.

Crockard, H. A., Gadian, D. G., Frackowiak, R. S., Proctor, E., Allen, K. L., Williams, S. R., and Ross Russell, R. W.(1987). Acute cerebral ischaemia: concurrent changes in cerebral blood flow, energy metabolism, pH, and lactate measured with hydrogen clearance and ^{13}P and ^{1}H nuclear magnetic resonance spectroscopy. II. changes during ischaemia. *J. Cereb. Blood Flow Metab.* **7**, 394-402.

D'Arceuil, H. E., De Crispigny, A. J., Rother, J., Seri, S., Moseley, M. E., Stevenson, D. K., and Rhine, W.(1998). Diffusion and perfusion magnetic resonance imaging of the evolution of hypoxic ischaemic encephalopathy in the neonatal rabbit. *J. Magn. Reson. imaging* **8**, 820-828.

Dardzinski, B. J., Sotak, C. H., Fisher, M., Hasegawa, Y., Li, L., and Minematsu, K.(1993). Apparent diffusion coefficient mapping of experimental focal cerebral ischemia using diffusion-weighted echo-planar imaging. *Magn. Reson. Med.* **30**, 318-325.

De Crispigny, A. J., Wendland, M. F., Derugin, N., Kozniewska, E., and Moseley, M. E.(1992). Real-time observation of transient focal ischemia and hyperemia in cat brain. *Magn. Reson. Med.* **27**, 391-397.

De Roo, M., Mortelmans, L., and Devos, P.(1989). Clinical experience with 99mTc-HMPAO high resolution SPECT of the brain in patients with cerebrovascular accidents. *Eur. J. Nucl. Med.* **15**, 9-15.

Decanniere, C., Eleff, S., Davis, D., and Van Zijl, P. C. M.(1995). Correlation of rapid changes in the average water diffusion constant and the concentrations of lactate and ATP breakdown products during global ischemia in cat brain. *Magn. Reson. Med.* **34**, 343-352.

Deichmann, R. and Haase, A.(1992). Quantitation of T_1 values by SNAPSHOT-FLASH NMR imaging. *J Magn Reson* **96**, 608-612.

Derugin, N. and Roberts, T. P. L.(1994). New and reproducible technique for experimentally induced middle cerebral artery stenosis. *Microsurgery* **15**, 70-72.

Detre, J. A., Leigh, J. S., Williams, D. S., and Koretsky, A. P.(1992). Perfusion imaging. *Magn. Reson. Med.* **23**, 37-45.

Di Rocco, R. J., Kuczynski, B. L., Pirro, J. P., Bauer, A., Linder, K. E., Ramalingam, K., Cyr, J. E., Chan, Y. W., Raju, N., Narra, R. K., Nowotnik, D. P., and Nunn, A. D.(1993). Imaging ischemic tissue at risk of infarction during stroke. *J. Cereb. Blood Flow Metab.* **13**, 755-762.

Dijkhuizen, R. M., Knollema, S., van der Worp, H. B., ter Horst, G. J., de Wildt, D. J., Berkelbach van der Spenkel, J. W., Tullenken, C. A. F., and Nicolay, K.(1998). Region-specific sensitivity and delayed damage after temporary hypoxia-ischaemia in rat brain. A multiparametric MRI study. *Stroke* **29**, 695-704.

Dijkhuizen, R. M., van Lookeren, M., Niendorf, T., Derher, W., van der Toorn, A., Hoehn-Berlage, M., Verheul, H. B., Tullenken, C. A. F., Leibfritz, D., Hossmann, K. A., and Nicolay, K.(1996). Correlation between brain tissue water diffusion changes and cerebral metabolic status in a neonatal rat model of excitotoxicity. *NMR. Biomed.* **9**, 84-92.

Doran, M., Hajnal, J. V., Van Bruggen, N., King, M. D., Young, I. R., and Bydder, G. M.(1990). Normal and abnormal white matter tracts shown by MR imaging using directional diffusion weighted sequences. *J. Comput. Assist. Tomogr.* **14**, 865-873.

Du, C., Hu, R., Csernansky, C. A., Hsu, C. Y., and Choi, D. W.(1996). Very delayed infarction after mild focal cerebral ischemia: A role for apoptosis. *J. Cereb. Blood Flow Metab.* **16**, 195-201.

Duong, T. Q., Ackerman, J. J. H., Ying, H. S., and Neil, J. J.(1998). Evaluation of extra- and intracellular apparent diffusion in normal and globally ischemic rat brain via ^{19}F NMR. *Magn. Reson. Med.* **40**, 1-13.

Ehrlich, P.(1885). Das Sauerstoff-Bederfuis des organismus: eine farbenalytishe studie. *Hirschward*

Eklof, B. and Siesjo, B. K.(1972). The effect of bilateral carotid ligation upon the blood flow and energy state of the rat brain. *Acta. Physiol. Scand.* **86**, 155-165.

Ell, P. J., Cullum, I. D., Costa, D. C., Jarritt, P. H., Hocknell, J. M. L., Lui, D., Jewkes, R. J., Steiner, T. J., Nowotnik, D. P., Pickett, R. D., and Neirinckx, R. D.(1985). A new regional cerebral blood flow agent with ^{99m}Tc-labelled compound. *Lancet* **II**, 50-51.

Ell, P. J., Hocknell, J. M. L., Jarritt, P. H., Cullum, I. D., Lui, D., Costa, D. C., Nowotnik, D. P., Pickett, R. D., Canning, L. R., and Neirinckx, R. D.(1985b). A ^{99}Tc^{m}-labelled radiotracer for the investigation of cerebrovascular disease. *Nuc. Med. Comm.* **6**, 437-441.

Ewing, J. R., Jiang, Q., Zhang, Z. G., Knight, R. A., Divine, G. W., and Chopp, M.(1998). T1 and magnetization transfer contrast at 7 Tesla in acute ischemic infarct in the rat. *Proc.ISMRM, 6th Annual Meeting, Sydney, 1998* 1662(Abstract)

Feldmann, M., Voth, E., Dressler, D., Henze, T., and Felgenauer, K.(1990). 99mTc-HMPAO SPECT and X-ray CT in acute cerebral ischaemia. *J. Neurol.* **237**, 475-479.

Fieschi, C., Battistini, N., Volante, F., Zanette, E., Weber, G., and Passero, S.(1975). Animal model of TIA: An experimental study with intracarotid ADP infusion in rabbits. *Stroke* **6**, 617-621.

Fisher, M.(1997). Characterizing the target of acute stroke therapy. *Stroke* **28**, 866-872.

Fisher, M., Bockhorst, K., Hoehn-Berlage, M., Schmitz, B., and Hossmann, K. A.(1995). Imaging of the apparent diffusion coeficient for the evaluation of cerebral metabolic recovery after cardiac arrest. *Magn. Reson. Imaging* **13**, 781-790.

Garcia, J. H.(1993). A reliable method to occlude a middle cerebral artery in wistar rats. *Stroke* **24**, 1423

Garcia, J. H., Liu, K. F., and Ho, K. L.(1995). Neuronal necrosis after middle cerebral artery occlusion in Wistar rats progresses ar different time intervals in the caudoputamen and the cortex. *Stroke* **26**, 636-643.

Gardner Medwin, A. R., Van Bruggen, N., Williams, S. R., and Ahier, R. G.(1994). Magnetic resonance imaging of propagating waves of spreading depression in the anaesthetised rat. *J. Cereb. Blood Flow Metab.* **14**, 7-11.

Goldmann, E. E.(1913). Vitalfarbung am zentralnervensystem. *Abh Preuss Akad Wiss Phys-Math* **1**, 1-60.

Gomori, J. M., Grossman, R. I., Yu-Ip, C., and Asakura, T.(1987). NMR relaxation times of blood: dependence on field strength, oxydation state, and cell integrity. *J. Comput. Assist. Tomogr.* **11**, 684-690.

Grohn, O. H. J., Lukkarinen, J. A., Oja, J. M. E., van Zijl, P. C., Ulatowski, J. A., Traystman, R. J., and Kauppinen, R. A.(1998). Noninvasive detection of cerebral hypoperfusion and reversible ischemia from reductions in the magnetic resonance imaging relaxation time,T2. *J. Cereb. Blood Flow Metab.* **18**, 911-920.

Groshar, D., McEwan, A. J. B., and Parliment, M. B.(1993). Imaging tumour hypoxia and tumor perfusion. *J. Nucl. Med.* **34**, 885-888.

Gurney, R. and Mott, N.(1948). *Proc. R. Soc. (Lond.)* **164**, 151

Gyngell, M. L., Back, T., Hoehn-Berlage, M., Kohno, K., and Hossmann, K. A.(1994). Transient cell depolarization after permanent middle cerebral artery occlusion: an observation by diffusion-weighted MRI and localised 1H-MRS. *Magn. Reson. Med.* **31**, 337-341.

Hahn, E. L.(1950). Spin echoes. *Phys. Rev.* **80**, 580-594.

Hanson, A. J.(1985). Effect of anoxia on ion distribution in the brain. *Physiol. Rev.* **65**, 101-148.

Hanson, S. K., Grotta, J. C., Rhoades, H., Tran, H. D., Lamkin, L. M., Barron, B. J., and Taylor, W. J.(1993). Value of single-photon emission-computed tomography in acute stroke therapeutic trials. *Stroke* **24**, 1322-1329.

Harris, R. J. and Symon, L.(1984). Extracellular pH, potassium, and calcium activities in progressive ischaemia of rat cortex. *J. Cereb. Blood Flow Metab.* **4**, 178-186.

Hasegawa, Y., Fisher, M., Latour, L. L., Dardzinski, B. J., and Sotak, C. H.(1994). MRI diffusion mapping of reversible and irreversible ischemic injury in focal brain ischemia. *Neurology* **44**, 1484-1490.

Hasegawa, Y., Formato, J. E., Latour, L. L., Gutierrez, J. A., Liu, K. F., Garcia, J. H., Sotak, C. H., and Fisher, M.(1996). Severe transient hypoglycemia causes reversible change in the apparent diffusion coeficient of water. *Stroke* **27**, 1648-1656.

Hasegawa, Y., Latour, L. L., Formato, J. E., Sotak, C. H., and Fisher, M.(1995). Spreading waves of reduced diffusion coefficient of water in normal and ischemic rat brain. *J. Cereb. Blood Flow Metab.* **15**, 179-187.

Hatano, S.(1976). Experience from a multicenter stroke register: A preliminary report. *Bull. World Health Organ.* **54**, 541-553.

Hekmatpanah, J.(1970). Cerebral circulation and perfusion in experimental increased intracranial pressure. *J. Neurosurg.* **32**, 21-29.

Helpern, J. A., Dereski, M. O., Knight, R. A., Ordidge, R. J., Chopp, M., and Qing, Z. X.(1993). Histopathological correlations of nuclear magnetic resonance imaging parameters in experimental cerebral ischemia. *Magn. Reson. Imaging* **11**, 241-246.

Helpern, J. A., Ordidge, R. J., and Knight, R. A.(1992). The effect of cell membrane water permeability on the diffusion coeficient of water. *Proc. XIth Annual Meeting of the Soc. Mag. Res. in Med.* **1**, 1201

Herscovitch, P. and Raichle, M. E.(1985). What is the correct value for the brain-blood partition coefficient for water? *J. Cereb. Blood Flow Metab.* **5**, 65-69.

Hoehn-Berlage, M.(1995). Diffusion-weighted NMR imaging:application to experimental focal cerebral ischemia. *NMR. Biomed.* **8**, 345-358.

Hoehn-Berlage, M., Eis, M., Back, T., Kohno, K., and Yamashita, K.(1995a). Changes of relaxation times (T1, T2) and apparent diffusion coefficient after permanent middle cerebral artery occlusion in the rat: temporal evolution, regional extent, and comparison with histology. *Magn. Reson. Med.* **34**, 824-834.

Hoehn-Berlage, M., Norris, D. G., Kohno, K., Mies, G., Leibfritz, D., and Hossmann, K. A.(1995b). Evolution of regional changes in apparent diffusion coefficient during focal ischemia of rat brain: the relationship of quantitative diffusion NMR imaging to reduction in cerebral blood flow and metabolic disturbances. *J. Cereb. Blood Flow Metab.* **15**, 1002-1011.

Hoffman, J. M., Rasey, J. S., Spence, A. M., Shaw, D. W., and Krohn, K. A.(1987). Binding of the hypoxic tracer [^{3}H]misonidazole in cerebral ischemia. *Stroke* **18**, 168-176.

Hoffman, T. J., Corlija, M., Chaplin, S. B., Volkert, W. A., and Holmes, R. A.(1988). Retention of [99mTc]-d,l-HM-PAO in rat brain: An autoradiographic study. *J. Cereb. Blood Flow Metab.* **8**, S38-S43.

Holland, J. P., Sydserff, S. G. C., Taylor, W. A. S., and Bell, A. B.(1993). Rat models of middle cerebral artery ischemia. *Stroke* **24**, 1423-1424.

Hope, P. L. and Reynolds, E. O. R.(1985). Investigation of cerebral energy metabolism in newborn infants by phosphorus nuclear magnetic resonance spectroscopy. *Clin. Perinatol* **12**, 261-275.

Hossmann, K. A. and Zimmermann, V.(1974). Resuscitation of the monkey brain after 1 hour complete ischemia. I. Physiological and morphological observations. *Brain Res.* **81**, 59-74.

Hossmann, K. A.(1979). Cerebral dysfunction related to local and global ischemia of the brain. *Brain Function in Old Age* **7**, 385-393.

Hossmann, K. A.(1985). *Progress in Brain Research* (Kogure, K., Hossmann, K. A., Siesjo, B. K., and Welsh, F. A. Eds.) Elsevier Science Publishers, New York. 3-17.

Hossmann, K. A.(1991). Animal models of cerebral ischemia. *Cerebrovasc. Dis.* **1**, 2-15.

Hossmann, K. A.(1994). Viability thresholds and the penumbra of focal ischemia. *Ann. Neurol.* **36**, 557-565.

Hossmann, K. A., Nagashima, G., and Klatzo, I.(1990). Repetitative ischemia of cat brain: pathophysiological observations. *Neurol. Res.* **12**, 158-163.

Hossmann, K. A., Sakaki, S., and Kimoto, K.(1976). Cerebral uptake of glucose and oxygen in the cat brain after prolonged ischemia. *Stroke* **7**, 301-305.

Infeld, B., Davis, S. M., Lichtenstein, M., Mitchell, P. J., and Hopper, J. L.(1995). Crossed cerebellar diaschisis and brain recovery after stroke. *Stroke* **26**, 90-95.

Ito, U., Ohno, K., Yamaguchi, T., Tomita, H., Inaba, Y., and Kashima, M.(1980). Transient appearance of "no-reflow" phenomenon in Mongolian gerbils. *Stroke* **11**, 517-521.

Jones, S. C., Bose, B., Furlan, A. J., Friel, H. T., Easly, K. A., Meredith, M. P., and Little, J. R.(1989). CO_2 reactivity and hetrogeneity of cerebral blood flow in ischemic, border zone, and normal cortex. *Am. J. Physiol.* **26**, H473-H482.

Jorgensen, H. S., Sperling, B., and Nakayama, H.(1994). Spontaneous reperfusion of cerebral infarcts in acute stroke patients. Incidence, time course and clinical outcome: The Copenhagen Stroke study. *Arch. Neurol.* **57**, 865-873.

Kagstrom, E., Smith, M. L., and Siesjo, B. K.(1983). Local cerebral blood flow in the recovery period following complete cerebral ischemia in the rat. *J. Cereb. Blood Flow Metab.* **3**, 170-182.

Kajima, T., Azuma, K., Itoh, K., Kagawa, R., Yamane, K., Okada, Y., and Shima, T.(1994). Diffusion anisotropy of cerebral ischaemia. *Acta Neurochir. Suppl. Wien.* **60**, 216-219.

Kato, H. and Kogure, K.(1990). Neuronal damage following non-lethal but repeated cerebral ischemia in the gerbil. *Acta. Neuropathol.* **79**, 494-500.

Kato, H., Araki, T., Kogure, K., Murakami, M., and Uemura, K.(1990). Sequential cerebral blood flow changes in short-term cerebral ischemia in gerbils. *Stroke* **21**, 1346-1349.

Kauppinen, R. A. and Williams, S. R.(1990). Cerebral energy metabolism and intracellular pH during severe hypoxia and recovery: a study using 1H, 31P, and 1H[13C] nuclear magnetic resonance spectroscopy in the guinea pig cerebral cortex in vitro. *J. Neurosci. Res* **26**, 356-369.

Kinouchi, H., Sharp, F. R., Koistinaho, J., Hicks, K., Kamii, H., and Chan, P. H.(1993). Induction of heat shock hsp70 mRNA and HSP70 kDa protein in neurons in the 'penumbra' following focal cerebral ischemia in the rat. *Brain Res.* **619**, 334-338.

Kirino, T.(1982). Delayed neuronal death in the gerbil hippocampus following ischemia. *Brain Res.* **239**, 57-69.

Klatza, I.(1967). Neuropathological aspects of brain edema. *J. Neuropathol. Exp. Neurol.* **26**, 1-14.

Knight, R. A., Dereski, M. O., Helpern, J. A., Ordidge, R. J., and Chopp, M.(1994). Magnetic resonance imaging assessment of evolving focal cerebral ischemia. Comparison with histopathology in rats. *Stroke* **25**, 1252-1261.

Knight, R. A., Ordidge, R. J., Helpern, J. A., Chopp, M., Rodolosi, L. C., and Peck, D.(1991). Temporal evolution of ischemic damage in rat brain measured by proton nuclear magnetic resonance imaging. *Stroke* **22**, 802-808.

Kocher, M.(1990). Metabolic and hemodynamic activation of postischaemic rat brain by cortical spreading depression. *J. Cereb. Blood Flow Metab.* **10**, 564-571.

Kohno, K., Back, T., Hoehn-Berlage, M., and Hossmann, K. A.(1995). A modified rat model of middle cerebral artery thread occlusion under electrophysiological control for magnetic resonance investigations. *Magn. Reson. Imaging* **13**, 65-71.

Kohno, K., Hoehn-Berlage, M., Mies, G., Back, T., and Hossmann, K. A.(1995b). Relationship between diffusion-weighted MR images, cerebral blood flow, and energy state in experimental brain infarction. *Magn. Reson. Imaging* **13**, 73-80.

Koizumi, J., Yoshida, Y., Nakazawa, T., and Ooneda, G.(1986). Experimental studies of ischaemic brain edema: 1. A new experimental model of cerebral embolism in rats in which recirculation can be introduced in the ischemic area. *Jpn J Stroke* **8**, 1-8.

Kriegelstein, G., Kriegelstein, J., and Urban, W.(1972). Long survival time of an isolated perfused rat brain. *J. Neurochem.* **19**, 885

Kudo, M., Aoyama, A., Ichimori, S., and Fukunaga, N.(1992). An animal model of cerebral infarction. Homologous blood clot emboli in rats. *Stroke* **13**, 505-508.

Kuge, Y., Minematsu, K., Yamaguchi, T., and Yoshihiro, M.(1995). Nylon monofilaments for intraluminal middle cerebral artery occlusion in rats. *Stroke* **26**, 1655-1658.

Lacassagne, A., Lattes, J., and Lavadan, J.(1925). Etude experimentale des effets biologiques du polonium introduit dans l'organism. *J. Radiol. Electrol.* **9**, 1

Lacombe, P., Meric, P., and Seylaz, J.(1980). Validation of cerebral blood flow measurements obtained with quantitative tracer techniques. *Brain Res. Rev.* **2**, 105-169.

Laing, R. J., Jakubowski, J., and Laing, R. W.(1993). Middle cerebral artery occlusion without craniectomy in rats which method works best? *Stroke* **24**, 294-298.

Landau, W., Freygang, W., Rowland, L., and Sokoloff, L.(1955). The local circulation of the living brain; values in the unanesthetized and anesthetized cat. *Trans. Am. Neurol. Assoc.* **80**, 125-129.

Lassen, N. A. and Astrup, J.(1987). *Cerebral blood flow* (Wood, J. H. Ed.) McGraw-Hill, New York. 458-466.

Lassen, N. A.(1966). The luxury-perfusion syndrome and its possible relation to acute metabolic acidosis localised within the brain. *Lancet* **2**, 1113-1115.

Lassen, N. A., Andersen, A. R., Friberg, L., and Paulson, O. B.(1988). The retention of [99mTc]-d,l,-HMPAO in the human brain after intracarotid bolus injection: a kinetic analysis. *J. Cereb. Blood Flow Metab.* **8**, S13-S22.

Latour, L. L., Hasegawa, Y., Formato, J. E., Fisher, M., and Sotak, C. H.(1994). Spreading waves of decreased diffusion coefficient after cortical stimulation in the rat brain. *Magn. Reson. Med.* **32**, 189-198.

Latour, L. L., Svoboda, K., Mitra, P. P., and Sotak, C. H.(1994). Time-dependent diffusion of water in a biological model system. *Proc. Natl. Acad. Sci. USA* **91**, 1229-1233.

Le Bihan, D., Breton, E., Lallemand, D., Grenier, P., Cabanis, E., and Laval Jeantet, M.(1986). MR imaging of intravoxel incoherent motions: application to diffusion and perfusion in neurologic disorders. *Radiology* **161**, 401-407.

Lear, J. L.(1988a). Quantitative local cerebral blood flow measurements with technetium-99m HMPAO: evaluation using multiple radionuclide digital quantitative autoradiography. *J. Nucl. Med.* **29**, 1387-1392.

Lear, J. L.(1988b). Initial cerebral HM-PAO distribution compared to LCBF: Use of a model which considers cerebral HM-PAO trapping kinetics. *J. Cereb. Blood Flow Metab.* **8**, S31-S37.

Leblond, C.(1934). Localisation of newly administered iodine in the thyroid gland as indicated by radio-iodine. *J. Anat.* **77**, 149

Levine, S. and Payne, H. M.(1966). Effects of ischaemia and other procedures on the brain and retina of the gerbil (Meriones uguiculatus). *Exp.Neurol.* **16**, 255-262.

Levy, D. E., Brierley, J. B., and Plum, F.(1975). Ischaemic brain damage in the gerbil in the absence of 'no-reflow'. *J. Neurol. Neurosurg. Psychiat.* **38**, 1197-1205.

Levy, D. E., Van Uitert, R. L., and Pike, C. L.(1979). Delayed postischemic hypoperfusion: A potentially damaging consequence of stroke. *Neurology* **29**, 1245-1252.

Li, F., Han, S., Tatlisumak, T., Carano, R. A. D., Irie, K., Sotak, C. H., and Fisher, M.(1998). A new method to improve in-bore middle cerebral artery occlusion in rats. *Stroke* **29**, 1715-1720.

Longa, E. Z., Weinstein, P. R., Carlson, S., and Cummins, R.(1989). Reversible middle cerebral artery occlusion without craniectomy in rats. *Stroke* **20**, 84-91.

Lorek, A., Takei, Y., Cady, E. B., Wyatt, J. S., Penrice, J., Edwards, A. D., Peebles, D., Wylezinska, M., Owen-Reece, H., Kirkbride, V., Cooper, C. E., Aldridge, R. F., Roth, S. C., Brown, G., Delpy, D. T., and Reynolds, E. O. R.(1994). Delayed ("secondary") cerebral energy failure after acute hypoxia-ischaemia in the newborn piglet: continuous 48-hour studies by phosphorus magnetic resonance spectroscopy. *Pediat. Res* **36**, 699-706.

Loubinoux, I., Volk, A., Borredon, J., Guirimand, S., Tiffon, B., Seylaz, J., and Meric, P.(1997). Spreading of vasogenic edema and cytotoxic edema assessed by quantative diffusion and T2 magnetic resonance imaging. *Stroke* **28**, 419-427.

Lust, W. D., Aral, H., Yasumoto, Y., Wittingham, T. S., Djuricic, H., Mrsulja, B. B., and Passonneau, J.(1985). *Cerebral energy metabolism and metabolic encephalopathy* (McCandless, D. W. Ed.) Plenum Press, Ney York. 79-112.

Lynch, L. J.(1983). *Magnetic resonance in biology* (Cohen, J. S. Ed.) John Wiley & Sons, New York. 280-286.

Mancuso, A., Karibe, H., Rooney, W. D., Zarow, G. J., Graham, S. H., Weiner, M. W., and Weinstein, P. R.(1995). Correlation of early reduction in the apparent diffusion coefficient of water with blood flow reduction during middle cerebral artery occlusion in rats. *Magn. Reson. Med.* **34**, 368-377.

Mannan, R. H., Somayaji, V. V., Lee, J., Mercer, J. R., Chapman, J. D., and Wiebe, L. I.(1991). Radioiodinated 1-(5-iodo-5-deoxy-beta-D-arabinofuranosyl)-2-nitroimidazole (iodoazomycin arabinoside: IAZA): a novel marker of tissue hypoxia. *J. Nucl. Med.* **32**, 1764-1770.

Mannan, R.(1991). Novel non-invasive markers of tumor hypoxia. 88-89. PhD thesis; Faculty of Pharancy, Albert, Canada.

Marchal, G., Beaudouin, V., Rioux, P., de la Sayette, V., Le Doze, F., Viader, F., Derlon, J. M., and Baron, J. C.(1996). Prolonged persistence of substantial volumes of potentially viable brain tissue after stroke: a correlative PET-CT study with voxel-based data analysis. *Stroke* **27**, 599-606.

Marshall, L. F., Durity, F., Lounsbury, R., Graham, D. I., Welsh, F., and Langfitt, T. W.(1975). Experimental cerebral oligemia and ischemia produced by intracranial hypertension. I. Pathophysiology, electroenchphalography, cerebral blood flow, blood brain barrier, neurological function. *J. Neurosurg.* **43**, 308-317.

Mas, J. L. and Zuber, M.(1991). Epidemiology of ischaemic stroke. *Cerebrovasc. Dis.* **1**, 36-44.

Matsuda, H., Oba, H., Seki, H., Higashi, S., Sumiya, H., Tsuji, S., Terada, H., Imai, K., and Hisada, K.(1988). Deterimination of flow and rate constants in a kinetic model of [99mTc]-Hexamethyl-Propylene Amine Oxime in the human brain. *J. Cereb. Blood Flow Metab.* **8**, S61-S68.

Matthews, J. N. S., Altman, D. G., Campbell, M. J., and Royston, P.(1990). Analysis of serial measurements in medical research. *Brit. Med. J.* **300**, 230-255.

McLaughlin, A. C., Ye, F. Q., Pekar, J., Santha, A. K. S., and Frank, J. A.(1997). Effect of magnetization transfer on the measurement of cerebral blood flow using steady-state arterial spin tagging approaches: A theoretical investigation. *Magn. Reson. Med.* **37**, 501-510.

Mehta, R. C., Pike, G. B., and Enzmann, D. R.(1996). Magnetization transfer magnetic resonance imaging: A clinical review. *Magn. Reson. Imaging* **8**, 214-230.

Messa, C., Fazio, F., Costa, D. C., and Ell, P. J.(1995). Clinical brain radionuclide imaging studies. *Semin. Nucl. Med.* **25**, 111-143.

Mies, G., Ishimaru, S., Xie, Y., Seo, K., and Hossmann, K. A.(1991). Ischemic thresholds of cerebral protein synthesis and energy state following middle cerebral artery occlusion in rat. *J. Cereb. Blood Flow Metab.* **11**, 753-761.

Mima, T.(1995). *Central nervous system trauma* (Ohnishi, S. T. and Ohnishi, T. Eds.) CRC Press, New York. 107-117.

Minematsu, K., Li, L., Sotak, C. H., Davis, M. A., and Fisher, M.(1992). Reversible focal ischemic injury demonstrated by diffusion-weighted magnetic resonance imaging in rats. *Stroke* **23**, 1304-1311.

Mintorovitch, J., Moseley, M. E., Chileuitt, L., Shimizu, H., Cohen, Y., and Weinstein, P. R.(1991). Comparison of diffusion- and T2-weighted MRI for the early detection of cerebral ischemia and reperfusion in rats. *Magn. Reson. Med.* **18**, 39-50.

Mintorovitch, J., Yang, G. Y., Shimizu, H., Kucharczyk, J., Chan, P. H., and Weinstein, P. R.(1994). Diffusion-weighted magnetic resonance imaging of acute focal cerebral ischaemia: comparison of signal intensity with changes in brain water and Na^+, K^+ - ATPase activity. *J. Cereb. Blood Flow Metab.* **14**, 332-336.

Miyabe, M., Mori, S., van Zijl, P. C., Kirsch, J. R., Eleff, S. M., Koehler, R. C., and Traystman, R. J.(1996). Correlation of the average water diffusion constant with cerebral blood flow and ischaemic damage after transient middle cerebral artery occlusion in cats. *J. Cereb. Blood Flow Metab.* **16**, 881-891.

Morawetz, R. B., Crowell, R. H., De Girolami, U., Marcoux, F. W., Jones, T. H., and Halsey, J. H.(1974). Regional cerebral blood flow thresholds during cerebral ischaemia. *Fed. Proc.* **38**, 2493-2494.

Mori, S. and van Zijl, P. C.(1995). Diffusion weighting by the trace of the diffusion tensor within a single scan. *Magn. Reson. Med.* **33**, 41-52.

Moseley, M. E., Cohen, Y., Mintorovitch, J., Chileuitt, L., Shimizu, H., Kucharczyk, J., Wendland, M. F., and Weinstein, P. R.(1990). Early detection of regional cerebral ischemia in cats: comparison of diffusion- and T2-weighted MRI and spectroscopy. *Magn. Reson. Med.* **14**, 330-346.

Nedergaard, M. and Astrup, J.(1986). Infarct rim: effect of hyperglycemia on direct current potential and (14C)-deoxyglucose phosphorylation. *J. Cereb. Blood Flow Metab.* **6**, 607-615.

Nemoto, E. M., Bleyaert, A. L., Stezoski, S. W., Moossy, J., Rao, G. R., and Safar, P.(1977). Global brain ischemia. A reproducible monkey model. *Stroke* **8**, 558-564.
Niepce de St.Victor, N.(1867). *Comp. Rend.* **65**, 505

Nitatori, T., Sato, N., Waguri, S., Karasawa, Y., Araki, H., Shibanai, K., Kominami, E., and Uchiyama, Y.(1995). Delayed neuronal death in CA1 pyramidal cell layer of the gerbil hippocampus following transient ischemia is appotosis. *J. Neurosci.* **15**, 1001-1011.

Norris, D. G. and Niendorf, T.(1995). Interpretation of DW-NMR data:dependence on experimental conditions. *NMR. Biomed.* **8**, 280-288.

Obrenovitch, T. P.(1995). The ischaemic penumbra: twenty years on. *Cerebrovasc. Brain Metab. Rev.* **7**, 297-323.

Obrenovitch, T. P., Garofalo, O., Harris, R. J., Bordi, L., Ono, M., Momma, F., Bachelard, H. S., and Symon, L.(1988). Brain tissue concentration of ATP, phosphocreatine, lactate, and tissue pH in relation to reduced cerebral blood flow following experimental acute middle cerebral artery occlusion. *J. Cereb. Blood Flow Metab.* **8**, 866-874.

O'Brien, M. D. and Waltz, A. G.(1973). Transorbital approach for occluding the middle cerebral artery without craniectomy. *Stroke* **4**, 201-206.

Ogawa, S., Lee, T. M., Kay, A. R., and Tank, D. W.(1990a). Brain magnetic resonance imaging with contrast dependent on blood oxygenation. *Proc. Natl. Acad. Sci. USA* **87**, 9868-9872.

Ogawa, S., Lee, T. M., Nayak, A. S., and Glynn, P.(1990b). Oxygenation-sensitive contrast in magnetic resonance image of rodent brain at high magnetic fields. *Magn. Reson. Med.* **14**, 68-78.

Ordidge, R. J., Helpern, J. A., Knight, R. A., Qing, Z. X., and Welch, K. M. A.(1991). Investigation of cerebral ischemia using magnetization transfer contrast (MTC) MR imaging. *Magn. Reson. Imaging* **9**, 895-902.

Ordidge, R. J., Wylezinska, M., Hugg, J. W., Butterworth, E., and Franconi, F.(1996). Frequency offset corrected inversion (FOCI) pulses for use in localised spectroscopy. *Magn. Reson. Med.* **36**, 562-566.

Pappata, S., Fiorelli, M., Rommel, T., Hartmann, A., Dettmers, C., Yamaguchi, T., Chabriat, H., Poline, J. B., Crouzel, C., Di Giamberardino, L., and Baron, J. C.(1993). PET studies of changes in local brain hemodynamics and oxygen metabolism after unilateral middle cerebral artery occlusion in baboons. *J. Cereb. Blood Flow Metab.* **13**, 416-424.

Paschen, W., Mies, G., and Hossmann, K. A.(1992). Threshold relationship between cerebral blood flow, glucose-utilazation, and energy metabolites during development of stroke in gerbils. *Exp.Neurol.* **117**, 325-333.

Paxinos, G. and Watson, C.(1986). *The rat brain in stereotaxic coordinates*, 2nd edition. Academic Press, San Diego.

Pekar, J., Jezzard, P., Roberts, D. A., Leigh, J. S. J., Frank, A. C., and McLaughlin, A. C.(1996). Perfusion imaging with compensation for asymmetric magnetization transfer effects. *Magn. Reson. Med.* **35**, 70-79

Pell, G., Lythgoe, M. F., Thomas, D. L., Calamante, F., King, M. D., Gadian, D. G., and Ordidge, R. J.(1999a). A study of reperfusion in a gerbil model of forebrain ischaemia using serial magnetic resonance perfusion and diffusion imaging. *Stroke* **In Press**,

Pell, G., Thomas, D. L., Lythgoe, M. F., Calamante, F., Howseman, A. M., Gadian, D. G., and Ordidge, R. J.(1999b). The implementation of quantative FAIR perfusion imaging with a short repetition time in time-course studies. *Magn. Reson. Med.* **In Press**,

Perez Trepichio, A. D., Xue, M., Ng, T. C., Majors, A. W., Furlan, A. J., Awad, I. A., and Jones, S. C.(1995). Sensitivity of magnetic resonance diffusion-weighted imaging and regional relationship between the apparent diffusion coefficient and cerebral blood flow in rat focal cerebral ischemia. *Stroke* **26**, 667-674.

Pierpaoli, C., Alger, J. R., Righini, A., Mattiello, J., Dickerson, R., Des Pres, D., Barnett, A., and Di Chiro, G.(1996). High temporal resolution diffusion MRI of global cerebral ischemia and reperfusion. *J. Cereb. Blood Flow Metab.* **16**, 892-905.

Pierpaoli, C., Righini, A., Linfante, I., Tao-Cheng, J. H., Alger, J. R., and Di Chiro, G.(1993). Histopathological correlates of abnormal water diffusion in cerebral ischaemia: Diffusion-weighted MR imaging and light and electron miscrosopy study. *Radiology* **189**, 439-448.

Powers, W. J.(1991). Cerebral hemodynamics in ischaemic cerebrovascular disease. *Ann. Neurol.* **29**, 231-240.

Pulsinelli, W. A. and Brierley, J. B.(1979). A new model of bilateral hemispheric ischemia in the unanesthetized rat. *Stroke* **10**, 267-272.

Pulsinelli, W. A.(1985). *Progress in Brain Research* (Kogure, K., Hossmann, K. A., Siesjo, B. K., and Welsh, F. A. Eds.) Elsevier Science Publishers, New York. 29-37.

Pulsinelli, W. A., Brierley, J. B., and Plum, F.(1982). Temporary profile of neuronal damage in a model of transient forebrain ischemia. *Ann. Neurol.* **11**, 491-498.

Punwani, S., Ordidge, R. J., Cooper, C. E., Amess, P., and Clemence, M.(1998). MRI measurements of cerebral deoxyhaemoglobin concentration [dHb]-correlation with near infrared spectroscopy (NIRS). *NMR. Biomed.* **11**, 281-289.

Quast, M. J., Huang, N. C., Hillman, G. R., and Kent, T. A.(1993). The evolution of acute stroke recording by multimodal magnetic resonance imaging. *Magn. Reson. Imaging* **11**, 465-471.

Rice, J. E., Vannucci, R. C., and Brierley, J. B.(1981). The influence of immaturity on hypoxic-ischemic brain damage in the rat. *Ann. Neurol.* **9**, 131-141.

Roberts, T. P. L., Vexler, Z., Derugin, N., Moseley, M. E., and Kucharczyk, J.(1993). Hight-speed MR imaging of ischemic brain injury following stenosis of the middle cerebral artery. *J. Cereb. Blood Flow Metab.* **13**, 940-946.

Robinson, R. G., Shoemaker, W. J., Schlumpf, M., Valk, T., and Bloom, F. E.(1975). Effect of experimental cerebral infarction in the rat brain on catecholamines and behaviour. *Nature* **255**, 332-334.

Rother, J., De Crispigny, A. J., D'Arceuil, H. E., Iwai, K., and Moseley, M. E.(1996). Recovery of the apparent diffusion coeficient after ischemia-induced spreading depression relates to cerebral perfusion gradient. *Stroke* **27**, 980-987.

Roussel, S. A., Van Bruggen, N., King, M. D., and Gadian, D. G.(1995). Identification of collaterally perfused areas following focal cerebral ischemia in the rat by comparison of gradient echo and diffusion-weighted MRI. *J. Cereb. Blood Flow Metab.* **15**, 578-586.

Roussel, S. A., Van Bruggen, N., King, M. D., Houseman, J., Williams, S. R., and Gadian, D. G.(1994). Monitoring the initial expansion of focal ischaemic changes by diffusion-weighted MRI using a remote controlled method of occlusion. *NMR. Biomed.* **7**, 21-28.

Sakurada, O., Kennedy, C., Jehle, J., Brown, J., Carbin, G., and Sokoloff, L.(1978). Measurement of local cerebral blood flow with iodo[^{14}C]antopyrine. *Am. J. Physiol.* **234**, H59-H66.

Schmid-Elsaesser, R., Zausinger, S., Hungerhuber, E., Baethmann, A., and Reulen, H. J.(1989). A critical reevaluation of the intraluminal thread model of focal cerebral ischaemia. Evidence of inadvertent premature reperfusion and subarachnoid hemorrhage in rats by laser-doppler flowmetry. *Stroke* **29**, 2162-2170.

Seimkowicz, E. and Hanson, A. J.(1978). Clinical restitution following cerebral ischemia in hypo-, normo- and hpyerglycemic rats. *Neurol. Scand.* **58**, 1-8.

Sharp, P. F., Smith, F. W., Gemmell, H. G., Lyall, D., Evans, N. T., Gvozdanovic, D., Davidson, J., Tyrrell, D. A., Pickett, R. D., and Neirinckx, R. D.(1986). Technetium-99m HM-PAO stereoisomers as potential agents for imaging regional cerebral blood flow: human volunteer studies. *J. Nucl. Med.* **27**, 171-177.

Shigeno, T., Teasdale, G. M., McCulloch, J., and Graham, D. I.(1985). Recirculation model following MCA occlusion in rats. Cerebral blood flow, cerebrovascular permeability, and brain edema. *J. Neurosurg.* **63**, 272-277.

Siesjo, B. K.(1978). *Brain energy metabolism*, John Wiley & Sons, New York.

Siesjo, B. K.(1992a). Pathophysiology and treatment of focal cerebral ischemia. Part II: Mechanisms of damage and treatment. *J. Neurosurg.* **77**, 337-354.

Siesjo, B. K.(1992b). Pathophisiology and treatment of focal cerebral ischemia. Part I: Pathophysiology. *J. Neurosurg.* **77**, 169-184.

Smith, M. L., Bendek, G., Dahlgren, N., Rosen, I., Wieloch, T., and Siesjo, B. K.(1985). Model for studying long term recovery following forebrain ischemia in the rat. 2. A 2-vessel occlusion model. *Acta. Neurol. Scand.* **69**, 385-401.

Sorensen, A. G., Gonzalez, R. G., Copen, W. A., Schwamm, L., Rordorf, G., Ostergaard, L., Weisskoff, R. M., and Rosen, B. R.(1997). Quantitaion of diffusion/perfusion MRI mismatch in acute human cerebral infarction. *Stroke* **28**, 252

Stejskal, E. O. and Tanner, J. E.(1965). Spin diffusion measurements: Spin echoes in the presence of a time-dependent field gradient. *J. Chem. Phys.* **42**, 288-292.

Stummer, W., Baethmann, A., Murr, R., Schurer, L., and Kempski, O. S.(1995). Cerebral protection against ischemia by locomotor activity in gerbils. Underlying mechanisms. *Stroke* **26**, 1423-1430.

Suzuki, R., Yamaguchi, T., Kirino, T., Orzi, F., and Klatzo, I.(1983). The effects of 5-minute ischemia in Mongolian gerbils: I. Blood-brain barrier, cerebral blood flow, and local cerebral glucose utilization changes. *Acta. Neuropathol.* **60**, 207-216.

Symon, L.(1980). The relationship between CBF, evoked potentials, and the clinial features in cerebral ischemia. *Acta. Neurol. Scand.* **62**, 175-190.

Tadamura, E., Hatabu, H., Li, W., Prasad, P. V., and Edelman, R. R.(1997). Effect of oxygen inhalation on relaxation times in various tissues. *J. Magn. Reson. imaging* **7**, 220-225.

Takaizawa, S. and Hakim, A. M.(1991). Animal models of cerebral ischemia. 2. Rat models. *Cerebrovasc. Dis.* **1**, 16-21.

Takano, K., Latour, L. L., Formato, J. E., Carano, R. A. D., Helmer, K. G., Hasegawa, Y., Sotak, C. H., and Fisher, M.(1996). The role of spreading depression in focal ischemia evaluated by diffusion mapping. *Ann. Neurol.* **39**, 308-318.

Tamura, A., Graham, D. I., McCulloch, J., and Teasdale, G. M.(1981). Focal cerebral ischemia in the rat: 1. Description of technique and early neuropathological consequences following middle cerebral artery occlusion. *J. Cereb. Blood Flow Metab.* **1**, 53-60.

Thilmann, R., Xie, Y., Kleihues, P., and Kiessling, M.(1986). Persistant inhibition of proteitn synthesis precedes delayed neuronal death in post-ischemic gerbil hippocampus. *Acta. Neuropathol.* **71**, 88-93.

Thornton, J. S., Ordidge, R. J., Penrice, J., Cady, E. B., Amess, P., Punwani, S., Clemence, M., and Wyatt, J. S.(1997). Anisotropic water diffusion in white and gray matter of the noenatal piglet brain before and after transient hypoxia-ischaemia. *Magn. Reson. Imaging* **15**, 433-440.

Thornton, J. S., Ordidge, R. J., Penrice, J., Punwani, S., Clemence, M., and Wyatt, J. S.(1996). Anisotropic diffusion in white and grey matter of the neonatal piglet brain pre and post hypoxia-ischaemia. *Procs SMR* **3**, 1330(Abstract)

Thulborn, K. R., Waterton, J. C., Matthews, P. W., and Radda, G. K.(1982). Oxygenation dependence of the transverse relaxation time of water protons in whole blood at high field. *Biochem. Biophys. Acta* **714**, 265-270.

Tomida, S., Nowak, T. S., Vass, K., Lohr, J. M., and Klatzo, I.(1987). Experimental model for repetitive ischemic attacks in the gerbil: The cumulative effect of repeated ischemic insults. *J. Cereb. Blood Flow Metab.* **7**, 773-783.

Tsuchidate, R., He, Q. ,P., Smith, M. L., and Siesjo, B. K.(1997). Regional cerebral blood flow during and after 2 hours of middle cerebral artery occlusion in the rat. *J. Cereb. Blood Flow Metab.* **17**, 1066-1073.

Tuor, U. I., Kozlowski, P., Del-Bigo, D. R., Ramjiawan, B., Su, S., Malisza, K., and Saunders, J. K.(1998). Diffusion- and T2-weighted increase in magnetic resonance images of immature brain during hypoxia-ischemia: transient reversal posthypoxia. *Exp.Neurol.* **150**, 321-328.

Turner, J. H.(1975). Brain scan in cerebral ischemia. An experimental model in rat. *Stroke* **6**, 703-706.

Van Bruggen, N., Cullen, B. M., King, M. D., Doran, M., Williams, S. R., Gadian, D. G., and Cremer, J. E.(1992). T2- and diffusion-weighted magnetic resonance imaging of a focal ischemic lesion in rat brain. *Stroke* **23**, 576-582.

Van Bruggen, N., Roberts, T. P., and Cremer, J. E.(1994). The application of magnetic resonance imaging to the study of experimental cerebral ischaemia. *Cerebrovasc. Brain Metab. Rev.* **6**, 180-210.

Van Bruggen, N., van Lookeren Campagne, M., Thibodeaux, H., Palmer, J. T., Williams, S. P., and Thomas, G. R.(1998). Evidence for delayed cerebral infarction following focal ischaemia in the rat: A diffusion-weighted imaging study. *Proc. ISMRM, 6th Annual Meeting, Sydney* **2**, 1180(Abstract)

van der Toorn, A., Verheul, H. B., Berkelbach van der Spenkel, J. W., Tullenken, C. A. F., and Nicolay, K.(1994). Changes in metabolites and tissue water status after focal ischemia in cat brain assessed with localized proton MR spectroscopy. *Magn. Reson. Med.* **32**, 685-691.

van Gelderen, P., de Vleeschouwer, M. H., DesPres, D., Pekar, J., van Zijl, P. C., and Moonen, C. T.(1994). Water diffusion and acute stroke. *Magn. Reson. Med.* **31**, 154-163.

van Zijl, P. C., Eleff, S. M., Ulatowski, J. A., Oja, J. M., Ulug, A. M., Traystman, R. J., and Kauppinen, R. A.(1998). Quantitative assessment of blood flow, blood volume and blood oxygenation effects in functional magnetic resonance imaging. *Nat. Med.* **4**, 159-167.

Verheul, H. B., Berkelbach van der Spenkel, J. W., Tullenken, C. A. F., Tamminga, K. S., and Nicolay, K.(1992). Temporal evolution of cerebral ischaemia in the rat assessed by T2-weighted and diffusion-weighted magnetic resonance imaging. *Brain Topogr.* **5**, 171-176.

Villringer, A., Rosen, B. R., Belliveau, J. W., Ackerman, J. L., Lauffer, R. B., Buxton, R. B., Chao, Y., Wedeen, V. J., and Brady, T. J.(1988). Dynamic imaging with lanthanide chelates in normal brain: contrast due to magnetic susceptibility effects. *Magn. Reson. Med.* **6**, 164-174.

Vise, W. M., Schuier, F. J., Hossmann, K. A., Takagi, S., and Zulch, K. J.(1977). Cerebral microembolization. I. Pathophysiological studies. *Ann. Neurol.* **34**, 660-665.

Warach, S., Chien, D., Li, W., Ronthal, M., and Edelman, R. R.(1992). Fast magnetic resonance diffusion-weighted imaging of acute human stroke [published erratum appears in Neurology 1992 Nov; 42(11):2192]. *Neurology* **42**, 1717-1723.

Watson, B. D., Dietrich, W. D., Busto, R., Wachtel, M. S., and Ginsberg, M. D.(1995). Induction of reproducible brain infarction by photochemically initiated thombosis. *Ann. Neurol.* **17**, 497-504.

White, B. C., Grossman, L. I., and Krause, G. S.(1993). Brain injury by global ischemia and reperfusion. *Neurology* **43**, 1656-1665.

Williams, D. S., Detre, J. A., Leigh, J. S. J., and Koretsky, A. P.(1992). Magnetic resonance imaging of perfusion using spin inversion of arterial water. *Proc. Natl. Acad. Sci. USA* **89**, 212-216.

Wolff, S. D. and Balaban, R. S.(1989). Magnetization transfer contrast (MTC) and tissue water proton relaxation in vivo. *Magn. Reson. Med.* **10**, 135-144.

Yang, G. Y. and Betz, A. L.(1994). Reperfusion-induced injury to the blood-brain barrier after middle cerebral artery occlusion in rats. *Stroke* **25**, 1658-1665.

Ye, F. Q., Mattay, V. S., Jezzard, P., Frank, J. A., Weinberger, D. R., and McLaughlin, A. C.(1997). Correction for vascular artifacts in cerebral blood flow measured by using steady-state arterial spin tagging approaches. *Magn. Reson. Med.* **37**, 226-235.

Yeh, S. H., Liu, R. S., Hu, H. H., Change, C. P., Chu, L. S., Chou, K. L., and Wu, L. C.(1994). Ischaemic penumbra in acute stroke:demonstration by PET with fluorine-18 fluoromisonidazole. *J. Nucl. Med.* **35**, 205P

Young, A. R., Sette, G., Touzani, O., Rioux, P., Derlon, J. M., MacKenzie, E. T., and Baron, J. C.(1996). Relationships between high oxygen extraction fraction in the acute stage and final infarction in reversible middle cerebral artery occlusion: an investigation in anesthetized baboons with positron emission tomography. *J. Cereb. Blood Flow Metab.* **16**, 1176-1188.

Zea Longa, E., Weinstein, P. R., Carlson, S., and Cummins, R.(1989). Reversible middle cerebral artery occlusion without craniectomy in rats. *Stroke* **20**, 84-91.

Zhang, W., Silva, A. C., Williams, D. S., and Koretsky, A. P.(1995). NMR measurements of perfusion using arterial spin labeling without saturation of macromolecular spins. *Magn. Reson. Med.* **33**, 370-376.

Zhang, W., Williams, D. S., and Koretsky, A. P.(1993). Measurement of rat brain perfusion by NMR using spin labeling of arterial water:*In vivo* determination of the degree of spin labeling. *Magn. Reson. Med.* **29**, 416-421.